This is to certify that the

dissertation entitled

Nondestructive Measurements of Electromagnetic Parameters of Anisotropic Materials Using An Open-Ended Waveguide Probe System

presented by

Chih-Wei Chang

has been accepted towards fulfillment
of the requirements for

Ph.D. degree in Electrical Engineering

Major professor

Date April 26, 1995

DATE DUE	DATE DUE	DATE DUE
MAY 17 2005 091605		

NONDESTRUCTIVE MEASUREMENTS OF ELECTROMAGNETIC PARAMETERS OF ANISOTROPIC MATERIALS USING AN OPEN-ENDED WAVEGUIDE PROBE SYSTEM

By

Chih-Wei Chang

A DISSERTATION

Submitted to
Michigan State University
in partial fulfillment of the requirements
for the degree of

DOCTOR OF PHILOSOPHY

Department of Electrical Engineering

1995

ABSTRACT

NONDESTRUCTIVE MEASUREMENTS OF ELECTROMAGNETIC PARAMETERS OF ANISOTROPIC MATERIALS USING A WAVEGUIDE PROBE SYSTEM

By

Chih-Wei Chang

A non-destructive measurement of electromagnetic (EM) properties of anisotropic materials using an open-ended waveguide probe has been conducted. Two different techniques, based on the Hertzian potential method and the transverse field method, are developed to facilitate the investigation of the subject. The technique employing Hertzian potentials is applied to isotropic materials only, however, the technique employing the transverse field method is suitable for both isotropic and anisotropic materials.

When a waveguide probe, which consists of an open-ended waveguide terminated on a flange, is placed against a material layer, two coupled electric field integral equations (EFIE's) for the aperture electric field can be derived by matching the boundary conditions at discontinuity interfaces. These EFIE's can be solved numerically with the Method of Moments (MoM) when the electric field on the waveguide aperture is expressed as a sum of waveguide modes. The reflection coefficient of the incident wave or other relevant quantities of the waveguide probe can be expressed as functions of the EM properties,

such

layer

the re

A

const

input

layer

adm

inver

prope

tenso

their

mate

such as the permittivity, permeability, and conductivity, and the thickness of the material layer. Therefore, the EM parameters of the material layer can be inversely determined if the reflection coefficient of the incident wave is experimentally measured.

A series of experiments have been conducted using the waveguide probe system constructed at MSU electromagnetics laboratory. The experimental results of the probe input admittances, with the probe attached to various isotropic and anisotropic material layers, using an HP 8720B network analyzer are presented. These probe input admittances are then used to determine the complex permittivity inversely by a numerical inverse procedure based on the Newton's iterative method. The inverse results on the EM properties of some known materials are found to be quite satisfactory. The results on the tensor permittivities of some anisotropic materials are found to be reasonable even though their exact values have not been determined before. Finally, an analysis of the effects of material parameters on the input admittance is presented.

To my wife

and

our lovely sons

ACKNOWLEDGEMENTS

I would like to express my heartfelt appreciation to my major professor, Dr. Kun-Mu Chen. His knowledgeable advice, technical competency as well as his patience and timely input made it possible for me to complete this work. I am also indebted to Dr. Dennis P. Nyquist, Dr. Edward J. Rothwell and Dr. Byron C. Drachman for their generous support and constructive suggestions during the course of this study. A special note of thanks is due Professor Jian Qian for his generous assistance and kind concern.

I owe a great deal to my parents for their love and continuous support. I must also acknowledge my wonderful wife, Uan-Li. Her love, sacrifice, constant encouragement and taking care of our children, Timmy (Ching-Chen) and Peter (Yao-Chen), have been invaluable in the successful completion of my graduate study.

Finally, the fundings of this research by the State of Michigan Research Excellence Fund through Michigan State University and Boeing Airplane Company are most gratefully acknowledged.

TABLE OF CONTENTS

LIST OF FIGURES

4.1

4.1

4.2

4.2

4.3(a

4.3(b

4.4.

4.5.

5.1.

5.2.

5.3.

5.4.

5.5.

5.6.

5.7.

5.8.

5.9.

5.10.

5.11.

5.12.

5.13

5.14

5.15

5.16

5.17

5.18

5.19

5.20

5.21

5.22

5.23

5.24.

5.25.

5.26.

5.27.

5.28.

5.29

5.30

5.31

5.32

5.33

5.34

A.1

A.2

LIST OF TABLES

CHAPTER 1

INTRODUCTION

The objective of this research is to conduct nondestructive measurement of the electromagnetic (EM) properties of material layers using a waveguide probe system. Two different techniques are established to facilitate the investigation of the subject. The technique employing Hertzian potentials is applied to isotropic materials only, however, the technique employing the transverse field method is suitable to both isotropic and anisotropic materials.

Techniques for the measurement of the material EM properties have been developed by numerous investigators using various structures such as open-ended coaxial line [1]-[12], stripline [13], microstrip line [14], cavity resonator [15]-[17] and waveguide [18]-[20] during the last two decades. In recent years, due to the rapid advance in material manufacturing, an increasing demand for accurate nondestructive measurements of the material parameters has emerged.

Several methods are available for measuring the EM properties of dielectric materials nondestructively. Some researchers employed an open-ended coaxial probe [1]-[12], while others used an open-ended waveguide probe [19]-[20]. However, all of them were

limited to the measurement of the EM parameters of isotropic materials only. In this research, we present an technique for accurate nondestructive measurement of the EM parameters of isotropic materials, and another technique for anisotropic materials, where both of them employ an open-ended waveguide probe system.

In the study of the nondestructive measurement of the EM parameters of materials with a waveguide probe system, we divide the study into steps: the forward and the inverse procedures. The forward procedure refers to the theoretical and numerical analysis of the waveguide probe system, which consists of an open-ended waveguide terminated on a flange, placed against a layer of material [21]-[32]. In this procedure, the reflection coefficient or the input admittance of the waveguide probe can be expressed as a function of the assumed EM parameters of the material layer. On the other hand, the inverse procedure deals with the problem of inversely determining the EM parameters of the material layer from the measured reflection coefficient or input admittance of the waveguide probe placed against the material layer [12].

This study is presented in three parts: the first part, Chapter 2, presents the basic theories for this research; the second part, Chapters 3 and 4, develops the forward procedure of the measurement for determining the EM properties of isotropic and anisotropic materials; and the last part, Chapter 5, describes the experiments and the inverse procedure of the measurement.

Chapter 2 presents the basic theories which are used to establish two different techniques for determining the EM parameters of materials using a waveguide probe system. Hertzian potentials are first reviewed in the chapter. The EM fields in the waveguide, the material layer and the open free space are then determined in terms of Hertzian potentials. These fields are used in Chapter 3 to match the boundary conditions at the interfaces between different regions. The transverse field method is also reviewed in this chapter. It generates a general case dealing with the EM fields inside an anisotropic

medium and a degenerate case with the EM fields inside an isotropic medium. The EM fields derived by this method are then used to match the boundary conditions at the discontinuity interfaces in Chapter 4.

In Chapter 3, the forward procedure of the measurement for determining the EM parameters of isotropic materials is studied. The EM fields expressed in terms of Hertzian potentials within various regions are first recalled from Chapter 2. Two coupled integral equations for the electric field are then derived by matching the tangential EM fields across the waveguide aperture. The method of moments is implemented to solve these coupled electric field integral equations (EFIE's) numerically. Finally, the numerical results on the input admittances of the waveguide probe placed against material layers are compared with the existing results published by other workers.

Chapter 4 deals with the forward procedure of the measurement for determining the EM parameters of anisotropic materials. The EM fields derived with the transverse field method are recalled from Chapter 2. The matching of the tangential EM fields at the probe aperture results in two coupled integral equations for the unknown aperture electric field. The method of moments is implemented to solve these EFIE's numerically. Also the numerical examples illustrated in Chapter 3 for isotropic materials are recalculated and compared with the existing results to validate the technique. In addition, the numerical results on the input admittances of the waveguide probe in contact with a layer of assumed known anisotropic material are presented.

Finally, the experiments and the inverse procedure of the measurement are described in Chapter 5. The experimental setups and the calibration procedures of the waveguide probe system are first described. The experimental results of the probe input admittances, with the probe attached to various isotropic and anisotropic material layers, using an HP 8720B network analyzer are then presented. In addition, the inverse procedure of the measurement to determine the EM parameters of the measured materials is developed.

The pro

by this

known

of some

have no

The probe input admittances are then used to inversely determine the complex permittivity by this numerical inverse procedure. The inverse results on the EM properties of some known materials are found to be quite satisfactory. The results on the tensor permittivities of some anisotropic materials are found to be reasonable even though their exact values have not been determined before.

CHAPTER 2

BASIC THEORIES

2.1. Introduction

In this chapter we review the basic theories which will be used to establish two different techniques for determining the electromagnetic (EM) parameters of materials using a waveguide probe system. As mentioned in the preceding chapter, the study of the first technique is limited to isotropic media. The second technique, however, is suitable for the application to both isotropic and anisotropic media.

The geometry of the problem is shown in Fig. 2.1 which depicts the cross-sectional view of the system. A layer of unknown dielectric material of thickness d which is backed by free space, is placed against a waveguide probe consisting of an open-ended rectangular waveguide terminated by an infinite metallic flange. Inside the waveguide region, a dominant TE_{10} mode of field is excited and it propagates toward the probe aperture. In addition to the reflected TE_{10} mode, higher order modes of fields are excited near this aperture due to the discontinuity between the waveguide and the slab material. The electromagnetic wave carried by the waveguide radiates into the material layer and through to the open space backing it. If the electromagnetic fields in the material layer

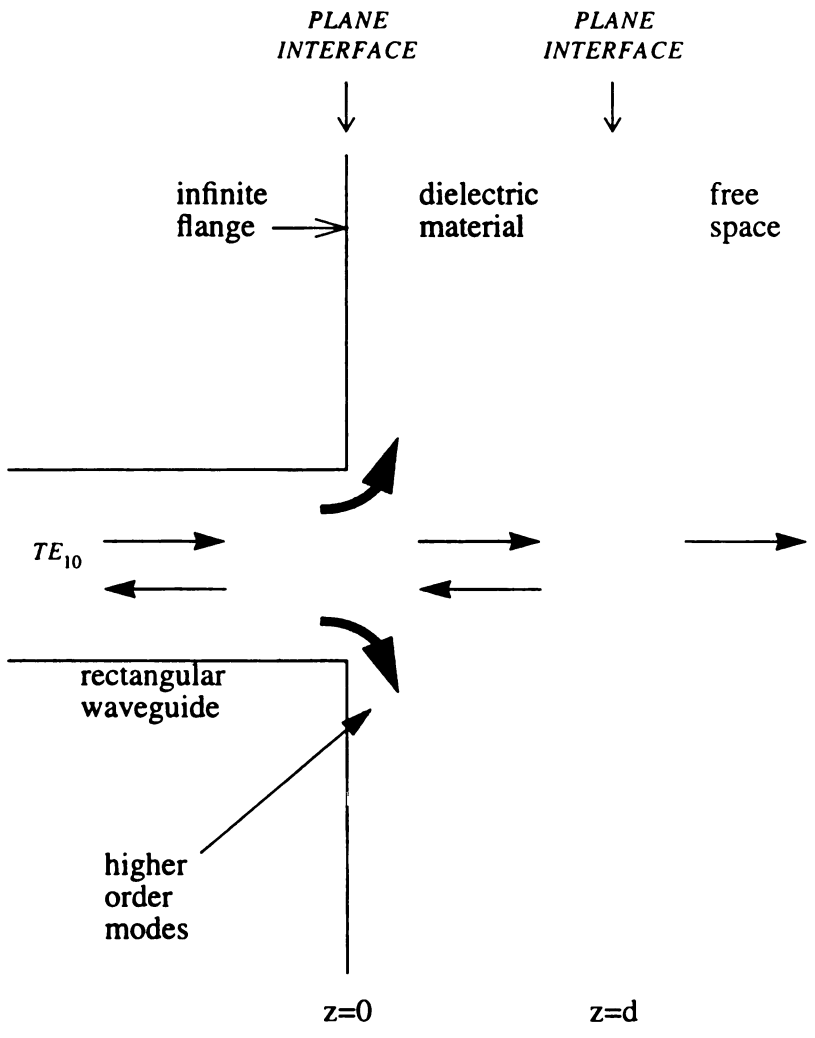

Figure 2.1 The geometric structure of nondestructive measurement using a waveguide probe system.

and the open space are established based on Maxwell's equations, the problem can be solved by matching the fields at the waveguide-material and the material-air interfaces.

In this chapter, the EM fields in the waveguide, the material layer and the open free space will be determined. The application of the boundary conditions at the interfaces will be discussed in the following chapters.

Section 2.2. presents the EM waves in an isotropic medium in terms of Hertzian potentials. In this section, the EM fields in both the waveguide region and the material layer are examined. In section 2.3. a partial differential equation is derived directly from the Maxwell's equations for the spectrum-domain transverse EM fields. This partial differential equation then leads to an eigenvalue problem for the EM fields in an anisotropic medium and a degenerate eigenvalue problem for the EM fields in an isotropic medium.

2.2. Derivation of EM Fields via Hertzian Potentials

For an isotropic medium, it is well known that the total EM fields inside the region can be regarded as a superposition of two types of waves: the transverse electric (TE) modes and the transverse magnetic (TM) modes which can be derived in terms of Hertzian potentials [33].

The definition of the TE and TM modes of waves will be addressed in the following subsection [34]. Also the definition of Hertzian potentials is introduced, and the EM fields based on Hertzian potentials are defined.

2.2.1 Introduction of Hertzian Potentials

In a homogeneous and isotropic medium, we can classify waves into two types; TE modes and TM modes. TE modes are field configurations which electric field components lie in a plane that is transverse to the direction of propagation; while for TM modes the

magn

TE a

to so

probl

In

poten

EM fi

In

satisfi

∇

and the

$\vec{E}$ =

$\vec{H}$ =

where k

Sim

$\nabla \cdot \vec{H}$

and the r

$\vec{E}$ =

$\vec{H}$ =

magnetic field components are transverse to the direction of propagation. Generally, the TE and TM modes that satisfy Maxwell's equations and the boundary conditions are used to solve electromagnetic boundary-value problems, especially for waveguide-related problems.

In general, there are two types of Hertzian potentials, the electric type Hertzian potential $\vec{\Pi}_e$ and the magnetic type Hertzian potential $\vec{\Pi}_h$, commonly used to describe the EM fields in a homogeneous and isotropic medium.

In a time harmonic and source free region, the electric type Hertzian potential, $\vec{\Pi}_e$, satisfies

$$\nabla^2\vec{\Pi}_e + k^2\vec{\Pi}_e = 0 \tag{2.2.1}$$

and the related electric and magnetic fields are derived from

$$\vec{E} = \nabla\nabla\cdot\vec{\Pi}_e + k^2\vec{\Pi}_e = \nabla\times\nabla\times\vec{\Pi}_e \tag{2.2.2}$$

$$\vec{H} = j\omega\varepsilon\nabla\times\vec{\Pi}_e \tag{2.2.3}$$

where $k = \omega\sqrt{\mu\varepsilon}$ is the wavenumber in the medium.

Similarly, the magnetic type Hertzian potential, $\vec{\Pi}_h$, satisfies

$$\nabla^2\vec{\Pi}_h + k^2\vec{\Pi}_h = 0 \tag{2.2.4}$$

and the related electric and magnetic fields are derived from

$$\vec{E} = -j\omega\mu\nabla\times\vec{\Pi}_h \tag{2.2.5}$$

$$\vec{H} = \nabla\nabla\cdot\vec{\Pi}_h + k^2\vec{\Pi}_h = \nabla\times\nabla\times\vec{\Pi}_h \tag{2.2.6}$$

eq

whe

dire

I

It

propa

Using

modif

Trans

Th

$\vec{\Pi}_n =$

$\nabla \cdot \Gamma$

$\vec{E}_t =$

$\vec{H} =$

where

Combination of eqs. from (2.2.1) to (2.2.6) shows that a general solution to Maxwell's equations can be written as

$$\vec{E} = \nabla\times\nabla\times\vec{\Pi}_e - j\omega\mu\nabla\times\vec{\Pi}_h \tag{2.2.7}$$

$$\vec{H} = j\omega\varepsilon\nabla\times\vec{\Pi}_e + \nabla\times\nabla\times\vec{\Pi}_h \tag{2.2.8}$$

where the electric and magnetic Hertzian potentials, $\vec{\Pi}_h$ and $\vec{\Pi}_e$, are pointed in a constant direction $\hat{a}$ [33]:

$$\vec{\Pi}_e = \hat{a}\Pi_e \tag{2.2.9}$$

$$\vec{\Pi}_h = \hat{a}\Pi_h \tag{2.2.10}$$

If the unit constant vector $\hat{a} = \hat{z}$ is chosen where $\hat{z}$ is in the direction of wave propagation, $\vec{\Pi}_h$ can produce TE modes while TM modes can be generated from $\vec{\Pi}_e$. Using eqs. (2.2.9) and (2.2.10) and the choice of $\hat{a} = \hat{z}$, these two kinds of modes can be modified as follows:

Transverse Electric Modes ($E_z = 0, H_z \neq 0$)

The TE modes can be derived from a magnetic Hertzian potential by letting $\vec{\Pi}_h = \hat{z}\Pi_h$ and be represented as

$$\nabla^2\Pi_h + k^2\Pi_h = 0 \tag{2.2.11}$$

$$\vec{E}_t = j\omega\mu\,(\hat{z}\times\nabla_t)\,\Pi_h \tag{2.2.12}$$

$$\vec{H} = \hat{z}\left(\frac{\partial^2}{\partial z^2} + k^2\right)\Pi_h + \nabla_t\frac{\partial}{\partial z}\Pi_h \tag{2.2.13}$$

where

$$\nabla_t = \nabla - \hat{z}\frac{\partial}{\partial z} \tag{2.2.14}$$

Transverse Magnetic Modes ($H_z = 0, E_z \neq 0$)

The TM modes can be derived from an electric Hertzian potential by letting $\vec{\Pi}_e = \hat{z}\Pi_e$ and be represented as

$$\nabla^2\Pi_e + k^2\Pi_e = 0 \tag{2.2.15}$$

$$\vec{E} = \hat{z}\left(\frac{\partial^2}{\partial z^2} + k^2\right)\Pi_e + \nabla_t\frac{\partial}{\partial z}\Pi_e \tag{2.2.16}$$

$$\vec{H}_t = -j\omega\mu\,(\hat{z}\times\nabla_t)\,\Pi_e \tag{2.2.17}$$

Total Fields (TE modes + TM modes)

The total EM fields within a homogeneous and isotropic medium can therefore be expressed as the combination of eqs. (2.2.12), (2.2.13), (2.2.16) and (2.2.17). Components of the EM fields are shown as follows:

$$E_x = -j\omega\mu\frac{\partial}{\partial y}\Pi_h + \frac{\partial^2}{\partial x\partial z}\Pi_e \tag{2.2.18}$$

$$E_y = j\omega\mu\frac{\partial}{\partial x}\Pi_h + \frac{\partial^2}{\partial y\partial z}\Pi_e \tag{2.2.19}$$

$$E_z = -\left(\frac{\partial^2}{\partial x^2} + \frac{\partial^2}{\partial y^2}\right)\Pi_e \tag{2.2.20}$$

$$H_x = \frac{\partial^2}{\partial x\partial z}\Pi_h + j\omega\varepsilon\frac{\partial}{\partial y}\Pi_e \tag{2.2.21}$$

$$H_y = \frac{\partial^2}{\partial y\partial z}\Pi_h - j\omega\varepsilon\frac{\partial}{\partial x}\Pi_e \tag{2.2.22}$$

$$H_z = -\left(\frac{\partial^2}{\partial x^2} + \frac{\partial^2}{\partial y^2}\right)\Pi_h \tag{2.2.23}$$

2.2.2 EM Fields inside A Rectangular Waveguide

As mentioned in the previous section, the scalar Hertzian potentials, Π_h and Π_e, satisfy two scalar Helmholtz equations as given in eqs. (2.2.11) and (2.2.15). Since both TE and TM modes in a rectangular waveguide are sought, the solutions for Π_h and Π_e can be assumed to have a form of

$$\Pi_h = \psi_h(x, y)\, e^{\pm \Gamma z} \tag{2.2.24}$$

$$\Pi_e = \psi_e(x, y)\, e^{\pm \Gamma z} \tag{2.2.25}$$

where the scalar wave functions ψ_h and ψ_e satisfy the two-dimensional Helmholtz equations;

$$\nabla_t^2 \psi_h + k_c^2 \psi_h = 0 \tag{2.2.26}$$

$$\nabla_t^2 \psi_e + k_c^2 \psi_e = 0 \tag{2.2.27}$$

with $k_c^2 = k_0^2 + \Gamma^2$ and ∇_t^2 as the transverse part of ∇^2 operator.

Thus the EM fields represented in eqs. (2.2.12), (2.2.13), (2.2.16) and (2.2.17) can be written as

$$\begin{aligned} H_z &= k_c^2 \psi_h e^{\mp \Gamma z} \\ \vec{H}_t &= \mp \Gamma \nabla_t \psi_h e^{\mp \Gamma z} \\ \vec{E}_t &= \mp Z_h \left(\hat{z} \times \vec{H}_t\right) \end{aligned} \tag{2.2.28}$$

for TE modes, and

$$E_z = k_c^2 \psi_e e^{\mp \Gamma z}$$

$$\vec{E}_t = \mp \Gamma \nabla_t \psi_e e^{\mp \Gamma z} \tag{2.2.29}$$

$$\vec{H}_t = \mp Y_e \left(\hat{z} \times \vec{E}_t \right)$$

for TM modes, where Z_h is the TE mode wave impedance and Y_e is the TM mode wave admittance.

For a waveguide with perfectly conducting walls, we observe from eq. (2.2.28) that ψ_h must satisfy the boundary condition if $\partial \psi_h / \partial n = 0$, in order for the tangential electric field to vanish in the case of TE modes. Also from eq. (2.2.29) we see that $\psi_e = 0$ is the condition to make the tangential electric field vanish on the boundary for TM modes. Thus, the scalar wave functions ψ_h and ψ_e can be determined from eqs. (2.2.26) and (2.2.27), using the separation of variables method, to be

$$\psi_{h,nm} = \cos\left(\frac{n'\pi x}{a}\right)\cos\left(\frac{m'\pi y}{b}\right), \begin{cases} n' = 0, 1, 2, \ldots \\ m' = 0, 1, 2, \ldots \\ m' \neq n' = 0 \end{cases} \tag{2.2.30}$$

$$\psi_{e,nm} = \sin\left(\frac{n''\pi x}{a}\right)\sin\left(\frac{m''\pi y}{b}\right), \begin{cases} n'' = 1, 2, \ldots \\ m'' = 1, 2, \ldots \end{cases} \tag{2.2.31}$$

The scalar Hertzian potentials can then be derived from ψ_h and ψ_e by means of eqs. (2.2.24) and (2.2.25) and are expressed as

$$\Pi_h = a_{10}\cos\left(\frac{\pi x}{a}\right)\left(e^{-\Gamma_{10}z} + Re^{\Gamma_{10}z}\right) + \sum_{n'}\sum_{m'} A_{n'm'}\cos\left(\frac{n'\pi x}{a}\right)\cos\left(\frac{m'\pi y}{b}\right)e^{\Gamma_{n'm'}z} \tag{2.2.32}$$

$$\Pi_e = \sum_{n''}\sum_{m''} B_{n''m''}\sin\left(\frac{n''\pi x}{a}\right)\sin\left(\frac{m''\pi y}{b}\right)e^{\Gamma_{n''m''}z} \tag{2.2.33}$$

where

$$\Gamma_{10} = j\sqrt{k_0^2 - \left(\frac{\pi}{a}\right)^2} \tag{2.2.34}$$

$$\Gamma_{nm} = j\sqrt{k_0^2 - \left(\frac{n\pi}{a}\right)^2 - \left(\frac{m\pi}{b}\right)^2} \tag{2.2.35}$$

$$k_0 = \omega\sqrt{\mu_0\varepsilon_0} \tag{2.2.36}$$

Also a_{10} and $A_{n'm'}$ represent the amplitude coefficients of the dominant TE_{10} mode and the TE higher order modes, respectively; and $B_{n''m''}$ represents the amplitude coefficients of the TM higher order modes. R denotes the reflection coefficient of the incident dominant mode and it is required that $Re\,(\Gamma_{nm}) \geq 0$ and $Im\,(\Gamma_{nm}) \geq 0$, for all values of n and m.

The EM fields inside the waveguide can then be derived via the substitution of Hertzian potentials into eqs (2.2.18) to (2.2.23):

The EM Fields inside the waveguide

$$\begin{aligned} E_x(x,y,z) &= j\omega\mu_0 \sum_{n'}\sum_{m'}\left(\frac{m'\pi}{b}\right)A_{n'm'}\cos\left(\frac{n'\pi x}{a}\right)\sin\left(\frac{m'\pi y}{b}\right)e^{\Gamma_{n'm'}z} \\ &\quad + \sum_{n''}\sum_{m''}\Gamma_{n''m''}\left(\frac{n''\pi}{a}\right)B_{n''m''}\cos\left(\frac{n''\pi x}{a}\right)\sin\left(\frac{m''\pi y}{b}\right)e^{\Gamma_{n''m''}z} \end{aligned} \tag{2.2.37}$$

$$\begin{aligned} E_y(x,y,z) &= -j\omega\mu_0\left(\frac{\pi}{a}\right)a_{10}\sin\left(\frac{\pi x}{a}\right)\left(e^{-\Gamma_{10}z} + Re^{\Gamma_{10}z}\right) \\ &\quad - j\omega\mu_0 \sum_{n'}\sum_{m'}\left(\frac{n'\pi}{a}\right)A_{n'm'}\sin\left(\frac{n'\pi x}{a}\right)\cos\left(\frac{m'\pi y}{b}\right)e^{\Gamma_{n'm'}z} \\ &\quad + \sum_{n''}\sum_{m''}\Gamma_{n''m''}\left(\frac{m''\pi}{b}\right)B_{n''m''}\sin\left(\frac{n''\pi x}{a}\right)\cos\left(\frac{m''\pi y}{b}\right)e^{\Gamma_{n''m''}z} \end{aligned} \tag{2.2.38}$$

$$E_z(x,y,z) = \sum_{n''}\sum_{m''}\left[\left(\frac{n''\pi}{a}\right)^2 + \left(\frac{m''\pi}{b}\right)^2\right]B_{n''m''}\sin\left(\frac{n''\pi x}{a}\right)\sin\left(\frac{m''\pi y}{b}\right)e^{\Gamma_{n''m''}z} \tag{2.2.39}$$

$$H_x(x,y,z) = \left(\frac{\pi}{a}\right)\Gamma_{10}a_{10}\sin\left(\frac{\pi x}{a}\right)\left(e^{-\Gamma_{10}z} - Re^{\Gamma_{10}z}\right)$$
$$-\sum_{n'}\sum_{m'}\Gamma_{n'm'}\left(\frac{n'\pi}{a}\right)A_{n'm'}\sin\left(\frac{n'\pi x}{a}\right)\cos\left(\frac{m'\pi y}{b}\right)e^{\Gamma_{n'm'}z}$$
$$+j\omega\varepsilon_0\sum_{n''}\sum_{m''}\left(\frac{m''\pi}{b}\right)B_{n''m''}\sin\left(\frac{n''\pi x}{a}\right)\cos\left(\frac{m''\pi y}{b}\right)e^{\Gamma_{n''m''}z} \quad (2.2.40)$$

$$H_y(x,y,z) = -\sum_{n'}\sum_{m'}\Gamma_{n'm'}\left(\frac{m'\pi}{b}\right)A_{n'm'}\cos\left(\frac{n'\pi x}{a}\right)\sin\left(\frac{m'\pi y}{b}\right)e^{\Gamma_{n'm'}z}$$
$$-j\omega\varepsilon_0\sum_{n''}\sum_{m''}\left(\frac{n''\pi}{a}\right)B_{n''m''}\cos\left(\frac{n''\pi x}{a}\right)\sin\left(\frac{m''\pi y}{b}\right)e^{\Gamma_{n''m''}z} \quad (2.2.41)$$

$$H_z(x,y,z) = \left(\frac{\pi}{a}\right)^2 a_{10}\cos\left(\frac{\pi x}{a}\right)\left(e^{-\Gamma_{10}z} + Re^{\Gamma_{10}z}\right)$$
$$+\sum_{n'}\sum_{m'}\left[\left(\frac{n'\pi}{a}\right)^2+\left(\frac{m'\pi}{b}\right)^2\right]A_{n'm'}\cos\left(\frac{n'\pi x}{a}\right)\cos\left(\frac{m'\pi y}{b}\right)e^{\Gamma_{n'm'}z} \quad (2.2.42)$$

2.2.3 EM Fields inside A Homogeneous, Isotropic Medium

The scalar Hertzian potentials inside a homogeneous and isotropic medium satisfy the scalar Helmholtz equations of eqs. (2.2.11) and (2.2.15). Since the isotropic medium is uniform and unbounded in the transverse directions, Fourier transform will be applied to the x and y directions. Let's define $\tilde{\Pi}(k_x, k_y, z)$ to be the two-dimensional Fourier transform of $\Pi(x, y, z)$ along the transverse directions, i.e.,

$$\tilde{\Pi}(k_x, k_y, z) = \int_{-\infty}^{\infty}\int \Pi(x, y, z)\, e^{-jk_x x} e^{-jk_y y} dxdy \quad (2.2.43)$$

Then

$$\Pi(x, y, z) = \left(\frac{1}{2\pi}\right)^2 \int_{-\infty}^{\infty}\int \tilde{\Pi}(k_x, k_y, z)\, e^{jk_x x} e^{jk_y y} dk_x dk_y \quad (2.2.44)$$

If we take the two-dimensional Fourier transform of the two scalar Helmholtz equations, we have

$$\left(\frac{1}{2\pi}\right)^2 \int_{-\infty}^{\infty}\int \left(\frac{\partial^2}{\partial z^2} + k_1^2 - k_x^2 - k_y^2\right)\tilde{\Pi}_h e^{jk_x x} e^{jk_y y} dk_x dk_y = 0 \tag{2.2.45}$$

$$\left(\frac{1}{2\pi}\right)^2 \int_{-\infty}^{\infty}\int \left(\frac{\partial^2}{\partial z^2} + k_1^2 - k_x^2 - k_y^2\right)\tilde{\Pi}_e e^{jk_x x} e^{jk_y y} dk_x dk_y = 0 \tag{2.2.46}$$

or

$$\left(\frac{\partial^2}{\partial z^2} + k_1^2 - k_x^2 - k_y^2\right)\tilde{\Pi}_h(k_x, k_y, z) = 0 \tag{2.2.47}$$

$$\left(\frac{\partial^2}{\partial z^2} + k_1^2 - k_x^2 - k_y^2\right)\tilde{\Pi}_e(k_x, k_y, z) = 0 \tag{2.2.48}$$

The solutions of $\tilde{\Pi}_h$ and $\tilde{\Pi}_e$ of eqs. (2.2.47) and (2.2.48) can be written as

$$\tilde{\Pi}_h(k_x, k_y, z) = F(k_x, k_y)\, e^{\pm\Gamma_1 z} \tag{2.2.49}$$

and

$$\tilde{\Pi}_e(k_x, k_y, z) = G(k_x, k_y)\, e^{\pm\Gamma_1 z} \tag{2.2.50}$$

where

$$\Gamma_1(k_x, k_y) = -j\sqrt{k_1^2 - k_x^2 - k_y^2} \tag{2.2.51}$$

$$k_1 = \omega\sqrt{\mu_1 \varepsilon_1} \tag{2.2.52}$$

Notice that Γ_1 should provide positive real and positive imaginary parts to satisfy the radiation condition of fields derived from eqs. (2.2.49) and (2.2.50).

The substitution of the two-dimensional Fourier transformed Hertzian potentials, $\tilde{\Pi}_h$ and $\tilde{\Pi}_e$, into eq. (2.2.44) gives the expressions of space domain Hertzian potentials inside a slab, isotropic medium as

$$\Pi_h(x, y, z) = \left(\frac{1}{2\pi}\right)^2 \int_{-\infty}^{\infty}\int F(k_x, k_y)\, e^{jk_x x} e^{jk_y y}\left(e^{-\Gamma_1 z} + R_a e^{\Gamma_1 z}\right) dk_x dk_y \tag{2.2.53}$$

$$\Pi_e(x, y, z) = \left(\frac{1}{2\pi}\right)^2 \int_{-\infty}^{\infty}\int G(k_x, k_y)\, e^{jk_x x} e^{jk_y y}\left(e^{-\Gamma_1 z} + R_b e^{\Gamma_1 z}\right) dk_x dk_y \tag{2.2.54}$$

Here the quantities $R_a(k_x, k_y)$ and $R_b(k_x, k_y)$ represent the ratios of the backward-to-forward wave at the plane interface $z = d$ as shown in Fig. 2.1.

Thus, the total EM fields within an isotropic material slab can be obtained by substituting eqs. (2.2.53) and (2.2.54) into eqs. (2.2.18) to (2.2.23) as follows:

Fields inside the isotropic material slab

$$E_x(x, y, z) = \left(\frac{1}{2\pi}\right)^2 \left[\omega\mu \int_{-\infty}^{\infty}\int k_y F(k_x, k_y)\, e^{jk_x x} e^{jk_y y}\left(e^{-\Gamma_1 z} + R_a e^{\Gamma_1 z}\right) dk_x dk_y \right.$$
$$\left. - j\int_{-\infty}^{\infty}\int k_x \Gamma_1 G(k_x, k_y)\, e^{jk_x x} e^{jk_y y}\left(e^{-\Gamma_1 z} - R_b e^{\Gamma_1 z}\right) dk_x dk_y \right] \tag{2.2.55}$$

$$E_y(x, y, z) = \left(\frac{1}{2\pi}\right)^2 \left[-\omega\mu \int_{-\infty}^{\infty}\int k_x F(k_x, k_y)\, e^{jk_x x} e^{jk_y y}\left(e^{-\Gamma_1 z} + R_a e^{\Gamma_1 z}\right) dk_x dk_y \right.$$
$$\left. - j\int_{-\infty}^{\infty}\int k_y \Gamma_1 G(k_x, k_y)\, e^{jk_x x} e^{jk_y y}\left(e^{-\Gamma_1 z} - R_b e^{\Gamma_1 z}\right) dk_x dk_y \right] \tag{2.2.56}$$

$$E_z(x, y, z) = \left(\frac{1}{2\pi}\right)^2 \int_{-\infty}^{\infty}\int \left(k_x^2 + k_y^2\right) G(k_x, k_y)\, e^{jk_x x} e^{jk_y y}\left(e^{-\Gamma_1 z} + R_b e^{\Gamma_1 z}\right) dk_x dk_y \tag{2.2.57}$$

$$H_x(x,y,z) = \left(\frac{1}{2\pi}\right)^2\left[-j\int_{-\infty}^{\infty}\int k_x\Gamma_1 F(k_x,k_y)\,e^{jk_x x}e^{jk_y y}\left(e^{-\Gamma_1 z}-R_a e^{\Gamma_1 z}\right)dk_x dk_y\right.$$

$$\left.-\omega\varepsilon\int_{-\infty}^{\infty}\int k_y G(k_x,k_y)\,e^{jk_x x}e^{jk_y y}\left(e^{-\Gamma_1 z}+R_b e^{\Gamma_1 z}\right)dk_x dk_y\right] \qquad (2.2.58)$$

$$H_y(x,y,z) = \left(\frac{1}{2\pi}\right)^2\left[-j\int_{-\infty}^{\infty}\int k_y\Gamma_1 F(k_x,k_y)\,e^{jk_x x}e^{jk_y y}\left(e^{-\Gamma_1 z}-R_a e^{\Gamma_1 z}\right)dk_x dk_y\right.$$

$$\left.+\omega\varepsilon\int_{-\infty}^{\infty}\int k_x G(k_x,k_y)\,e^{jk_x x}e^{jk_y y}\left(e^{-\Gamma_1 z}+R_b e^{\Gamma_1 z}\right)dk_x dk_y\right] \qquad (2.2.59)$$

$$H_z(x,y,z) = \left(\frac{1}{2\pi}\right)^2\int_{-\infty}^{\infty}\int\left(k_x^2+k_y^2\right)F(k_x,k_y)\,e^{jk_x x}e^{jk_y y}\left(e^{-\Gamma_1 z}+R_a e^{\Gamma_1 z}\right)dk_x dk_y \qquad (2.2.60)$$

The symmetry condition in the waveguide excitation can be used to simplify the problem. Let's observe the field distributions at the waveguide's aperture, $(z = 0)$. The transverse electric fields derived from eqs. (2.2.28) to (2.2.31) for both TE and TM modes are proportional to the following sinusoidal functions.

$$\vec{E}_t \propto \begin{cases}\hat{x}\cos\left(\dfrac{n\pi x}{a}\right)\sin\left(\dfrac{m\pi y}{b}\right)\\ \hat{y}\sin\left(\dfrac{n\pi x}{a}\right)\cos\left(\dfrac{m\pi y}{b}\right)\end{cases} \qquad (2.2.61)$$

Since the dominant TE_{10} mode,

$$\overrightarrow{E_{10}} \propto \hat{y}\sin\left(\frac{\pi x}{a}\right), \qquad (2.2.62)$$

which is evenly symmetrical to the center of the aperture located at $(a/2,b/2)$, is used to excite the waveguide, only the higher order modes with *odd n* and *even m* can be excited.

Thus, the x-component of the electric field of higher order modes appeared at the aperture is antisymmetric with respect to the center of the aperture, and the y-component of the electric field of higher order modes is symmetrical with respect to the aperture center. The excited modes are determined to be $(1,0)$, $(3,0)$, $(1,2)$, ... , $(2k+1, 2k)$, ... , for $k \geq 0$, in an ascending order of cut-off frequencies. Expressing the aperture field in terms of these excited modes will result in an accurate and rapidly convergent solution.

2.3. Derivation of EM Fields via Transverse Field Method

Due to rapid technological advance in material manufacturing in recent years, the study on the behavior of electromagnetic fields in anisotropic materials has become increasingly important. Numerical methods are commonly used to solve the problems dealing with materials with complex structures.

In this section the electromagnetic fields inside an electric anisotropic medium, which electric properties vary in different directions, is investigated. The method used in this section is based on the concept of eigenmodes of the spectrum-domain transverse EM fields. The EM fields derived in this section are used in chapter 4 to match the tangential electric and magnetic fields at the interfaces between regions as illustrated in Fig. 2.1.

2.3.1 Dielectric Tensor Properties of Anisotropic Media

The constitutive relations for a homogeneous, nonmagnetic anisotropic medium are derived as

$$\vec{D} = \bar{\bar{\varepsilon}} \cdot \vec{E} \tag{2.3.1}$$

$$\vec{B} = \mu_0 \vec{H} \tag{2.3.2}$$

where $\bar{\bar{\varepsilon}}$ is called the tensor permittivity and is a complex constant dyadic or tensor if the medium is a lossy material. The basic form of the complex tensor permittivity containing only the diagonal elements is of the form

$$\bar{\bar{\varepsilon}} = \begin{bmatrix} \varepsilon_1 & 0 & 0 \\ 0 & \varepsilon_2 & 0 \\ 0 & 0 & \varepsilon_3 \end{bmatrix} \tag{2.3.3}$$

where

$$\varepsilon_j = \varepsilon_r - j\sigma_j/\omega \tag{2.3.4}$$

and ε_r is the real-valued dielectric constant and σ_j is the real-valued conductivity. The orthogonal coordinate axes in which the diagonal tensor $\bar{\bar{\varepsilon}}$ takes are referred to as the principal axes.

Let us now consider that coordinates of the medium are lines up with the principal axes of the anisotropy and the z-axis is considered to be the direction of wave propagation. To rotate the transverse plane of the medium with a rotated angle θ, it will give us an alternative form of the tensor permittivity:

$$\bar{\bar{\varepsilon}} = \begin{bmatrix} \varepsilon_{xx} & \varepsilon_{xy} & 0 \\ \varepsilon_{yx} & \varepsilon_{yy} & 0 \\ 0 & 0 & \varepsilon_z \end{bmatrix} \tag{2.3.5}$$

where

$$\varepsilon_{xx} = \varepsilon_1 \cos^2\theta + \varepsilon_2 \sin^2\theta \tag{2.3.6}$$

$$\varepsilon_{yy} = \varepsilon_1 \sin^2\theta + \varepsilon_2 \cos^2\theta \tag{2.3.7}$$

$$\varepsilon_z = \varepsilon_3 \tag{2.3.8}$$

$$\varepsilon_{xy} = \varepsilon_{yx} = (\varepsilon_1 - \varepsilon_2) \sin\theta \cos\theta \tag{2.3.9}$$

The relationship of matrix components between eqs. (2.3.3) and (2.3.5) is based on the change basis of the transverse plane. It can be easily found in the following derivation.

Let $\overline{\overline{W}}$ be a square matrix that transforms vectors in accordance with the equation $\vec{u} = \overline{\overline{W}} \cdot \vec{v}$. Suppose we now change basis and write $\vec{v}$ and $\vec{u}$ in the new basis as $\vec{v}^*$ and $\vec{u}^*$, and there is a matrix $\overline{\overline{W}}^*$ that can transform vectors $\vec{v}^*$ and $\vec{u}^*$ in accordance with the equation $\vec{u}^* = \overline{\overline{W}}^* \cdot \vec{v}^*$. Now if we know that the coordinates in the new basis relates to the coordinates in the old basis by a transform matrix $\overline{\overline{Y}}$, we can then write relations for the coordinate transformation as

$$\vec{u} = \overline{\overline{Y}} \cdot \vec{u}^* \tag{2.3.10}$$

$$\vec{v} = \overline{\overline{Y}} \cdot \vec{v}^* \tag{2.3.11}$$

Simply applying the vector transformation of $\vec{u}$ and $\vec{u}^*$ for the new and old basis respectively into eq. (2.3.10) and taking the inverse coordinate transformation leads to the solution to the matrix $\overline{\overline{W}}^*$, i.e.,

$$\begin{aligned} \vec{u}^* &= \overline{\overline{Y}}^{-1} \cdot \vec{u} \\ &= \overline{\overline{Y}}^{-1} \cdot \overline{\overline{W}} \cdot \vec{v} \\ &= \left(\overline{\overline{Y}}^{-1} \cdot \overline{\overline{W}} \cdot \overline{\overline{Y}} \right) \cdot \vec{v}^* \end{aligned} \tag{2.3.12}$$

or

$$\overline{\overline{W}}^* = \overline{\overline{Y}}^{-1} \cdot \overline{\overline{W}} \cdot \overline{\overline{Y}} \tag{2.3.13}$$

If we rotate an angle θ of the transverse plane, the coordinate transform matrix $\overline{\overline{Y}}$ can be represented as

$$\bar{\bar{Y}} = \begin{bmatrix} \cos\theta & \sin\theta \\ -\sin\theta & \cos\theta \end{bmatrix} \tag{2.3.14}$$

and the inverse matrix $\bar{\bar{Y}}^{-1}$ is

$$\bar{\bar{Y}}^{-1} = \begin{bmatrix} \cos\theta & -\sin\theta \\ \sin\theta & \cos\theta \end{bmatrix} \tag{2.3.15}$$

As a result, with the aid of $\bar{\bar{Y}}$ and $\bar{\bar{Y}}^{-1}$, the vector transform matrix $\bar{\bar{W}}^*$ in the new basis is derived as

$$\begin{aligned} \bar{\bar{W}}^* = \bar{\bar{Y}}^{-1} \cdot \bar{\bar{W}} \cdot \bar{\bar{Y}} &= \begin{bmatrix} \cos\theta & -\sin\theta \\ \sin\theta & \cos\theta \end{bmatrix} \begin{bmatrix} \varepsilon_1 & 0 \\ 0 & \varepsilon_2 \end{bmatrix} \begin{bmatrix} \cos\theta & \sin\theta \\ -\sin\theta & \cos\theta \end{bmatrix} \\ &= \begin{bmatrix} \varepsilon_1\cos^2\theta + \varepsilon_2\sin^2\theta & (\varepsilon_1 - \varepsilon_2)\sin\theta\cos\theta \\ (\varepsilon_1 - \varepsilon_2)\sin\theta\cos\theta & \varepsilon_1\sin^2\theta + \varepsilon_2\cos^2\theta \end{bmatrix} \end{aligned} \tag{2.3.16}$$

2.3.2 General Eigenvalue Problem

Assuming a suppressed $e^{j\omega t}$ harmonic time dependence of the fields, the electric and magnetic field vectors satisfy the Maxwell's equations

$$\nabla \times \vec{E} = -j\omega\mu_0 \vec{H} \tag{2.3.17}$$

$$\nabla \times \vec{H} = j\omega \bar{\bar{\varepsilon}} \cdot \vec{E} \tag{2.3.18}$$

Expanding above equations gives

$$\frac{\partial E_z}{\partial y} - \frac{\partial E_y}{\partial z} = -j\omega\mu_0 H_x \tag{2.3.19}$$

$$\frac{\partial E_x}{\partial z} - \frac{\partial E_z}{\partial x} = -j\omega\mu_0 H_y \tag{2.3.20}$$

$$\frac{\partial E_y}{\partial x} - \frac{\partial E_x}{\partial y} = -j\omega\mu_0 H_z \tag{2.3.21}$$

$$\frac{\partial H_z}{\partial y} - \frac{\partial H_y}{\partial z} = j\omega\varepsilon_{xx} E_x + j\omega\varepsilon_{xy} E_y \tag{2.3.22}$$

$$\frac{\partial H_x}{\partial z} - \frac{\partial H_z}{\partial x} = j\omega\varepsilon_{yx} E_x + j\omega\varepsilon_{yy} E_y \tag{2.3.23}$$

$$\frac{\partial H_y}{\partial x} - \frac{\partial H_x}{\partial y} = j\omega\varepsilon_z E_z \tag{2.3.24}$$

As mentioned before, a two-dimensional Fourier transform can be used to facilitate the solution of the three-dimensional Maxwell's equations derived above if an uniform and unbounded medium along the transverse directions is involved. Let us now define a two-dimensional Fourier transform pair as

$$\tilde{f}(k_x, k_y, z) = \int_{-\infty}^{\infty}\int f(x, y, z)\, e^{-jk_x x} e^{-jk_y y}\, dxdy \tag{2.3.25}$$

$$f(x, y, z) = \left(\frac{1}{2\pi}\right)^2 \int_{-\infty}^{\infty}\int \tilde{f}(k_x, k_y, z)\, e^{jk_x x} e^{jk_y y}\, dk_x dk_y \tag{2.3.26}$$

where $f(x, y, z)$ denotes a three-dimensional spatial function and $\tilde{f}(k_x, k_y, z)$ is defined to be the two-dimensional Fourier transform of $f(x, y, z)$ along the transverse directions.

If we take the two-dimensional Fourier transform of eqs. (2.3.19) to (2.3.24), we then have

$$jk_y \tilde{E}_z - \frac{\partial \tilde{E}_y}{\partial z} = -j\omega\mu_0 \tilde{H}_x \tag{2.3.27}$$

$$\frac{\partial \tilde{E}_x}{\partial z} - jk_x \tilde{E}_z = -j\omega\mu_0 \tilde{H}_y \tag{2.3.28}$$

$$jk_x\tilde{E}_y - jk_y\tilde{E}_x = -j\omega\mu_0\tilde{H}_z \tag{2.3.29}$$

$$jk_y\tilde{H}_z - \frac{\partial\tilde{H}_y}{\partial z} = j\omega\varepsilon_{xx}\tilde{E}_x + j\omega\varepsilon_{xy}\tilde{E}_y \tag{2.3.30}$$

$$\frac{\partial\tilde{H}_x}{\partial z} - jk_x\tilde{H}_z = j\omega\varepsilon_{yx}\tilde{E}_x + j\omega\varepsilon_{yy}\tilde{E}_y \tag{2.3.31}$$

$$jk_x\tilde{H}_y - jk_y\tilde{H}_x = j\omega\varepsilon_z\tilde{E}_z \tag{2.3.32}$$

Among these expressions, the partial derivatives of the spatial domain electromagnetic fields with respect to x and y are replaced by jk_x and jk_y and the derivative with respect to z is left as the only variable in the spectrum-domain. Rewriting eqs. (2.3.29) and (2.3.32) gives

$$\tilde{E}_z = -\frac{k_y}{\omega\varepsilon_z}\tilde{H}_x + \frac{k_x}{\omega\varepsilon_z}\tilde{H}_y \tag{2.3.33}$$

$$\tilde{H}_z = \frac{k_y}{\omega\mu}\tilde{E}_x - \frac{k_x}{\omega\mu}\tilde{E}_y \tag{2.3.34}$$

The substitution of eqs. (2.3.33) and (2.3.34) back into eqs. (2.3.27), (2.3.28), (2.3.30) and (2.3.31) leads to

$$\frac{\partial\tilde{E}_x}{\partial z} = -\frac{j}{\omega\varepsilon_z}\left[k_xk_y\tilde{H}_x + \left(\omega^2\mu_0\varepsilon_z - k_x^2\right)\tilde{H}_y\right] \tag{2.3.35}$$

$$\frac{\partial\tilde{E}_y}{\partial z} = -\frac{j}{\omega\varepsilon_z}\left[\left(-\omega^2\mu_0\varepsilon_z + k_y^2\right)\tilde{H}_x - k_xk_y\tilde{H}_y\right] \tag{2.3.36}$$

$$\frac{\partial\tilde{H}_x}{\partial z} = -\frac{j}{\omega\mu}\left[\left(-\omega^2\mu_0\varepsilon_{yx} - k_xk_y\right)\tilde{E}_x + \left(-\omega^2\mu_0\varepsilon_{yy} + k_x^2\right)\tilde{E}_y\right] \tag{2.3.37}$$

$$\frac{\partial\tilde{H}_y}{\partial z} = -\frac{j}{\omega\mu}\left[\left(\omega^2\mu_0\varepsilon_{xx} - k_y^2\right)\tilde{E}_x + \left(\omega^2\mu_0\varepsilon_{xy} + k_xk_y\right)\tilde{E}_y\right] \tag{2.3.38}$$

These equations constitute a set of one-dimensional linear partial differential equation for the spectrum-domain transverse electromagnetic fields, and they can be expressed by a matrix equation as

$$\frac{d}{dz}\tilde{T} = \bar{\bar{S}} \cdot \tilde{T} \tag{2.3.39}$$

where

$$\tilde{T} \equiv \left(\tilde{E}_x, \tilde{E}_y, \eta_0 \tilde{H}_x, \eta_0 \tilde{H}_y \right)^T \tag{2.3.40}$$

with $\eta_0 = 120\pi$, and

$$\bar{\bar{S}} \equiv -\begin{bmatrix} 0 & 0 & a & b \\ 0 & 0 & c & d \\ \alpha & \beta & 0 & 0 \\ \gamma & \delta & 0 & 0 \end{bmatrix} \tag{2.3.41}$$

$$\begin{bmatrix} a & b \\ c & d \end{bmatrix} \equiv \frac{j}{\omega \varepsilon_z \eta_0} \begin{bmatrix} k_x k_y & \omega^2 \mu_0 \varepsilon_z - k_x^2 \\ -\omega^2 \mu_0 \varepsilon_z + k_y^2 & -k_x k_y \end{bmatrix} \tag{2.3.42}$$

$$\begin{bmatrix} \alpha & \beta \\ \gamma & \delta \end{bmatrix} \equiv \frac{j\eta_0}{\omega \mu_0} \begin{bmatrix} -\omega^2 \mu_0 \varepsilon_{yx} - k_x k_y & -\omega^2 \mu_0 \varepsilon_{yy} + k_x^2 \\ \omega^2 \mu_0 \varepsilon_{xx} - k_y^2 & \omega^2 \mu_0 \varepsilon_{xy} + k_x k_y \end{bmatrix} \tag{2.3.43}$$

The longitudinal components, E_z and H_z, can be obtained from

$$\tilde{E}_z = -\frac{k_y}{\omega \varepsilon_z} \tilde{H}_x + \frac{k_x}{\omega \varepsilon_z} \tilde{H}_y \tag{2.3.44}$$

$$\tilde{H}_z = \frac{k_y}{\omega \mu_0} \tilde{E}_x - \frac{k_x}{\omega \mu_0} \tilde{E}_y \tag{2.3.45}$$

To find the solutions for the spectrum-domain transverse EM fields we need to solve the eigenvalue problem of the one-dimensional partial differential equation. Its general solution can be represented as

$$\tilde{T} = \sum_{m=1}^{4} A_m \vec{v}_m e^{\lambda_m z} \tag{2.3.46}$$

where A_m denotes the unknown coefficient of the m^{th} eigenvector, $\vec{v}_m$, which with a corresponding eigenvalue λ_m satisfies the relation $\bar{\bar{S}} \cdot \vec{v}_m = \lambda_m \vec{v}_m$. Since $\bar{\bar{S}}$ is a 4x4 matrix in our case, there exists four eigenmodes in this problem and the complete solution of the spectrum-domain transverse EM fields is a linear combination of these four eigenmodes.

The nontrivial solutions to eigenvalues and eigenvectors can be determined by solving $det\left(\lambda \bar{\bar{I}} - \bar{\bar{S}}\right) = 0$. This leads to

$$det\begin{bmatrix} \lambda & 0 & a & b \\ 0 & \lambda & c & d \\ \alpha & \beta & \lambda & 0 \\ \gamma & \delta & 0 & \lambda \end{bmatrix} = \lambda \begin{vmatrix} \lambda & c & d \\ \beta & \lambda & 0 \\ \delta & 0 & \lambda \end{vmatrix} + a \begin{vmatrix} 0 & \lambda & d \\ \alpha & \beta & 0 \\ \gamma & \delta & \lambda \end{vmatrix} - b \begin{vmatrix} 0 & \lambda & c \\ \alpha & \beta & \lambda \\ \gamma & \delta & 0 \end{vmatrix}$$

$$= \lambda^4 - \lambda^2 (a\alpha + b\gamma + c\beta + d\delta) + (ad - bc)(\alpha\delta - \beta\gamma)$$

$$\equiv \lambda^4 - \lambda^2 \sum + \Delta S = 0 \tag{2.3.47}$$

With the aid of the quadratic formula, four eigenvalues are obtained from the solutions of eq. (2.3.47) as

$$\lambda_1 (k_x, k_y) \equiv \Gamma_{1+} = \sqrt{\frac{\sum + \sqrt{\sum^2 - 4\Delta S}}{2}} \tag{2.3.48}$$

$$\lambda_2 (k_x, k_y) \equiv \Gamma_{1-} = -\Gamma_{1+} \tag{2.3.49}$$

$$\lambda_3(k_x, k_y) \equiv \Gamma_{2+} = \sqrt{\frac{\sum - \sqrt{\sum^2 - 4\Delta S}}{2}} \tag{2.3.50}$$

$$\lambda_4(k_x, k_y) \equiv \Gamma_{2-} = -\Gamma_{2+} \tag{2.3.51}$$

These eigenvalues represent right and left traveling waves which are denoted by the propagation constants Γ_{i+} and Γ_{i-} for the subscript $i = 1$ or 2.

The corresponding eigenvector, denoted by $\vec{v}_m = [e, f, g, h]^T$, satisfies a matrix equation as

$$\begin{bmatrix} \lambda_m & 0 & a & b \\ 0 & \lambda_m & c & d \\ \alpha & \beta & \lambda_m & 0 \\ \gamma & \delta & 0 & \lambda_m \end{bmatrix} \begin{bmatrix} e \\ f \\ g \\ h \end{bmatrix} = 0 \tag{2.3.52}$$

For a specific eigenvalue λ_m, expanding this matrix equation gives four homogeneous linear equations for four unknown components of the corresponding eigenvector. It can be written out as

Homogeneous system of four linear equations:

$$e\lambda_m + 0 + ag + bh = 0$$

$$0 + f\lambda_m + cg + dh = 0$$

$$e\alpha + f\beta + g\lambda_m + 0 = 0$$

$$e\gamma + f\delta + 0 + h\lambda_m = 0$$

The algorithm used to solve this homogeneous system is that one of the equations is selected and the unknown term containing the eigenvalue is transferred to the right-hand side and treated as a known value. Next by transferring the selected unknown terms on the left-hand sides to the right-hand sides of the remaining equations, we can solve the

remaining three unknowns in terms of the unknown treated as a known value. Thus, four different sets of nontrivial solutions, or four different eigenvectors, can be constructed. Since the four eigenvalues represent two pairs of forward and backward waves of two different waves, two different eigenvectors are used to construct four possible eigenmodes in the medium. The selection of appropriate eigenvectors to create eigenmodes is dictated by the numerical convergence.

Case I

$$ag + bh = -e\lambda_m \tag{2.3.53}$$

$$\begin{bmatrix} \lambda_m & c & d \\ \beta & \lambda_m & 0 \\ \delta & 0 & \lambda_m \end{bmatrix} \cdot \begin{bmatrix} f \\ g \\ h \end{bmatrix} = \begin{bmatrix} 0 \\ -e\alpha \\ -e\gamma \end{bmatrix} \tag{2.3.54}$$

Solving these equations with the Gauss elimination method leads to,

$$\begin{bmatrix} \left(\lambda_m^2 - c\beta - d\delta\right) & 0 & 0 \\ \beta & \lambda_m & 0 \\ \delta & 0 & \lambda_m \end{bmatrix} \cdot \begin{bmatrix} f \\ g \\ h \end{bmatrix} = \begin{bmatrix} e\,(c\alpha + d\gamma) \\ -e\alpha \\ -e\gamma \end{bmatrix} \tag{2.3.55}$$

The value of unknown f is first determined from the top of above expression, and unknowns g and h are then solved by substituting f back into the subsequent equations. This gives

$$f = \left[\frac{c\alpha + d\gamma}{\lambda_m^2 - c\beta - d\delta}\right] e \tag{2.3.56}$$

$$g = -\frac{e}{\lambda_m}\left[\alpha + \frac{\beta\,(c\alpha + d\gamma)}{\lambda_m^2 - c\beta - d\delta}\right] = -\left[\frac{\alpha\left(\lambda_m^2 - c\beta - d\delta\right) + \beta\,(c\alpha + d\gamma)}{\lambda_m\left(\lambda_m^2 - c\beta - d\delta\right)}\right] e \tag{2.3.57}$$

$$h = -\frac{e}{\lambda_m}\left[\gamma + \frac{\delta(c\alpha + d\gamma)}{\lambda_m^2 - c\beta - d\delta}\right] = -\left[\frac{\gamma\left(\lambda_m^2 - c\beta - d\delta\right) + \delta(c\alpha + d\gamma)}{\lambda_m\left(\lambda_m^2 - c\beta - d\delta\right)}\right]e \tag{2.3.58}$$

If we multiply $\lambda_m\left(\lambda_m^2 - c\beta - d\delta\right)$ to and divide e from above equations, the eigenvector becomes

$$\vec{v}_m = \begin{bmatrix} e \\ f \\ g \\ h \end{bmatrix} = \begin{bmatrix} \lambda_m\left(\lambda_m^2 - c\beta - d\delta\right) \\ \lambda_m(c\alpha + d\gamma) \\ -\left[\alpha\left(\lambda_m^2 - c\beta - d\delta\right) + \beta(c\alpha + d\gamma)\right] \\ -\left[\gamma\left(\lambda_m^2 - c\beta - d\delta\right) + \delta(c\alpha + d\gamma)\right] \end{bmatrix} \tag{2.3.59}$$

Notice that e should be a nonzero value.

Case II

$$e\alpha + f\beta = -g\lambda_n \tag{2.3.60}$$

$$\begin{bmatrix} \lambda_n & 0 & b \\ 0 & \lambda_n & d \\ \gamma & \delta & \lambda_n \end{bmatrix} \cdot \begin{bmatrix} e \\ f \\ h \end{bmatrix} = \begin{bmatrix} -ag \\ -cg \\ 0 \end{bmatrix} \tag{2.3.61}$$

Using the Gauss elimination method, eq. (2.3.61) becomes

$$\begin{bmatrix} \lambda_n & 0 & b \\ 0 & \lambda_n & d \\ 0 & 0 & \left(\lambda_n^2 - b\gamma - d\delta\right) \end{bmatrix} \cdot \begin{bmatrix} e \\ f \\ h \end{bmatrix} = \begin{bmatrix} -ag \\ -cg \\ g(a\gamma + c\delta) \end{bmatrix} \tag{2.3.62}$$

From eq. (2.3.62) the components of the eigenvector are then solved in terms of the selected unknown g as

$$h = \left[\frac{a\gamma + c\delta}{\lambda_n^2 - b\gamma - d\delta}\right] g \tag{2.3.63}$$

$$e = -\frac{g}{\lambda_n}\left[a + \frac{b(a\gamma + c\delta)}{\lambda_n^2 - b\gamma - d\delta}\right] = -\left[\frac{a\left(\lambda_n^2 - b\gamma - d\delta\right) + b(a\gamma + c\delta)}{\lambda_n\left(\lambda_n^2 - b\gamma - d\delta\right)}\right] g \tag{2.3.64}$$

$$f = -\frac{g}{\lambda_n}\left[c + \frac{d(a\gamma + c\delta)}{\lambda_n^2 - b\gamma - d\delta}\right] = -\left[\frac{c\left(\lambda_n^2 - b\gamma - d\delta\right) + d(a\gamma + c\delta)}{\lambda_n\left(\lambda_n^2 - b\gamma - d\delta\right)}\right] g \tag{2.3.65}$$

Finally, multiplying $\lambda_n\left(\lambda_n^2 - b\gamma - d\delta\right)$ to and dividing nonzero value g from each component of the eigenvector, we have

$$\vec{v}_n = \begin{bmatrix} e \\ f \\ g \\ h \end{bmatrix} = \begin{bmatrix} -\left[a\left(\lambda_n^2 - b\gamma - d\delta\right) + b(a\gamma + c\delta)\right] \\ -\left[c\left(\lambda_n^2 - b\gamma - d\delta\right) + d(a\gamma + c\delta)\right] \\ \lambda_n\left(\lambda_n^2 - b\gamma - d\delta\right) \\ \lambda_n(a\gamma + c\delta) \end{bmatrix} \tag{2.3.66}$$

Let us now denote the n^{th} eigenvector of the four eigenmodes of the system as

$$\vec{v}_n = \begin{bmatrix} v_{n1} \\ v_{n2} \\ v_{n3} \\ v_{n4} \end{bmatrix}, \qquad n=1, 2, 3, 4 \tag{2.3.67}$$

We will generate the first and second eigenvectors based on eq. (2.3.59) and the third and fourth eigenvectors on eq. (2.3.66). Finally, the spectrum-domain transverse electromagnetic fields represented in eq. (2.3.46) for an anisotropic medium can be rewritten as

$$\begin{bmatrix} \tilde{E}_x \\ \tilde{E}_y \\ \eta_0\tilde{H}_x \\ \eta_0\tilde{H}_y \end{bmatrix} = A_1\vec{v}_1 e^{\lambda_1 z} + A_2\vec{v}_2 e^{\lambda_2 z} + A_3\vec{v}_3 e^{\lambda_3 z} + A_4\vec{v}_4 e^{\lambda_4 z} \tag{2.3.68}$$

2.3.3 Degenerate Eigenvalue Problem

In this section the electromagnetic fields within an isotropic medium will be derived in the same way as we did in the preceding section using the transverse Fourier transform and eigenmode representation. As shown in Fig. 2.1, the free space backing the material layer will be recognized as an isotropic medium and used as an example.

In free space the permittivity tensor is reduced to a complex scalar value by setting $\varepsilon_1 = \varepsilon_2 = \varepsilon_3 = \varepsilon_0$ and the permeability remains as $\mu = \mu_0$. Substituting back into eqs. (2.3.6) to (2.3.9), we have

$$\varepsilon_{xx} = \varepsilon_{yy} = \varepsilon_z = \varepsilon_0, \qquad \varepsilon_{xy} = \varepsilon_{yx} = 0 \tag{2.3.69}$$

The two-dimensional Fourier transform of Maxwell's equations expressed in the preceding section gives the following simplified relations.

$$\frac{d\tilde{T}_a}{dz} = \bar{\bar{S}}_a \cdot \tilde{T}_a \tag{2.3.70}$$

$$\tilde{E}_{za} = -\frac{k_y}{\omega\varepsilon_0}\tilde{H}_{xa} + \frac{k_x}{\omega\varepsilon_0}\tilde{H}_{ya} \tag{2.3.71}$$

$$\tilde{H}_{za} = \frac{k_y}{\omega\mu_0}\tilde{E}_{xa} - \frac{k_x}{\omega\mu_0}\tilde{E}_{ya} \tag{2.3.72}$$

where

$$\tilde{T}_a \equiv \left(\tilde{E}_{xa}, \tilde{E}_{ya}, \eta_0 \tilde{H}_{xa}, \eta_0 \tilde{H}_{ya} \right)^T \tag{2.3.73}$$

and

$$\bar{\bar{S}}_a \equiv -\begin{bmatrix} 0 & 0 & a' & b' \\ 0 & 0 & c' & d' \\ \alpha' & \beta' & 0 & 0 \\ \gamma' & \delta' & 0 & 0 \end{bmatrix} \tag{2.3.74}$$

$$\begin{bmatrix} a' & b' \\ c' & d' \end{bmatrix} \equiv \frac{j}{\omega \varepsilon_0 \eta_0} \begin{bmatrix} k_x k_y & \omega^2 \mu_0 \varepsilon_0 - k_x^2 \\ -\omega^2 \mu_0 \varepsilon_0 + k_y^2 & -k_x k_y \end{bmatrix} \tag{2.3.75}$$

$$\begin{bmatrix} \alpha' & \beta' \\ \gamma' & \delta' \end{bmatrix} \equiv \frac{j\eta_0}{\omega \mu_0} \begin{bmatrix} -k_x k_y & -\omega^2 \mu_0 \varepsilon_0 + k_x^2 \\ \omega^2 \mu_0 \varepsilon_0 - k_y^2 & k_x k_y \end{bmatrix} \tag{2.3.76}$$

The nontrivial solution to the eigenvalues of matrix $\bar{\bar{S}}_a$ can be proven to have degenerate λ. This means that multiple eigenvectors of $\bar{\bar{S}}_a$ correspond to the same eigenvalue. Let's calculate the coefficients of the quadratic equation (2.3.47) and find the solutions for eigenvalues via eqs. (2.3.48) to (2.3.51).

$$a'\alpha' = \frac{1}{\omega^2 \mu_0 \varepsilon_0} k_x^2 k_y^2$$

$$b'\gamma' = \frac{-1}{\omega^2 \mu_0 \varepsilon_0} \left(\omega^2 \mu_0 \varepsilon_0 - k_x^2 \right) \left(\omega^2 \mu_0 \varepsilon_0 - k_y^2 \right)$$

$$= \frac{-1}{\omega^2 \mu_0 \varepsilon_0} \left[\left(\omega^2 \mu_0 \varepsilon_0 \right)^2 - \left(k_x^2 + k_y^2 \right) \omega^2 \mu_0 \varepsilon_0 + k_x^2 k_y^2 \right]$$

$$c'\beta' = \frac{-1}{\omega^2 \mu_0 \varepsilon_0} \left(-\omega^2 \mu_0 \varepsilon_0 + k_y^2 \right) \left(-\omega^2 \mu_0 \varepsilon_0 + k_x^2 \right)$$

$$= \frac{-1}{\omega^2\mu_0\varepsilon_0}\left[\left(\omega^2\mu_0\varepsilon_0\right)^2 - \left(k_x^2 + k_y^2\right)\omega^2\mu_0\varepsilon_0 + k_x^2 k_y^2\right]$$

$$d'\delta' = \frac{1}{\omega^2\mu_0\varepsilon_0}k_x^2 k_y^2$$

$$\Rightarrow \sum' = \left(a'\alpha' + b'\gamma' + c'\beta' + d'\delta'\right) = -2\left[\omega^2\mu_0\varepsilon_0 - k_x^2 - k_y^2\right] \tag{2.3.77}$$

$$a'd' = \frac{1}{\omega^2\varepsilon_0^2}k_x^2 k_y^2$$

$$b'c' = \frac{-1}{\omega^2\varepsilon_0^2}\left(\omega^2\mu_0\varepsilon_0 - k_x^2\right)\left(-\omega^2\mu_0\varepsilon_0 + k_y^2\right)$$

$$= \frac{1}{\omega^2\varepsilon_0^2}\left[\left(\omega^2\mu_0\varepsilon_0\right)^2 - \left(k_x^2 + k_y^2\right)\omega^2\mu_0\varepsilon_0 + k_x^2 k_y^2\right]$$

$$\alpha'\delta' = \frac{1}{\omega^2\mu_0^2}k_x^2 k_y^2$$

$$\beta'\gamma' = \frac{-1}{\omega^2\mu_0^2}\left(-\omega^2\mu_0\varepsilon_0 + k_x^2\right)\left(\omega^2\mu_0\varepsilon_0 - k_y^2\right)$$

$$= \frac{1}{\omega^2\mu_0^2}\left[\left(\omega^2\mu_0\varepsilon_0\right)^2 - \left(k_x^2 + k_y^2\right)\omega^2\mu_0\varepsilon_0 + k_x^2 k_y^2\right]$$

$$\Rightarrow \Delta S' = \left(a'd' - b'c'\right)\left(\alpha'\delta' - \beta'\gamma'\right) = \left[\omega^2\mu_0\varepsilon_0 - k_x^2 - k_y^2\right]^2 \tag{2.3.78}$$

From eqs. (2.3.77) and (2.3.78) we obtain

$$\left(\sum'\right)^2 - 4\Delta S' = 0 \tag{2.3.79}$$

If we substitute eq. (2.3.79) back into the formulas for the roots of a quadratic equation, it will lead to a condition of eigenvalue degeneracy meaning the multiple roots of the eigenvalues. The eigenvalues are

$$\lambda_1 = \lambda_3 \equiv \lambda_a = \sqrt{\frac{\sum'}{2}} = -j\sqrt{\omega^2\mu_0\varepsilon_0 - k_x^2 - k_y^2} \tag{2.3.80}$$

$$\lambda_2 = \lambda_4 \equiv -\lambda_a = j\sqrt{\omega^2\mu_0\varepsilon_0 - k_x^2 - k_y^2} \tag{2.3.81}$$

The corresponding eigenvectors associated with these two degenerate eigenvalues can also be determined by using a similar algorithm as shown in the preceding section. Since eigenvalues are degenerate within an isotropic medium, this algorithm doesn't need to yield linear independent eigenvectors. Let's write one eigenvector by setting zero in one component and normalizing the other two nonzero components by the other remaining nonzero component in a form like $\begin{bmatrix} 0 & f & 1 & h \end{bmatrix}^T$, or $\begin{bmatrix} e & 0 & g & 1 \end{bmatrix}^T$, or $\begin{bmatrix} 1 & f & 0 & h \end{bmatrix}^T$, or $\begin{bmatrix} e & 1 & g & 0 \end{bmatrix}^T$. The other eigenvector that has the same eigenvalue can be constructed with a 0 where the first eigenvector has a 1 and with a 1 where the other has a 0. The derivation of these eigenvectors is given below.

Case I

Let the first eigenvector which corresponds to the eigenvalue λ_a be chosen as $\vec{v}_{1a} = \begin{bmatrix} 0 & f & 1 & h \end{bmatrix}^T$. Substituting this into eq. (2.3.52) gives

$$\begin{bmatrix} \lambda_a & 0 & a & b \\ 0 & \lambda_a & c & d \\ \alpha & \beta & \lambda_a & 0 \\ \gamma & \delta & 0 & \lambda_a \end{bmatrix} \begin{bmatrix} 0 \\ f \\ 1 \\ h \end{bmatrix} = 0 \tag{2.3.82}$$

This will give us four linear equations to determine unknowns f and h. Expanding the matrix equation yields a system of four homogeneous linear equations:

$$a + bh = 0$$

$$f\lambda_a + c + dh = 0$$

$$f\beta + \lambda_a = 0$$

$$f\delta + h\lambda_a = 0$$

It is obviously that the solution to f and h are

$$f = -\frac{\lambda_a}{\beta} \tag{2.3.83}$$

$$h = -\frac{a}{b} = \frac{\delta}{\beta} \tag{2.3.84}$$

The other eigenvector which corresponds to the same eigenvalue is then expressed as $\vec{v}_{3a} = \begin{bmatrix} 1 & f & 0 & h \end{bmatrix}^T$. Substituting this back into eq. (2.3.52) and expanding this matrix equation gives

$$\lambda_a + bh = 0$$

$$f\lambda_a + dh = 0$$

$$\alpha + f\beta = 0$$

$$\gamma + f\delta + h\lambda_a = 0$$

Similarly the solutions to unknowns f and h are obtained as

$$h = -\frac{\lambda_a}{b} \tag{2.3.85}$$

$$f = -\frac{\beta}{\alpha} = \frac{d}{b} \tag{2.3.86}$$

Finally, the eigenvectors in this case are summarized as

$$\vec{v}_{1a} = \begin{bmatrix} 0 & -\frac{\lambda_a}{\beta} & 1 & \frac{\delta}{\beta} \end{bmatrix}^T \tag{2.3.87}$$

$$\vec{v}_{2a} = \left[0 \ \frac{\lambda_a}{\beta} \ 1 \ \frac{\delta}{\beta}\right]^T \tag{2.3.88}$$

$$\vec{v}_{3a} = \left[1 \ \frac{d}{b} \ 0 \ -\frac{\lambda_a}{b}\right]^T \tag{2.3.89}$$

$$\vec{v}_{4a} = \left[1 \ \frac{d}{b} \ 0 \ \frac{\lambda_a}{b}\right]^T \tag{2.3.90}$$

Case II

Now let the first eigenvector which corresponds to the eigenvalue λ_a be chosen as $\vec{v}_{1a} = \left[e \ 0 \ g \ 1\right]^T$. Substituting this into eq. (2.3.52) leads to

$$\begin{bmatrix} \lambda_a & 0 & a & b \\ 0 & \lambda_a & c & d \\ \alpha & \beta & \lambda_a & 0 \\ \gamma & \delta & 0 & \lambda_a \end{bmatrix} \begin{bmatrix} e \\ 0 \\ g \\ 1 \end{bmatrix} = 0 \tag{2.3.91}$$

Expanding the matrix expression gives a system of four homogeneous linear equations:

$$e\lambda_a + ag + b = 0$$

$$cg + d = 0$$

$$e\alpha + g\lambda_a = 0$$

$$e\gamma + \lambda_a = 0$$

The solutions to unknowns e and g are obtained as

$$e = -\frac{\lambda_a}{\gamma} \tag{2.3.92}$$

$$g = -\frac{d}{c} = \frac{\alpha}{\gamma} \tag{2.3.93}$$

The other eigenvector corresponding to the same eigenvalue is then written as $\vec{v}_{3a} = \left[e \; 1 \; g \; 0\right]^T$. With this eigenvector, four linear equations are obtained when the matrix equation is expanded:

$$e\lambda_a + ag = 0$$

$$\lambda_a + cg = 0$$

$$e\alpha + \beta + g\lambda_a = 0$$

$$e\gamma + \delta = 0$$

The solutions to unknowns e and g are obtained as

$$g = -\frac{\lambda_a}{c} \tag{2.3.94}$$

$$e = -\frac{\delta}{\gamma} = \frac{a}{c} \tag{2.3.95}$$

Finally, the eigenvectors in this case are summarized as

$$\vec{v}_{1a} = \left[-\frac{\lambda_a}{\gamma} \; 0 \; \frac{\alpha}{\gamma} \; 1\right]^T \tag{2.3.96}$$

$$\vec{v}_{2a} = \left[\frac{\lambda_a}{\gamma} \; 0 \; \frac{\alpha}{\gamma} \; 1\right]^T \tag{2.3.97}$$

$$\vec{v}_{3a} = \left[\frac{a}{c} \; 1 \; -\frac{\lambda_a}{c} \; 0\right]^T \tag{2.3.98}$$

$$\vec{v}_{4a} = \left[\frac{a}{c} \; 1 \; \frac{\lambda_a}{c} \; 0\right]^T \tag{2.3.99}$$

We will use the notation of the n^{th} eigenvector of the eigenmodes within an isotropic medium as

$$\vec{v}_{na} = \begin{bmatrix} v_{n1a} \\ v_{n2a} \\ v_{n3a} \\ v_{n4a} \end{bmatrix}, \qquad n=1, 2, 3, 4 \tag{2.3.100}$$

Let's use the eigenvector of *case I* to create the first two eigenmodes with two different eigenvalues and the eigenvector of *case II* to generate the last two eigenvectors with two different eigenvalues. The spectrum-domain transverse electromagnetic fields can then be expressed as

$$\begin{bmatrix} \tilde{E}_{xa} \\ \tilde{E}_{ya} \\ \eta_0 \tilde{H}_{xa} \\ \eta_0 \tilde{H}_{ya} \end{bmatrix} = B_1 \vec{v}_{1a} e^{\lambda_a (z-t)} + B_2 \vec{v}_{2a} e^{-\lambda_a (z-t)} + B_3 \vec{v}_{3a} e^{\lambda_a (z-t)} + B_4 \vec{v}_{4a} e^{-\lambda_a (z-t)} \tag{2.3.101}$$

If we let λ_a satisfy $Re\{\lambda_a\} > 0$ and $Im\{\lambda_a\} > 0$, the terms with complex-valued coefficients B_1 and B_3 will represent the backward propagating waves, while the terms with B_2 and B_4 will represent the forward propagating waves.

By considering only the forward plane waves in an infinite half space, the spectrum-domain transverse fields inside free space can be expressed as

$$\begin{bmatrix} \tilde{E}_{xa} \\ \tilde{E}_{ya} \\ \eta_0 \tilde{H}_{xa} \\ \eta_0 \tilde{H}_{ya} \end{bmatrix} = B_2 \vec{v}_{2a} e^{-\lambda_a (z-t)} + B_4 \vec{v}_{4a} e^{-\lambda_a (z-t)} \tag{2.3.102}$$

In summary of this chapter, the EM fields inside a homogeneous medium have been derived based on two different techniques. Those derived in section 2.2. will be further

used in

an isot

chapte

anisot

used in matching the boundary conditions in chapter 3 for measuring the EM properties of an isotropic slab material. On the other hand, those derived in section 2.3. will be used in chapter 4 to match the boundary conditions for measuring the EM properties of an anisotropic slab material.

CHAPTER 3

OPEN-ENDED RECTANGULAR WAVEGUIDE PROBE TO MEASURE EM PROPERTIES OF ISOTROPIC MATERIALS

3.1. Introduction

There are demands for measuring the EM parameters of materials nondestructively. A waveguide probe which consists of an open-ended waveguide terminated with a flange can be used for this purpose. When a waveguide probe is placed against a material layer and the reflection coefficient of the incident wave at the waveguide aperture is determined, the EM properties of the material layer can be inversely determined.

The goal of this chapter is to derive two coupled integral equations for the electric field on the waveguide aperture. After the determination of the aperture electric field by solving the electric field integral equations (EFIE's) numerically, the reflection coefficient of the incident wave can be expressed as a function of the EM parameters of the material layer. Thus, the EM parameters of the material layer can be inversely determined if the reflection coefficient of the incident wave is experimentally measured.

In section 3.2., the electromagnetic fields in the waveguide, the material layer and the free space derived using Hertzian potentials in section 2.2. are employed to match the boundary conditions at the material-air interface and the material-waveguide aperture

interface. This will lead to two coupled electric field integral equations. In section 3.3., the moment method is implemented to solve the EFIEs numerically. Numerical results on the input admittance of the waveguide probe are then compared with the existing results published by other workers.

3.2. Coupled Integral Equations for Aperture Electric Fields

The geometry of the problem is shown in Fig. 2.1, where there are two discontinuity interfaces; the material-free space interface at $z = d$ where the material to be tested is backed by free space, and the waveguide-material interface at $z = 0$ where the material slab is placed against the waveguide flange.

Using the EM fields in the waveguide, the material layer and the free space derived in section 2.2., the tangential components of the electric and magnetic fields can be matched at the two interfaces. This will lead to two coupled integral equations for aperture electric field. After the aperture electric field is determined, the reflection coefficient or other quantities of interest such as the input impedance and admittance of the waveguide probe can be determined.

3.2.1 Reflection Coefficients at a Discontinuity Interface

When a *TE* or a *TM* wave is incident upon an interface plane which separates two different media, a part of the wave is reflected back from the discontinuity. The ratio of the complex amplitudes of the reflected wave to the incident wave is defined as *the reflection coefficient.*

In section 2.2.3 we have derived the EM fields in a layer of material which is backed by free space. In that section two unknown quantities, $R_a(k_x, k_y)$ and $R_b(k_x, k_y)$, appeared in the field components given in eqs. (2.2.55) to (2.2.60) represent the reflection coefficients of propagating *TE* and *TM* modes, respectively, at the plane interface at

$z = d$. These quantities can be determined when the transverse EM fields within the material layer and that in free space are matched at the interface at $z = d$. Since the free space is of infinite extent, only the forward propagating wave is assumed in the free space region.

The forward propagating transverse fields inside the free space can be derived as follows:

$$E_x^a = \left(\frac{1}{2\pi}\right)^2 \int_{-\infty}^{\infty}\int [\omega\mu_0 k_y H(k_x, k_y) - jk_x\Gamma_2 I(k_x, k_y)]\, e^{-\Gamma_2(z-d)} e^{jk_x x} e^{jk_y y} dk_x dk_y \quad (3.2.1)$$

$$E_y^a = \left(\frac{1}{2\pi}\right)^2 \int_{-\infty}^{\infty}\int [-\omega\mu_0 k_x H(k_x, k_y) - jk_y\Gamma_2 I(k_x, k_y)]\, e^{-\Gamma_2(z-d)} e^{jk_x x} e^{jk_y y} dk_x dk_y \quad (3.2.2)$$

$$H_x^a = \left(\frac{1}{2\pi}\right)^2 \int_{-\infty}^{\infty}\int [-jk_x\Gamma_2 H(k_x, k_y) - \omega\varepsilon_0 k_y I(k_x, k_y)]\, e^{-\Gamma_2(z-d)} e^{jk_x x} e^{jk_y y} dk_x dk_y \quad (3.2.3)$$

$$H_y^a = \left(\frac{1}{2\pi}\right)^2 \int_{-\infty}^{\infty}\int [-jk_y\Gamma_2 H(k_x, k_y) + \omega\varepsilon_0 k_x I(k_x, k_y)]\, e^{-\Gamma_2(z-d)} e^{jk_x x} e^{jk_y y} dk_x dk_y \quad (3.2.4)$$

where

$$\Gamma_2(k_x, k_y) = -j\sqrt{k_0^2 - k_x^2 - k_y^2} \quad (3.2.5)$$

$$k_2 = \omega\sqrt{\mu_0\varepsilon_0} \quad (3.2.6)$$

The quantities of $H(k_x, k_y)$ and $I(k_x, k_y)$ represent the corresponding coefficients of fields of *TE* and *TM* modes at the spectrum location (k_x, k_y). The superscript, a, appeared in the field components signify that existing in the free space.

Using the transverse EM fields in the material layer given in eqs. (2.2.55) to (2.2.60) and the transverse EM fields in the free space given in eqs. (3.2.1) to (3.2.4), the matching

of these transverse EM fields at the interface at $z = d$ will generate the following relations:

$$\text{for } E_x\Big|_{z=d^-} = E_x^a\Big|_{z=d^+}$$

$$\left[\omega\mu k_y F\left(1 + R_a e^{2\Gamma_1 d}\right) - jk_x\Gamma_1 G\left(1 - R_b e^{2\Gamma_1 d}\right)\right] e^{-\Gamma_1 d} = [\omega\mu_0 k_y H - jk_x\Gamma_2 I] \tag{3.2.7}$$

$$\text{for } E_y\Big|_{z=d^-} = E_y^a\Big|_{z=d^+}$$

$$\left[-\omega\mu k_x F\left(1 + R_a e^{2\Gamma_1 d}\right) - jk_y\Gamma_1 G\left(1 - R_b e^{2\Gamma_1 d}\right)\right] e^{-\Gamma_1 d} = [-\omega\mu_0 k_x H - jk_y\Gamma_2 I] \tag{3.2.8}$$

$$\text{for } H_x\Big|_{z=d^-} = H_x^a\Big|_{z=d^+}$$

$$\left[-jk_x\Gamma_1 F\left(1 - R_a e^{2\Gamma_1 d}\right) - \omega\varepsilon k_y G\left(1 + R_b e^{2\Gamma_1 d}\right)\right] e^{-\Gamma_1 d} = [-jk_x\Gamma_2 H - \omega\varepsilon_0 k_y I] \tag{3.2.9}$$

$$\text{for } H_y\Big|_{z=d^-} = H_y^a\Big|_{z=d^+}$$

$$\left[-jk_y\Gamma_1 F\left(1 - R_a e^{2\Gamma_1 d}\right) + \omega\varepsilon k_x G\left(1 + R_b e^{2\Gamma_1 d}\right)\right] e^{-\Gamma_1 d} = [-jk_y\Gamma_2 H + \omega\varepsilon_0 k_x I] \tag{3.2.10}$$

The unknown quantity $I(k_x, k_y)$ can be eliminated from eqs. (3.2.7) and (3.2.8) by subtraction to yield

$$\mu F\left(1 + R_a e^{2\Gamma_1 d}\right) e^{-\Gamma_1 d} = \mu_0 H \tag{3.2.11}$$

Similarly, $I(k_x, k_y)$ can be eliminated from eqs. (3.2.9) and (3.2.10) to yield

$$\Gamma_1 F\left(1 - R_a e^{2\Gamma_1 d}\right) e^{-\Gamma_1 d} = \Gamma_2 H \tag{3.2.12}$$

Now, the reflection coefficient of propagating *TE* modes, R_a, at the interface at $z = d$ can be obtained from eqs. (3.2.11) and (3.2.12) after eliminating $H(k_x, k_y)$. The result for R_a is

$$R_a(k_x, k_y) = \left(\frac{\mu_0\Gamma_1 - \mu\Gamma_2}{\mu_0\Gamma_1 + \mu\Gamma_2}\right)e^{-2\Gamma_1 d} \tag{3.2.13}$$

On the other hand, after eliminating the unknown quantity $H(k_x, k_y)$ from eqs. (3.2.7) and (3.2.8), we have

$$\Gamma_1 G\left(1 - R_b e^{2\Gamma_1 d}\right)e^{-\Gamma_1 d} = \Gamma_2 I \tag{3.2.14}$$

Similarly, eliminating $H(k_x, k_y)$ from eqs. (3.2.9) and (3.2.10), we have

$$\varepsilon G\left(1 + R_b e^{2\Gamma_1 d}\right)e^{-\Gamma_1 d} = \varepsilon_0 I \tag{3.2.15}$$

The reflection coefficient of propagating *TM* modes, R_b, at the interface at $z = d$ can now be obtained from eqs. (3.2.14) and (3.2.15) after eliminating $I(k_x, k_y)$. The result for R_b is

$$R_b(k_x, k_y) = \left(\frac{\varepsilon_0\Gamma_1 - \varepsilon\Gamma_2}{\varepsilon_0\Gamma_1 + \varepsilon\Gamma_2}\right)e^{-2\Gamma_1 d} \tag{3.2.16}$$

3.2.2 Matching Boundary Conditions at Waveguide Aperture

After deriving the reflection coefficients of the *TE* and *TM* modes at the interface at $z = d$ by matching the tangential EM fields across this interface, we can now proceed to match the boundary conditions at the waveguide aperture at $z = 0$.

The field components derived in section 2.2. for both the waveguide and the material layer are recalled in this section. Since a discontinuity is presented at the waveguide aperture, higher order modes are excited near the aperture. Therefore the aperture fields should contain not only a dominant mode but also an infinite number of higher order modes. Due to the orthogonality property of waveguide eigenmodes, the unknown amplitudes of these higher order modes can be derived in terms of the aperture fields. As

a result, two coupled integral equations for the aperture fields can be obtained after matching the boundary condition at the aperture.

First, we will give the aperture fields at the side of the waveguide, i.e. at $z = 0^-$. According to eqs. (2.2.37) and (2.2.38), the aperture electric fields E_{xo} and E_{yo} can be expressed as:

$$E_{xo}(x,y) = j\omega\mu_0 \sum_{n'}\sum_{m'}\left(\frac{m'\pi}{b}\right)A_{n'm'}\cos\left(\frac{n'\pi x}{a}\right)\sin\left(\frac{m'\pi y}{b}\right) + \sum_{n''}\sum_{m''}\Gamma_{n''m}\left(\frac{n''\pi}{a}\right)B_{n''m'}\cos\left(\frac{n''\pi x}{a}\right)\sin\left(\frac{m''\pi y}{b}\right) \tag{3.2.17}$$

$$E_{yo}(x,y) = -j\omega\mu_0\left(\frac{\pi}{a}\right)a_{10}\sin\left(\frac{\pi x}{a}\right)(1+R) - j\omega\mu_0\sum_{n'}\sum_{m'}\left(\frac{n'\pi}{a}\right)A_{n'm'}\sin\left(\frac{n'\pi x}{a}\right)\cos\left(\frac{m'\pi y}{b}\right) + \sum_{n''}\sum_{m''}\Gamma_{n''m}\left(\frac{m''\pi}{b}\right)B_{n''m'}\sin\left(\frac{n''\pi x}{a}\right)\cos\left(\frac{m''\pi y}{b}\right) \tag{3.2.18}$$

Since the *TM* modes do not exist if one of the mode indices is zero, we can write the above equations in more compact forms as

$$E_{xo}(x,y) = \sum_{n'}\sum_{m'}\left[j\omega\mu_0\left(\frac{m'\pi}{b}\right)A_{n'm'} + \Gamma_{n'm}\left(\frac{n'\pi}{a}\right)B_{n'm'}\right]\cos\left(\frac{n'\pi x}{a}\right)\sin\left(\frac{m'\pi y}{b}\right) \tag{3.2.19}$$

$$E_{yo}(x,y) = -j\omega\mu_0\left(\frac{\pi}{a}\right)a_{10}\sin\left(\frac{\pi x}{a}\right)(1+R) + \sum_{n'}\sum_{m'}\left[-j\omega\mu_0\left(\frac{n'\pi}{a}\right)A_{n'm'} + \Gamma_{n'm}\left(\frac{m'\pi}{b}\right)B_{n'm'}\right]\sin\left(\frac{n'\pi x}{a}\right)\cos\left(\frac{m'\pi y}{b}\right) \tag{3.2.20}$$

By using the orthogonality properties of the sinusoidal functions, we can determine the unknown amplitudes a_{10}, $A_{n'm'}$ and $B_{n'm'}$ from eqs. (3.2.19) and (3.2.20). We have

$$\int_0^b\int_0^a E_{yo}\sin\left(\frac{\pi x}{a}\right)dxdy = -j\omega\mu_0\left(\frac{\pi}{a}\right)\frac{ab}{2}a_{10}(1+R) \tag{3.2.21}$$

$$\int_0^b\int_0^a E_{xo}\cos\left(\frac{n'\pi x}{a}\right)\sin\left(\frac{m'\pi y}{b}\right)dxdy = \frac{ab}{4}\left[j\omega\mu_0\left(\frac{m'\pi}{b}\right)\varepsilon_{n'}A_{n'm'} + \Gamma_{n'm'}\left(\frac{n'\pi}{a}\right)B_{n'm'}\right] \tag{3.2.22}$$

$$\int_0^b\int_0^a E_{yo}\sin\left(\frac{n'\pi x}{a}\right)\cos\left(\frac{m'\pi y}{b}\right)dxdy = \frac{ab}{4}\left[-j\omega\mu_0\left(\frac{n'\pi}{a}\right)\varepsilon_{m'}A_{n'm'} + \Gamma_{n'm'}\left(\frac{m'\pi}{b}\right)B_{n'm'}\right] \tag{3.2.23}$$

or these unknown amplitudes can be expressed in terms of the aperture electric fields as

$$a_{10} = \frac{2/-j\omega\mu_0}{b\pi(1+R)}\int_0^b\int_0^a E_{yo}\sin\left(\frac{\pi x}{a}\right)dxdy \tag{3.2.24}$$

$$A_{n'm'} = \frac{4/j\omega\mu_0}{ab}\frac{\left[\left(\frac{m'\pi}{b}\right)\iint E_{xo} - \left(\frac{n'\pi}{a}\right)\iint E_{yo}\right]}{\left[\varepsilon_{m'}\left(\frac{n'\pi}{a}\right)^2 + \varepsilon_{n'}\left(\frac{m'\pi}{b}\right)^2\right]} \tag{3.2.25}$$

$$B_{n'm'} = \frac{4/\Gamma_{n'm'}}{ab}\frac{\left[\left(\frac{n'\pi}{a}\right)\iint E_{xo} + \left(\frac{m'\pi}{b}\right)\iint E_{yo}\right]}{\left[\varepsilon_{m'}\left(\frac{n'\pi}{a}\right)^2 + \varepsilon_{n'}\left(\frac{m'\pi}{b}\right)^2\right]} \tag{3.2.26}$$

where, for the sake of brevity,

$$\iint E_{xo} \equiv \int_0^b\int_0^a E_{xo}\cos\left(\frac{n'\pi x}{a}\right)\sin\left(\frac{m'\pi y}{b}\right)dxdy \tag{3.2.27}$$

$$\iint E_{yo} \equiv \int_0^b\int_0^a E_{yo}\sin\left(\frac{n'\pi x}{a}\right)\cos\left(\frac{m'\pi y}{b}\right)dxdy \tag{3.2.28}$$

$$\varepsilon_{n'} \equiv \begin{cases} 2 & n' = 0 \\ 1 & n' \neq 0 \end{cases}, \qquad \varepsilon_{m'} \equiv \begin{cases} 2 & m' = 0 \\ 1 & m' \neq 0 \end{cases} \tag{3.2.29}$$

In eq. (3.2.24) if we let the amplitude of the incident wave, a_{10}, to be 1, then we can obtain an expression for the reflection coefficient of this incident TE_{10} mode in terms of the aperture electric field. That is

$$R = \left(\frac{2/-j\omega\mu_0}{b\pi} \int_0^b \int_0^a E_{yo} \sin\left(\frac{\pi x}{a}\right) dx dy \right) - 1 \tag{3.2.30}$$

Substituting $A_{n'm'}$, $B_{n'm'}$ and R back into the aperture magnetic field in eq. (2.2.40) leads to

$$\begin{aligned} H_x(x,y)\Big|_{z=0^-} &= \left(\frac{\pi}{a}\right)\Gamma_{10}\sin\left(\frac{\pi x}{a}\right)(1-R) \\ &\quad + \sum_{n'}\sum_{m'}\left[-\Gamma_{n'm'}\left(\frac{n'\pi}{a}\right)A_{n'm'} + j\omega\varepsilon_0\left(\frac{m'\pi}{b}\right)B_{n'm'}\right]\sin\left(\frac{n'\pi x}{a}\right)\cos\left(\frac{m'\pi y}{b}\right) \\ &= 2\left(\frac{\pi}{a}\right)\Gamma_{10}\sin\left(\frac{\pi x}{a}\right) + \frac{2\Gamma_{10}}{j\omega\mu_0 ab}\sin\left(\frac{\pi x}{a}\right)\int_0^b\int_0^a E_{yo}\sin\left(\frac{\pi x'}{a}\right)dx'dy' \\ &\quad + \sum_{n'}\sum_{m'}\frac{4\sin\left(\frac{n'\pi x}{a}\right)\cos\left(\frac{m'\pi y}{b}\right)}{ab\left[\varepsilon_{m'}\left(\frac{n'\pi}{a}\right)^2 + \varepsilon_{n'}\left(\frac{m'\pi}{b}\right)^2\right]}\Bigg(\left(\frac{n'\pi}{a}\right)\left(\frac{m'\pi}{b}\right)\left[\frac{-\Gamma_{n'm'}}{j\omega\mu_0} + \frac{j\omega\varepsilon_0}{\Gamma_{n'm'}}\right]\int\int E_{xo} \\ &\quad + \left[\left(\frac{n'\pi}{a}\right)^2\frac{\Gamma_{n'm'}}{j\omega\mu_0} + \left(\frac{m'\pi}{b}\right)^2\frac{j\omega\varepsilon_0}{\Gamma_{n'm'}}\right]\int\int E_{yo}\Bigg) \\ &= 2\left(\frac{\pi}{a}\right)\Gamma_{10}\sin\left(\frac{\pi x}{a}\right) + \frac{2\Gamma_{10}}{j\omega\mu_0 ab}\sin\left(\frac{\pi x}{a}\right)\int_0^b\int_0^a E_{yo}\sin\left(\frac{\pi x'}{a}\right)dx'dy' \\ &\quad + \sum_{n'}\sum_{m'}\frac{4j\sin\left(\frac{n'\pi x}{a}\right)\cos\left(\frac{m'\pi y}{b}\right)}{ab\omega\mu_0\Gamma_{n'm'}\left[\varepsilon_{m'}\left(\frac{n'\pi}{a}\right)^2 + \varepsilon_{n'}\left(\frac{m'\pi}{b}\right)^2\right]}\Bigg(\left(\frac{n'\pi}{a}\right)\left(\frac{m'\pi}{b}\right)\left[\Gamma_{n'm'}^2 + k_0^2\right]\int\int E_{xo} \\ &\quad - \left[\left(\frac{n'\pi}{a}\right)^2\Gamma_{n'm'}^2 - \left(\frac{m'\pi}{b}\right)^2 k_0^2\right]\int\int E_{yo}\Bigg) \end{aligned} \tag{3.2.31}$$

Employing the following identities,

$$\Gamma_{n'm'}^2 + k_0^2 = \left(\frac{n'\pi}{a}\right)^2 + \left(\frac{m'\pi}{b}\right)^2 \tag{3.2.32}$$

$$\left(\frac{n'\pi}{a}\right)^2 \Gamma_{n'm'}^2 - \left(\frac{m'\pi}{b}\right)^2 k_0^2 = \left(\frac{n'\pi}{a}\right)^2 \left[\left(\frac{n'\pi}{a}\right)^2 + \left(\frac{m'\pi}{b}\right)^2 - k_0^2\right] - \left(\frac{m'\pi}{b}\right)^2 k_0^2$$

$$= \left[\left(\frac{n'\pi}{a}\right)^2 + \left(\frac{m'\pi}{b}\right)^2\right]\left[\left(\frac{n'\pi}{a}\right)^2 - k_0^2\right] \tag{3.2.33}$$

and substituting them into eq. (3.2.31) yields

$$H_x\Big|_{z=0^-} = \frac{1}{\omega\mu_0 ab}\Bigg(2b\pi\omega\mu_0\Gamma_{10}\sin\left(\frac{\pi x}{a}\right) - j2\,\Gamma_{10}\sin\left(\frac{\pi x}{a}\right)\int_0^b\int_0^a E_{yo}\sin\left(\frac{\pi x'}{a}\right)dx'dy'$$

$$+ \sum_{n'}\sum_{m'}\frac{j4\varepsilon_{n'm'}}{\Gamma_{n'm'}}\sin\left(\frac{n'\pi x}{a}\right)\cos\left(\frac{m'\pi y}{b}\right)\left[\left(\frac{n'\pi}{a}\right)\left(\frac{m'\pi}{b}\right)\iint E_{xo}\right.$$

$$\left. + \left[k_0^2 - \left(\frac{n'\pi}{a}\right)^2\right]\iint E_{yo}\right]\Bigg) \tag{3.2.34}$$

where

$$\varepsilon_{n'm'} \equiv \frac{\left(\frac{n'\pi}{a}\right)^2 + \left(\frac{m'\pi}{b}\right)^2}{\varepsilon_{m'}\left(\frac{n'\pi}{a}\right)^2 + \varepsilon_{n'}\left(\frac{m'\pi}{b}\right)^2} \tag{3.2.35}$$

Similarly, substituting $A_{n'm'}$, $B_{n'm'}$ and R back into the aperture magnetic field in eq. (2.2.41) leads to

$$H_y(x,y)\Big|_{z=0^-} = \sum_{n'}\sum_{m'}\left[-\Gamma_{n'm'}\left(\frac{m'\pi}{b}\right)A_{n'm'} - j\omega\varepsilon_0\left(\frac{m'\pi}{b}\right)B_{n'm'}\right]\cos\left(\frac{n'\pi x}{a}\right)\sin\left(\frac{m'\pi y}{b}\right)$$

$$= \sum_{n'}\sum_{m'}\frac{-4\cos\left(\frac{n'\pi x}{a}\right)\sin\left(\frac{m'\pi y}{b}\right)}{ab\left[\varepsilon_{m'}\left(\frac{n'\pi}{a}\right)^2 + \varepsilon_{n'}\left(\frac{m'\pi}{b}\right)^2\right]}\Bigg(\left[\left(\frac{m'\pi}{b}\right)^2\frac{\Gamma_{n'm'}}{j\omega\mu_0} + \left(\frac{n'\pi}{a}\right)^2\frac{j\omega\varepsilon_0}{\Gamma_{n'm'}}\right]\iint E_{xo}$$

$$+ \left(\frac{n'\pi}{a}\right)\left(\frac{m'\pi}{b}\right)\left[\frac{-\Gamma_{n'm'}}{j\omega\mu_0} + \frac{j\omega\varepsilon_0}{\Gamma_{n'm'}}\right]\iint E_{yo}\Bigg)$$

$$= \sum_{n'}\sum_{m'} \frac{4j\cos\left(\frac{n'\pi x}{a}\right)\sin\left(\frac{m'\pi y}{b}\right)}{ab\omega\mu_0\Gamma_{n'm'}\left[\varepsilon_{m'}\left(\frac{n'\pi}{a}\right)^2+\varepsilon_{n'}\left(\frac{m'\pi}{b}\right)^2\right]}\Bigg(\left[\left(\frac{m'\pi}{b}\right)^2\Gamma_{n'm'}^2-\left(\frac{n'\pi}{a}\right)^2k_0^2\right]\iint E_{xo}$$

$$-\left(\frac{n'\pi}{a}\right)\left(\frac{m'\pi}{b}\right)\left[\Gamma_{n'm'}^2+k_0^2\right]\iint E_{yo}\Bigg) \tag{3.2.36}$$

Using the identities of

$$\Gamma_{n'm'}^2+k_0^2=\left(\frac{n'\pi}{a}\right)^2+\left(\frac{m'\pi}{b}\right)^2 \tag{3.2.37}$$

$$\left(\frac{m'\pi}{b}\right)^2\Gamma_{n'm'}^2-\left(\frac{n'\pi}{a}\right)^2k_0^2=\left(\frac{m'\pi}{b}\right)^2\left[\left(\frac{n'\pi}{a}\right)^2+\left(\frac{m'\pi}{b}\right)^2-k_0^2\right]-\left(\frac{n'\pi}{a}\right)^2k_0^2$$

$$=\left[\left(\frac{n'\pi}{a}\right)^2+\left(\frac{m'\pi}{b}\right)^2\right]\left[\left(\frac{m'\pi}{b}\right)^2-k_0^2\right] \tag{3.2.38}$$

and substituting them into (3.2.36) yields

$$H_y\Big|_{z=0^-}=\sum_{n'}\sum_{m'}\frac{-j4\varepsilon_{n'm'}}{ab\omega\mu_0\Gamma_{n'm'}}\cos\left(\frac{n'\pi x}{a}\right)\sin\left(\frac{m'\pi y}{b}\right)\Bigg(\left[k_0^2-\left(\frac{m'\pi}{b}\right)^2\right]\iint E_{xo}$$

$$+\left(\frac{n'\pi}{a}\right)\left(\frac{m'\pi}{b}\right)\iint E_{yo}\Bigg) \tag{3.2.39}$$

As a consequence, eqs. (3.2.34) and (3.2.39) show that the aperture magnetic field at the waveguide side are related to the integrals of the aperture electric field as defined in eqs. (3.2.27) and (3.2.28).

Next, we will give the aperture fields at the side of the material layer, i.e. at $z = 0^+$. From eqs. (2.2.55) and (2.2.56), the aperture electric fields E_{xo} and E_{yo} are expressed as:

$$E_{xo}(x,y)=\left(\frac{1}{2\pi}\right)^2\int_{-\infty}^{\infty}\int\left[\omega\mu k_y F(1+R_a)-jk_x\Gamma_1 G(1-R_b)\right]e^{jk_x x}e^{jk_y y}dk_x dk_y \tag{3.2.40}$$

$$E_{yo}(x,y) = \left(\frac{1}{2\pi}\right)^2 \int_{-\infty}^{\infty}\int [-\omega\mu k_x F(1+R_a) - jk_y \Gamma_1 G(1-R_b)]\, e^{jk_x x} e^{jk_y y} dk_x dk_y \tag{3.2.41}$$

Using the orthogonality properties of the exponential functions, the above two equations can yield the following relations:

$$\int_{-\infty}^{\infty}\int E_{xo} e^{-jk_x x} e^{-jk_y y} dxdy = \omega\mu k_y F(1+R_a) - jk_x \Gamma_1 G(1-R_b) \tag{3.2.42}$$

$$\int_{-\infty}^{\infty}\int E_{yo} e^{-jk_x x} e^{-jk_y y} dxdy = -\omega\mu k_x F(1+R_a) - jk_y \Gamma_1 G(1-R_b) \tag{3.2.43}$$

Since the aperture electric field components E_{xo} and E_{yo} only exist over the aperture region, $0<x<a$, $0<y<b$, and vanish on the flange, the double infinite integrals can be replaced by the two double finite integrals as

$$\iint E_{xo}^{e} \equiv \int_0^b\int_0^a E_{xo} e^{-jk_x x} e^{-jk_y y} dxdy \tag{3.2.44}$$

$$\iint E_{yo}^{e} \equiv \int_0^b\int_0^a E_{yo} e^{-jk_x x} e^{-jk_y y} dxdy \tag{3.2.45}$$

The unknown amplitudes F and G can then be solved from eqs. (3.2.42) and (3.2.43) as

$$F(k_x,k_y) = \frac{1/\omega\mu}{\left(k_x^2+k_y^2\right)(1+R_a)}\left[k_y\iint E_{xo}^{e} - k_x\iint E_{yo}^{e}\right] \tag{3.2.46}$$

$$G(k_x,k_y) = \frac{j/\Gamma_1}{\left(k_x^2+k_y^2\right)(1-R_b)}\left[k_x\iint E_{xo}^{e} + k_y\iint E_{yo}^{e}\right] \tag{3.2.47}$$

Substituting F and G back into the aperture magnetic field given in eqs. (2.2.58) and (2.2.59) leads to

$$H_x(x,y)\Big|_{z=0^+} = \left(\frac{1}{2\pi}\right)^2 \int_{-\infty}^{\infty}\int [-jk_x\Gamma_1 F(1-R_a) - \omega\varepsilon k_y G(1+R_b)]\, e^{jk_x x} e^{jk_y y} dk_x dk_y$$

$$= \left(\frac{1}{2\pi}\right)^2 \int_{-\infty}^{\infty}\int \left[\frac{-j\Gamma_1}{\omega\mu}\frac{1-R_a}{1+R_a}\frac{e^{jk_x x}e^{jk_y y}}{k_x^2+k_y^2}\left(k_x k_y \iint E_{xo}^e - k_x^2 \iint E_{yo}^e\right)\right.$$

$$\left. -\frac{j\omega\varepsilon}{\Gamma_1}\frac{1+R_b}{1-R_b}\frac{e^{jk_x x}e^{jk_y y}}{k_x^2+k_y^2}\left(k_x k_y \iint E_{xo}^e + k_y^2 \iint E_{yo}^e\right)\right] dk_x dk_y$$

$$= \left(\frac{1}{2\pi}\right)^2 \int_{-\infty}^{\infty}\int \frac{je^{jk_x x}e^{jk_y y}}{\omega\mu}\left[\frac{-k_x k_y}{\Gamma_1\left(k_x^2+k_y^2\right)}\left(\Gamma_1^2\frac{1-R_a}{1+R_a} + k_1^2\frac{1+R_b}{1-R_b}\right)\iint E_{xo}^e\right.$$

$$\left. + \frac{1}{\Gamma_1\left(k_x^2+k_y^2\right)}\left(\Gamma_1^2 k_x^2\frac{1-R_a}{1+R_a} - k_1^2 k_y^2\frac{1+R_b}{1-R_b}\right)\iint E_{yo}^e\right] dk_x dk_y \qquad (3.2.48)$$

or

$$H_x\Big|_{z=0^+} = \frac{j}{\omega\mu}\int_{-\infty}^{\infty}\int e^{jk_x x}e^{jk_y y}\left[M(k_x,k_y)\iint E_{xo}^e + N_y(k_x,k_y)\iint E_{yo}^e\right] dk_x dk_y \qquad (3.2.49)$$

where

$$M(k_x,k_y) \equiv \frac{-k_x k_y/(2\pi)^2}{\Gamma_1\left(k_x^2+k_y^2\right)}\left(\Gamma_1^2\frac{1-R_a}{1+R_a} + k_1^2\frac{1+R_b}{1-R_b}\right) \qquad (3.2.50)$$

$$N_y(k_x,k_y) \equiv \frac{1/(2\pi)^2}{\Gamma_1\left(k_x^2+k_y^2\right)}\left(\Gamma_1^2 k_x^2\frac{1-R_a}{1+R_a} - k_1^2 k_y^2\frac{1+R_b}{1-R_b}\right) \qquad (3.2.51)$$

and

$$H_y(x,y)\Big|_{z=0^+} = \left(\frac{1}{2\pi}\right)^2 \int_{-\infty}^{\infty}\int [-jk_y\Gamma_1 F(1-R_a) + \omega\varepsilon k_x G(1+R_b)]\, e^{jk_x x} e^{jk_y y} dk_x dk_y$$

$$= \left(\frac{1}{2\pi}\right)^2 \int\int_{-\infty}^{\infty} \left[\frac{-j\Gamma_1}{\omega\mu} \frac{1-R_a}{1+R_a} \frac{e^{jk_x x} e^{jk_y y}}{k_x^2 + k_y^2} \left(k_y^2 \int\int E_{xo}^e - k_x k_y \int\int E_{yo}^e \right) \right.$$

$$\left. + \frac{j\omega\varepsilon}{\Gamma_1} \frac{1+R_b}{1-R_b} \frac{e^{jk_x x} e^{jk_y y}}{k_x^2 + k_y^2} \left(k_x^2 \int\int E_{xo}^e + k_x k_y \int\int E_{yo}^e \right) \right] dk_x dk_y$$

$$= \left(\frac{1}{2\pi}\right)^2 \int\int_{-\infty}^{\infty} \frac{j e^{jk_x x} e^{jk_y y}}{\omega\mu} \left[\frac{1}{\Gamma_1 \left(k_x^2 + k_y^2 \right)} \left(-\Gamma_1^2 k_y^2 \frac{1-R_a}{1+R_a} + k_1^2 k_x^2 \frac{1+R_b}{1-R_b} \right) \int\int E_{xo}^e \right.$$

$$\left. + \frac{k_x k_y}{\Gamma_1 \left(k_x^2 + k_y^2 \right)} \left(\Gamma_1^2 \frac{1-R_a}{1+R_a} + k_1^2 \frac{1+R_b}{1-R_b} \right) \int\int E_{yo}^e \right] dk_x dk_y \qquad (3.2.52)$$

or

$$H_y\Big|_{z=0^+} = \frac{-j}{\omega\mu} \int\int_{-\infty}^{\infty} e^{jk_x x} e^{jk_y y} \left[N_x(k_y, k_x) \int\int E_{xo}^e + M(k_y, k_x) \int\int E_{yo}^e \right] dk_x dk_y \qquad (3.2.53)$$

where

$$N_x(k_y, k_x) \equiv \frac{1/(2\pi)^2}{\Gamma_1 \left(k_x^2 + k_y^2 \right)} \left(\Gamma_1^2 k_y^2 \frac{1-R_a}{1+R_a} - k_1^2 k_x^2 \frac{1+R_b}{1-R_b} \right) \qquad (3.2.54)$$

Equations (3.2.49) and (3.2.53) indicate that the aperture magnetic field at the material side can also be expressed in terms of the aperture electric field as defined in eqs. (3.2.44) and (3.2.45).

It is also important to note that the roots of $1 + R_a = 0$ and $1 - R_b = 0$, the factors appeared in eqs. (3.2.50), (3.2.51) and (3.2.54), lead to the surface wave pole singularities in an isotropic dielectric slab. Let us substitute eqs. (3.2.13) and (3.2.16) into $1 + R_a = 0$ and $1 - R_b = 0$. We have

$$1 + R_a = 1 + \left(\frac{\mu_0 \Gamma_1 - \mu \Gamma_2}{\mu_0 \Gamma_1 + \mu \Gamma_2} \right) e^{-2\Gamma_1 d} = 0 \qquad (3.2.55)$$

$$1 - R_b = 1 - \left(\frac{\varepsilon_0 \Gamma_1 - \varepsilon \Gamma_2}{\varepsilon_0 \Gamma_1 + \varepsilon \Gamma_2} \right) e^{-2\Gamma_1 d} = 0 \tag{3.2.56}$$

These relations can be rearranged to become

$$\frac{1 - e^{-2\Gamma_1 d}}{1 + e^{-2\Gamma_1 d}} = -\frac{\mu_0 \Gamma_1}{\mu \Gamma_2} \tag{3.2.57}$$

$$\frac{1 - e^{-2\Gamma_1 d}}{1 + e^{-2\Gamma_1 d}} = -\frac{\varepsilon \Gamma_2}{\varepsilon_0 \Gamma_1} \tag{3.2.58}$$

If surface wave modes are excited in the dielectric slab, we can let $\Gamma_1 = jK_1$ in above two equations. This leads to

$$\tan K_1 d = -\frac{\mu_0 K_1}{\mu \Gamma_2} \tag{3.2.59}$$

$$\tan K_1 d = \frac{\varepsilon \Gamma_2}{\varepsilon_0 K_1} \tag{3.2.60}$$

It is noted that eq. (3.2.59) is the well known *TE-odd* mode eigenvalue equation and eq. (3.2.60) is the well known *TM-even* mode eigenvalue equation for the guided surface waves.

Next, we will derive two coupled integral equations for the aperture electric field. Since the tangential magnetic field components, H_x and H_y, are continuous at the aperture plane, $z = 0$, the equality of eqs. (3.2.34) and (3.2.49), and that of eqs. (3.2.39) and (3.2.53) will yield two coupled integral equations for the aperture electric field. We have

For $H_y\big|_{z=0^-} = H_y\big|_{z=0^+}$

$$\sum_{n'}\sum_{m'}\frac{-j4\varepsilon_{n'm'}}{ab\omega\mu_0\Gamma_{n'm'}}\cos\left(\frac{n'\pi x}{a}\right)\sin\left(\frac{m'\pi y}{b}\right)\left(\left[k_0^2-\left(\frac{m'\pi}{b}\right)^2\right]\iint E_{xo}+\left(\frac{n'\pi}{a}\right)\left(\frac{m'\pi}{b}\right)\iint E_{yo}\right)$$

$$=\frac{-j}{\omega\mu}\int_{-\infty}^{\infty}\int e^{jk_x x}e^{jk_y y}\left[N_x(k_y,k_x)\iint E_{xo}^{e}+M(k_y,k_x)\iint E_{yo}^{e}\right]dk_x dk_y \qquad (3.2.61)$$

or

$$\sum_{n'}\sum_{m'}\frac{-4\varepsilon_{n'm'}}{ab\Gamma_{n'm'}}\left(\frac{\mu}{\mu_0}\right)\cos\left(\frac{n'\pi x}{a}\right)\sin\left(\frac{m'\pi y}{b}\right)\left(\left[k_0^2-\left(\frac{m'\pi}{b}\right)^2\right]\iint E_{xo}+\left(\frac{n'\pi}{a}\right)\left(\frac{m'\pi}{b}\right)\iint E_{yo}\right)$$

$$+\int_{-\infty}^{\infty}\int e^{jk_x x}e^{jk_y y}\left[N_x(k_y,k_x)\iint E_{xo}^{e}+M(k_y,k_x)\iint E_{yo}^{e}\right]dk_x dk_y=0 \qquad (3.2.62)$$

For $H_x\big|_{z=0^-}=H_x\big|_{z=0^+}$

$$\frac{2\pi}{a}\Gamma_{10}\sin\left(\frac{\pi x}{a}\right)-\frac{j2\Gamma_{10}}{ab\omega\mu_0}\sin\left(\frac{\pi x}{a}\right)\int_0^b\int_0^a E_{yo}\sin\left(\frac{\pi x'}{a}\right)dx'dy'+\sum_{n'}\sum_{m'}\frac{j4\varepsilon_{n'm'}}{ab\omega\mu_0\Gamma_{n'm'}}\times$$

$$\sin\left(\frac{n'\pi x}{a}\right)\cos\left(\frac{m'\pi y}{b}\right)\left[\left(\frac{n'\pi}{a}\right)\left(\frac{m'\pi}{b}\right)\iint E_{xo}+\left(k_0^2-\left(\frac{n'\pi}{a}\right)^2\right)\iint E_{yo}\right]$$

$$=\frac{j}{\omega\mu}\int_{-\infty}^{\infty}\int e^{jk_x x}e^{jk_y y}\left[M(k_x,k_y)\iint E_{xo}^{e}+N_y(k_x,k_y)\iint E_{yo}^{e}\right]dk_x dk_y \qquad (3.2.63)$$

or

$$\frac{2\Gamma_{10}}{ab}\left(\frac{\mu}{\mu_0}\right)\sin\left(\frac{\pi x}{a}\right)\int_0^b\int_0^a E_{yo}\sin\left(\frac{\pi x'}{a}\right)dx'dy'-\sum_{n'}\sum_{m'}\frac{4\varepsilon_{n'm'}}{ab\Gamma_{n'm'}}\left(\frac{\mu}{\mu_0}\right)\times$$

$$\sin\left(\frac{n'\pi x}{a}\right)\cos\left(\frac{m'\pi y}{b}\right)\left[\left(\frac{n'\pi}{a}\right)\left(\frac{m'\pi}{b}\right)\iint E_{xo}+\left(k_0^2-\left(\frac{n'\pi}{a}\right)^2\right)\iint E_{yo}\right]$$

$$+\int_{-\infty}^{\infty}\int e^{jk_x x}e^{jk_y y}\left[M(k_x,k_y)\iint E_{xo}^{e}+N_y(k_x,k_y)\iint E_{yo}^{e}\right]dk_x dk_y=C\sin\left(\frac{\pi x}{a}\right) \qquad (3.2.64)$$

where

$$C \equiv -j\frac{2\pi}{a}\omega\mu\Gamma_{10} \tag{3.2.65}$$

Equations (3.2.62) and (3.2.64) are the key coupled electric field integral equations to be used in the further development.

3.3. Numerical Simulation

In our study, the numerical simulation includes two procedures, the *forward* procedure and the *inverse* procedure. In the *forward* procedure, the reflection coefficient or the input admittance of the waveguide probe is determined with assumed EM properties of the material layer. In this procedure, two coupled electric field integral equations (EFIE's) for the aperture electric field are numerically determined. The unknown aperture electric field is expressed as a sum of incident and reflected dominant mode and a number of higher order modes due to the discontinuity presented at the aperture. In the *inverse* procedure, the reflection coefficient or the input admittance of the waveguide aperture is measured, and the EM parameters of the material layer are inversely determined through an inverse technique. In this procedure, a number of higher order modes are included in the unknown aperture electric field to improve the accuracy of the solutions for the EM parameters of the material layer. The *forward* procedure will be discussed in the present and subsequent chapters, while, the *inverse* procedure will be discussed in Chapter 5.

In section 3.3.1, the method of moments is employed to convert the EFIE's to a matrix equation. Here the EFIE's are solved by the Galerkin's method using the waveguide eigenmodes as the basis and testing functions. Section 3.3.2 develops formulas which are needed in carrying out the numerical calculation of the matrix equation transforming from rectangular coordinates into cylindrical coordinates. Finally, section 3.3.3 presents numerical results of this study, and compares them with the published results to verify the accuracy of this technique.

3.3.1 Application of Method of Moments

The coupled integral equations given in eqs. (3.2.62) and (3.2.64) for the unknown aperture electric field are solved by using the moment method technique. The unknown aperture electric field is first expanded into a set of appropriately chosen basis functions $\{e_\beta(x, y)\}$. Since the aperture fields of a waveguide can be expressed as a sum of a dominant mode and a number of higher order modes, the appropriate basis functions are the eigenmodes of the waveguide. Let us expand the unknown aperture electric field components into two finite sums of eigenmodes of the waveguide as follows:

$$E_{xo}(x, y) = \sum_\beta a_\beta e_\beta^x(x, y) \tag{3.3.1}$$

$$E_{yo}(x, y) = \sum_\beta b_\beta e_\beta^y(x, y) \tag{3.3.2}$$

where $\sum_\beta$ represents $\sum_p \sum_q$ for summation of all possible higher order modes which have mode indices $[(2p-1), (2q-2)]$ with $p, q = 1, 2, 3, \ldots$. The set of basis functions are expressed as

$$e_\beta^x(x, y) \equiv \cos\left[\frac{(2p-1)\pi x}{a}\right] \sin\left[\frac{(2q-2)\pi y}{b}\right] \tag{3.3.3}$$

$$e_\beta^y(x, y) \equiv \sin\left[\frac{(2p-1)\pi x}{a}\right] \cos\left[\frac{(2q-2)\pi y}{b}\right] \tag{3.3.4}$$

Substituting eqs. (3.3.1) and (3.3.2) into the coupled EFIE's yields

$$\sum_\beta a_\beta \cdot \left[W_{dx}^x + W_{cx}^x\right] + \sum_\beta b_\beta \cdot \left[W_{dx}^y + W_{cx}^y\right] = 0 \tag{3.3.5}$$

$$\sum_\beta a_\beta \cdot \left[W_{dy}^x + W_{cy}^x\right] + \sum_\beta b_\beta \cdot \left[W_{dy}^y + W_{cy}^y\right] = C\sin\left(\frac{\pi x}{a}\right) \tag{3.3.6}$$

where

$$W_{dx}^{x} \equiv \sum_{n'}\sum_{m'} \frac{-4\varepsilon_{n'm'}}{ab\Gamma_{n'm'}}\left(\frac{\mu}{\mu_0}\right)\cos\left(\frac{n'\pi x}{a}\right)\sin\left(\frac{m'\pi y}{b}\right)\left[k_0^2-\left(\frac{m'\pi}{b}\right)^2\right]\iint e_x \tag{3.3.7}$$

$$W_{cx}^{x} \equiv \int_{-\infty}^{\infty}\int e^{jk_x x}e^{jk_y y}N_x(k_y, k_x)\left(\iint e_x^e\right)dk_x dk_y \tag{3.3.8}$$

$$W_{dx}^{y} \equiv \sum_{n'}\sum_{m'} \frac{-4\varepsilon_{n'm'}}{ab\Gamma_{n'm'}}\left(\frac{\mu}{\mu_0}\right)\cos\left(\frac{n'\pi x}{a}\right)\sin\left(\frac{m'\pi y}{b}\right)\left(\frac{n'\pi}{a}\right)\left(\frac{m'\pi}{b}\right)\iint e_y \tag{3.3.9}$$

$$W_{cx}^{y} \equiv \int_{-\infty}^{\infty}\int e^{jk_x x}e^{jk_y y}M(k_y, k_x)\left(\iint e_y^e\right)dk_x dk_y \tag{3.3.10}$$

$$W_{dy}^{x} \equiv \sum_{n'}\sum_{m'} \frac{-4\varepsilon_{n'm'}}{ab\Gamma_{n'm'}}\left(\frac{\mu}{\mu_0}\right)\sin\left(\frac{n'\pi x}{a}\right)\cos\left(\frac{m'\pi y}{b}\right)\left(\frac{n'\pi}{a}\right)\left(\frac{m'\pi}{b}\right)\iint e_x \tag{3.3.11}$$

$$W_{cy}^{x} \equiv \int_{-\infty}^{\infty}\int e^{jk_x x}e^{jk_y y}M(k_x, k_y)\left(\iint e_x^e\right)dk_x dk_y \tag{3.3.12}$$

$$W_{dy}^{y} \equiv \frac{2\Gamma_{10}}{ab}\left(\frac{\mu}{\mu_0}\right)\sin\left(\frac{\pi x}{a}\right)\int_0^b\int_0^a e_\beta^y(x', y')\sin\left(\frac{\pi x'}{a}\right)dx'dy'$$

$$+\sum_{n'}\sum_{m'} \frac{-4\varepsilon_{n'm'}}{ab\Gamma_{n'm'}}\left(\frac{\mu}{\mu_0}\right)\sin\left(\frac{n'\pi x}{a}\right)\cos\left(\frac{m'\pi y}{b}\right)\left[k_0^2-\left(\frac{n'\pi}{a}\right)^2\right]\iint e_y \tag{3.3.13}$$

$$W_{cy}^{y} \equiv \int_{-\infty}^{\infty}\int e^{jk_x x}e^{jk_y y}N_y(k_x, k_y)\left(\iint e_y^e\right)dk_x dk_y \tag{3.3.14}$$

and

$$\iint e_x \equiv \int_0^b\int_0^a e_\beta^x(x', y')\cos\left(\frac{n'\pi x'}{a}\right)\sin\left(\frac{m'\pi y'}{b}\right)dx'dy' \tag{3.3.15}$$

$$\iint e_y \equiv \int_0^b\int_0^a e_\beta^y(x', y')\sin\left(\frac{n'\pi x'}{a}\right)\cos\left(\frac{m'\pi y'}{b}\right)dx'dy' \tag{3.3.16}$$

$$\iint e_x^e \equiv \int_0^b \int_0^a e_\beta^x(x', y')\, e^{-jk_x x'} e^{-jk_y y'} dx' dy' \tag{3.3.17}$$

$$\iint e_y^e \equiv \int_0^b \int_0^a e_\beta^y(x', y')\, e^{-jk_x x'} e^{-jk_y y'} dx' dy' \tag{3.3.18}$$

The EFIE's for the aperture electric field are now expanded into the waveguide eigenmodes with unknown expansion coefficients a_β and b_β which represent the amplitudes of the eigenmodes for the x and y components of the aperture electric field, respectively. Next, we will use the Galerkin's method to determine a_β and b_β. Since the Galerkin's method uses the same set of basis functions as the testing functions, we write the set of testing functions as

$$t_\alpha^x(x, y) \equiv \cos\left[\frac{(2l-1)\pi x}{a}\right] \sin\left[\frac{(2r-2)\pi y}{b}\right] \tag{3.3.19}$$

$$t_\alpha^y(x, y) \equiv \sin\left[\frac{(2l-1)\pi x}{a}\right] \cos\left[\frac{(2r-2)\pi y}{b}\right] \tag{3.3.20}$$

After taking the inner products of eqs. (3.3.5) and (3.3.6) with the set of testing functions, we have the following results.

$$\sum_\beta a_\beta \cdot D_{\alpha\beta}^{xx} + \sum_\beta b_\beta \cdot D_{\alpha\beta}^{xy} = 0 \tag{3.3.21}$$

$$\sum_\beta a_\beta \cdot D_{\alpha\beta}^{yx} + \sum_\beta b_\beta \cdot D_{\alpha\beta}^{yy} = F_\alpha \tag{3.3.22}$$

which can be represented in a matrix form of

$$\begin{bmatrix} D_{\alpha\beta}^{xx} & D_{\alpha\beta}^{xy} \\ D_{\alpha\beta}^{yx} & D_{\alpha\beta}^{yy} \end{bmatrix} \begin{bmatrix} a_\beta \\ b_\beta \end{bmatrix} = \begin{bmatrix} 0 \\ F_\alpha \end{bmatrix} \tag{3.3.23}$$

where

$$D_{\alpha\beta}^{xx} \equiv \int_0^b \int_0^a t_\alpha^x(x,y)\left[W_{dx}^x(x,y) + W_{cx}^x(x,y)\right]dxdy \tag{3.3.24}$$

$$D_{\alpha\beta}^{xy} \equiv \int_0^b \int_0^a t_\alpha^x(x,y)\left[W_{dx}^y(x,y) + W_{cx}^y(x,y)\right]dxdy \tag{3.3.25}$$

$$D_{\alpha\beta}^{yx} \equiv \int_0^b \int_0^a t_\alpha^y(x,y)\left[W_{dy}^x(x,y) + W_{cy}^x(x,y)\right]dxdy \tag{3.3.26}$$

$$D_{\alpha\beta}^{yy} \equiv \int_0^b \int_0^a t_\alpha^y(x,y)\left[W_{dy}^y(x,y) + W_{cy}^y(x,y)\right]dxdy \tag{3.3.27}$$

and

$$F_\alpha \equiv C \int_0^b \int_0^a t_\alpha^y(x,y)\sin\left(\frac{\pi x}{a}\right)dxdy \tag{3.3.28}$$

3.3.2 Evaluation of Matrix Elements

In this section, elements of the matrix will be evaluated into compact forms to facilitate the computer programing. Among the evaluations in this section, two-dimensional Fourier transforms of the sinusoidal functions over the aperture are evaluated analytically in Appendix.

In the matrix, the component $D_{\alpha\beta}^{yy}$ which represents the self-interaction of the y-component of the aperture electric field is first discussed. Let us divide $D_{\alpha\beta}^{yy}$ into three parts:

$$D_{\alpha\beta}^{yy} \equiv \int_0^b \int_0^a t_\alpha^y(x,y)\left[W_{dy}^y(x,y) + W_{cy}^y(x,y)\right]dxdy$$

$$= \Phi_1^{yy} + \Phi_2^{yy} + \Phi_3^{yy} \tag{3.3.29}$$

where Φ_1^{yy} represents the contribution coming from the material layer which has continuous spectrum property, Φ_2^{yy} represents the contribution from discrete higher order modes of the waveguide and Φ_3^{yy} represents the contribution from the incident dominant mode. They are expressed as

$$\begin{aligned}
\Phi_1^{yy} &\equiv \int_0^b \int_0^a t_\alpha^y(x, y)\, W_{cy}^y(x, y)\, dxdy \\
&= \int_0^b \int_0^a t_\alpha^y(x, y) \left(\int_{-\infty}^{\infty} \int e^{jk_x x} e^{jk_y y} N(k_x, k_y) \left(\int\int e_y^e \right) dk_x dk_y \right) dxdy \\
&= \int_{-\infty}^{\infty} \int N_y(k_x, k_y) \left(\int\int t_y^e \right) \left(\int\int e_y^e \right) dk_x dk_y
\end{aligned} \tag{3.3.30}$$

$$\begin{aligned}
\Phi_2^{yy} &\equiv \int_0^b \int_0^a t_\alpha^y(x, y) \left(\sum_{n'} \sum_{m'} \frac{-4\varepsilon_{n'm'}}{ab\Gamma_{n'm'}} \left(\frac{\mu}{\mu_0} \right) \sin\left(\frac{n'\pi x}{a} \right) \cos\left(\frac{m'\pi y}{b} \right) \left[k_0^2 - \left(\frac{n'\pi}{a} \right)^2 \right] \int\int e_y \right) dxdy \\
&= \sum_{n'} \sum_{m'} \frac{-4\varepsilon_{n'm'}}{ab\Gamma_{n'm'}} \left(\frac{\mu}{\mu_0} \right) \left[k_0^2 - \left(\frac{n'\pi}{a} \right)^2 \right] \left(\int\int t_y \right) \left(\int\int e_y \right)
\end{aligned} \tag{3.3.31}$$

$$\begin{aligned}
\Phi_3^{yy} &\equiv \int_0^b \int_0^a t_\alpha^y(x, y) \left(\frac{2\Gamma_{10}}{ab} \left(\frac{\mu}{\mu_0} \right) \sin\left(\frac{\pi x}{a} \right) \int_0^b \int_0^a e_\beta^y(x', y') \sin\left(\frac{\pi x'}{a} \right) dx'dy' \right) dxdy \\
&= \frac{2\Gamma_{10}}{ab} \left(\frac{\mu}{\mu_0} \right) \left(\int_0^b \int_0^a t_\alpha^y(x, y) \sin\left(\frac{\pi x}{a} \right) dxdy \right) \left(\int_0^b \int_0^a e_\beta^y(x', y') \sin\left(\frac{\pi x'}{a} \right) dx'dy' \right) \\
&= \frac{2\Gamma_{10}}{ab} \left(\frac{\mu}{\mu_0} \right) \left(\int_0^b \int_0^a \sin\left[\frac{(2l-1)\pi x}{a} \right] \cos\left[\frac{(2r-2)\pi y}{b} \right] \sin\left(\frac{\pi x}{a} \right) dxdy \right) \times \\
&\quad \left(\int_0^b \int_0^a \sin\left[\frac{(2p-1)\pi x'}{a} \right] \cos\left[\frac{(2q-2)\pi y'}{b} \right] \sin\left(\frac{\pi x'}{a} \right) dx'dy' \right) \\
&= \frac{2\Gamma_{10}}{ab} \left(\frac{\mu}{\mu_0} \right) \left[\frac{ab}{2} \delta_{l,1} \delta_{r,1} \right] \left[\frac{ab}{2} \delta_{p,1} \delta_{q,1} \right]
\end{aligned}$$

$$= \frac{ab}{2}\left(\frac{\mu}{\mu_0}\right)\Gamma_{10}\delta_{l,1}\delta_{r,1}\delta_{p,1}\delta_{q,1} \tag{3.3.32}$$

where some shorthand notations are expressed as

$$\iint t_y^e \equiv \int_0^b\int_0^a t_\alpha^y(x,y)\, e^{jk_x x} e^{jk_y y}\, dxdy$$

$$= \left(\int_0^a \sin\left[\frac{(2l-1)\pi x}{a}\right][\cos(k_x x) + j\sin(k_x x)]\, dx\right)\times$$

$$\left(\int_0^b \cos\left[\frac{(2r-2)\pi y}{b}\right][\cos(k_y y) + j\sin(k_y y)]\, dy\right)$$

$$\equiv [s_{11}(k_x) + s_{12}(k_x)]\,[s_{13}(k_y) + s_{14}(k_y)] \tag{3.3.33}$$

$$\iint t_y \equiv \int_0^b\int_0^a t_\alpha^y(x,y)\, \sin\left(\frac{n'\pi x}{a}\right)\cos\left(\frac{m'\pi y}{b}\right)dxdy$$

$$= \int_0^b\int_0^a \sin\left[\frac{(2l-1)\pi x}{a}\right]\cos\left[\frac{(2r-2)\pi y}{b}\right]\sin\left(\frac{n'\pi x}{a}\right)\cos\left(\frac{m'\pi y}{b}\right)dxdy$$

$$= \frac{ab}{4}\delta_{n',(2l-1)}\delta_{m',(2r-2)}\varepsilon_{m'} \tag{3.3.34}$$

$$s_{11}(k_x) \equiv \int_0^a \sin\left[\frac{(2l-1)\pi x}{a}\right]\cos(k_x x)\, dx \tag{3.3.35}$$

$$s_{12}(k_x) \equiv j\int_0^a \sin\left[\frac{(2l-1)\pi x}{a}\right]\sin(k_x x)\, dx \tag{3.3.36}$$

$$s_{13}(k_y) \equiv \int_0^b \cos\left[\frac{(2r-2)\pi y}{b}\right]\cos(k_y y)\, dy \tag{3.3.37}$$

$$s_{14}(k_y) \equiv j\int_0^b \cos\left[\frac{(2r-2)\pi y}{b}\right]\sin(k_y y)\, dy \tag{3.3.38}$$

Similar forms for $\iint e_y^e$ and $\iint e_y$ are expressed as

$$\iint e_y^e \equiv \int_0^b \int_0^a e_\beta^y(x', y')\, e^{-jk_x x'} e^{-jk_y y'}\, dx'dy'$$

$$= \left(\int_0^a \sin\left[\frac{(2p-1)\pi x'}{a}\right] [\cos(k_x x') - j\sin(k_x x')]\, dx' \right) \times$$

$$\left(\int_0^b \cos\left[\frac{(2q-2)\pi y'}{b}\right] [\cos(k_y y') - j\sin(k_y y')]\, dy' \right)$$

$$\equiv [s_{21}(k_x) + s_{22}(k_x)]\, [s_{23}(k_y) + s_{24}(k_y)] \tag{3.3.39}$$

$$\iint e_y \equiv \int_0^b \int_0^a e_\beta^y(x', y') \sin\left(\frac{n'\pi x'}{a}\right) \cos\left(\frac{m'\pi y'}{b}\right) dx'dy'$$

$$= \int_0^b \int_0^a \sin\left[\frac{(2p-1)\pi x'}{a}\right] \cos\left[\frac{(2q-2)\pi y'}{b}\right] \sin\left(\frac{n'\pi x'}{a}\right) \cos\left(\frac{m'\pi y'}{b}\right) dx'dy'$$

$$= \frac{ab}{4} \delta_{n',\,(2p-1)}\, \delta_{m',\,(2q-2)}\, \varepsilon_{m'} \tag{3.3.40}$$

$$s_{21}(k_x) \equiv \int_0^a \sin\left[\frac{(2p-1)\pi x'}{a}\right] \cos(k_x x')\, dx' \tag{3.3.41}$$

$$s_{22}(k_x) \equiv -j \int_0^a \sin\left[\frac{(2p-1)\pi x'}{a}\right] \sin(k_x x')\, dx' \tag{3.3.42}$$

$$s_{23}(k_y) \equiv \int_0^b \cos\left[\frac{(2q-2)\pi y'}{b}\right] \cos(k_y y')\, dy' \tag{3.3.43}$$

$$s_{24}(k_y) \equiv -j \int_0^b \cos\left[\frac{(2q-2)\pi y'}{b}\right] \sin(k_y y')\, dy' \tag{3.3.44}$$

If we further define

$$\phi_{12u}(k_x) \equiv [s_{11}(k_x) + s_{12}(k_x)]\,[s_{21}(k_x) + s_{22}(k_x)] \tag{3.3.45}$$

$$\phi_{12v}(k_y) \equiv [s_{13}(k_y) + s_{14}(k_y)]\,[s_{23}(k_y) + s_{24}(k_y)]\,, \tag{3.3.46}$$

the multiplication of the shorthand notations given in eqs. (3.3.30) and (3.3.31) become

$$\left(\iint t_y^e\right)\left(\iint e_y^e\right) \equiv \phi_{12u}(k_x)\,\phi_{12v}(k_y) \tag{3.3.47}$$

and

$$\left(\iint t_y\right)\left(\iint e_y\right) = \left(\frac{ab}{4}\right)^2 \delta_{n',\,(2l-1)}\,\delta_{m',\,(2r-2)}\,\delta_{n',\,(2p-1)}\,\delta_{m',\,(2q-2)}\,\varepsilon_{m'}^2 \tag{3.3.48}$$

Substituting them into eqs. (3.3.30) and (3.3.31) gives

$$\Phi_1^{yy} = \int_{-\infty}^{\infty}\!\!\int N_y(k_x, k_y)\,\phi_{12u}(k_x)\,\phi_{12v}(k_y)\,dk_x dk_y \tag{3.3.49}$$

$$\begin{aligned}\Phi_2^{yy} &= \sum_{n'}\sum_{m'} \frac{-4\varepsilon_{n'm'}}{ab\Gamma_{n'm'}}\left(\frac{\mu}{\mu_0}\right)\left[k_0^2 - \left(\frac{n'\pi}{a}\right)^2\right]\left(\iint t_y\right)\left(\iint e_y\right) \\ &= \frac{ab}{4}\left(\frac{\mu}{\mu_0}\right)\sum_{n'}\sum_{m'} \frac{\varepsilon_{n'm'}\varepsilon_{m'}^2}{\Gamma_{n'm'}}\left[\left(\frac{n'\pi}{a}\right)^2 - k_0^2\right]\delta_{n',\,(2l-1)}\,\delta_{m',\,(2r-2)}\,\delta_{n',\,(2p-1)}\,\delta_{m',\,(2q-2)}\end{aligned} \tag{3.3.50}$$

Moreover, since

$$N_y(k_x, k_y) \equiv \frac{1/(2\pi)^2}{\Gamma_1\left(k_x^2 + k_y^2\right)}\left(\Gamma_1^2 k_x^2 \frac{1 - R_a}{1 + R_a} - k_1^2 k_y^2 \frac{1 + R_b}{1 - R_b}\right)$$

is an even function of k_x and k_y, Φ_1^{yy} can be further simplified to

$$\Phi_1^{yy} = 4\int_0^\infty\int N_y(k_x, k_y)\,\phi_{12u}^e(k_x)\,\phi_{12v}^e(k_y)\,dk_x dk_y \tag{3.3.51}$$

where $\phi_{12u}^e(k_x)$ and $\phi_{12v}^e(k_y)$ denote the even components of $\phi_{12u}(k_x)$ and $\phi_{12v}(k_y)$, respectively, and are derived in detail in Appendix.

Since it becomes highly oscillatory if the two-dimensional semi-infinite spectral integration given in eq. (3.3.51) is calculated in rectangular coordinates, this spectral integration is computed in cylindrical coordinates to sidestep this difficulty. Let's change the coordinates from rectangular to cylindrical with the relations of

$$\begin{cases} k_x = k\cos\varphi \\ k_y = k\sin\varphi \end{cases} \tag{3.3.52}$$

where φ is a real variable with range of $[0, 2\pi]$ and k is a real variable of $[0, \infty]$. The substitution of eq. (3.3.52) in eq. (3.3.51) yields

$$\begin{aligned} \Phi_1^{yy} &= 4\int_0^\infty\int_0^{\pi/2} N_y(k, \varphi)\,\phi_{12u}^e(k, \varphi)\,\phi_{12v}^e(k, \varphi)\,k\,d\varphi dk \\ &= 4\int_0^\infty G_{yy}(k)\,k\,dk \end{aligned} \tag{3.3.53}$$

where

$$G_{yy}(k) \equiv \int_0^{\pi/2} N_y(k, \varphi)\,\phi_{12u}^e(k, \varphi)\,\phi_{12v}^e(k, \varphi)\,d\varphi \tag{3.3.54}$$

Next we will discuss the component $D_{\alpha\beta}^{xx}$ which represents the self-interaction of the x-component of the aperture electric field in the matrix. Divide $D_{\alpha\beta}^{xx}$ into two parts as follows:

$$D_{\alpha\beta}^{xx} \equiv \int_0^b \int_0^a t_\alpha^x(x,y)\left[W_{dx}^x(x,y) + W_{cx}^x(x,y)\right]dxdy$$

$$= \Phi_1^{xx} + \Phi_2^{xx} \tag{3.3.55}$$

where

$$\Phi_1^{xx} \equiv \int_0^b \int_0^a t_\alpha^x(x,y)\, W_{cx}^x(x,y)\, dxdy$$

$$= \int_0^b \int_0^a t_\alpha^x(x,y)\left(\int_{-\infty}^{\infty}\int e^{jk_x x} e^{jk_y y} N(k_y,k_x)\left(\iint e_x^e\right)dk_x dk_y\right)dxdy$$

$$= \int_{-\infty}^{\infty}\int N_x(k_y,k_x)\left(\iint t_x^e\right)\left(\iint e_x^e\right)dk_x dk_y \tag{3.3.56}$$

$$\Phi_2^{xx} \equiv \int_0^b \int_0^a t_\alpha^x(x,y)\, W_{dx}^x(x,y)\, dxdy$$

$$= \int_0^b \int_0^a t_\alpha^x(x,y)\left(\sum_{n'}\sum_{m'}\frac{-4\varepsilon_{n'm'}}{ab\Gamma_{n'm'}}\left(\frac{\mu}{\mu_0}\right)\cos\left(\frac{n'\pi x}{a}\right)\sin\left(\frac{m'\pi y}{b}\right)\left[k_0^2 - \left(\frac{m'\pi}{b}\right)^2\right]\iint e_x\right)dxdy$$

$$= \sum_{n'}\sum_{m'}\frac{-4\varepsilon_{n'm'}}{ab\Gamma_{n'm'}}\left(\frac{\mu}{\mu_0}\right)\left[k_0^2 - \left(\frac{m'\pi}{b}\right)^2\right]\left(\iint t_x\right)\left(\iint e_x\right) \tag{3.3.57}$$

and the shorthand notations are expressed as

$$\iint t_x^e \equiv \int_0^b \int_0^a t_\alpha^x(x,y)\, e^{jk_x x} e^{jk_y y}\, dxdy$$

$$= \left(\int_0^a \cos\left[\frac{(2l-1)\pi x}{a}\right]\left[\cos(k_x x) + j\sin(k_x x)\right]dx\right)\times$$

$$\left(\int_0^b \sin\left[\frac{(2r-2)\pi y}{b}\right]\left[\cos(k_y y) + j\sin(k_y y)\right]dy\right)$$

$$\equiv \left[s_{31}(k_x) + s_{32}(k_x)\right]\left[s_{33}(k_y) + s_{34}(k_y)\right] \tag{3.3.58}$$

$$\iint t_x \equiv \int_0^b \int_0^a t_\alpha^x (x, y) \cos\left(\frac{n'\pi x}{a}\right) \sin\left(\frac{m'\pi y}{b}\right) dx dy$$

$$= \int_0^b \int_0^a \cos\left[\frac{(2l-1)\pi x}{a}\right] \sin\left[\frac{(2r-2)\pi y}{b}\right] \cos\left(\frac{n'\pi x}{a}\right) \sin\left(\frac{m'\pi y}{b}\right) dx dy$$

$$= \frac{ab}{4} \delta_{n',\,(2l-1)}\, \delta_{m',\,(2r-2)} \tag{3.3.59}$$

$$s_{31}(k_x) \equiv \int_0^a \cos\left[\frac{(2l-1)\pi x}{a}\right] \cos(k_x x)\, dx \tag{3.3.60}$$

$$s_{32}(k_x) \equiv j \int_0^a \cos\left[\frac{(2l-1)\pi x}{a}\right] \sin(k_x x)\, dx \tag{3.3.61}$$

$$s_{33}(k_y) \equiv \int_0^b \sin\left[\frac{(2r-2)\pi y}{b}\right] \cos(k_y y)\, dy \tag{3.3.62}$$

$$s_{34}(k_y) \equiv j \int_0^b \sin\left[\frac{(2r-2)\pi y}{b}\right] \sin(k_y y)\, dy \tag{3.3.63}$$

Similar forms for $\iint e_x^e$ and $\iint e_x$ are expressed as

$$\iint e_x^e \equiv \int_0^b \int_0^a e_\beta^x (x', y')\, e^{-jk_x x'} e^{-jk_y y'} dx' dy'$$

$$= \left(\int_0^a \cos\left[\frac{(2p-1)\pi x'}{a}\right] [\cos(k_x x') - j \sin(k_x x')]\, dx' \right) \times$$

$$\left(\int_0^b \sin\left[\frac{(2q-2)\pi y'}{b}\right] [\cos(k_y y') - j \sin(k_y y')]\, dy' \right)$$

$$\equiv [s_{41}(k_x) + s_{42}(k_x)]\, [s_{43}(k_y) + s_{44}(k_y)] \tag{3.3.64}$$

$$\iint e_x \equiv \int_0^b \int_0^a e_\beta^x (x', y') \cos\left(\frac{n'\pi x'}{a}\right) \sin\left(\frac{m'\pi y'}{b}\right) dx' dy'$$

$$= \int_0^b \int_0^a \cos\left[\frac{(2p-1)\pi x'}{a}\right] \sin\left[\frac{(2q-2)\pi y'}{b}\right] \cos\left(\frac{n'\pi x'}{a}\right) \sin\left(\frac{m'\pi y'}{b}\right) dx' dy'$$

$$= \frac{ab}{4}\delta_{n',\,(2p-1)}\,\delta_{m',\,(2q-2)} \tag{3.3.65}$$

$$s_{41}(k_x) \equiv \int_0^a \cos\left[\frac{(2p-1)\,\pi x'}{a}\right]\cos(k_x x')\,dx' \tag{3.3.66}$$

$$s_{42}(k_x) \equiv -j\int_0^a \cos\left[\frac{(2p-1)\,\pi x'}{a}\right]\sin(k_x x')\,dx' \tag{3.3.67}$$

$$s_{43}(k_y) \equiv \int_0^b \sin\left[\frac{(2q-2)\,\pi y'}{b}\right]\cos(k_y y')\,dy' \tag{3.3.68}$$

$$s_{44}(k_y) \equiv -j\int_0^b \sin\left[\frac{(2q-2)\,\pi y'}{b}\right]\sin(k_y y')\,dy' \tag{3.3.69}$$

If we define the following notations,

$$\phi_{34u}(k_x) \equiv [s_{31}(k_x) + s_{32}(k_x)]\,[s_{41}(k_x) + s_{42}(k_x)] \tag{3.3.70}$$

$$\phi_{34v}(k_y) \equiv [s_{33}(k_y) + s_{34}(k_y)]\,[s_{43}(k_y) + s_{44}(k_y)] \tag{3.3.71}$$

the multiplication of the shorthand notations which given in eqs. (3.3.56) and (3.3.57) become

$$\left(\iint t_x^e\right)\left(\iint e_x^e\right) \equiv \phi_{34u}(k_x)\,\phi_{34v}(k_y) \tag{3.3.72}$$

and

$$\left(\iint t_x\right)\left(\iint e_x\right) = \left(\frac{ab}{4}\right)^2 \delta_{n',\,(2l-1)}\,\delta_{m',\,(2r-2)}\,\delta_{n',\,(2p-1)}\,\delta_{m',\,(2q-2)} \tag{3.3.73}$$

Substituting them in eqs. (3.3.56) and (3.3.57) gives

$$\Phi_1^{xx} = \int_{-\infty}^{\infty}\int N_x(k_y, k_x)\,\phi_{34u}(k_x)\,\phi_{34v}(k_y)\,dk_x dk_y \tag{3.3.74}$$

$$\Phi_2^{xx} = \sum_{n'}\sum_{m'}\frac{-4\varepsilon_{n'm'}}{ab\Gamma_{n'm'}}\left(\frac{\mu}{\mu_0}\right)\left[k_0^2-\left(\frac{m'\pi}{b}\right)^2\right]\left(\int t_x\right)\left(\int e_x\right)$$

$$= \frac{ab}{4}\left(\frac{\mu}{\mu_0}\right)\sum_{n'}\sum_{m'}\frac{\varepsilon_{n'm'}}{\Gamma_{n'm'}}\left[\left(\frac{m'\pi}{b}\right)^2 - k_0^2\right]\delta_{n',\,(2l-1)}\,\delta_{m',\,(2r-2)}\,\delta_{n',\,(2p-1)}\,\delta_{m',\,(2q-2)} \tag{3.3.75}$$

Since

$$N_x(k_y, k_x) \equiv \frac{1/(2\pi)^2}{\Gamma_1\left(k_x^2+k_y^2\right)}\left(\Gamma_1^2 k_y^2\frac{1-R_a}{1+R_a} - k_1^2 k_x^2\frac{1+R_b}{1-R_b}\right)$$

is an even functions of k_x and k_y, Φ_1^{xx} can be modified to

$$\Phi_1^{xx} = 4\int_0^{\infty}\int N_x(k_y, k_x)\,\phi_{34u}^{e}(k_x)\,\phi_{34v}^{e}(k_y)\,dk_x dk_y \tag{3.3.76}$$

where $\phi_{34u}^{e}(k_x)$ and $\phi_{34v}^{e}(k_y)$ represent the even components of $\phi_{34u}(k_x)$ and $\phi_{34v}(k_y)$, respectively. As done earlier, changing coordinates from rectangular to cylindrical, the two-dimensional semi-infinite spectral integration becomes

$$\Phi_1^{xx} = 4\int_0^{\infty}\int_0^{\pi/2} N_x(k, \varphi)\,\phi_{34u}^{e}(k, \varphi)\,\phi_{34v}^{e}(k, \varphi)\,k\,d\varphi\,dk$$

$$= 4\int_0^{\infty} G_{xx}(k)\,k\,dk \tag{3.3.77}$$

where

$$G_{xx}(k) \equiv \int_0^{\pi/2} N_x(k, \varphi)\,\phi_{34u}^{e}(k, \varphi)\,\phi_{34v}^{e}(k, \varphi)\,d\varphi \tag{3.3.78}$$

Next, let's evaluate the component $D_{\alpha\beta}^{xy}$ in the matrix which represents the mutual-interaction of the x-component of the aperture electric field as the testing function and the y-component of the aperture electric field as the basis function. Divide $D_{\alpha\beta}^{xy}$ into two parts as follows:

$$D_{\alpha\beta}^{xy} \equiv \int_0^b \int_0^a t_\alpha^x(x,y)\left[W_{dx}^y(x,y) + W_{cx}^y(x,y)\right]dxdy$$

$$= \Phi_1^{xy} + \Phi_2^{xy} \tag{3.3.79}$$

where

$$\Phi_1^{xy} \equiv \int_0^b \int_0^a t_\alpha^x(x,y)\, W_{cx}^y(x,y)\, dxdy$$

$$= \int_0^b \int_0^a t_\alpha^x(x,y)\left(\int_{-\infty}^{\infty}\int e^{jk_x x} e^{jk_y y} M(k_y,k_x)\left(\iint e_y^e\right)dk_x dk_y\right)dxdy$$

$$= \int_{-\infty}^{\infty}\int M(k_y,k_x)\left(\iint t_x^e\right)\left(\iint e_y^e\right)dk_x dk_y \tag{3.3.80}$$

$$\Phi_2^{xy} \equiv \int_0^b \int_0^a t_\alpha^x(x,y)\, W_{dx}^y(x,y)\, dxdy$$

$$= \int_0^b \int_0^a t_\alpha^x(x,y)\left(\sum_{n'}\sum_{m'}\frac{-4\varepsilon_{n'm'}}{ab\Gamma_{n'm'}}\left(\frac{\mu}{\mu_0}\right)\cos\left(\frac{n'\pi x}{a}\right)\sin\left(\frac{m'\pi y}{b}\right)\left(\frac{n'\pi}{a}\right)\left(\frac{m'\pi}{b}\right)\iint e_y\right)dxdy$$

$$= \sum_{n'}\sum_{m'}\frac{-4\varepsilon_{n'm'}}{ab\Gamma_{n'm'}}\left(\frac{\mu}{\mu_0}\right)\left(\frac{n'\pi}{a}\right)\left(\frac{m'\pi}{b}\right)\left(\iint t_x\right)\left(\iint e_y\right) \tag{3.3.81}$$

According to eqs. (3.3.39) and (3.3.58), we obtain

$$\left(\iint t_x^e\right)\left(\iint e_y^e\right) \equiv \phi_{32u}(k_x)\,\phi_{32v}(k_y) \tag{3.3.82}$$

with the new shorthand notations defined as

$$\phi_{32u}(k_x) \equiv [s_{31}(k_x) + s_{32}(k_x)]\,[s_{21}(k_x) + s_{22}(k_x)] \tag{3.3.83}$$

$$\phi_{32v}(k_y) \equiv [s_{33}(k_y) + s_{34}(k_y)]\,[s_{23}(k_y) + s_{24}(k_y)] \tag{3.3.84}$$

and according to eqs. (3.3.40) and (3.3.59), we get

$$\left(\iint t_x\right)\left(\iint e_y\right) = \left(\frac{ab}{4}\right)^2 \delta_{n',\,(2l-1)}\,\delta_{m',\,(2r-2)}\,\delta_{n',\,(2p-1)}\,\delta_{m',\,(2q-2)}\,\varepsilon_{m'} \tag{3.3.85}$$

Substituting them in eqs. (3.3.80) and (3.3.81) gives,

$$\Phi_1^{xy} = \int_{-\infty}^{\infty}\!\!\int M(k_y, k_x)\,\phi_{32u}(k_x)\,\phi_{32v}(k_y)\,dk_x dk_y \tag{3.3.86}$$

$$\begin{aligned}\Phi_2^{xy} &= \sum_{n'}\sum_{m'} \frac{-4\varepsilon_{n'm'}}{ab\Gamma_{n'm'}}\left(\frac{\mu}{\mu_0}\right)\left(\frac{n'\pi}{a}\right)\left(\frac{m'\pi}{b}\right)\left(\iint t_x\right)\left(\iint e_y\right) \\ &= -\frac{ab}{4}\left(\frac{\mu}{\mu_0}\right)\sum_{n'}\sum_{m'}\frac{\varepsilon_{n'm'}}{\Gamma_{n'm'}}\left(\frac{n'\pi}{a}\right)\left(\frac{m'\pi}{b}\right)\delta_{n',\,(2l-1)}\,\delta_{m',\,(2r-2)}\,\delta_{n',\,(2p-1)}\,\delta_{m',\,(2q-2)}\end{aligned} \tag{3.3.87}$$

Since

$$M(k_y, k_x) \equiv \frac{-k_x k_y/(2\pi)^2}{\Gamma_1\left(k_x^2 + k_y^2\right)}\left(\Gamma_1^2\frac{1-R_a}{1+R_a} + k_1^2\frac{1+R_b}{1-R_b}\right)$$

is an odd functions of k_x and k_y, Φ_1^{xy} can be written as

$$\Phi_1^{xy} = 4\int_0^{\infty}\!\!\int M(k_y, k_x)\,\phi_{32u}^{o}(k_x)\,\phi_{32v}^{o}(k_y)\,dk_x dk_y \tag{3.3.88}$$

where $\phi_{32u}^{o}(k_x)$ and $\phi_{32v}^{o}(k_y)$ represented the odd components of $\phi_{32u}(k_x)$ and $\phi_{32v}(k_y)$, respectively. As before, changing coordinates from rectangular to cylindrical, Φ_1^{xy} in eq. (3.3.88) becomes

$$\Phi_1^{xy} = 4\int_0^{\infty}\int_0^{\pi/2} M(k,\varphi)\,\phi_{32u}^{o}(k,\varphi)\,\phi_{32v}^{o}(k,\varphi)\,k\,d\varphi\,dk$$

$$= 4\int_0^{\infty} G_{xy}(k)\,k\,dk \tag{3.3.89}$$

where

$$G_{xy}(k) \equiv \int_0^{\pi/2} M(k,\varphi)\,\phi_{32u}^{o}(k,\varphi)\,\phi_{32v}^{o}(k,\varphi)\,d\varphi \tag{3.3.90}$$

The last step is to evaluate the component $D_{\alpha\beta}^{yx}$ in the matrix which represents the mutual-interaction of the y-component of the aperture electric field as the testing function and the x-component of the aperture electric field as the basis function. Let's divide $D_{\alpha\beta}^{yx}$ into two parts as follows:

$$D_{\alpha\beta}^{yx} \equiv \int_0^{b}\int_0^{a} t_\alpha^y(x,y)\left[W_{dy}^{x}(x,y) + W_{cy}^{x}(x,y)\right]dxdy$$

$$= \Phi_1^{yx} + \Phi_2^{yx} \tag{3.3.91}$$

where

$$\Phi_1^{yx} \equiv \int_0^{b}\int_0^{a} t_\alpha^y(x,y)\,W_{cy}^{x}(x,y)\,dxdy$$

$$= \int_0^{b}\int_0^{a} t_\alpha^y(x,y)\left(\int_{-\infty}^{\infty}\int e^{jk_x x}e^{jk_y y}M(k_x,k_y)\left(\iint e_x^e\right)dk_x dk_y\right)dxdy$$

$$= \int_{-\infty}^{\infty}\int M(k_x,k_y)\left(\iint t_y^e\right)\left(\iint e_x^e\right)dk_x dk_y \tag{3.3.92}$$

$$\Phi_2^{yx} \equiv \int_0^{b}\int_0^{a} t_\alpha^y(x,y)\,W_{dy}^{x}(x,y)\,dxdy$$

$$= \int_0^b \int_0^a t_\alpha^y(x,y) \left(\sum_{n'} \sum_{m'} \frac{-4\varepsilon_{n'm'}}{ab\Gamma_{n'm'}} \left(\frac{\mu}{\mu_0}\right) \sin\left(\frac{n'\pi x}{a}\right) \cos\left(\frac{m'\pi y}{b}\right) \left(\frac{n'\pi}{a}\right) \left(\frac{m'\pi}{b}\right) \iint e_x \right) dxdy$$

$$= \sum_{n'} \sum_{m'} \frac{-4\varepsilon_{n'm'}}{ab\Gamma_{n'm'}} \left(\frac{\mu}{\mu_0}\right) \left(\frac{n'\pi}{a}\right) \left(\frac{m'\pi}{b}\right) \left(\iint t_y\right) \left(\iint e_x\right) \tag{3.3.93}$$

Based on eqs. (3.3.33) and (3.3.64), we have

$$\left(\iint t_y^e\right)\left(\iint e_x^e\right) \equiv \phi_{14u}(k_x)\, \phi_{14v}(k_y) \tag{3.3.94}$$

With the new shorthand notations defined as

$$\phi_{14u}(k_x) \equiv [s_{11}(k_x) + s_{12}(k_x)]\, [s_{41}(k_x) + s_{42}(k_x)] \tag{3.3.95}$$

$$\phi_{14v}(k_y) \equiv [s_{13}(k_y) + s_{14}(k_y)]\, [s_{43}(k_y) + s_{44}(k_y)] \tag{3.3.96}$$

and with eqs. (3.3.34) and (3.3.65), we obtain

$$\left(\iint t_y\right)\left(\iint e_x\right) = \left(\frac{ab}{4}\right)^2 \delta_{n',\,(2l-1)}\, \delta_{m',\,(2r-2)}\, \delta_{n',\,(2p-1)}\, \delta_{m',\,(2q-2)}\, \varepsilon_{m'} \tag{3.3.97}$$

Substituting them in eqs. (3.3.92) and (3.3.93) gives

$$\Phi_1^{yx} = \int_{-\infty}^{\infty} \int M(k_x, k_y)\, \phi_{14u}(k_x)\, \phi_{14v}(k_y)\, dk_x dk_y \tag{3.3.98}$$

$$\Phi_2^{yx} = \sum_{n'} \sum_{m'} \frac{-4\varepsilon_{n'm'}}{ab\Gamma_{n'm'}} \left(\frac{\mu}{\mu_0}\right) \left(\frac{n'\pi}{a}\right) \left(\frac{m'\pi}{b}\right) \left(\iint t_y\right) \left(\iint e_x\right)$$

$$= -\frac{ab}{4} \left(\frac{\mu}{\mu_0}\right) \sum_{n'} \sum_{m'} \frac{\varepsilon_{n'm'}}{\Gamma_{n'm'}} \left(\frac{n'\pi}{a}\right) \left(\frac{m'\pi}{b}\right) \delta_{n',\,(2l-1)}\, \delta_{m',\,(2r-2)}\, \delta_{n',\,(2p-1)}\, \delta_{m',\,(2q-2)} \tag{3.3.99}$$

Since

$$M(k_x, k_y) \equiv \frac{-k_x k_y / (2\pi)^2}{\Gamma_1 \left(k_x^2 + k_y^2\right)} \left(\Gamma_1^2 \frac{1 - R_a}{1 + R_a} + k_1^2 \frac{1 + R_b}{1 - R_b} \right)$$

is an odd functions of k_x and k_y, Φ_1^{yx} can be written as

$$\Phi_1^{yx} = 4\int_0^{\infty}\int M(k_x, k_y)\,\phi_{14u}^{o}(k_x)\,\phi_{14v}^{o}(k_y)\,dk_x dk_y \tag{3.3.100}$$

where $\phi_{14u}^{o}(k_x)$ and $\phi_{14v}^{o}(k_y)$ are the odd components of $\phi_{14u}(k_x)$ and $\phi_{14v}(k_y)$, respectively. If we change coordinates from rectangular to cylindrical as before, Φ_1^{yx} in eq. (3.3.100) becomes

$$\begin{aligned}\Phi_1^{yx} &= 4\int_0^{\infty}\int_0^{\pi/2} M(k, \varphi)\,\phi_{14u}^{o}(k, \varphi)\,\phi_{14v}^{o}(k, \varphi)\,k\,d\varphi\,dk \\ &= 4\int_0^{\infty} G_{yx}(k)\,k\,dk\end{aligned} \tag{3.3.101}$$

where

$$G_{yx}(k) \equiv \int_0^{\pi/2} M(k, \varphi)\,\phi_{14u}^{o}(k, \varphi)\,\phi_{14v}^{o}(k, \varphi)\,d\varphi \tag{3.3.102}$$

3.3.3 Numerical Results and Comparison with Existing Results

For a specific material layer, the numerical evaluation of the components of the matrix equation given in eq. (3.3.23) for solving the aperture electric field and other relevant quantities of the waveguide probe is performed in a FORTRAN computer program. Once the matrix equation is solved, the aperture electric field is first obtained by summing up a finite number of modes that we have taken into account in the program. Then the reflection coefficient or the input impedance of the waveguide probe is determined via these aperture electric field.

To verify the accuracy of this technique, as well as the validity of the computer program, data of the input admittance of the waveguide probe placed against various

material layers which have been published using a waveguide (RG 52U rectangular waveguide, X band) are recalculated and compared with the existing results.

Figures 3.1(a) and (b) show the real and imaginary components of the input admittances of a waveguide probe when the probe is placed against a layer of quartz with a dielectric constant of $\varepsilon_r = 3.76$ and a thickness of 0.1299 inch. Our results are compared to the theoretical and experimental results of Croswell et al. [22] where only a dominant TE_{10} mode was considered in their theoretical calculation. These figures show that our numerical results compare quite well with the theoretical value of Croswell et al. when we considered only a dominant mode in our calculation. However, when higher order *TE* and *TM* modes are taken into account in our calculation, our numerical results match very well with their experimental results, much better than their theoretical results do.

We considered two multi-mode cases; the one with a dominant TE_{10} mode plus three higher order modes (TE_{30}, TE_{12} and TM_{12}) and the other one with a dominant TE_{10} mode plus eight higher order modes (TE_{30}, TE_{12}, TM_{12}, TE_{50}, TE_{32}, TM_{32}, TE_{52} and TM_{52}). It is noted in Figs. 3.1(a) and (b) that the 4 modes case and the 9 modes case yielded almost identical results. This indicates that a good convergence can be obtained when only the first four modes are used in the numerical calculation.

Figures 3.2(a) and (b) show the real and imaginary components of the input admittances of a waveguide probe which is placed against a material layer with a dielectric constant $\varepsilon_r = 2.25$ and a thickness of 0.3201 cm. For this case our numerical results obtained by using one, four and nine modes are compared to the theoretical and experimental results of Bodnar et al. [24]. These figures show a good agreement between our numerical results with multi-mode consideration and their theoretical and experimental results.

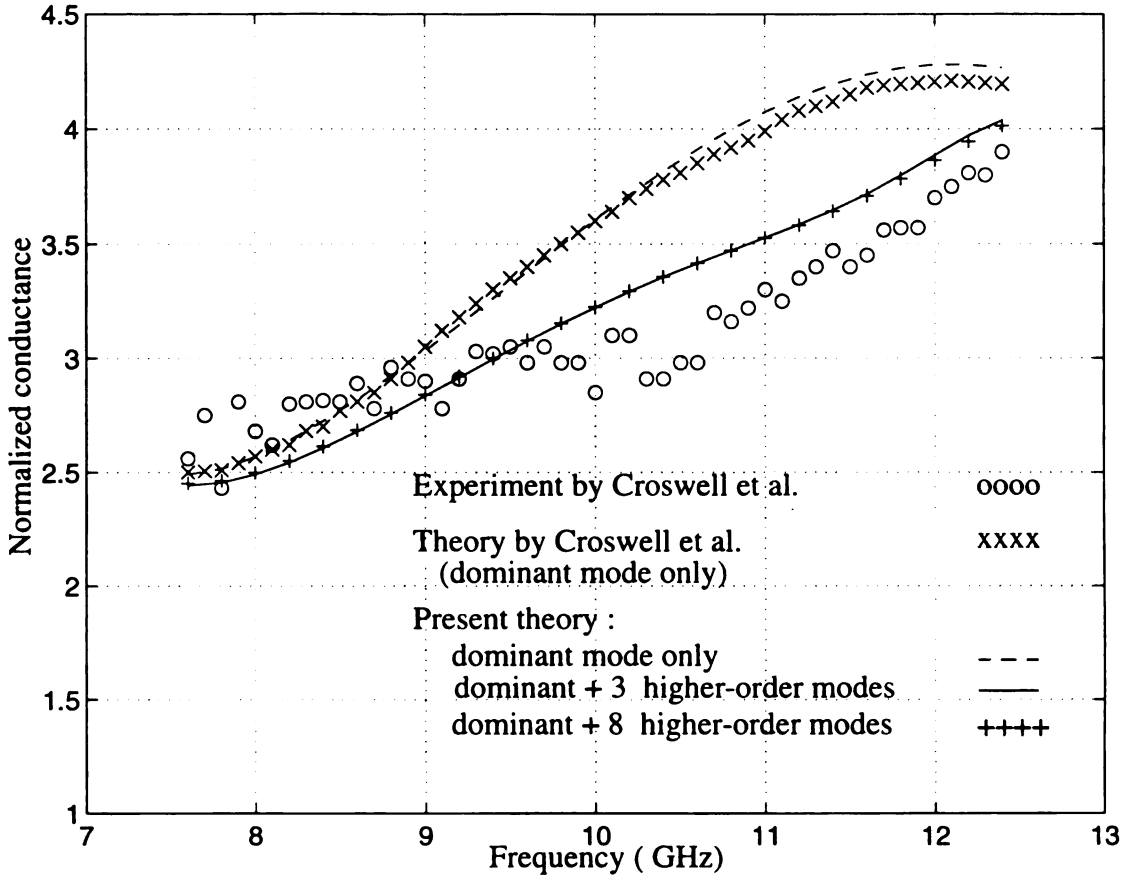

Figure 3.1(a) Input conductances of a waveguide probe ($a = 0.4$ *in*, $b = 0.9$ *in*) as a function of frequency when the probe is placed against a material layer with a dielectric constant of $\varepsilon_r = 3.76$ and a thickness of 0.1299 *in*. The comparisons are made between our numerical results and theoretical and experimental results of Croswell et al. [22].

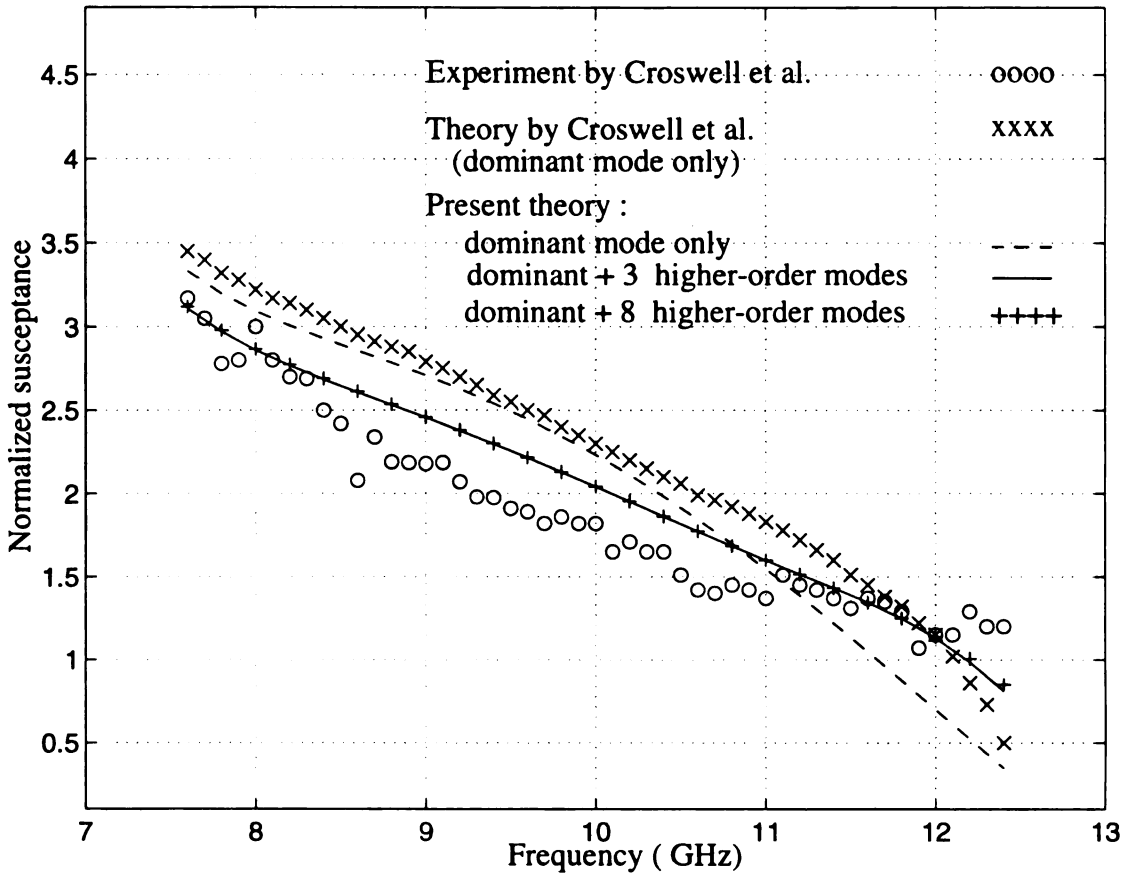

Figure 3.1(b) Input susceptances of a waveguide probe ($a = 0.4$ *in*, $b = 0.9$ *in*) as a function of frequency when the probe is placed against a material layer with a dielectric constant of $\varepsilon_r = 3.76$ and a thickness of 0.1299 *in*. The comparisons are made between our numerical results and theoretical and experimental results of Croswell et al. [22].

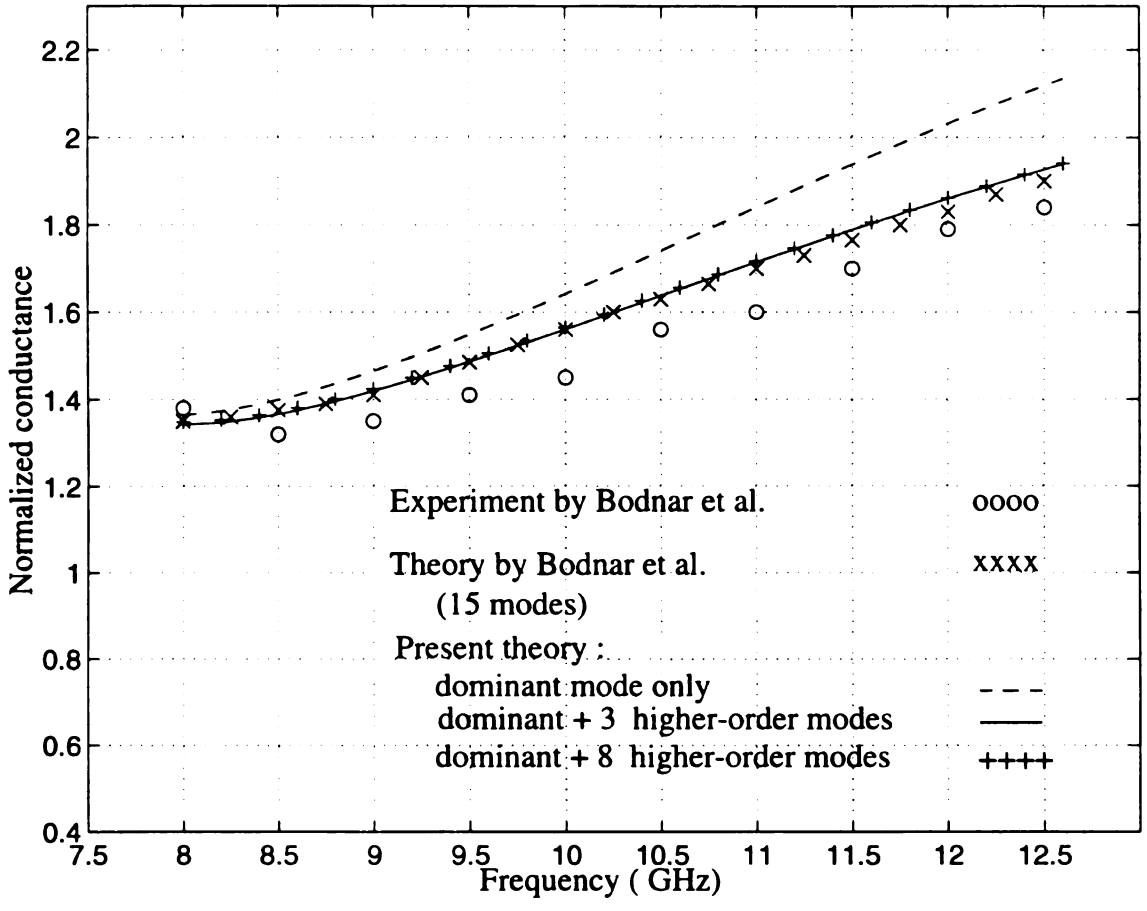

Figure 3.2(a) Input conductances of a waveguide probe ($a = 0.4$ *in*, $b = 0.9$ *in*) as a function of frequency when the probe is placed against a material layer with a dielectric constant of $\varepsilon_r = 2.25$ and a thickness of 0.3201 *cm*. The comparisons are made between our numerical results and theoretical and experimental results of Bodnar et al. [24].

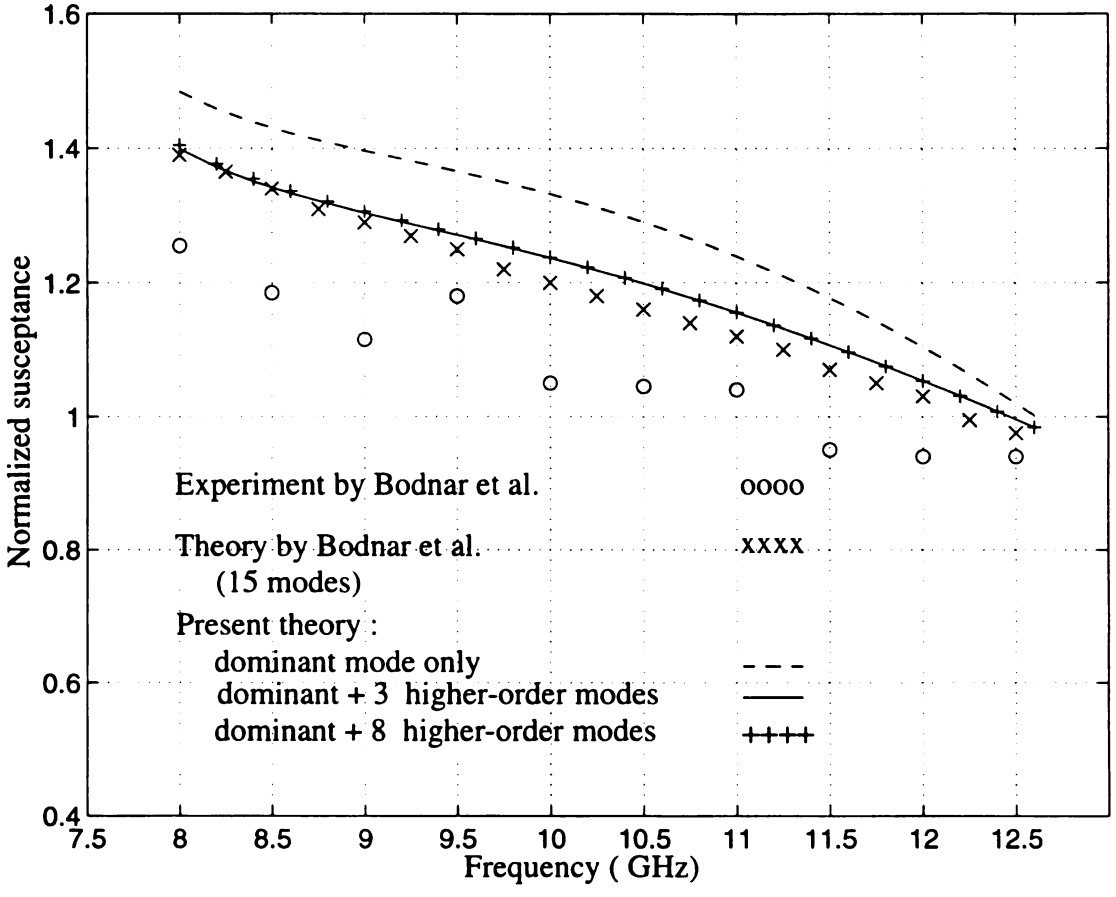

Figure 3.2(b) Input susceptances of a waveguide probe ($a = 0.4$ *in*, $b = 0.9$ *in*) as a function of frequency when the probe is placed against a material layer with a dielectric constant of $\varepsilon_r = 2.25$ and a thickness of 0.3201 *cm*. The comparisons are made between our numerical results and theoretical and experimental results of Bodnar et al. [24].

The last comparisons are shown in Figs. 3.3(a) and (b) which show the real and imaginary components of the input admittances of a waveguide probe that is open to free space. Our numerical results are compared to the theoretical results of Baudrand et al. [30] and the experimental results of Bondar et al. [24]. Our results using four modes and nine modes agree well with above published results.

In this chapter, we established a *forward* procedure for the theoretical study of measuring EM parameters of isotropic materials using an open-ended waveguide probe system. The accuracy of the technique and the validity of the computer program have been verified by comparing our numerical results with the published results.

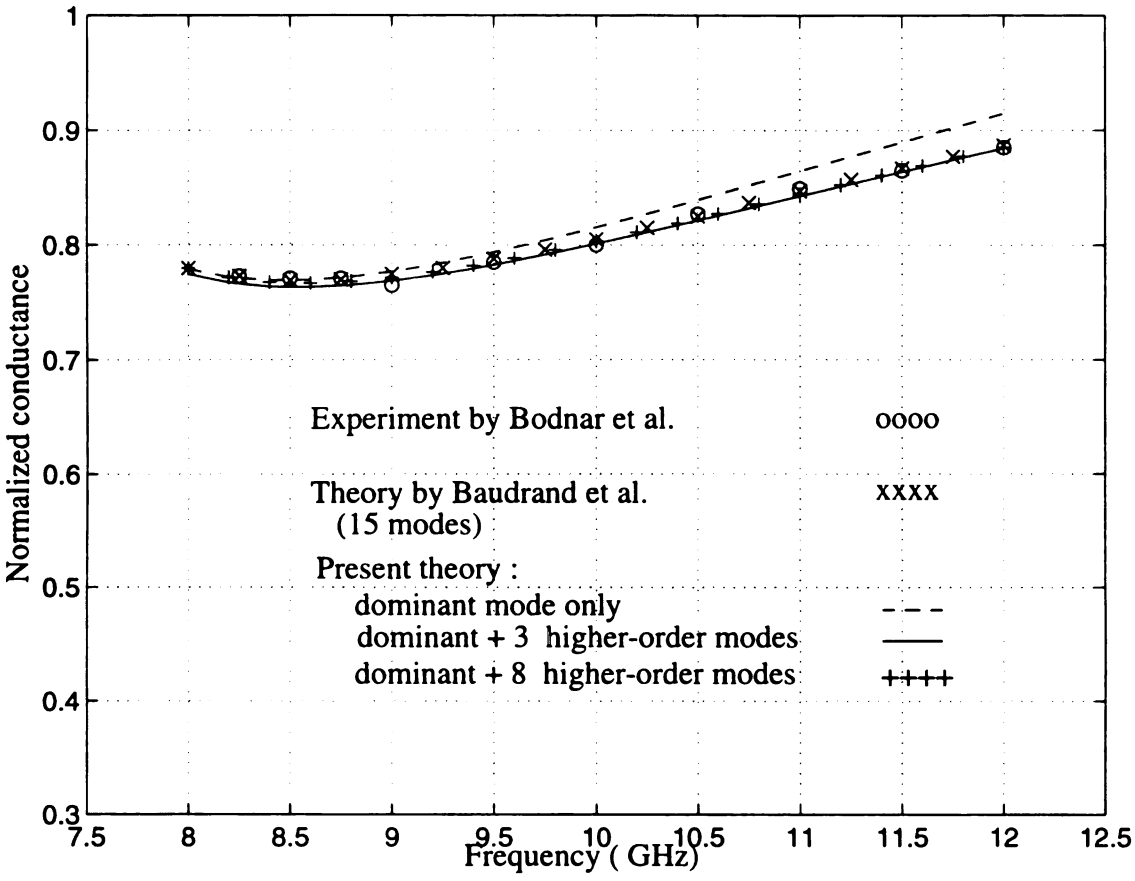

Figure 3.3(a) Input conductances of a waveguide probe ($a = 0.4$ *in*, $b = 0.9$ *in*) as a function of frequency when the probe is opening onto free space. The comparisons are made between our numerical results and theoretical of Baudrand et al. [30] and experimental results of Bodnar et al. [24].

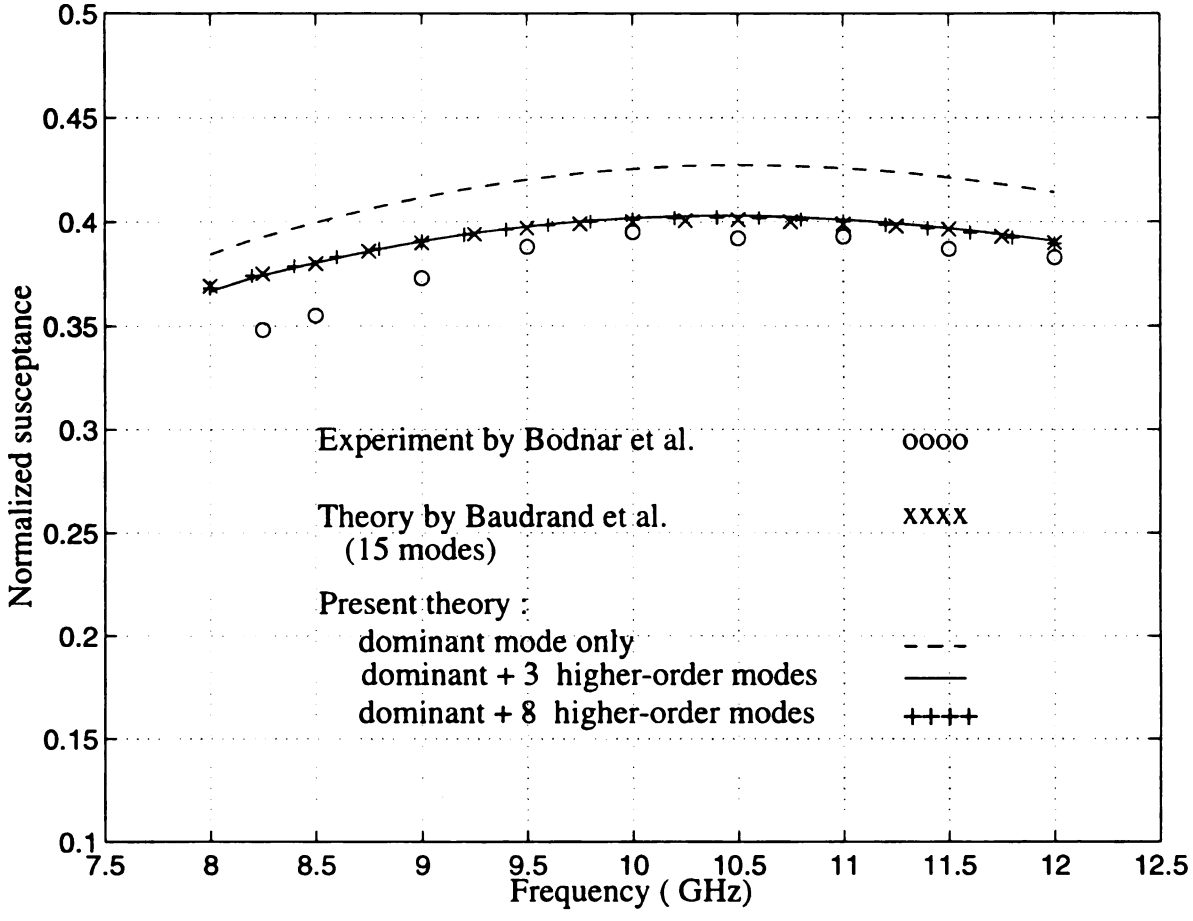

Figure 3.3(b) Input susceptances of a waveguide probe ($a = 0.4$ *in*, $b = 0.9$ *in*) as a function of frequency when the probe is opening onto free space. The comparisons are made between our numerical results and theoretical of Baudrand et al. [30] and experimental results of Bodnar et al. [24].

CHAPTER 4

OPEN-ENDED RECTANGULAR WAVEGUIDE PROBE TO MEASURE EM PROPERTIES OF ANISOTROPIC MATERIALS

4.1. Introduction

In Chapter 3 we have studied the *forward* procedure of the nondestructive measurement of material parameters using a waveguide probe system. However, it is limited to isotropic materials because the EM fields inside the material layer are expressed in terms of Hertzian potentials which are only suitable in an isotropic medium.

In this chapter we will employ the similar procedure to conduct the *forward* procedure for measuring the parameters of anisotropic materials using the transverse field method to express the EM fields inside the material layer. The EM fields derived with the transverse field method were presented in section 2.3. where a general case dealt with the fields inside an anisotropic medium and a degenerate case with the fields inside an isotropic medium. As presented in Chapter 3, after matching the boundary conditions at the discontinuity interfaces, two coupled electric field integral equations (EFIE's) for the aperture electric field can be obtained. Similarly, this chapter will include the derivation of the EFIE's, as well as the numerical solutions to these EFIE's. Also the numerical

examples illustrated in the preceding chapter will be recalculated and compared with the existing results to validate this technique.

The derivation of the coupled EFIE's for the aperture electric field is first presented in section 4.2.. After the EFIE's are derived, the reflection coefficient or other quantities of interest such as the input impedance or admittance of the waveguide probe can then be determined to be a function of the aperture electric field. In section 4.3. the method of moments is implemented to convert the EFIE's to a matrix equation. In that section, the elements of the matrix are evaluated in detail. Finally, some numerical results are compared to the published results by other workers to verify the accuracy of the technique. The numerical results on the input admittances of the waveguide probe attached to a layer of assumed known anisotropic material are also presented.

4.2. Coupled Integral Equations for Aperture Electric Field

Two coupled EFIE's via matching the tangential electric and magnetic fields at discontinuity interfaces are derived in this section. The EM fields inside the waveguide are given in the previous chapter, while the EM fields inside the material layer and the open free space are established based on the transverse field method as described in section 2.3..

4.2.1 Matching Boundary Conditions at z=t

Let's assume that the waveguide probe is placed against a layer of anisotropic material which is backed by open free space and has a tensor permittivity $\bar{\bar{\varepsilon}}$ and the free-space permeability μ_0.

Recalling from section 2.3., the spectrum-domain transverse EM fields inside an anisotropic medium can be expressed as

$$\begin{bmatrix} \tilde{E}_x \\ \tilde{E}_y \\ \eta_0\tilde{H}_x \\ \eta_0\tilde{H}_y \end{bmatrix} = A_1\vec{v}_1 e^{\lambda_1 z} + A_2\vec{v}_2 e^{\lambda_2 z} + A_3\vec{v}_3 e^{\lambda_3 z} + A_4\vec{v}_4 e^{\lambda_4 z} \tag{4.2.1}$$

and that inside the open free space as

$$\begin{bmatrix} \tilde{E}_{xa} \\ \tilde{E}_{ya} \\ \eta_0\tilde{H}_{xa} \\ \eta_0\tilde{H}_{ya} \end{bmatrix} = B_2\vec{v}_{2a} e^{-\lambda_a (z-t)} + B_4\vec{v}_{4a} e^{-\lambda_a (z-t)} \tag{4.2.2}$$

where the eigenvectors, $\vec{v}_n$ and $\vec{v}_{ma}$, are given as

$$\vec{v}_n = \begin{bmatrix} v_{n1} \\ v_{n2} \\ v_{n3} \\ v_{n4} \end{bmatrix} \qquad \vec{v}_{ma} = \begin{bmatrix} v_{m1a} \\ v_{m2a} \\ v_{m3a} \\ v_{m4a} \end{bmatrix}, \qquad \begin{matrix} n = 1, 2, 3, 4 \\ m = 2, 4 \end{matrix} \tag{4.2.3}$$

and A_1, A_2, A_3, A_4, B_2 and B_4 represent the unknown amplitudes of eigenmodes for both regions. Notice that these unknown quantities are all functions of k_x and k_y.

At $z = t$, the spectrum-domain transverse fields satisfy

$$\tilde{E}_x(k_x, k_y, t) = \tilde{E}_{xa}(k_x, k_y, t) \tag{4.2.4}$$

$$\tilde{E}_y(k_x, k_y, t) = \tilde{E}_{ya}(k_x, k_y, t) \tag{4.2.5}$$

$$\eta_0\tilde{H}_x(k_x, k_y, t) = \eta_0\tilde{H}_{xa}(k_x, k_y, t) \tag{4.2.6}$$

$$\eta_0\tilde{H}_y(k_x, k_y, t) = \eta_0\tilde{H}_{ya}(k_x, k_y, t) \tag{4.2.7}$$

Substitute eq. (4.2.3) into eqs. (4.2.1) and (4.2.2) and define the following notations for the field components as

$$
\begin{aligned}
r_{11} &\equiv v_{11}e^{\lambda_1 t}, & r_{21} &\equiv v_{12}e^{\lambda_1 t} \\
r_{12} &\equiv v_{21}e^{\lambda_2 t}, & r_{22} &\equiv v_{22}e^{\lambda_2 t} \\
r_{13} &\equiv v_{31}e^{\lambda_3 t}, & r_{23} &\equiv v_{32}e^{\lambda_3 t} \\
r_{14} &\equiv v_{41}e^{\lambda_4 t}, & r_{24} &\equiv v_{42}e^{\lambda_4 t} \\
r_{15} &\equiv v_{21a}, & r_{25} &\equiv v_{22a} \\
r_{16} &\equiv v_{41a}, & r_{26} &\equiv v_{42a} \\
r_{31} &\equiv v_{13}e^{\lambda_1 t}, & r_{41} &\equiv v_{14}e^{\lambda_1 t} \\
r_{32} &\equiv v_{23}e^{\lambda_2 t}, & r_{42} &\equiv v_{24}e^{\lambda_2 t} \\
r_{33} &\equiv v_{33}e^{\lambda_3 t}, & r_{43} &\equiv v_{34}e^{\lambda_3 t} \\
r_{34} &\equiv v_{43}e^{\lambda_4 t}, & r_{44} &\equiv v_{44}e^{\lambda_4 t} \\
r_{35} &\equiv v_{23a}, & r_{45} &\equiv v_{24a} \\
r_{36} &\equiv v_{43a}, & r_{46} &\equiv v_{44a}
\end{aligned}
\tag{4.2.8}
$$

Then eqs. (4.2.4) to (4.2.7) can be rewritten as

$$A_1 r_{11} + A_2 r_{12} + A_3 r_{13} + A_4 r_{14} = B_2 r_{15} + B_4 r_{16} \tag{4.2.9}$$

$$A_1 r_{21} + A_2 r_{22} + A_3 r_{23} + A_4 r_{24} = B_2 r_{25} + B_4 r_{26} \tag{4.2.10}$$

$$A_1 r_{31} + A_2 r_{32} + A_3 r_{33} + A_4 r_{34} = B_2 r_{35} + B_4 r_{36} \tag{4.2.11}$$

$$A_1 r_{41} + A_2 r_{42} + A_3 r_{43} + A_4 r_{44} = B_2 r_{45} + B_4 r_{46} \tag{4.2.12}$$

If we transfer all the terms with unknown amplitudes A_1 and A_2 on the left-hand side of the equations to the right-hand side and transfer the terms with B_2 and B_4 on the right-hand side to the left-hand side of the equations, we have

$$A_3 r_{13} + A_4 r_{14} - B_2 r_{15} - B_4 r_{16} = -A_1 r_{11} - A_2 r_{12} \tag{4.2.13}$$

$$A_3 r_{23} + A_4 r_{24} - B_2 r_{25} - B_4 r_{26} = -A_1 r_{21} - A_2 r_{22} \tag{4.2.14}$$

$$A_3 r_{33} + A_4 r_{34} - B_2 r_{35} - B_4 r_{36} = -A_1 r_{31} - A_2 r_{32} \tag{4.2.15}$$

$$A_3 r_{43} + A_4 r_{44} - B_2 r_{45} - B_4 r_{46} = -A_1 r_{41} - A_2 r_{42} \tag{4.2.16}$$

To eliminate the unknown quantity $B_2(k_x, k_y)$ first, subtract eq. (4.2.13) multiplied by r_{45} from eq. (4.2.16) multiplied by r_{15}:

$$A_3 (r_{15} r_{43} - r_{13} r_{45}) + A_4 (r_{15} r_{44} - r_{14} r_{45}) + B_4 (r_{16} r_{45} - r_{15} r_{46}) = A_1 (r_{11} r_{45} - r_{15} r_{41}) + A_2 (r_{12} r_{45} - r_{15} r_{42}) \tag{4.2.17}$$

Subtracting eq. (4.2.14) multiplied by r_{45} from eq. (4.2.16) multiplied by r_{25} yields

$$A_3 (r_{25} r_{43} - r_{23} r_{45}) + A_4 (r_{25} r_{44} - r_{24} r_{45}) + B_4 (r_{26} r_{45} - r_{25} r_{46}) = A_1 (r_{21} r_{45} - r_{25} r_{41}) + A_2 (r_{22} r_{45} - r_{25} r_{42}) \tag{4.2.18}$$

Subtracting eq. (4.2.15) multiplied by r_{45} from eq. (4.2.16) multiplied by r_{35} yields

$$A_3 (r_{35} r_{43} - r_{33} r_{45}) + A_4 (r_{35} r_{44} - r_{34} r_{45}) + B_4 (r_{36} r_{45} - r_{35} r_{46}) = A_1 (r_{31} r_{45} - r_{35} r_{41}) + A_2 (r_{32} r_{45} - r_{35} r_{42}) \tag{4.2.19}$$

By defining the following notations

$$r_a \equiv r_{15} r_{43} - r_{13} r_{45}, \qquad r_i \equiv r_{21} r_{45} - r_{25} r_{41}$$

$$r_b \equiv r_{15} r_{44} - r_{14} r_{45}, \qquad r_j \equiv r_{22} r_{45} - r_{25} r_{42}$$

$$r_c \equiv r_{16} r_{45} - r_{15} r_{46}, \qquad r_k \equiv r_{35} r_{43} - r_{33} r_{45}$$

$$r_d \equiv r_{11}r_{45} - r_{15}r_{41}, \qquad r_l \equiv r_{35}r_{44} - r_{34}r_{45} \tag{4.2.20}$$

$$r_e \equiv r_{12}r_{45} - r_{15}r_{42}, \qquad r_m \equiv r_{36}r_{45} - r_{35}r_{46}$$

$$r_f \equiv r_{25}r_{43} - r_{23}r_{45}, \qquad r_n \equiv r_{31}r_{45} - r_{35}r_{41}$$

$$r_g \equiv r_{25}r_{44} - r_{24}r_{45}, \qquad r_o \equiv r_{32}r_{45} - r_{35}r_{42}$$

$$r_h \equiv r_{26}r_{45} - r_{25}r_{46},$$

eqs. (4.2.17) to (4.2.19) are simplified to

$$A_3 r_a + A_4 r_b + B_4 r_c = A_1 r_d + A_2 r_e \tag{4.2.21}$$

$$A_3 r_f + A_4 r_g + B_4 r_h = A_1 r_i + A_2 r_j \tag{4.2.22}$$

$$A_3 r_k + A_4 r_l + B_4 r_m = A_1 r_n + A_2 r_o \tag{4.2.23}$$

Similarly, $B_4\,(k_x, k_y)$ can be eliminated from eqs. (4.2.21) to (4.2.23) to give

$$A_3\,(r_a r_h - r_c r_f) + A_4\,(r_b r_h - r_c r_g) = A_1\,(r_d r_h - r_c r_i) + A_2\,(r_e r_h - r_c r_j) \tag{4.2.24}$$

$$A_3\,(r_a r_m - r_c r_k) + A_4\,(r_b r_m - r_c r_l) = A_1\,(r_d r_m - r_c r_n) + A_2\,(r_e r_m - r_c r_o) \tag{4.2.25}$$

Let us define

$$r_p \equiv r_a r_h - r_c r_f, \qquad r_v \equiv r_a r_m - r_c r_k$$

$$r_q \equiv r_b r_h - r_c r_g, \qquad r_w \equiv r_b r_m - r_c r_l \tag{4.2.26}$$

$$r_r \equiv r_d r_h - r_c r_i, \qquad r_x \equiv r_d r_m - r_c r_n$$

$$r_u \equiv r_e r_h - r_c r_j, \qquad r_y \equiv r_e r_m - r_c r_o$$

and rewrite eqs. (4.2.24) and (4.2.25) as a form of

$$A_3 r_p + A_4 r_q = A_1 r_r + A_2 r_u \tag{4.2.27}$$

$$A_3 r_v + A_4 r_w = A_1 r_x + A_2 r_y \tag{4.2.28}$$

Now, using eqs. (4.2.27) and (4.2.28), two unknown quantities $A_3(k_x, k_y)$ and $A_4(k_x, k_y)$ can be expressed in terms of $A_1(k_x, k_y)$ and $A_2(k_x, k_y)$ as follows:

$$A_3(k_x, k_y) = A_1\left(\frac{r_r r_w - r_q r_x}{r_p r_w - r_q r_v}\right) + A_2\left(\frac{r_u r_w - r_q r_y}{r_p r_w - r_q r_v}\right) \equiv A_1 r_1 + A_2 r_2 \tag{4.2.29}$$

$$A_4(k_x, k_y) = A_1\left(\frac{r_p r_x - r_r r_v}{r_p r_w - r_q r_v}\right) + A_2\left(\frac{r_p r_y - r_u r_v}{r_p r_w - r_q r_v}\right) \equiv A_1 r_3 + A_2 r_4 \tag{4.2.30}$$

Substituting eqs. (4.2.29) and (4.2.30) back into eq. (4.2.1) yields

$$\begin{bmatrix} \tilde{E}_x \\ \tilde{E}_y \\ \eta_0 \tilde{H}_x \\ \eta_0 \tilde{H}_y \end{bmatrix} = A_1\left(\vec{v}_1 e^{\lambda_1 z} + r_1 \vec{v}_3 e^{\lambda_3 z} + r_3 \vec{v}_4 e^{\lambda_4 z}\right) + A_2\left(\vec{v}_2 e^{\lambda_2 z} + r_2 \vec{v}_3 e^{\lambda_3 z} + r_4 \vec{v}_4 e^{\lambda_4 z}\right) \tag{4.2.31}$$

It is important to note that to derive these formulas for numerical calculations, it needs to avoid creating singularities during the process of elimination of a term from a set of equations. Once a singularity occurs in the elimination process, an alternative process needs to be found. Since the process of choosing an alternative elimination is straightforward and explicit, it will be considered directly in the computer program.

4.2.2 Matching Boundary Conditions at Waveguide Aperture

Equation (4.2.31) indicates that the spectrum-domain transverse fields inside a material layer are expressed in terms of two unknown quantities only. If the aperture fields are studied (i.e. at $z = 0$) and the electric field is chosen as the reference, the two unknown quantities can be represented as functions of the aperture electric field first. Then the aperture magnetic field at the material side can be expressed in terms of the aperture electric field in terms of these two unknown quantities. Recalling from section 3.2.2 that the aperture magnetic field at the waveguide side can also be expressed in terms

of the aperture electric field. As a result, two coupled EFIE's for the aperture electric field can be derived after matching the tangential magnetic fields at the waveguide aperture.

By eq. (4.2.8), eigenvectors $\vec{v}_1$, $\vec{v}_2$, $\vec{v}_3$ and $\vec{v}_4$ can be rewritten as

$$\vec{v}_1 = \begin{bmatrix} r_{11} \\ r_{21} \\ r_{31} \\ r_{41} \end{bmatrix} e^{-\lambda_1 t}, \qquad \vec{v}_2 = \begin{bmatrix} r_{12} \\ r_{22} \\ r_{32} \\ r_{42} \end{bmatrix} e^{\lambda_1 t}, \qquad \vec{v}_3 = \begin{bmatrix} r_{13} \\ r_{23} \\ r_{33} \\ r_{43} \end{bmatrix} e^{-\lambda_3 t}, \qquad \vec{v}_4 = \begin{bmatrix} r_{14} \\ r_{24} \\ r_{34} \\ r_{44} \end{bmatrix} e^{\lambda_3 t}.$$

This leads the spectrum-domain transverse fields in eq. (4.2.31) to an alternative form as

$$\begin{bmatrix} \tilde{E}_x \\ \tilde{E}_y \\ \eta_0 \tilde{H}_x \\ \eta_0 \tilde{H}_y \end{bmatrix} = A_1 \left(\begin{bmatrix} r_{11} \\ r_{21} \\ r_{31} \\ r_{41} \end{bmatrix} e^{\lambda_1 (z-t)} + r_1 \begin{bmatrix} r_{13} \\ r_{23} \\ r_{33} \\ r_{43} \end{bmatrix} e^{\lambda_3 (z-t)} + r_3 \begin{bmatrix} r_{14} \\ r_{24} \\ r_{34} \\ r_{44} \end{bmatrix} e^{-\lambda_3 (z-t)} \right)$$

$$+ A_2 \left(\begin{bmatrix} r_{12} \\ r_{22} \\ r_{32} \\ r_{42} \end{bmatrix} e^{-\lambda_1 (z-t)} + r_2 \begin{bmatrix} r_{13} \\ r_{23} \\ r_{33} \\ r_{43} \end{bmatrix} e^{\lambda_3 (z-t)} + r_4 \begin{bmatrix} r_{14} \\ r_{24} \\ r_{34} \\ r_{44} \end{bmatrix} e^{-\lambda_3 (z-t)} \right) \tag{4.2.32}$$

Let's write out the spectrum-domain aperture electric field components (at $z = 0$) as

$$\tilde{E}_x(k_x, k_y, 0) = A_1 \left[r_{11} e^{-\lambda_1 t} + r_1 r_{13} e^{-\lambda_3 t} + r_3 r_{14} e^{\lambda_3 t} \right]$$
$$+ A_2 \left[r_{12} e^{\lambda_1 t} + r_2 r_{13} e^{-\lambda_3 t} + r_4 r_{14} e^{\lambda_3 t} \right] \tag{4.2.33}$$

$$\tilde{E}_y(k_x, k_y, 0) = A_1 \left[r_{21} e^{-\lambda_1 t} + r_1 r_{23} e^{-\lambda_3 t} + r_3 r_{24} e^{\lambda_3 t} \right]$$
$$+ A_2 \left[r_{22} e^{\lambda_1 t} + r_2 r_{23} e^{-\lambda_3 t} + r_4 r_{24} e^{\lambda_3 t} \right] \tag{4.2.34}$$

If we define

$$C_1(k_x, k_y) \equiv r_{11}e^{-\lambda_1 t} + r_1 r_{13}e^{-\lambda_3 t} + r_3 r_{14}e^{\lambda_3 t} \tag{4.2.35}$$

$$C_2(k_x, k_y) \equiv r_{12}e^{\lambda_1 t} + r_2 r_{13}e^{-\lambda_3 t} + r_4 r_{14}e^{\lambda_3 t} \tag{4.2.36}$$

$$C_3(k_x, k_y) \equiv r_{21}e^{-\lambda_1 t} + r_1 r_{23}e^{-\lambda_3 t} + r_3 r_{24}e^{\lambda_3 t} \tag{4.2.37}$$

$$C_4(k_x, k_y) \equiv r_{22}e^{\lambda_1 t} + r_2 r_{23}e^{-\lambda_3 t} + r_4 r_{24}e^{\lambda_3 t} \tag{4.2.38}$$

and employ the definition of the inverse Fourier transform of the aperture fields, eqs. (4.2.33) and (4.2.34) become

$$\int_{-\infty}^{\infty}\int E_x(x, y, 0)\, e^{-jk_x x} e^{-jk_y y} dxdy = A_1 \cdot C_1 + A_2 \cdot C_2 \tag{4.2.39}$$

$$\int_{-\infty}^{\infty}\int E_y(x, y, 0)\, e^{-jk_x x} e^{-jk_y y} dxdy = A_1 \cdot C_3 + A_2 \cdot C_4 \tag{4.2.40}$$

As mentioned in the preceding chapter, since the aperture electric field components, $E_{xo} = E_x(x, y, 0)$ and $E_{yo} = E_y(x, y, 0)$, only exist over the aperture region $0<x<a$, $0<y<b$, and vanish on the flange, the double infinite integrals can be replaced by the two double finite integrals as

$$\int_0^b\int_0^a E_{xo} e^{-jk_x x} e^{-jk_y y} dxdy = A_1 \cdot C_1 + A_2 \cdot C_2 \tag{4.2.41}$$

$$\int_0^b\int_0^a E_{yo} e^{-jk_x x} e^{-jk_y y} dxdy = A_1 \cdot C_3 + A_2 \cdot C_4 \tag{4.2.42}$$

Let's denote

$$\iint E_{xo}^{e} \equiv \int_{0}^{b}\int_{0}^{a} E_{xo} e^{-jk_x x} e^{-jk_y y} dxdy \tag{4.2.43}$$

$$\iint E_{yo}^{e} \equiv \int_{0}^{b}\int_{0}^{a} E_{yo} e^{-jk_x x} e^{-jk_y y} dxdy \tag{4.2.44}$$

and substitute back into eqs. (4.2.41) and (4.2.42) to solve for the unknown quantities $A_1(k_x, k_y)$ and $A_2(k_x, k_y)$. We have

$$A_1(k_x, k_y) = \frac{1}{C_1 C_4 - C_2 C_3}\left[C_4 \iint E_{xo}^{e} - C_2 \iint E_{yo}^{e}\right] \tag{4.2.45}$$

$$A_2(k_x, k_y) = \frac{-1}{C_1 C_4 - C_2 C_3}\left[C_3 \iint E_{xo}^{e} - C_1 \iint E_{yo}^{e}\right] \tag{4.2.46}$$

Similarly, the aperture magnetic fields can be derived by defining

$$D_1(k_x, k_y) \equiv r_{31} e^{-\lambda_1 t} + r_1 r_{33} e^{-\lambda_3 t} + r_3 r_{34} e^{\lambda_3 t} \tag{4.2.47}$$

$$D_2(k_x, k_y) \equiv r_{32} e^{\lambda_1 t} + r_2 r_{33} e^{-\lambda_3 t} + r_4 r_{34} e^{\lambda_3 t} \tag{4.2.48}$$

$$D_3(k_x, k_y) \equiv r_{41} e^{-\lambda_1 t} + r_1 r_{43} e^{-\lambda_3 t} + r_3 r_{44} e^{\lambda_3 t} \tag{4.2.49}$$

$$D_4(k_x, k_y) \equiv r_{42} e^{\lambda_1 t} + r_2 r_{43} e^{-\lambda_3 t} + r_4 r_{44} e^{\lambda_3 t} \tag{4.2.50}$$

and taking the two-dimensional inverse Fourier transform of the spectrum-domain magnetic field components given in eq. (4.2.32) after substituting $z = 0$. We obtain

$$H_x(x, y)\Big|_{z=0^+} = \left(\frac{1}{2\pi}\right)^2 \frac{1}{\eta_0} \int_{-\infty}^{\infty}\int [A_1 \cdot D_1 + A_2 \cdot D_2] e^{jk_x x} e^{jk_y y} dk_x dk_y \tag{4.2.51}$$

$$H_y(x, y)\Big|_{z=0^+} = \left(\frac{1}{2\pi}\right)^2 \frac{1}{\eta_0} \int_{-\infty}^{\infty}\int [A_1 \cdot D_3 + A_2 \cdot D_4] e^{jk_x x} e^{jk_y y} dk_x dk_y \tag{4.2.52}$$

Substituting eqs. (4.2.45) and (4.2.46) into above two equations yields

$$H_x\Big|_{z=0^+} = \frac{j}{\omega\mu}\int_{-\infty}^{\infty}\int e^{jk_x x}e^{jk_y y}\left[M_y(k_x,k_y)\iint E_{xo}^e + N_y(k_x,k_y)\iint E_{yo}^e\right]dk_x dk_y \qquad (4.2.53)$$

$$H_y\Big|_{z=0^+} = \frac{-j}{\omega\mu}\int_{-\infty}^{\infty}\int e^{jk_x x}e^{jk_y y}\left[N_x(k_y,k_x)\iint E_{xo}^e + M_x(k_y,k_x)\iint E_{yo}^e\right]dk_x dk_y \qquad (4.2.54)$$

where

$$M_y(k_x,k_y) \equiv \frac{\omega\mu}{j\eta_0(2\pi)^2}\frac{C_4D_1 - C_3D_2}{C_1C_4 - C_2C_3}, \quad N_y(k_x,k_y) \equiv \frac{\omega\mu}{j\eta_0(2\pi)^2}\frac{C_1D_2 - C_2D_1}{C_1C_4 - C_2C_3}$$

$$N_x(k_x,k_y) \equiv \frac{\omega\mu}{j\eta_0(2\pi)^2}\frac{C_3D_4 - C_4D_3}{C_1C_4 - C_2C_3}, \quad M_x(k_x,k_y) \equiv \frac{\omega\mu}{j\eta_0(2\pi)^2}\frac{C_2D_3 - C_1D_4}{C_1C_4 - C_2C_3} \qquad (4.2.55)$$

Recalling from section 3.2.2 that the aperture magnetic field components in the waveguide side are derived as

$$H_x\Big|_{z=0^-} = \frac{1}{\omega\mu_0 ab}\Bigg(2b\pi\omega\mu_0\Gamma_{10}\sin\left(\frac{\pi x}{a}\right) - j2\Gamma_{10}\sin\left(\frac{\pi x}{a}\right)\int_0^b\int_0^a E_{yo}\sin\left(\frac{\pi x'}{a}\right)dx'dy'$$
$$+\sum_{n'}\sum_{m'}\frac{j4\varepsilon_{n'm'}}{\Gamma_{n'm'}}\sin\left(\frac{n'\pi x}{a}\right)\cos\left(\frac{m'\pi y}{b}\right)\left[\left(\frac{n'\pi}{a}\right)\left(\frac{m'\pi}{b}\right)\iint E_{xo}\right.$$
$$\left.+\left[k_0^2 - \left(\frac{n'\pi}{a}\right)^2\right]\iint E_{yo}\right]\Bigg) \qquad (4.2.56)$$

$$H_y\Big|_{z=0^-} = \sum_{n'}\sum_{m'}\frac{-j4\varepsilon_{n'm'}}{ab\omega\mu_0\Gamma_{n'm'}}\cos\left(\frac{n'\pi x}{a}\right)\sin\left(\frac{m'\pi y}{b}\right)\left(\left[k_0^2 - \left(\frac{m'\pi}{b}\right)^2\right]\iint E_{xo}\right.$$
$$\left.+\left(\frac{n'\pi}{a}\right)\left(\frac{m'\pi}{b}\right)\iint E_{yo}\right) \qquad (4.2.57)$$

where

$$\varepsilon_{n'm'} \equiv \frac{\left(\frac{n'\pi}{a}\right)^2 + \left(\frac{m'\pi}{b}\right)^2}{\varepsilon_{m'}\left(\frac{n'\pi}{a}\right)^2 + \varepsilon_{n'}\left(\frac{m'\pi}{b}\right)^2} \tag{4.2.58}$$

$$\iint E_{xo} \equiv \int_0^b \int_0^a E_{xo} \cos\left(\frac{n'\pi x}{a}\right) \sin\left(\frac{m'\pi y}{b}\right) dx dy \tag{4.2.59}$$

$$\iint E_{yo} \equiv \int_0^b \int_0^a E_{yo} \sin\left(\frac{n'\pi x}{a}\right) \cos\left(\frac{m'\pi y}{b}\right) dx dy \tag{4.2.60}$$

$$\varepsilon_{n'} \equiv \begin{cases} 2 & n' = 0 \\ 1 & n' \neq 0 \end{cases}, \qquad \varepsilon_{m'} \equiv \begin{cases} 2 & m' = 0 \\ 1 & m' \neq 0 \end{cases} \tag{4.2.61}$$

Since the tangential magnetic field components, H_x and H_y, are continuous at the aperture plane, $z = 0$, the equality of eqs. (4.2.53) and (4.2.56), and that of eqs. (4.2.54) and (4.2.57) will yield two coupled integral equations for the aperture electric fields. We have

For $H_x\big|_{z=0^-} = H_x\big|_{z=0^+}$,

$$\frac{2\Gamma_{10}}{ab}\left(\frac{\mu}{\mu_0}\right)\sin\left(\frac{\pi x}{a}\right)\int_0^b \int_0^a E_{yo} \sin\left(\frac{\pi x'}{a}\right) dx' dy' - \sum_{n'} \sum_{m'} \frac{4\varepsilon_{n'm'}}{ab\Gamma_{n'm'}}\left(\frac{\mu}{\mu_0}\right) \times$$

$$\sin\left(\frac{n'\pi x}{a}\right)\cos\left(\frac{m'\pi y}{b}\right)\left[\left(\frac{n'\pi}{a}\right)\left(\frac{m'\pi}{b}\right)\iint E_{xo} + \left(k_0^2 - \left(\frac{n'\pi}{a}\right)^2\right)\iint E_{yo}\right]$$

$$+ \int_{-\infty}^{\infty}\int e^{jk_x x} e^{jk_y y}\left[M_y(k_x, k_y)\iint E^e_{xo} + N_y(k_x, k_y)\iint E^e_{yo}\right] dk_x dk_y = C\sin\left(\frac{\pi x}{a}\right) \tag{4.2.62}$$

and for $H_y\big|_{z=0^-} = H_y\big|_{z=0^+}$,

$$\sum_{n'}\sum_{m'}\frac{-4\varepsilon_{n'm'}}{ab\Gamma_{n'm'}}\left(\frac{\mu}{\mu_0}\right)\cos\left(\frac{n'\pi x}{a}\right)\sin\left(\frac{m'\pi y}{b}\right)\left(\left[k_0^2-\left(\frac{m'\pi}{b}\right)^2\right]\iint E_{xo}+\left(\frac{n'\pi}{a}\right)\left(\frac{m'\pi}{b}\right)\iint E_{yo}\right)$$

$$+\int_{-\infty}^{\infty}\int e^{jk_x x}e^{jk_y y}\left[N_x(k_y,k_x)\iint E_{xo}^{e}+M_x(k_y,k_x)\iint E_{yo}^{e}\right]dk_x dk_y = 0 \quad (4.2.63)$$

where

$$C \equiv -j\frac{2\pi}{a}\omega\mu\Gamma_{10} \quad (4.2.64)$$

Equations (4.2.62) and (4.2.63) are the two coupled integral equations for the aperture electric field components, E_{xo} and E_{yo}. These EFIE's are the key equations to be used for further development.

4.3. Numerical Simulation

In this section the similar scheme used in seçtion 3.3. will be employed to solve two coupled EFIE's for the aperture electric field. As mentioned before, the unknown aperture electric field is expressed as a sum of incident and reflected dominant mode and a number of higher order modes due to the discontinuity presented at the aperture.

In section 4.3.1, the method of moments is employed to convert the EFIE's to a matrix equation. This matrix equation is then solved by the Galerkin's method using the waveguide eigenmodes as the basis and testing functions . Section 4.3.2 develops formulas which are needed in carrying out the numerical calculation of the matrix equation transforming from rectangular coordinates into cylindrical coordinates. Finally, section 4.3.3 presents numerical results compared to the published results to verify the accuracy of this technique.

4.3.1 Application of Method of Moments

The coupled integral equations given in eqs. (4.2.62) and (4.2.63) for the unknown aperture electric field components are solved by using the moment method technique. The unknown aperture electric field components are first expanded into a set of appropriately chosen basis functions $\{e_\beta(x, y)\}$. Since the aperture fields of a waveguide can be expressed as a sum of a dominant mode and a number of higher order modes, the appropriate basis functions are the eigenmodes of the waveguide. Let us expand the unknown aperture electric field components into two finite sums of eigenmodes of the waveguide as follows:

$$E_{xo}(x, y) = \sum_\beta a_\beta e_\beta^x(x, y) \tag{4.3.1}$$

$$E_{yo}(x, y) = \sum_\beta b_\beta e_\beta^y(x, y) \tag{4.3.2}$$

where $\sum_\beta$ stands for $\sum_p \sum_q$ for summation of all possible higher order modes which have mode indices $[p, q]$ with $p, q = 1, 2, 3, \ldots$. The set of basis functions are expressed as

$$e_\beta^x(x, y) \equiv \cos\left[\frac{p\pi x}{a}\right] \sin\left[\frac{q\pi y}{b}\right] \tag{4.3.3}$$

$$e_\beta^y(x, y) \equiv \sin\left[\frac{p\pi x}{a}\right] \cos\left[\frac{q\pi y}{b}\right] \tag{4.3.4}$$

Substituting eqs. (4.3.1) and (4.3.2) into the coupled EFIE's yields

$$\sum_\beta a_\beta \cdot \left[W_{dx}^x + W_{cx}^x\right] + \sum_\beta b_\beta \cdot \left[W_{dx}^y + W_{cx}^y\right] = 0 \tag{4.3.5}$$

$$\sum_\beta a_\beta \cdot \left[W_{dy}^x + W_{cy}^x\right] + \sum_\beta b_\beta \cdot \left[W_{dy}^y + W_{cy}^y\right] = C\sin\left(\frac{\pi x}{a}\right) \tag{4.3.6}$$

where

$$W_{dx}^{x} \equiv \sum_{n'}\sum_{m'} \frac{-4\varepsilon_{n'm'}}{ab\Gamma_{n'm'}}\left(\frac{\mu}{\mu_0}\right)\cos\left(\frac{n'\pi x}{a}\right)\sin\left(\frac{m'\pi y}{b}\right)\left[k_0^2-\left(\frac{m'\pi}{b}\right)^2\right]\iint e_x \tag{4.3.7}$$

$$W_{cx}^{x} \equiv \int_{-\infty}^{\infty}\int e^{jk_x x}e^{jk_y y}N_x(k_y, k_x)\left(\iint e_x^e\right)dk_x dk_y \tag{4.3.8}$$

$$W_{dx}^{y} \equiv \sum_{n'}\sum_{m'} \frac{-4\varepsilon_{n'm'}}{ab\Gamma_{n'm'}}\left(\frac{\mu}{\mu_0}\right)\cos\left(\frac{n'\pi x}{a}\right)\sin\left(\frac{m'\pi y}{b}\right)\left(\frac{n'\pi}{a}\right)\left(\frac{m'\pi}{b}\right)\iint e_y \tag{4.3.9}$$

$$W_{cx}^{y} \equiv \int_{-\infty}^{\infty}\int e^{jk_x x}e^{jk_y y}M_x(k_y, k_x)\left(\iint e_y^e\right)dk_x dk_y \tag{4.3.10}$$

$$W_{dy}^{x} \equiv \sum_{n'}\sum_{m'} \frac{-4\varepsilon_{n'm'}}{ab\Gamma_{n'm'}}\left(\frac{\mu}{\mu_0}\right)\sin\left(\frac{n'\pi x}{a}\right)\cos\left(\frac{m'\pi y}{b}\right)\left(\frac{n'\pi}{a}\right)\left(\frac{m'\pi}{b}\right)\iint e_x \tag{4.3.11}$$

$$W_{cy}^{x} \equiv \int_{-\infty}^{\infty}\int e^{jk_x x}e^{jk_y y}M_y(k_x, k_y)\left(\iint e_x^e\right)dk_x dk_y \tag{4.3.12}$$

$$\begin{aligned} W_{dy}^{y} \equiv{}& \frac{2\Gamma_{10}}{ab}\left(\frac{\mu}{\mu_0}\right)\sin\left(\frac{\pi x}{a}\right)\int_0^b\int_0^a e_\beta^y(x', y')\sin\left(\frac{\pi x'}{a}\right)dx'dy' \\ &+ \sum_{n'}\sum_{m'} \frac{-4\varepsilon_{n'm'}}{ab\Gamma_{n'm'}}\left(\frac{\mu}{\mu_0}\right)\sin\left(\frac{n'\pi x}{a}\right)\cos\left(\frac{m'\pi y}{b}\right)\left[k_0^2-\left(\frac{n'\pi}{a}\right)^2\right]\iint e_y \end{aligned} \tag{4.3.13}$$

$$W_{cy}^{y} \equiv \int_{-\infty}^{\infty}\int e^{jk_x x}e^{jk_y y}N_y(k_x, k_y)\left(\iint e_y^e\right)dk_x dk_y \tag{4.3.14}$$

and

$$\iint e_x \equiv \int_0^b\int_0^a e_\beta^x(x', y')\cos\left(\frac{n'\pi x'}{a}\right)\sin\left(\frac{m'\pi y'}{b}\right)dx'dy' \tag{4.3.15}$$

$$\iint e_y \equiv \int_0^b \int_0^a e_\beta^y(x', y') \sin\left(\frac{n'\pi x'}{a}\right)\cos\left(\frac{m'\pi y'}{b}\right)dx'dy' \tag{4.3.16}$$

$$\iint e_x^e \equiv \int_0^b \int_0^a e_\beta^x(x', y')\, e^{-jk_x x'} e^{-jk_y y'} dx'dy' \tag{4.3.17}$$

$$\iint e_y^e \equiv \int_0^b \int_0^a e_\beta^y(x', y')\, e^{-jk_x x'} e^{-jk_y y'} dx'dy' \tag{4.3.18}$$

The EFIE's for the aperture electric field are now expanded into the waveguide eigenmodes with unknown expansion coefficients a_β and b_β which represent the amplitudes of the eigenmodes for the x and y components of the aperture electric field, respectively. Next, we will use the Galerkin's method to determine a_β and b_β. Since the Galerkin's method uses the same set of basis functions as the testing functions, we write the set of testing functions as

$$t_\alpha^x(x, y) \equiv \cos\left[\frac{l\pi x}{a}\right]\sin\left[\frac{r\pi y}{b}\right] \tag{4.3.19}$$

$$t_\alpha^y(x, y) \equiv \sin\left[\frac{l\pi x}{a}\right]\cos\left[\frac{r\pi y}{b}\right] \tag{4.3.20}$$

After taking the inner products of eqs. (4.3.5) and (4.3.6) with the set of testing functions, we have the following results.

$$\sum_\beta a_\beta \cdot D_{\alpha\beta}^{xx} + \sum_\beta b_\beta \cdot D_{\alpha\beta}^{xy} = 0 \tag{4.3.21}$$

$$\sum_\beta a_\beta \cdot D_{\alpha\beta}^{yx} + \sum_\beta b_\beta \cdot D_{\alpha\beta}^{yy} = F_\alpha \tag{4.3.22}$$

which can be represented in a matrix form of

$$\begin{bmatrix} D_{\alpha\beta}^{xx} & D_{\alpha\beta}^{xy} \\ D_{\alpha\beta}^{yx} & D_{\alpha\beta}^{yy} \end{bmatrix} \begin{bmatrix} a_\beta \\ b_\beta \end{bmatrix} = \begin{bmatrix} 0 \\ F_\alpha \end{bmatrix} \tag{4.3.23}$$

where

$$D_{\alpha\beta}^{xx} \equiv \int_0^b \int_0^a t_\alpha^x(x,y) \left[W_{dx}^x(x,y) + W_{cx}^x(x,y) \right] dxdy \tag{4.3.24}$$

$$D_{\alpha\beta}^{xy} \equiv \int_0^b \int_0^a t_\alpha^x(x,y) \left[W_{dx}^y(x,y) + W_{cx}^y(x,y) \right] dxdy \tag{4.3.25}$$

$$D_{\alpha\beta}^{yx} \equiv \int_0^b \int_0^a t_\alpha^y(x,y) \left[W_{dy}^x(x,y) + W_{cy}^x(x,y) \right] dxdy \tag{4.3.26}$$

$$D_{\alpha\beta}^{yy} \equiv \int_0^b \int_0^a t_\alpha^y(x,y) \left[W_{dy}^y(x,y) + W_{cy}^y(x,y) \right] dxdy \tag{4.3.27}$$

and

$$F_\alpha \equiv C \int_0^b \int_0^a t_\alpha^y(x,y) \sin\left(\frac{\pi x}{a}\right) dxdy \tag{4.3.28}$$

4.3.2 Evaluation of Matrix Elements

In this section, elements of the matrix will be evaluated into compact forms to facilitate the computer programing. Among the evaluations in this section, two-dimensional Fourier transforms of the sinusoidal functions over the aperture are evaluated analytically in Appendix.

In the matrix, the component $D_{\alpha\beta}^{yy}$ which represents the self-interaction of the y-component of the aperture electric field is first discussed. Let us divide $D_{\alpha\beta}^{yy}$ into three parts as follow:

$$D_{\alpha\beta}^{yy} \equiv \int_0^b \int_0^a t_\alpha^y(x,y)\left[W_{dy}^y(x,y) + W_{cy}^y(x,y)\right]dxdy$$

$$= \Phi_1^{yy} + \Phi_2^{yy} + \Phi_3^{yy} \tag{4.3.29}$$

where Φ_1^{yy} represents the contribution coming from the material layer which has continuous spectrum property, Φ_2^{yy} represents the contribution from discrete higher order modes of the waveguide and Φ_3^{yy} represents the contribution from the incident dominant mode. They are expressed as

$$\Phi_1^{yy} \equiv \int_0^b \int_0^a t_\alpha^y(x,y)\, W_{cy}^y(x,y)\, dxdy$$

$$= \int_0^b \int_0^a t_\alpha^y(x,y)\left(\int_{-\infty}^{\infty}\int e^{jk_x x} e^{jk_y y} N_y(k_x,k_y)\left(\iint e_y^e\right)dk_x dk_y\right)dxdy$$

$$= \int_{-\infty}^{\infty}\int N_y(k_x,k_y)\left(\iint t_y^e\right)\left(\iint e_y^e\right)dk_x dk_y \tag{4.3.30}$$

$$\Phi_2^{yy} \equiv \int_0^b \int_0^a t_\alpha^y(x,y)\left(\sum_{n'}\sum_{m'}\frac{-4\varepsilon_{n'm'}}{ab\Gamma_{n'm'}}\left(\frac{\mu}{\mu_0}\right)\sin\left(\frac{n'\pi x}{a}\right)\cos\left(\frac{m'\pi y}{b}\right)\left[k_0^2-\left(\frac{n'\pi}{a}\right)^2\right]\iint e_y\right)dxdy$$

$$= \sum_{n'}\sum_{m'}\frac{-4\varepsilon_{n'm'}}{ab\Gamma_{n'm'}}\left(\frac{\mu}{\mu_0}\right)\left[k_0^2-\left(\frac{n'\pi}{a}\right)^2\right]\left(\iint t_y\right)\left(\iint e_y\right) \tag{4.3.31}$$

$$\Phi_3^{yy} \equiv \int_0^b \int_0^a t_\alpha^y(x,y)\left(\frac{2\Gamma_{10}}{ab}\left(\frac{\mu}{\mu_0}\right)\sin\left(\frac{\pi x}{a}\right)\int_0^b\int_0^a e_\beta^y(x',y')\sin\left(\frac{\pi x'}{a}\right)dx'dy'\right)dxdy$$

$$= \frac{2\Gamma_{10}}{ab}\left(\frac{\mu}{\mu_0}\right)\left(\int_0^b\int_0^a t_\alpha^y(x,y)\sin\left(\frac{\pi x}{a}\right)dxdy\right)\left(\int_0^b\int_0^a e_\beta^y(x',y')\sin\left(\frac{\pi x'}{a}\right)dx'dy'\right)$$

$$= \frac{2\Gamma_{10}}{ab}\left(\frac{\mu}{\mu_0}\right)\left(\int_0^b\int_0^a \sin\left[\frac{l\pi x}{a}\right]\cos\left[\frac{r\pi y}{b}\right]\sin\left(\frac{\pi x}{a}\right)dxdy\right)\times$$

$$\left(\int_0^b\int_0^a \sin\left[\frac{p\pi x'}{a}\right]\cos\left[\frac{q\pi y'}{b}\right]\sin\left(\frac{\pi x'}{a}\right)dx'dy'\right)$$

$$= \frac{2\Gamma_{10}}{ab}\left(\frac{\mu}{\mu_0}\right)\left[\frac{ab}{2}\delta_{l,1}\delta_{r,0}\right]\left[\frac{ab}{2}\delta_{p,1}\delta_{q,0}\right]$$

$$= \frac{ab}{2}\left(\frac{\mu}{\mu_0}\right)\Gamma_{10}\delta_{l,1}\delta_{r,0}\delta_{p,1}\delta_{q,0} \tag{4.3.32}$$

where some notations are expressed as

$$\iint t_y^e \equiv \int_0^b\int_0^a t_\alpha^y(x,y)\, e^{jk_x x} e^{jk_y y}\, dxdy$$

$$= \left(\int_0^a \sin\left[\frac{l\pi x}{a}\right]\left[\cos(k_x x) + j\sin(k_x x)\right]dx\right)\times$$

$$\left(\int_0^b \cos\left[\frac{r\pi y}{b}\right]\left[\cos(k_y y) + j\sin(k_y y)\right]dy\right)$$

$$\equiv \left[s_{11}(k_x) + s_{12}(k_x)\right]\left[s_{13}(k_y) + s_{14}(k_y)\right] \tag{4.3.33}$$

$$\iint t_y \equiv \int_0^b\int_0^a t_\alpha^y(x,y)\sin\left(\frac{n'\pi x}{a}\right)\cos\left(\frac{m'\pi y}{b}\right)dxdy$$

$$= \int_0^b\int_0^a \sin\left[\frac{l\pi x}{a}\right]\cos\left[\frac{r\pi y}{b}\right]\sin\left(\frac{n'\pi x}{a}\right)\cos\left(\frac{m'\pi y}{b}\right)dxdy$$

$$= \frac{ab}{4}\delta_{n',l}\delta_{m',r}\varepsilon_{m'} \tag{4.3.34}$$

$$s_{11}(k_x) \equiv \int_0^a \sin\left[\frac{l\pi x}{a}\right]\cos(k_x x)\, dx \tag{4.3.35}$$

$$s_{12}(k_x) \equiv j\int_0^a \sin\left[\frac{l\pi x}{a}\right]\sin(k_x x)\, dx \tag{4.3.36}$$

$$s_{13}(k_y) \equiv \int_0^b \cos\left[\frac{r\pi y}{b}\right] \cos(k_y y)\, dy \tag{4.3.37}$$

$$s_{14}(k_y) \equiv j\int_0^b \cos\left[\frac{r\pi y}{b}\right] \sin(k_y y)\, dy \tag{4.3.38}$$

Similar forms for $\iint e_y^e$ and $\iint e_y$ are expressed as

$$\iint e_y^e \equiv \int_0^b \int_0^a e_\beta^y(x', y')\, e^{-jk_x x'} e^{-jk_y y'}\, dx' dy'$$

$$= \left(\int_0^a \sin\left[\frac{p\pi x'}{a}\right] [\cos(k_x x') - j\sin(k_x x')]\, dx'\right) \times$$

$$\left(\int_0^b \cos\left[\frac{q\pi y'}{b}\right] [\cos(k_y y') - j\sin(k_y y')]\, dy'\right)$$

$$\equiv [s_{21}(k_x) + s_{22}(k_x)]\, [s_{23}(k_y) + s_{24}(k_y)] \tag{4.3.39}$$

$$\iint e_y \equiv \int_0^b \int_0^a e_\beta^y(x', y') \sin\left(\frac{n'\pi x'}{a}\right) \cos\left(\frac{m'\pi y'}{b}\right) dx' dy'$$

$$= \int_0^b \int_0^a \sin\left[\frac{p\pi x'}{a}\right] \cos\left[\frac{q\pi y'}{b}\right] \sin\left(\frac{n'\pi x'}{a}\right) \cos\left(\frac{m'\pi y'}{b}\right) dx' dy'$$

$$= \frac{ab}{4} \delta_{n',p} \delta_{m',q} \varepsilon_{m'} \tag{4.3.40}$$

$$s_{21}(k_x) \equiv \int_0^a \sin\left[\frac{p\pi x'}{a}\right] \cos(k_x x')\, dx' \tag{4.3.41}$$

$$s_{22}(k_x) \equiv -j\int_0^a \sin\left[\frac{p\pi x'}{a}\right] \sin(k_x x')\, dx' \tag{4.3.42}$$

$$s_{23}(k_y) \equiv \int_0^b \cos\left[\frac{q\pi y'}{b}\right] \cos(k_y y')\, dy' \tag{4.3.43}$$

$$s_{24}(k_y) \equiv -j\int_0^b \cos\left[\frac{q\pi y'}{b}\right] \sin(k_y y')\, dy' \tag{4.3.44}$$

If we further define

$$\phi_{12u}(k_x) \equiv [s_{11}(k_x) + s_{12}(k_x)]\,[s_{21}(k_x) + s_{22}(k_x)] \tag{4.3.45}$$

$$\phi_{12v}(k_y) \equiv [s_{13}(k_y) + s_{14}(k_y)]\,[s_{23}(k_y) + s_{24}(k_y)] \tag{4.3.46}$$

the multiplication of the notations given in eqs. (4.3.30) and (4.3.31) become

$$\left(\iint t_y^e\right)\left(\iint e_y^e\right) \equiv \phi_{12u}(k_x)\,\phi_{12v}(k_y) \tag{4.3.47}$$

and

$$\left(\iint t_y\right)\left(\iint e_y\right) = \left(\frac{ab}{4}\right)^2 \delta_{n',l}\delta_{m',r}\delta_{n',p}\delta_{m',q}\varepsilon_{m'}^2 \tag{4.3.48}$$

Substiting them back into eqs. (4.3.30) and (4.3.31) gives

$$\Phi_1^{yy} = \int_{-\infty}^{\infty}\int N_y(k_x, k_y)\,\phi_{12u}(k_x)\,\phi_{12v}(k_y)\, dk_x dk_y \tag{4.3.49}$$

$$\Phi_2^{yy} = \sum_{n'}\sum_{m'} \frac{-4\varepsilon_{n'm'}}{ab\Gamma_{n'm'}}\left(\frac{\mu}{\mu_0}\right)\left[k_0^2 - \left(\frac{n'\pi}{a}\right)^2\right]\left(\iint t_y\right)\left(\iint e_y\right)$$

$$= \frac{ab}{4}\left(\frac{\mu}{\mu_0}\right)\sum_{n'}\sum_{m'} \frac{\varepsilon_{n'm'}\varepsilon_{m'}^2}{\Gamma_{n'm'}}\left[\left(\frac{n'\pi}{a}\right)^2 - k_0^2\right]\delta_{n',l}\delta_{m',r}\delta_{n',p}\delta_{m',q} \tag{4.3.50}$$

Since it becomes highly oscillatory when the two-dimensional infinite spectral integration given in eq. (4.3.49) is evaluated in the rectangular coordinates, this spectral

integration is computed in the cylindrical coordinates to sidestep this difficulty. Let's change the coordinates from rectangular to cylindrical with the relations of

$$\begin{cases} k_x = k\cos\varphi \\ k_y = k\sin\varphi \end{cases} \tag{4.3.51}$$

where φ is a real variable with range of $[0, 2\pi]$ and k is a real variable of $[0, \infty]$. The substitution of eq. (4.3.51) in eq. (4.3.49) yields

$$\begin{aligned} \Phi_1^{yy} &= \int_0^{\infty}\int_0^{2\pi} N_y(k, \varphi)\, \phi_{12u}(k, \varphi)\, \phi_{12v}(k, \varphi)\, k d\varphi dk \\ &= \int_0^{\infty} G_{yy}(k)\, k dk \end{aligned} \tag{4.3.52}$$

where

$$G_{yy}(k) \equiv \int_0^{2\pi} N_y(k, \varphi)\, \phi_{12u}(k, \varphi)\, \phi_{12v}(k, \varphi)\, d\varphi \tag{4.3.53}$$

Next we will discuss the component $D_{\alpha\beta}^{xx}$ which represents the self-interaction of the x-component of the aperture electric field in the matrix. Divide $D_{\alpha\beta}^{xx}$ into two parts as follows:

$$\begin{aligned} D_{\alpha\beta}^{xx} &\equiv \int_0^b\int_0^a t_\alpha^x(x, y)\left[W_{dx}^x(x, y) + W_{cx}^x(x, y)\right] dxdy \\ &= \Phi_1^{xx} + \Phi_2^{xx} \end{aligned} \tag{4.3.54}$$

where

$$\Phi_1^{xx} \equiv \int_0^b\int_0^a t_\alpha^x(x, y)\, W_{cx}^x(x, y)\, dxdy$$

$$= \int_0^b \int_0^a t_\alpha^x(x,y) \left(\int_{-\infty}^{\infty} \int e^{jk_x x} e^{jk_y y} N_x(k_y, k_x) \left(\iint e_x^e \right) dk_x dk_y \right) dx dy$$

$$= \int_{-\infty}^{\infty} \int N_x(k_y, k_x) \left(\iint t_x^e \right) \left(\iint e_x^e \right) dk_x dk_y \tag{4.3.55}$$

$$\Phi_2^{xx} \equiv \int_0^b \int_0^a t_\alpha^x(x,y)\, W_{dx}^x(x,y)\, dx dy$$

$$= \int_0^b \int_0^a t_\alpha^x(x,y) \left(\sum_{n'} \sum_{m'} \frac{-4\varepsilon_{n'm'}}{ab\Gamma_{n'm'}} \left(\frac{\mu}{\mu_0} \right) \cos\left(\frac{n'\pi x}{a} \right) \sin\left(\frac{m'\pi y}{b} \right) \left[k_0^2 - \left(\frac{m'\pi}{b} \right)^2 \right] \iint e_x \right) dx dy$$

$$= \sum_{n'} \sum_{m'} \frac{-4\varepsilon_{n'm'}}{ab\Gamma_{n'm'}} \left(\frac{\mu}{\mu_0} \right) \left[k_0^2 - \left(\frac{m'\pi}{b} \right)^2 \right] \left(\iint t_x \right) \left(\iint e_x \right) \tag{4.3.56}$$

and the shorthand notations are expressed as

$$\iint t_x^e \equiv \int_0^b \int_0^a t_\alpha^x(x,y)\, e^{jk_x x} e^{jk_y y} dx dy$$

$$= \left(\int_0^a \cos\left[\frac{l\pi x}{a} \right] [\cos(k_x x) + j \sin(k_x x)]\, dx \right) \times$$

$$\left(\int_0^b \sin\left[\frac{r\pi y}{b} \right] [\cos(k_y y) + j \sin(k_y y)]\, dy \right)$$

$$\equiv [s_{31}(k_x) + s_{32}(k_x)]\, [s_{33}(k_y) + s_{34}(k_y)] \tag{4.3.57}$$

$$\iint t_x \equiv \int_0^b \int_0^a t_\alpha^x(x,y) \cos\left(\frac{n'\pi x}{a} \right) \sin\left(\frac{m'\pi y}{b} \right) dx dy$$

$$= \int_0^b \int_0^a \cos\left[\frac{l\pi x}{a} \right] \sin\left[\frac{r\pi y}{b} \right] \cos\left(\frac{n'\pi x}{a} \right) \sin\left(\frac{m'\pi y}{b} \right) dx dy$$

$$= \frac{ab}{4} \delta_{n',l} \delta_{m',r} \varepsilon_{n'} \tag{4.3.58}$$

$$s_{31}(k_x) \equiv \int_0^a \cos\left[\frac{l\pi x}{a} \right] \cos(k_x x)\, dx \tag{4.3.59}$$

$$s_{32}(k_x) \equiv j\int_0^a \cos\left[\frac{l\pi x}{a}\right] \sin(k_x x)\, dx \tag{4.3.60}$$

$$s_{33}(k_y) \equiv \int_0^b \sin\left[\frac{r\pi y}{b}\right] \cos(k_y y)\, dy \tag{4.3.61}$$

$$s_{34}(k_y) \equiv j\int_0^b \sin\left[\frac{r\pi y}{b}\right] \sin(k_y y)\, dy \tag{4.3.62}$$

Similar forms for $\iint e_x^e$ and $\iint e_x$ are expressed as

$$\begin{aligned}\iint e_x^e &\equiv \int_0^b\int_0^a e_\beta^x(x', y')\, e^{-jk_x x'} e^{-jk_y y'} dx'dy' \\ &= \left(\int_0^a \cos\left[\frac{p\pi x'}{a}\right] [\cos(k_x x') - j\sin(k_x x')]\, dx'\right)\times \\ &\qquad \left(\int_0^b \sin\left[\frac{q\pi y'}{b}\right] [\cos(k_y y') - j\sin(k_y y')]\, dy'\right) \\ &\equiv [s_{41}(k_x) + s_{42}(k_x)]\,[s_{43}(k_y) + s_{44}(k_y)]\end{aligned} \tag{4.3.63}$$

$$\begin{aligned}\iint e_x &\equiv \int_0^b\int_0^a e_\beta^x(x', y') \cos\left(\frac{n'\pi x'}{a}\right)\sin\left(\frac{m'\pi y'}{b}\right)dx'dy' \\ &= \int_0^b\int_0^a \cos\left[\frac{p\pi x'}{a}\right]\sin\left[\frac{q\pi y'}{b}\right]\cos\left(\frac{n'\pi x'}{a}\right)\sin\left(\frac{m'\pi y'}{b}\right)dx'dy' \\ &= \frac{ab}{4}\delta_{n',p}\delta_{m',q}\varepsilon_{n'}\end{aligned} \tag{4.3.64}$$

$$s_{41}(k_x) \equiv \int_0^a \cos\left[\frac{p\pi x'}{a}\right] \cos(k_x x')\, dx' \tag{4.3.65}$$

$$s_{42}(k_x) \equiv -j\int_0^a \cos\left[\frac{p\pi x'}{a}\right] \sin(k_x x')\, dx' \tag{4.3.66}$$

$$s_{43}(k_y) \equiv \int_0^b \sin\left[\frac{q\pi y'}{b}\right] \cos(k_y y')\, dy' \tag{4.3.67}$$

$$s_{44}(k_y) \equiv -j\int_0^b \sin\left[\frac{q\pi y'}{b}\right] \sin(k_y y')\, dy' \tag{4.3.68}$$

If we further define the following notations,

$$\phi_{34u}(k_x) \equiv [s_{31}(k_x) + s_{32}(k_x)]\,[s_{41}(k_x) + s_{42}(k_x)] \tag{4.3.69}$$

$$\phi_{34v}(k_y) \equiv [s_{33}(k_y) + s_{34}(k_y)]\,[s_{43}(k_y) + s_{44}(k_y)]\,, \tag{4.3.70}$$

the multiplication of the shorthand notations given in eqs. (4.3.55) and (4.3.56) become

$$\left(\iint t_x^e\right)\left(\iint e_x^e\right) \equiv \phi_{34u}(k_x)\,\phi_{34v}(k_y) \tag{4.3.71}$$

and

$$\left(\iint t_x\right)\left(\iint e_x\right) = \left(\frac{ab}{4}\right)^2 \delta_{n',l}\delta_{m',r}\delta_{n',p}\delta_{m',q}\varepsilon_{n'}^2 \tag{4.3.72}$$

Substituting them back into eqs. (4.3.55) and (4.3.56) gives

$$\Phi_1^{xx} = \int_{-\infty}^{\infty}\int N_x(k_y, k_x)\,\phi_{34u}(k_x)\,\phi_{34v}(k_y)\, dk_x dk_y \tag{4.3.73}$$

$$\begin{aligned}\Phi_2^{xx} &= \sum_{n'}\sum_{m'} \frac{-4\varepsilon_{n'm'}}{ab\Gamma_{n'm'}}\left(\frac{\mu}{\mu_0}\right)\left[k_0^2 - \left(\frac{m'\pi}{b}\right)^2\right]\left(\iint t_x\right)\left(\iint e_x\right) \\ &= \frac{ab}{4}\left(\frac{\mu}{\mu_0}\right)\sum_{n'}\sum_{m'} \frac{\varepsilon_{n'm'}\varepsilon_{n'}^2}{\Gamma_{n'm'}}\left[\left(\frac{m'\pi}{b}\right)^2 - k_0^2\right]\delta_{n',l}\delta_{m',r}\delta_{n',p}\delta_{m',q}\end{aligned} \tag{4.3.74}$$

As mentioned before, changing the coordinates from rectangular to cylindrical, the two-dimensional infinite spectral integration becomes

$$\Phi_1^{xx} = \int_0^{\infty}\int_0^{2\pi} N_x(k,\varphi)\,\phi_{34u}(k,\varphi)\,\phi_{34v}(k,\varphi)\,k\,d\varphi\,dk$$

$$= \int_0^{\infty} G_{xx}(k)\,k\,dk \tag{4.3.75}$$

where

$$G_{xx}(k) \equiv \int_0^{2\pi} N_x(k,\varphi)\,\phi_{34u}(k,\varphi)\,\phi_{34v}(k,\varphi)\,d\varphi \tag{4.3.76}$$

Next, let's evaluate the component $D_{\alpha\beta}^{xy}$ which represents the mutual-interaction of the x-component of the aperture electric field as the testing function and the y-component of the aperture electric field as the basis function in the matrix. Divide $D_{\alpha\beta}^{xy}$ into two parts as follows:

$$D_{\alpha\beta}^{xy} \equiv \int_0^b\int_0^a t_\alpha^x(x,y)\left[W_{dx}^{y}(x,y) + W_{cx}^{y}(x,y)\right]dxdy$$

$$= \Phi_1^{xy} + \Phi_2^{xy} \tag{4.3.77}$$

where

$$\Phi_1^{xy} \equiv \int_0^b\int_0^a t_\alpha^x(x,y)\,W_{cx}^{y}(x,y)\,dxdy$$

$$= \int_0^b\int_0^a t_\alpha^x(x,y)\left(\int_{-\infty}^{\infty}\int e^{jk_x x}e^{jk_y y}M(k_y,k_x)\left(\iint e_y^e\right)dk_x dk_y\right)dxdy$$

$$= \int_{-\infty}^{\infty}\int M_x(k_y,k_x)\left(\iint t_x^e\right)\left(\iint e_y^e\right)dk_x dk_y \tag{4.3.78}$$

$$\Phi_2^{xy} \equiv \int_0^b\int_0^a t_\alpha^x(x,y)\,W_{dx}^{y}(x,y)\,dxdy$$

$$= \int_0^b \int_0^a t_\alpha^x(x, y) \left(\sum_{n'} \sum_{m'} \frac{-4\varepsilon_{n'm'}}{ab\Gamma_{n'm'}} \left(\frac{\mu}{\mu_0} \right) \cos\left(\frac{n'\pi x}{a} \right) \sin\left(\frac{m'\pi y}{b} \right) \left(\frac{n'\pi}{a} \right) \left(\frac{m'\pi}{b} \right) \iint e_y \right) dx dy$$

$$= \sum_{n'} \sum_{m'} \frac{-4\varepsilon_{n'm'}}{ab\Gamma_{n'm'}} \left(\frac{\mu}{\mu_0} \right) \left(\frac{n'\pi}{a} \right) \left(\frac{m'\pi}{b} \right) \left(\iint t_x \right) \left(\iint e_y \right) \tag{4.3.79}$$

According to eqs. (4.3.39) and (4.3.57), we obtain

$$\left(\iint t_x^e \right) \left(\iint e_y^e \right) \equiv \phi_{32u}(k_x)\, \phi_{32v}(k_y) \tag{4.3.80}$$

with new shorthand notations defined as

$$\phi_{32u}(k_x) \equiv [s_{31}(k_x) + s_{32}(k_x)]\, [s_{21}(k_x) + s_{22}(k_x)] \tag{4.3.81}$$

$$\phi_{32v}(k_y) \equiv [s_{33}(k_y) + s_{34}(k_y)]\, [s_{23}(k_y) + s_{24}(k_y)] \tag{4.3.82}$$

and according to eqs. (4.3.40) and (4.3.58), we have

$$\left(\iint t_x \right) \left(\iint e_y \right) = \left(\frac{ab}{4} \right)^2 \delta_{n',l} \delta_{m',r} \delta_{n',p} \delta_{m',q} \varepsilon_{m'} \varepsilon_{n'} \tag{4.3.83}$$

Substituting them back into eqs. (4.3.78) and (4.3.79) yields

$$\Phi_1^{xy} = \int_{-\infty}^{\infty} \int M_x(k_y, k_x)\, \phi_{32u}(k_x)\, \phi_{32v}(k_y)\, dk_x dk_y \tag{4.3.84}$$

$$\Phi_2^{xy} = \sum_{n'} \sum_{m'} \frac{-4\varepsilon_{n'm'}}{ab\Gamma_{n'm'}} \left(\frac{\mu}{\mu_0} \right) \left(\frac{n'\pi}{a} \right) \left(\frac{m'\pi}{b} \right) \left(\iint t_x \right) \left(\iint e_y \right)$$

$$= -\frac{ab}{4} \left(\frac{\mu}{\mu_0} \right) \sum_{n'} \sum_{m'} \frac{\varepsilon_{n'm'}}{\Gamma_{n'm'}} \left(\frac{n'\pi}{a} \right) \left(\frac{m'\pi}{b} \right) \delta_{n',l} \delta_{m',r} \delta_{n',p} \delta_{m',q} \tag{4.3.85}$$

Like before, changing the coordinates from rectangular to cylindrical, Φ_1^{xy} given in eq. (4.3.84) becomes

$$\Phi_1^{xy} = \int_0^{\infty} \int_0^{2\pi} M_x(k, \varphi)\, \phi_{32u}(k, \varphi)\, \phi_{32v}(k, \varphi)\, k d\varphi dk$$

$$= \int_0^{\infty} G_{xy}(k)\, k dk \tag{4.3.86}$$

where

$$G_{xy}(k) \equiv \int_0^{2\pi} M_x(k, \varphi)\, \phi_{32u}(k, \varphi)\, \phi_{32v}(k, \varphi)\, d\varphi \tag{4.3.87}$$

The last step is to evaluate the component $D_{\alpha\beta}^{yx}$ which represents the mutual-interaction of the y-component of aperture electric field as the testing function and the x-component of aperture electric field as the basis function in the matrix. Let's divide $D_{\alpha\beta}^{yx}$ into two parts as follows:

$$D_{\alpha\beta}^{yx} \equiv \int_0^b \int_0^a t_\alpha^y(x, y) \left[W_{dy}^x(x, y) + W_{cy}^x(x, y) \right] dxdy$$

$$= \Phi_1^{yx} + \Phi_2^{yx} \tag{4.3.88}$$

where

$$\Phi_1^{yx} \equiv \int_0^b \int_0^a t_\alpha^y(x, y)\, W_{cy}^x(x, y)\, dxdy$$

$$= \int_0^b \int_0^a t_\alpha^y(x, y) \left(\int_{-\infty}^{\infty} \int e^{jk_x x} e^{jk_y y} M_y(k_x, k_y) \left(\iint e_x^e \right) dk_x dk_y \right) dxdy$$

$$= \int_{-\infty}^{\infty} \int M_y(k_x, k_y) \left(\iint t_y^e \right) \left(\iint e_x^e \right) dk_x dk_y \tag{4.3.89}$$

$$\Phi_2^{yx} \equiv \int_0^b \int_0^a t_\alpha^y(x, y)\, W_{dy}^x(x, y)\, dxdy$$

$$= \int_0^b \int_0^a t_\alpha^y(x, y) \left(\sum_{n'} \sum_{m'} \frac{-4\varepsilon_{n'm'}}{ab\Gamma_{n'm'}} \left(\frac{\mu}{\mu_0} \right) \sin\left(\frac{n'\pi x}{a} \right) \cos\left(\frac{m'\pi y}{b} \right) \left(\frac{n'\pi}{a} \right) \left(\frac{m'\pi}{b} \right) \iint e_x \right) dxdy$$

$$= \sum_{n'}\sum_{m'} \frac{-4\varepsilon_{n'm'}}{ab\Gamma_{n'm'}} \left(\frac{\mu}{\mu_0}\right)\left(\frac{n'\pi}{a}\right)\left(\frac{m'\pi}{b}\right)\left(\iint t_y\right)\left(\iint e_x\right) \tag{4.3.90}$$

Based on eqs. (4.3.33) and (4.3.63), we have

$$\left(\iint t_y^e\right)\left(\iint e_x^e\right) \equiv \phi_{14u}(k_x)\,\phi_{14v}(k_y) \tag{4.3.91}$$

With new shorthand notations defined as

$$\phi_{14u}(k_x) \equiv [s_{11}(k_x) + s_{12}(k_x)]\,[s_{41}(k_x) + s_{42}(k_x)] \tag{4.3.92}$$

$$\phi_{14v}(k_y) \equiv [s_{13}(k_y) + s_{14}(k_y)]\,[s_{43}(k_y) + s_{44}(k_y)] \tag{4.3.93}$$

and with eqs. (4.3.34) and (4.3.64), we obtain

$$\left(\iint t_y\right)\left(\iint e_x\right) = \left(\frac{ab}{4}\right)^2 \delta_{n',l}\delta_{m',r}\delta_{n',p}\delta_{m',q}\varepsilon_{m'}\varepsilon_{n'} \tag{4.3.94}$$

Substituting them back into eqs. (4.3.89) and (4.3.90) yields

$$\Phi_1^{xy} = \int_{-\infty}^{\infty}\int M_y(k_x, k_y)\,\phi_{14u}(k_x)\,\phi_{14v}(k_y)\,dk_x dk_y \tag{4.3.95}$$

$$\begin{aligned}\Phi_2^{xy} &= \sum_{n'}\sum_{m'} \frac{-4\varepsilon_{n'm'}}{ab\Gamma_{n'm'}} \left(\frac{\mu}{\mu_0}\right)\left(\frac{n'\pi}{a}\right)\left(\frac{m'\pi}{b}\right)\left(\iint t_y\right)\left(\iint e_x\right) \\ &= -\frac{ab}{4}\left(\frac{\mu}{\mu_0}\right)\sum_{n'}\sum_{m'} \frac{\varepsilon_{n'm'}}{\Gamma_{n'm'}}\left(\frac{n'\pi}{a}\right)\left(\frac{m'\pi}{b}\right)\delta_{n',l}\delta_{m',r}\delta_{n',p}\delta_{m',q}\end{aligned} \tag{4.3.96}$$

If we change the coordinates from rectangular to cylindrical as before, Φ_1^{yx} in eq. (4.3.95) becomes

$$\Phi_1^{yx} = \int_0^{\infty}\int_0^{2\pi} M_y(k, \varphi)\,\phi_{14u}(k, \varphi)\,\phi_{14v}(k, \varphi)\,k\,d\varphi\,dk$$

$$= \int_0^{\infty} G_{yx}(k)\, k dk \tag{4.3.97}$$

where

$$G_{yx}(k) \equiv \int_0^{2\pi} M_y(k, \varphi)\, \phi_{14u}(k, \varphi)\, \phi_{14v}(k, \varphi)\, d\varphi \tag{4.3.98}$$

4.3.3 Numerical Results and Comparison with Existing Results

For a specific material layer, the numerical evaluation of the components of the matrix equation given in eq. (4.3.23) for solving the aperture electric field and other relevant quantities of the waveguide probe is performed in a FORTRAN computer program. Once the matrix equation is solved, the aperture electric field is first determined by summing up a finite number of modes that we have taken into account in the program. Then the reflection coefficient or the input impedance of the waveguide probe is determined via the aperture electric field.

To verify the accuracy of this technique, as well as the validity of the computer program, numerical examples illustrated in the previous chapter are recalculated and compared with the existing results.

Figures 4.1(a) and (b) show the real and imaginary components of the input admittances of a waveguide probe when the probe is placed against a layer of quartz with a dielectric constant of $\varepsilon_r = 3.76$ and a thickness of 0.1299 inch. Our results are compared to the theoretical and experimental results of Croswell et al. [22] where they only considered a dominant TE_{10} mode in their theoretical calculation. These figures show that our numerical results employed by two different techniques given in Chapters 3 and 4 compare quite well to each other. Also our numerical results used a dominant TE_{10}

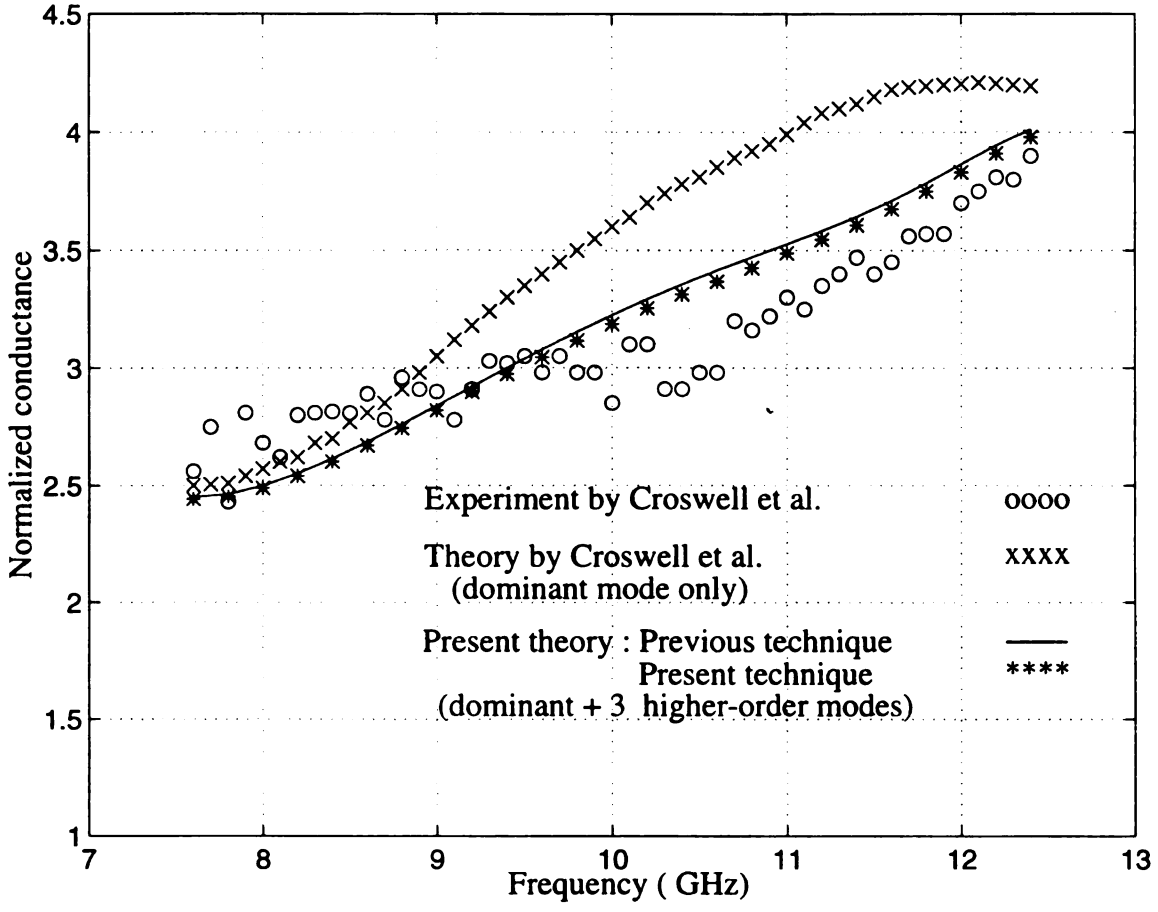

Figure 4.1(a) Input conductances of a waveguide probe (a = 0.4 *in*, b = 0.9 *in*) as a function of frequency when the probe is placed against a material layer with a dielectric constant of ε_r = 3.76 and a thickness of 0.1299 *in*. The comparisons are made between our numerical results and theoretical and experimental results of Croswell et al. [22].

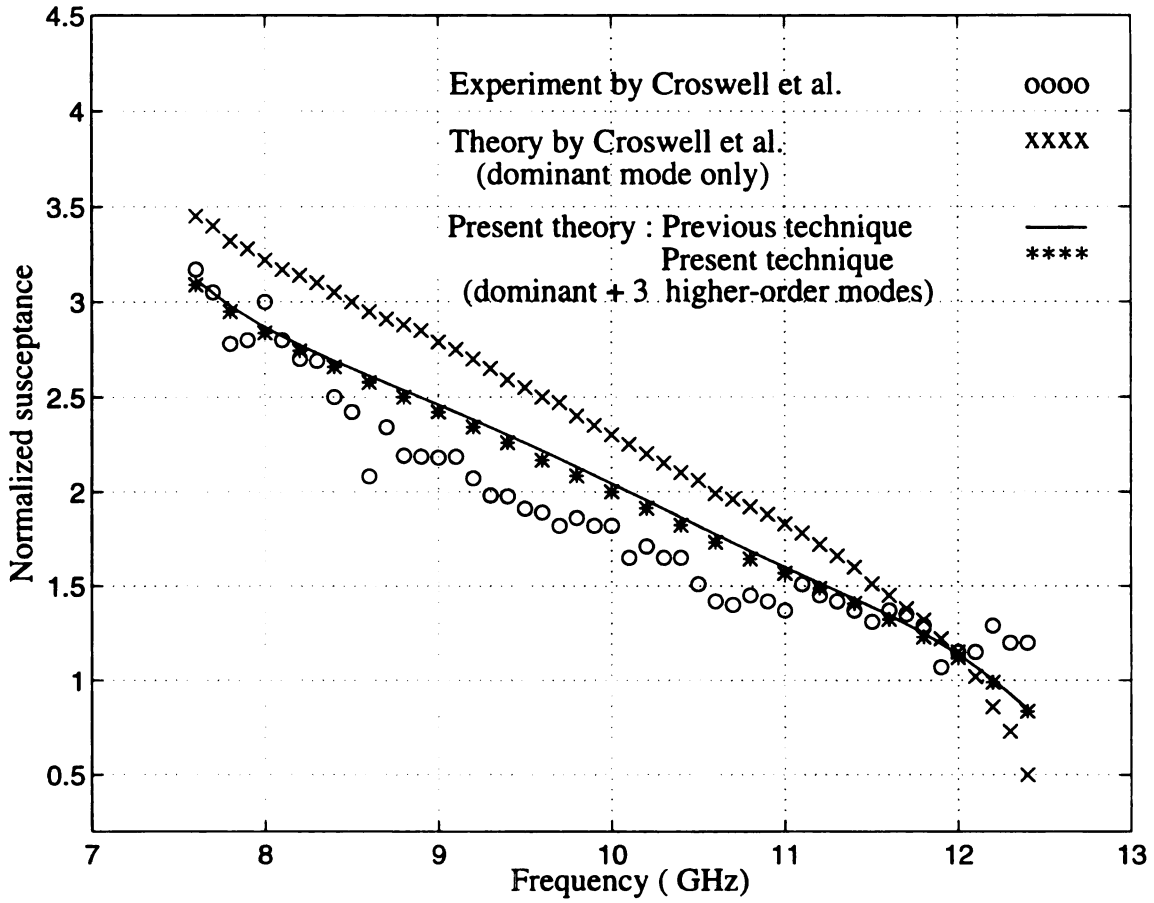

Figure 4.1(b) Input susceptances of a waveguide probe ($a = 0.4$ *in*, $b = 0.9$ *in*) as a function of frequency when the probe is placed against a material layer with a dielectric constant of $\varepsilon_r = 3.76$ and a thickness of 0.1299 *in*. The comparisons are made between our numerical results and theoretical and experimental results of Croswell et al. [22].

mode plus three higher order modes (TE_{30}, TE_{12} and TM_{12}) match very well with their experimental results, much better than their theoretical results do.

Figures 4.2(a) and (b) show the real and imaginary components of the input admittances of a waveguide probe which is placed against a material layer with a dielectric constant $\varepsilon_r = 2.25$ and a thickness of 0.3201 cm. As mentioned before, our numerical results are obtained by using four modes in our theoretical calculation; and in these figures, they compare quite good for both techniques we used. These figures also show a good agreement between our numerical results and the theoretical and experimental values of Bodnar et al. [24].

The last comparisons are shown in Figs. 4.3(a)-(b) which show the real and imaginary components of the input admittances of a waveguide probe that is open to free space. Our numerical results are compared to the theoretical results of Baudrand et al. [30] and the experimental results of Bondar et al. [24]. Our results using four modes for both techniques agree well to each other, as well as to the above published results.

Now if we use the waveguide probe to measure an assumed known anisotropic material layer with a thickness of 0.11 inch and three principal permittivities of $\varepsilon_1 = 5.4 - j0.3$, $\varepsilon_2 = 5.8 - j0.4$ and $\varepsilon_3 = 3.8 - j1.7$, the theoretical input admittance at the probe aperture can be obtained. Figure 4.4 shows the real and imaginary components of the input admittance of a waveguide probe which is placed against the assumed known anisotropic material layer at the orientation of 0 degree. In this figure, we considered three cases; (a) with a dominant TE_{10} mode only, (b) with a dominant TE_{10} mode plus one higher order mode (TE_{20}) and (c) with a dominant TE_{10} mode and two higher order modes (TE_{20} and TE_{01}). Since two multi-mode cases yield almost identical results over the frequency range of 8 to 12 GHz, it is then obvious that a good convergence can be obtained when the first two modes (TE_{10} and TE_{20}) are employed in the numerical calculation. It is also noted that the numerical results obtained by considering the

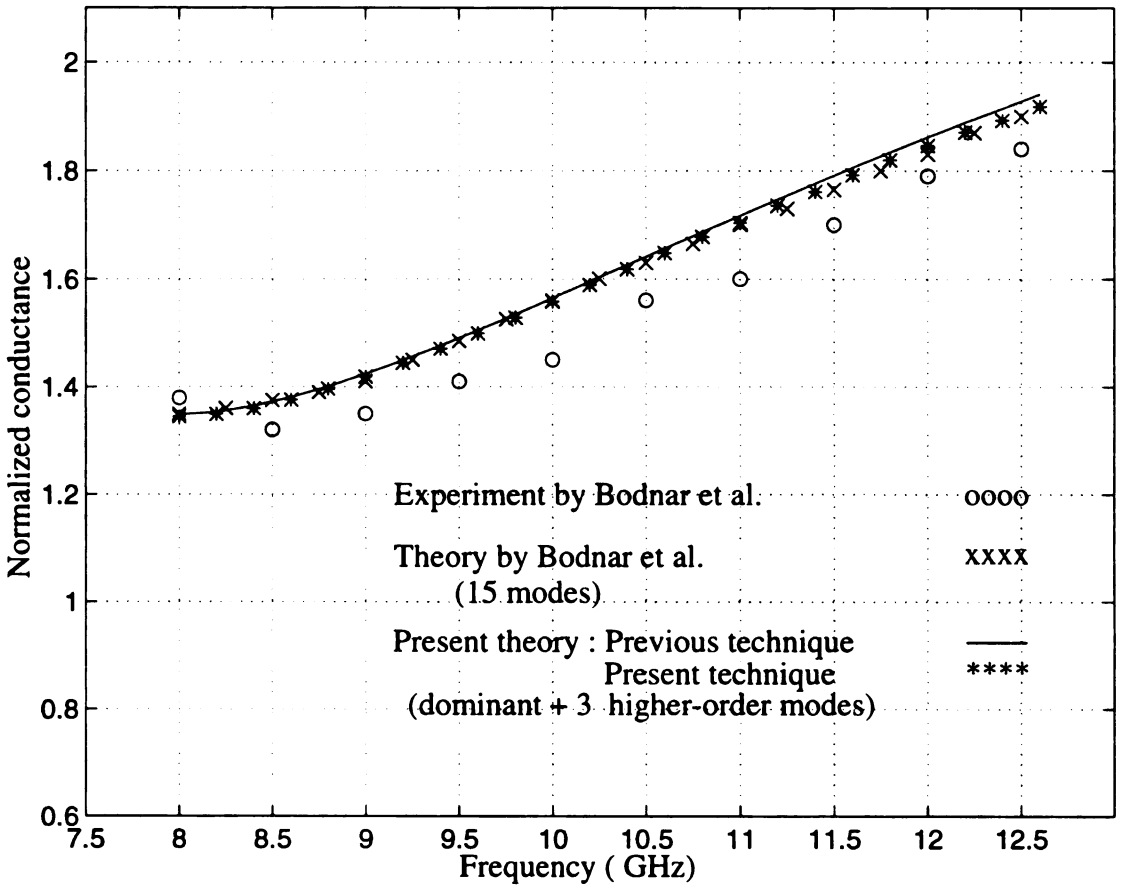

Figure 4.2(a) Input conductances of a waveguide probe ($a = 0.4$ *in*, $b = 0.9$ *in*) as a function of frequency when the probe is placed against a material layer with a dielectric constant of $\varepsilon_r = 2.25$ and a thickness of 0.3201 *cm*. The comparisons are made between our numerical results and theoretical and experimental results of Bodnar et al. [24].

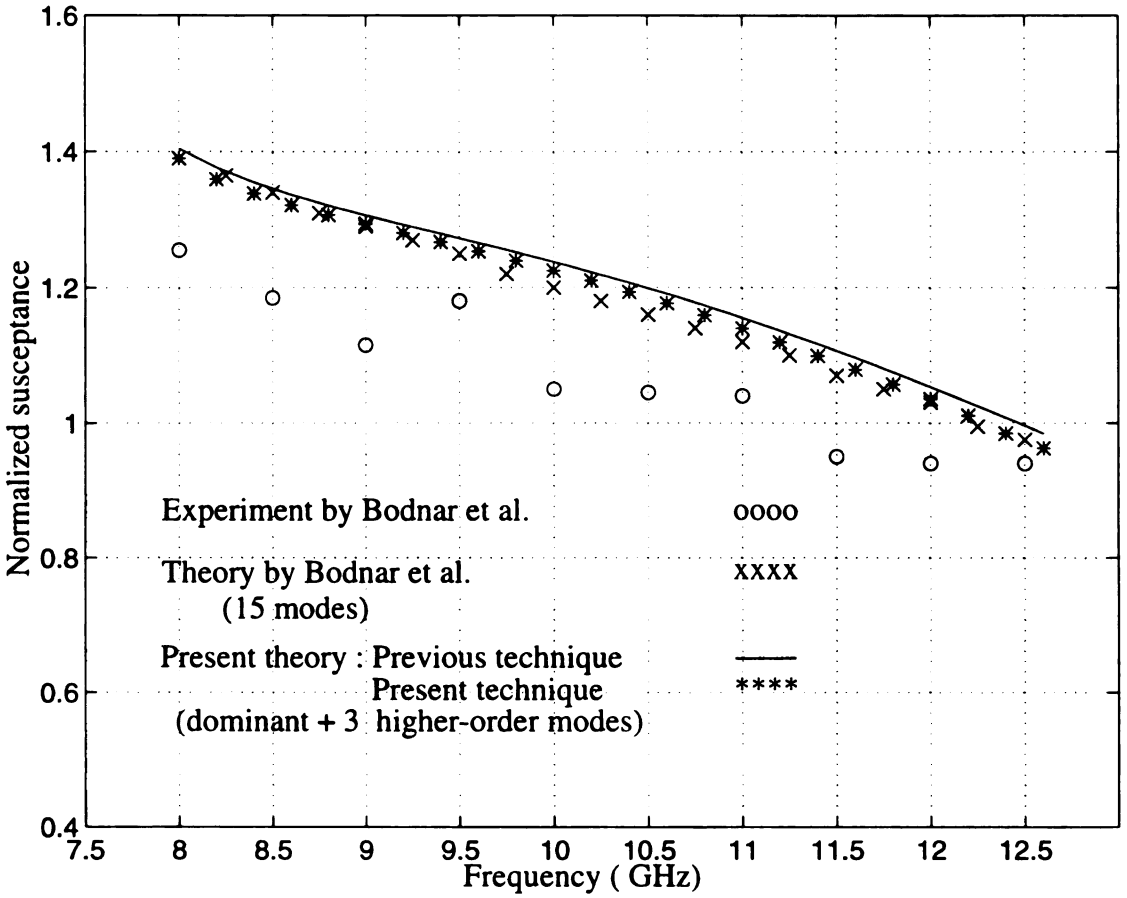

Figure 4.2(b) Input susceptances of a waveguide probe ($a = 0.4$ *in*, $b = 0.9$ *in*) as a function of frequency when the probe is placed against a material layer with a dielectric constant of $\varepsilon_r = 2.25$ and a thickness of 0.3201 *cm*. The comparisons are made between our numerical results and theoretical and experimental results of Bodnar et al. [24].

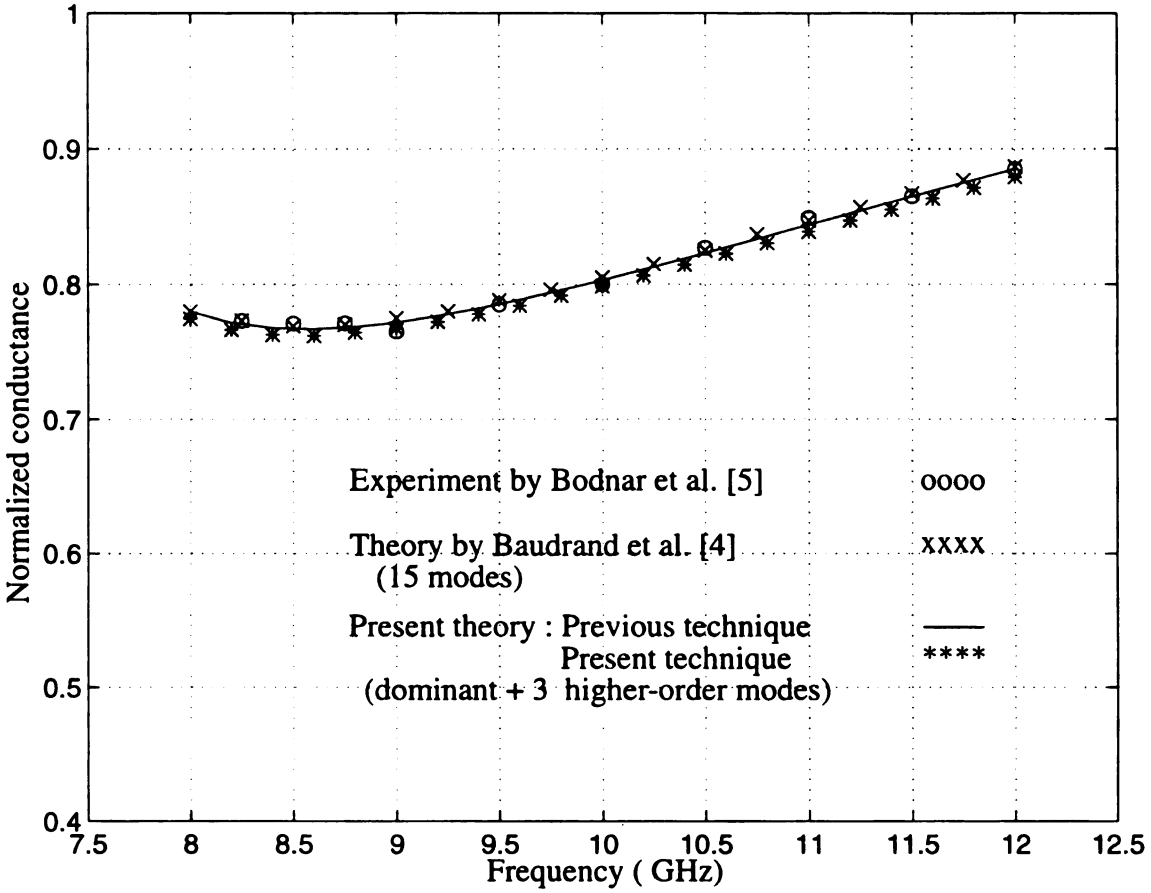

Figure 4.3(a) Input conductances of a waveguide probe ($a = 0.4$ *in*, $b = 0.9$ *in*) as a function of frequency when the probe is open into free space. The comparisons are made between our numerical results and theoretical results of Baudrand et al. [30] and experimental results of Bodnar et al. [24].

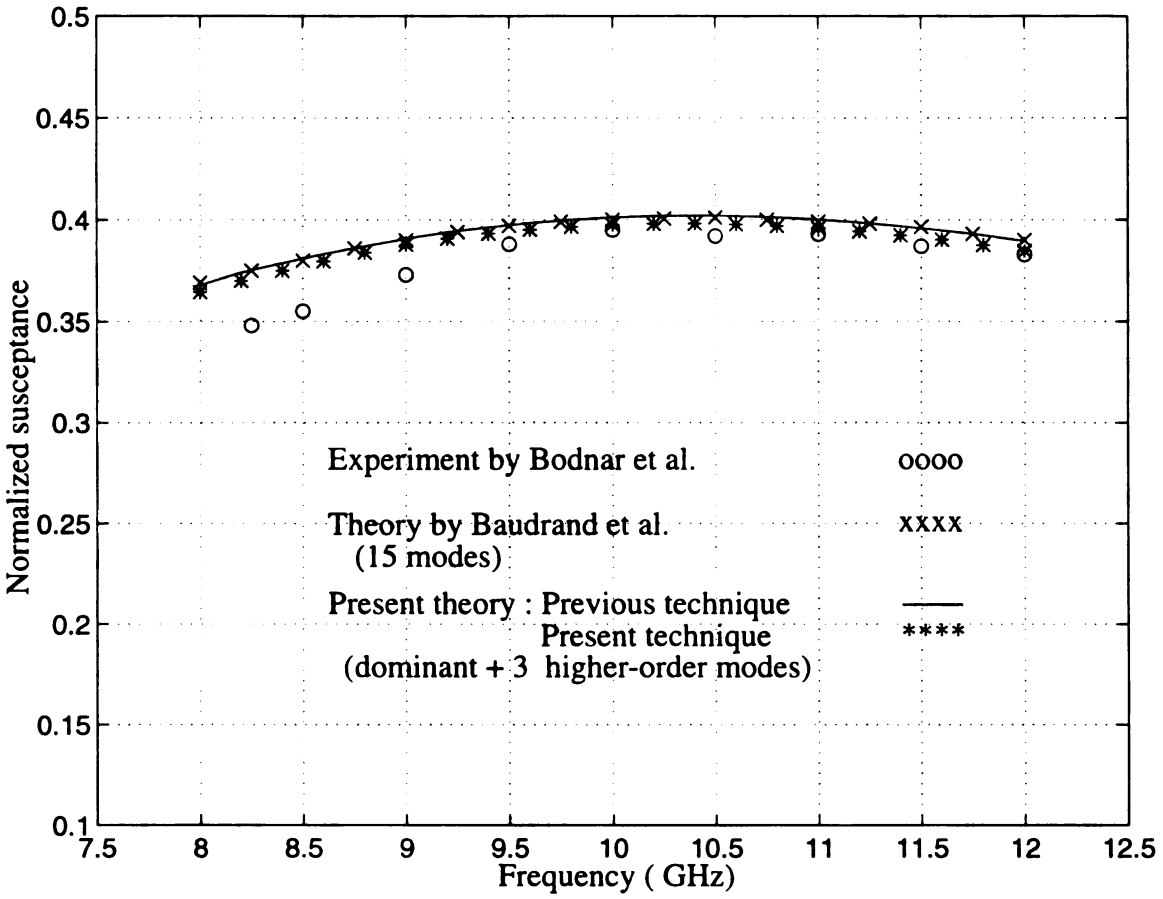

Figure 4.3(b) Input susceptances of a waveguide probe ($a = 0.4$ *in*, $b = 0.9$ *in*) as a function of frequency when the probe is open into free space. The comparisons are made between our numerical results and theoretical results of Baudrand et al. [30] and experimental results of Bodnar et al. [24].

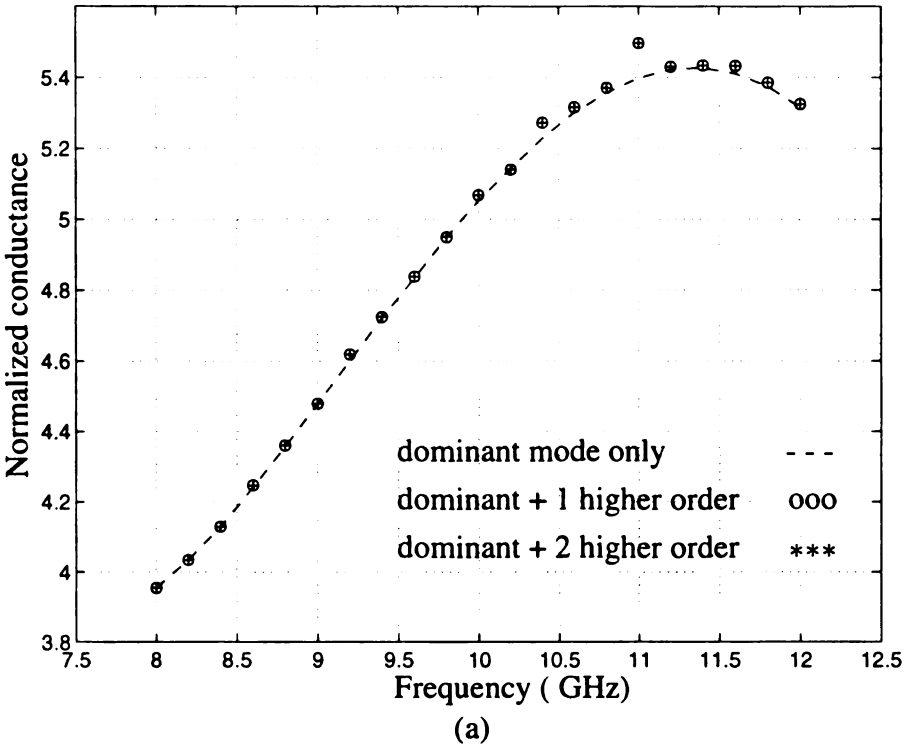

Figure 4.4 Input admittance of a waveguide probe ($a = 0.4$ *in*, $b = 0.9$ *in*) as a function of frequency when the probe is placed against an assumed known anisotropic material layer with a thickness of 0.11 inch and three principal permittivities of $\varepsilon_1 = 5.4 - j0.3$, $\varepsilon_2 = 5.8 - j0.4$ and $\varepsilon_3 = 3.8 - j1.7$.

dominant mode only in the theoretical calculation match very close with the results using the multi-mode cases. This indicates that the aperture electric field is dominated by the dominant TE_{10} mode and when the waveguide probe is attached to an anisotropic material layer, higher order modes contribute insignificantly to the electric field at the input admittance of the waveguide probe.

To further verify this observation, we use the waveguide probe to measure another assumed known anisotropic material layer which has higher permittivity and conductivity in the principal direction perpendicular to the waveguide aperture. Figure 4.4 shows the real and imaginary components of the input admittance of a waveguide probe which is placed against a layer of anisotropic material, with a thickness of 0.053 inch and three principal permittivities of $\varepsilon_1 = 5.4 - j5.3$, $\varepsilon_2 = 5.8 - j6.4$ and $\varepsilon_3 = 30.8 - j100.5$, at the orientation of 0 degree. As observed earlier, our numerical results obtained by using the first two and three modes in the theoretical calculation are almost identical, while the theoretical results obtained by using only the dominant mode match very well with those of multi-mode cases. Therefore, using a dominant TE_{10} mode plus one higher order mode TE_{20} in the numerical calculation, we can expect a good convergence on the probe input admittance; even using a dominant TE_{10} mode only, good results can be obtained over the major portion of the frequency range. As a result, in the interest of saving computation time, only the dominant TE_{10} mode will be assumed for the aperture field if the waveguide probe is attached to an anisotropic material layer. This approximation will be used in the next chapter to inversely determine the measured EM parameters of anisotropic material layers.

In this chapter, we established a *forward* procedure for the theoretical study of measuring EM parameters of anisotropic materials using an open-ended waveguide probe system. The accuracy of the technique and the validity of the computer program have been verified by comparing our numerical results with the published results. The

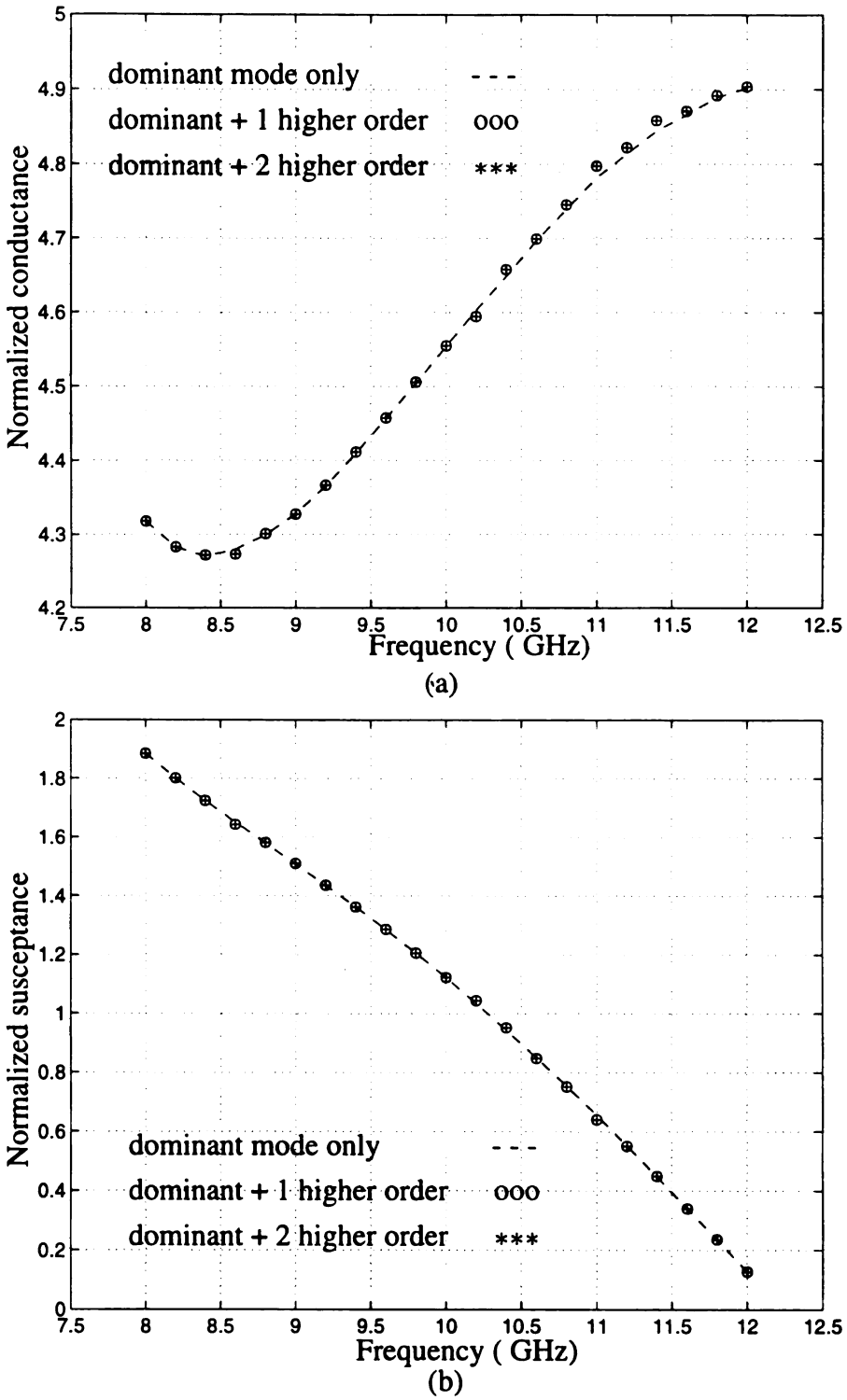

Figure 4.5 Input admittance of a waveguide probe ($a = 0.4\ in,\ b = 0.9\ in$) as a function of frequency when the probe is placed against an assumed known anisotropic material layer with a thickness of 0.053 inch and three principal permittivities of $\varepsilon_1 = 5.4 - j5.3$, $\varepsilon_2 = 5.8 - j6.4$ and $\varepsilon_3 = 30.8 - j100.5$.

theoretical calculation on the input admittance of the waveguide probe placed against a layer of assumed known anisotropic material was also presented and discussed in detail. The experiments for measuring the reflection coefficient or the input admittance of the waveguide probe and the *inverse* technique of this measurement method for determining the EM parameters of the material layer will be discussed in the following chapter.

CHAPTER 5

EXPERIMENTS

5.1. Introduction

In this chapter we discuss the experiments for determining the EM parameters of isotropic and anisotropic samples using an open-ended rectangular waveguide probe system. The calibration procedures of this waveguide probe system and the measurement procedures to obtain the complex permittivity ε of isotropic and anisotropic materials are explained. Also, the experimental input admittances of the waveguide probe when placed against various material layers and their complex permittivities determined from the inverse procedure are presented.

Section 5.2. presents, experimental setups and calibration procedures of the waveguide probe system. In this section, two different calibration procedures for the waveguide probe system are discussed in detail. Also the reactive characteristics property of the adjustable shorting device used for the calibration procedure is studied. Section 5.3. includes the experimental results of the input admittances of the waveguide probe placed against various isotropic and anisotropic material layers. Section 5.4. develops an inversion technique to determine the material parameters such as permittivity, permeability and the thickness of the material, etc., using the Newton's iterative method.

After the theoretical analysis of the parameter retrieval and technique descriptions, the inverted results of the EM parameters for various material layers measured in the preceding section are presented.

5.2. Experimental Setups and Calibration

A waveguide probe system for measuring the complex permittivity ε of isotropic and anisotropic materials has been constructed at MSU electromagnetics laboratory. The waveguide probe system and associated equipment are schematically shown in Fig. 5.1.

The waveguide probe consists of an X-band open-ended rectangular waveguide with a cross-sectional dimensions of 0.4"x0.9" terminated on a 18"x18"x0.25" metallic flange. It was experimentally found that the metallic flange is sufficient large to act as an infinite plate as the theory assumes. An acrylic tank is also built to measure liquid materials. In case the EM parameters of a liquid material are measured by this waveguide probe, a thin Scotch 3M Mailing tape is taped on the aperture to prevent the leakage of the liquid into the probe. It was also found that the effect due to this thin tape is neglible when we measured the input impedance of the probe open into space with and without the tape on the aperture.

An HP 8720B Network analyzer is connected to the waveguide probe and it excites a dominant TE_{10} mode of wave into the waveguide in the frequency range of 8 GHz to 12 GHz. The waveguide used in the system is 16" in length and it is sufficient long to permit only the dominant TE_{10} mode of wave to be reflected back to the network analyzer. That is higher-order modes excited near the waveguide aperture have attenuated greatly and will not reach to the network analyzer.

A layer of material to be measured is placed against the waveguide aperture and it is backed by free space. The material layer is also required to be sufficiently large to reduce

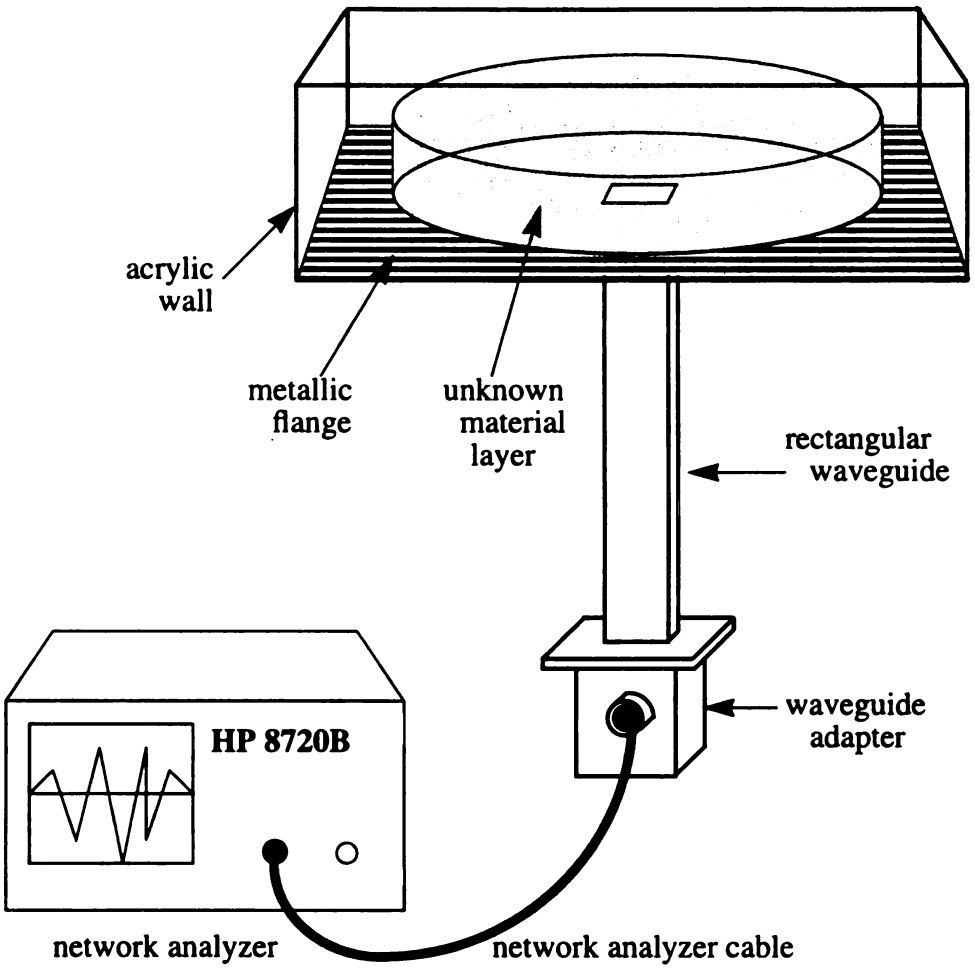

Figure 5.1 Experimental setup of a waveguide probe system to measure the EM parameters of materials.

the possible edge effect of a layer of finite size. Due to the discontinuity presented at the aperture, a part of the incident TE_{10} mode of wave penetrates into the material layer and the rest of it is reflected back to the waveguide. Additionally, higher-order waveguide modes are excited near the probe aperture. The theoretical analysis of the EM fields at the probe aperture was conducted in the preceding chapters and it showed that the reflected dominant mode of wave at the aperture is dependent on the material parameters such as permittivity, permeability and the thickness, etc.. Therefore, by measuring the reflection coefficient of the dominant mode at the waveguide aperture, the material parameters can be determined inversely.

The experimental reflection coefficient at the probe aperture is automatically measured and recorded with an HP network analyzer. As shown in Fig. 5.2, the equivalent two-port network between the probe aperture and the measurement reference plane of the network analyzer can be represented as a equivalent network characterized by $[S]$ matrix. The scattering (S) parameters of the equivalent network can be determined via a calibration procedure. In this section two different calibration procedures for this equivalent two-port network are developed and will be discussed in the following subsections. With these S parameters, the measured reflection coefficient at the reference plane of a network analyzer can then be converted to the reflection coefficient at the probe aperture.

For a layer of anisotropic material with a diagonal form of the complex tensor permittivity as given in eq. (2.3.3), there are three complex permittivities with respect to the principal axes of the anisotropic material layer. Since the electric and magnetic fields of the dominant mode inside the waveguide are orientated in specific directions, the tensor EM parameters of an anisotropic material layer can then be determined by measuring the reflection coefficient of the dominant mode at various orientations of the waveguide with respect to a reference axis of the material layer. Thus, for this kind of anisotropic material layer, it is required to make measurements of the probe input admittance at three or more

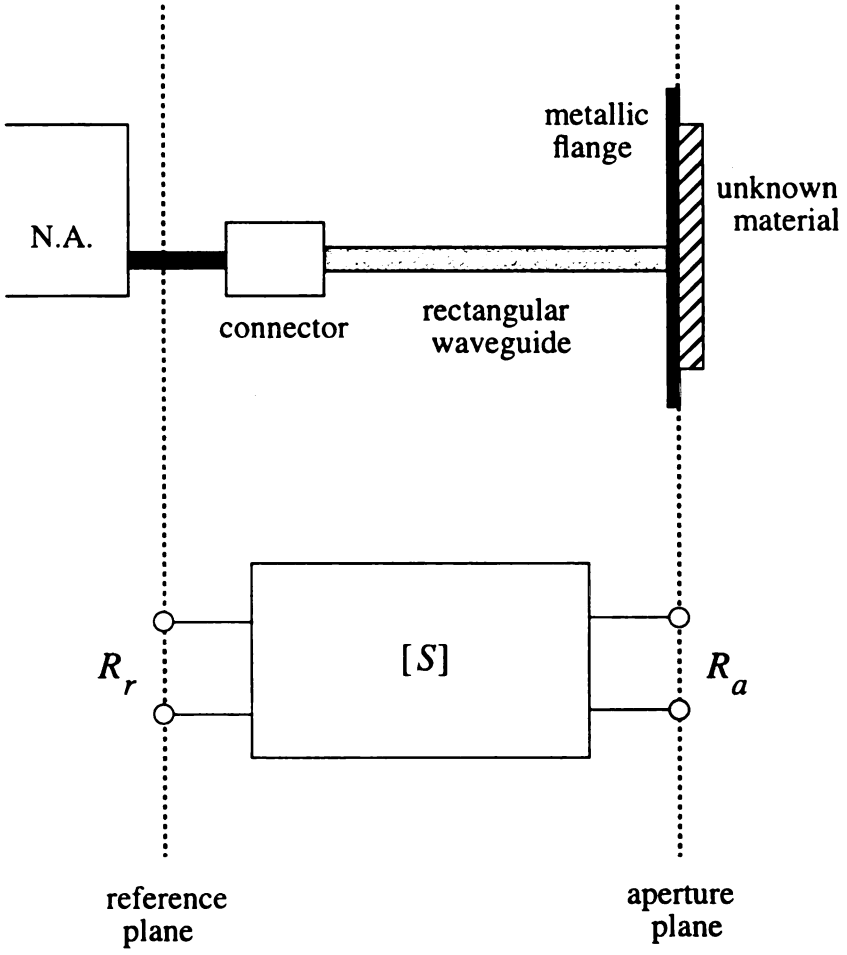

Figure 5.2 Representation of the equivalent two-port network between the waveguide aperture and the measurement reference plane of a network analyzer.

different orientations for inversely determine the three unknown quantities of the tensor permittivity. In a serious of experiments for an anisotropic material layer, we measured the reflection coefficient or the input admittance of the probe aperture at four different angles, 0, 30, 45 and 90 degrees, with respect to a reference axis of the material layer. If a laminated composite material is concerned, the reference axis of the material layer is chosen to be the axis parallel to the fibers in the first ply of the laminated composite.

5.2.1 Fixed-Stub Calibration

It is common practice to use combined calibration devices of short circuit, offset short circuit, perfect matched load and open circuit to calibrate the equivalent network between the actually measured plane of a material sample and the reference plane of a network analyzer. Usually, these calibration devices are assumed to be lossless and their lengths introduce only phase changes between the terminations[43].

For a waveguide probe system, the calibration scheme using all short circuits is most convenient. The signal flow diagram of the calibration scheme using short circuit devices is shown in Fig. 5.3. It is noted that R_r^1, R_r^2 and R_r^3 denote the measured reflection coefficients at the terminal of the network analyzer with the offset short circuits connected in the waveguide probe, while R_b^1, R_b^2 and R_b^3 denote the respective theoretical reflection coefficients at the probe base plane $l = l_1$. Since the shorting circuits are assumed to be lossless, we can express the theoretical reflection coefficients as

$$R_b^1 = -1 \tag{5.2.1}$$

$$R_b^2 = -e^{-j2\beta(l_2 - l_1)} \tag{5.2.2}$$

$$R_b^3 = -e^{-j2\beta(l_3 - l_1)} \tag{5.2.3}$$

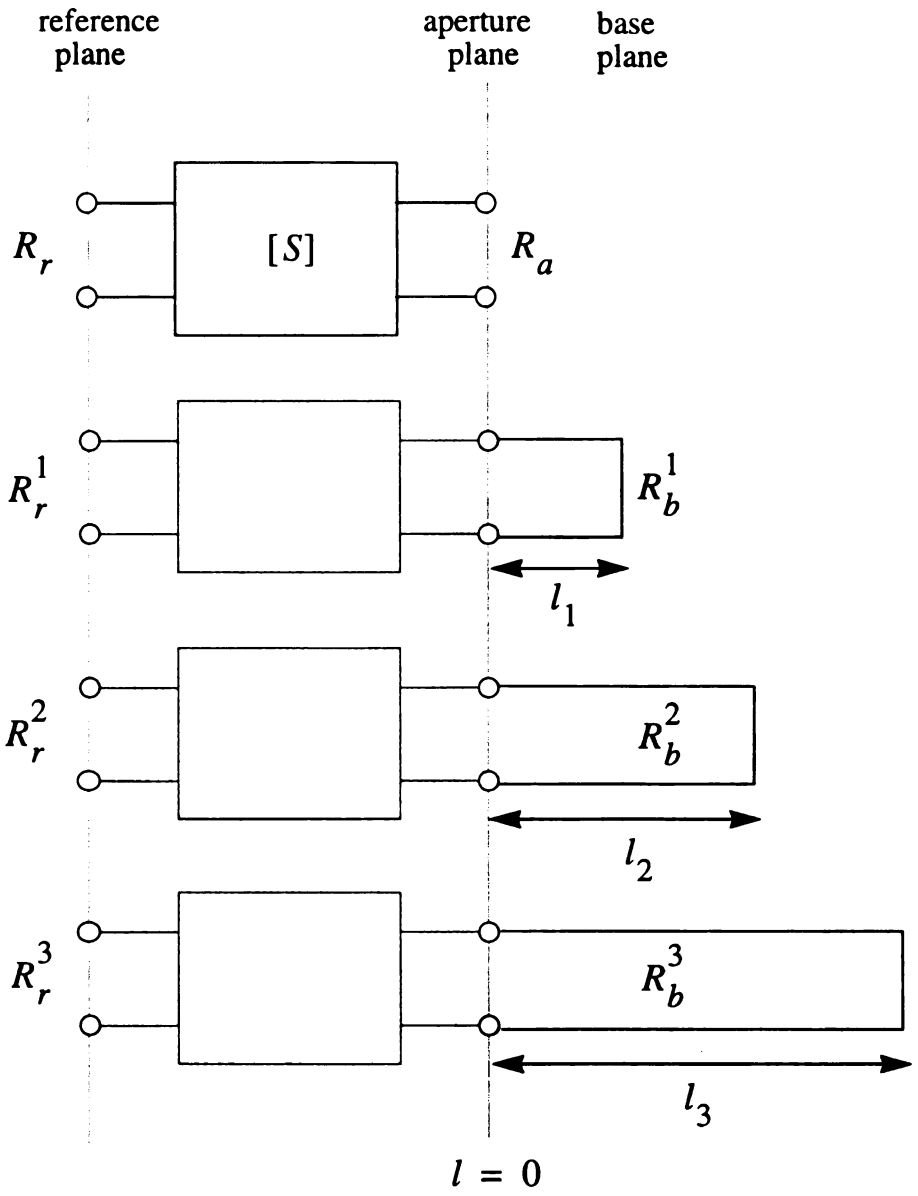

Figure 5.3 Signal flow diagram of the calibration scheme for the measurement system.

where $\beta = \frac{2\pi}{\lambda_g}$ with $\lambda_g = \frac{\lambda}{\sqrt{1-(f_c/f)^2}}$.

According to [12], the equivalent network characterized by $[S]$ matrix as shown in Fig. 5.2 can convert the measured input impedance or reflection coefficient at the reference plane of a network analyzer to the input impedance or reflection coefficient at the probe aperture plane, or vice verse. The relation between the reflection coefficient R_r at the reference plane and that R_a at the probe aperture plane is expressed as

$$R_a = \frac{R_r - S_{11}}{(R_r - S_{11})S_{22} + S_{12}S_{21}} \tag{5.2.4}$$

or

$$R_r = \frac{S_{12}S_{21}R_a}{1 - S_{22}R_a} + S_{11} \tag{5.2.5}$$

This shows that only three scattering parameters S_{11}, S_{22} and $S_{12}S_{21}$ need to be determined if both R_r and R_a are known.

With reference to Fig. 5.3, three offset short circuits are used to determine the S parameters of the equivalent network. Using eqs. (5.2.4) and (5.2.5) for the three short circuits, the S parameters of the equivalent network can determined as

$$S_{22} = \frac{\left(R_r^3 - R_r^2\right)\left(R_b^1 - R_b^2\right) - \left(R_r^1 - R_r^2\right)\left(R_b^3 - R_b^2\right)}{\left(R_r^3 - R_r^2\right)\left(R_b^1 - R_b^2\right)R_b^3 - \left(R_r^1 - R_r^2\right)\left(R_b^3 - R_b^2\right)R_b^1} \tag{5.2.6}$$

$$S_{12}S_{21} = \frac{\left(R_r^3 - R_r^2\right)}{\left(R_b^3 - R_b^2\right)}\left(1 - S_{22}R_b^3\right)\left(1 - S_{22}R_b^2\right) \tag{5.2.7}$$

$$S_{11} = R_r^3 - \frac{S_{12}S_{21}R_b^3}{1 - S_{22}R_b^3}. \tag{5.2.8}$$

Based on these S parameters, the reflection coefficient of the probe aperture R_a can be transformed to be

$$R_a = R_b e^{j2\beta l_1} \tag{5.2.9}$$

where the reflection coefficient at the probe base plane R_b is

$$R_b = \frac{R_r - S_{11}}{(R_r - S_{11})S_{22} + S_{12}S_{21}}. \tag{5.2.10}$$

The easiest calibration scheme using three offset short circuits is to use three fixed shorting stubs which can be attached tightly on the probe aperture. Since the operating frequency covers the range of 8 GHz to 12 GHz, and in order to provide sufficient phase differences over this frequency range, three shorting stubs are chosen to have 5 mm, 10 mm and 20 mm in length, respectively. When these shorting stubs are used, we use a short circuit at the aperture and two offset short circuits with 5 mm and 10 mm in length to calibrate the frequency range of 8 GHz to 10 GHz. On the other hand, a short circuit and two offset short circuits with 10 mm and 20 mm in length are used to calibrate the frequency range of 10 GHz to 12 GHz. That is, three shorting stubs with lengths $l_1 = 0\ mm$, $l_2 = 5\ mm$ and $l_3 = 10\ mm$, or $l_1 = 0\ mm$, $l_2 = 10\ mm$ and $l_3 = 20\ mm$ are used to calibrate the equivalent network for the two frequency ranges. It is noted that the reflection coefficient of the probe aperture in eq. (5.2.9) is now becomes $R_a = R_b$ since the probe base plane is chosen to be the same as the aperture plane in the present arrangement. The calibration scheme discussed here is referred to the "*fixed-stub calibration*" since this calibration uses fixed shorting stubs.

The drawback of this fixed-stub calibration is the problem caused by poor contact between the edges of the stubs and the inner surface of the waveguide. This may affect the accuracy of the calibration greatly. In order to overcome this difficulty, an adjustable shorter is used instead of fixed shorting stubs. This alternate scheme will be discussed in the next section.

5.2.2 Adjustable Shorter Calibration

An adjustable shorter with a dumbbell-shaped loading in front of the termination provides a reactive contact with the waveguide and ensures a very large standing-wave ratio (SWR) in the waveguide. This allows the adjustable shorter to reduce the resistive loss at the contact point with the waveguide and become an ideal short circuit device. However, due to the reactive characteristics of the adjustable shorter, it is difficult to determine the actual offset shorting length of the shorter directly by measuring the distance from the probe aperture to the shorting termination inside the shorter. Therefore, to use the adjustable shorter in the calibration, the offset shorting length of the shorter over the frequency range of 8 GHz to 12 GHz needs to be found first.

The offset shorting length of the shorter for various frequencies can be found by comparing the equivalent phase of the shorter to the phase of the shorting plate at the aperture and they can be determined accurately by using a slotted-line measurement[44]. The simplified block diagram as shown in Fig. 5.4 illustrates the arrangement of the instrumental setup in the slotted-line measurement. An HP 809B slotted line consists of a section of waveguide into which a small antenna, or probe, can be introduced through a slot. The probe extracts a small fraction of the power flowing in the waveguide, and is connected to an HP 415E SWR meter. An HP 8620B sweep oscillator is used to generate the dominant TE_{10} mode of wave inside the waveguide at the X-band frequencies. Also, an HP X532A frequency meter is used to monitor the frequency. Between the oscillator

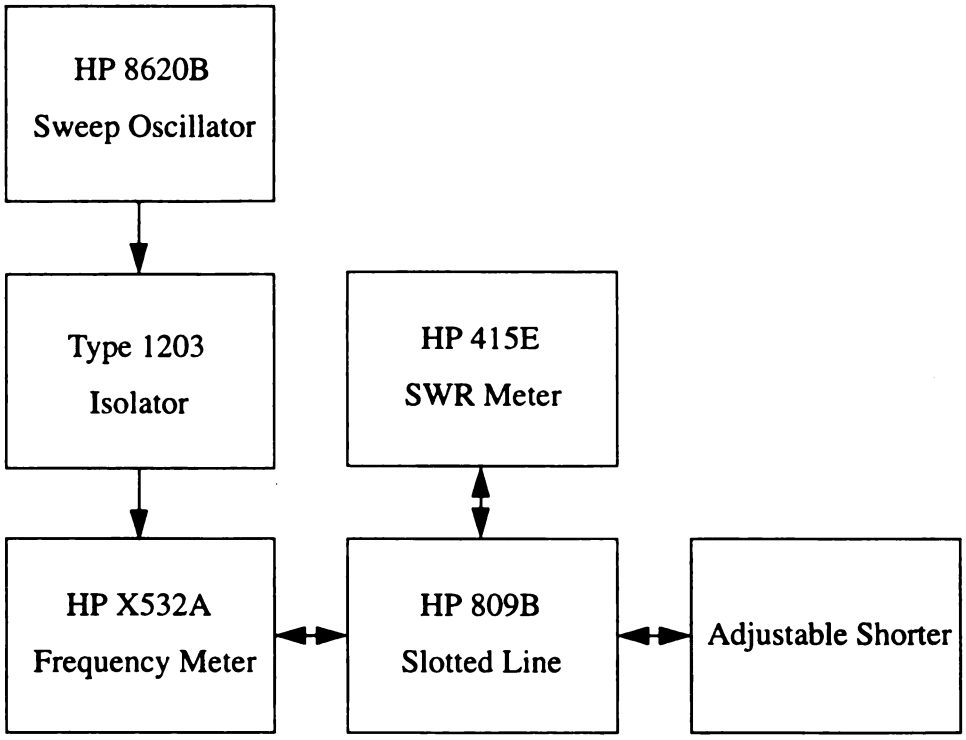

Figure 5.4 The block diagram of the slotted-line measurement.

and the slotted line, a type 1203 isolator is connected to block the reflected wave back to the generator.

When a shorting plate is connected to the end of the slotted line, using the movable probe in the slotted line and monitoring the SWR meter, the position of a voltage minimum at a specific frequency can be found. Replacing the shorting plate with the adjustable shorter, the equivalent shorting location of the shorter can then be determined. Also the measured half-wavelength at this specific frequency can be obtained by measuring the distance between one voltage maximum and the adjacent voltage minimum. Repeating above procedure over discrete frequencies between 8.5 GHz to 12 GHz, the equivalent shorting locations of the shorter are obtained and they are shown in Fig. 5.5. In this figure, the '+' marks represent the measured data by the slotted-line measurement at discrete frequencies, and the solid line represents the fitting curve interpolarized from the measured data by using MATLAB's LEASTSQ program.

From above measured data, we can also plot a figure to show the reactive characteristics of the adjustable shorter. In Fig. 5.6, we compared the half-wavelength differences of the experimental results with that of the theoretical results versus frequency. Both of them represent the differences of the half-wavelengths measured over the frequency range of 8.5 to 12 GHz and that at 12 GHz. If this adjustable shorter is a simple waveguide shorting terminator, the experimental and theoretical differences should be identical. However, as shown in the figure, there are some small discrepancies between theoretical and experimental results over the frequency range. Therefore, a proper calibration procedure is needed for using this adjustable shorter.

To calibrate the system with the adjustable shorter, the following procedure was designed.

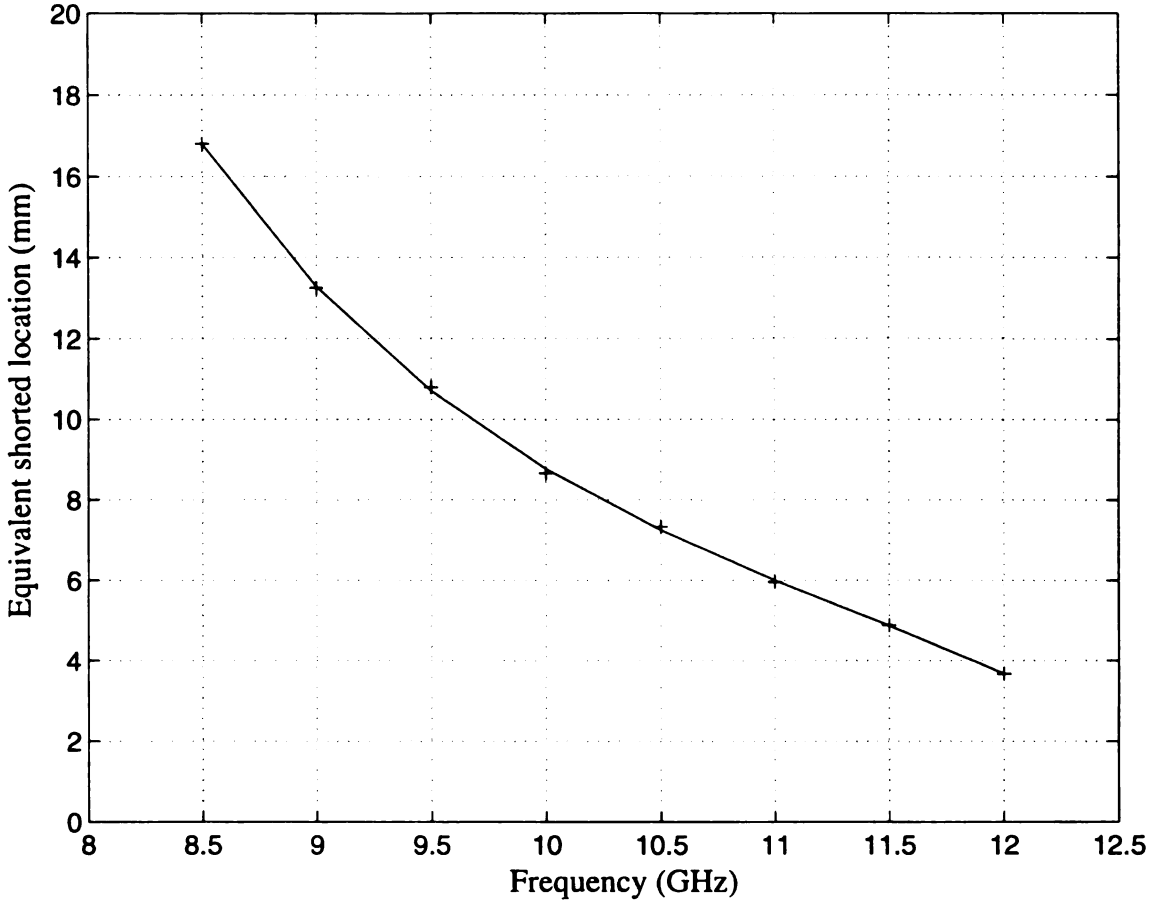

Figure 5.5 The equivalent shorting locations of the adjustable shorter obtained by the measurement of the slotted line over frequencies between 8.5 GHz to 12 GHz. The '+' marks represent the measured equivalent shorting locations of the adjustable shorter at discrete frequencies. The solid line represents the fitting curve of the equivalent shorting locations.

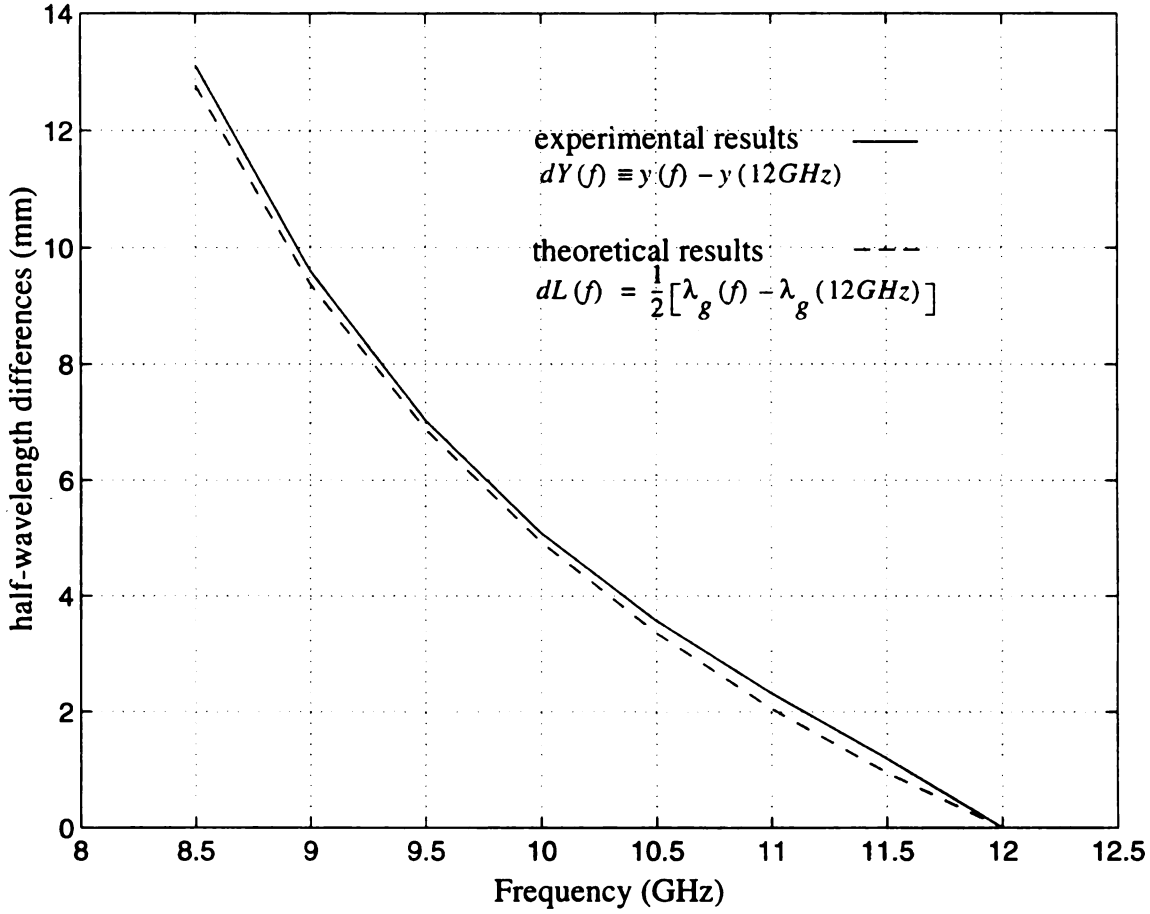

Figure 5.6 The reactive characteristics of the adjustable shorter over frequencies between 8.5 GHz to 12 GHz. The discrepancy of these two curves shows that this adjustable shorter is not a simple waveguide shorting terminator.

Based on the scales indicated on the surface of the adjustable shorter, 40 evenly spaced positions are chosen to be the reference offset shorting locations. Also, in order to obtain sufficient calibration data for the calibration procedure, the distance between the first and the last reference shorting locations should be sufficient long to provide at least one wavelength in length over the frequency range of 8 GHz to 12 GHz.

When the adjustable shorter set at a specific reference position is attached to the waveguide aperture, an HP network analyzer automatically measures 201 measured reflection coefficients of the waveguide probe sweeping over the frequency range of 8 to 12 GHz. Repeating the measurements for all 40 reference shorting positions, the database (40 x 201) of the probe reflection coefficients can be obtained. Now if we replace the adjustable shorter with a shorting plate, 201 measured reflection coefficients of the waveguide probe placed against the shorting plate are recorded. Therefore, for each specific frequency, the location of the equivalent short circuit corresponding to the aperture shorting plate can be determined by selecting the equivalent phase of the probe reflection coefficient from the database. Two reference locations whose phases lag 120 and 240 degrees with respect to that of the equivalent short circuit are also determined to be two offset short circuits for the calibration procedure and their corresponding offset shorting lengths are denoted as l_2 and l_3 as shown in Fig. 5.7. Thus, an equivalent short circuit with $l_1 = 0$ and two offset short circuits with l_2 and l_3 in length are used in the calibration procedure. Once the equivalent network characterized by S parameters is calibrated, the reflection coefficient at the probe aperture placed against a layer of unknown material can be obtained using eqs. (5.2.9) and (5.2.10).

The primary advantage of using the adjustable shorter as a short circuit device is that it provides a low resistive loss at the contact point with the waveguide and a high SWR for the system. It was also found that the calibration procedure designed for this adjustable shorter is a direct and stable method to deal with the reactive characteristics of this shorter.

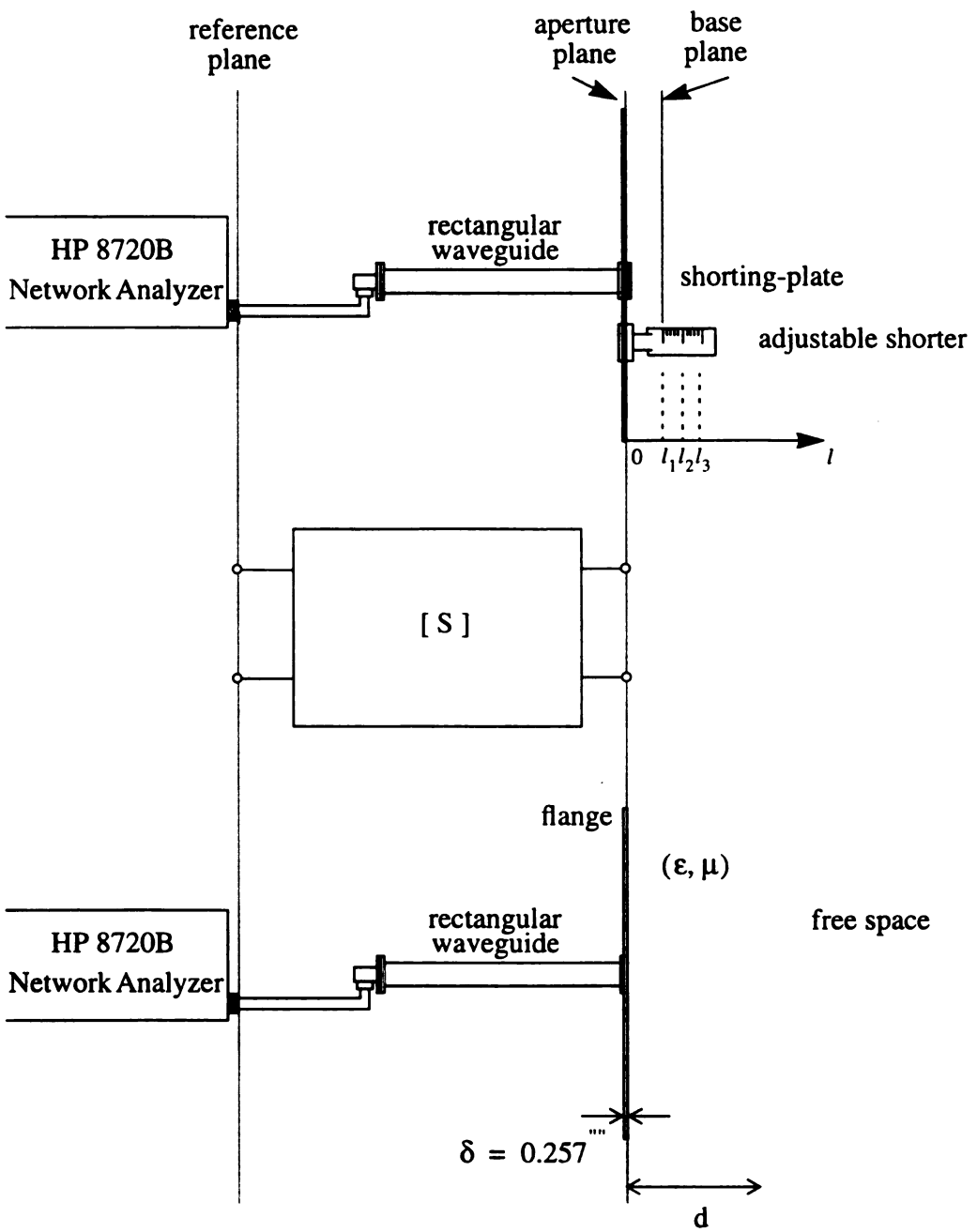

Figure 5.7 Calibration procedure of the waveguide probe system using an adjustable shorter. The S parameters of the transmission network is determined to convert the reflection coefficient or the input admittance measured at the reference plane of the network analyzer to that at the aperture plane of the waveguide probe.

However, this calibration procedure turns out to be rather time consuming. Moreover, a small oscillation (less than 5%) occurs to follow the curve of the calibrated data. This is probably due to the inaccuracy of the numerical interpolation process in finding the offset shorting lengths in the calibration procedure. This may be improved by increasing the number of the reference offset shorting locations to 400 or 800 points in the calibration process, if this practice is not too cumbersome. A better method may be to use an HP waveguide calibration kits for calibrating the system. Unfortunately, such a calibration kit system is not available to us at the present.

5.3. Experimental Results for Materials

We have conducted a serious of experiments to measure the reflection coefficients or the input admittances of a waveguide probe system attached to various material samples as shown in Fig. 5.1. As discussed in the preceding section and shown in Fig. 5.7, the waveguide probe system can be represented by an equivalent two-port network characterized by [S] matrix and calibrated by using an adjustable shorter with a proper calibration procedure.

The reflection coefficients or the input admittances of the waveguide probe attached to various material layers are first measured at the reference plane of the network analyzer. After calibrating the data by the scattering parameters of the equivalent network, these quantities of interest can be converted from that measured at the reference plane to that at the aperture plane. In this section, we present the results of the input admittances at the probe aperture attached to various material layers over the frequency range of 8 to 12 GHz. These material layers include isotropic materials such as air, acrylic, plexiglass, teflon and liquid materials such as distilled water and acetone, and anisotropic materials such as an epoxy/glass-fiber manufactured by Composite Materials and Structures Center laboratory of MSU and a dielectric-fiber manufactured by Boeing Airplane Company.

Figure 5.8 shows the real and imaginary components of the experimental input admittances of a waveguide probe when the probe is open to free space. In these figures, the solid line represents the experimental data, while the '*' marks represents the smoothed curve of the experimental data. As mentioned earlier, an oscillation of less than 5% magnitude along the measured data is probably due to the inaccuracy of the numerical interpolation process. It seems reasonable to treat the smoothed curve of the experimental data as the measured input admittance at the probe aperture.

As shown in Fig. 5.9, the results of Fig. 5.8 are also compared with our theoretical calculations based on two different techniques, Hertzian potential method and transverse field method, with four mode assumption and the published experimental results by Bodnar[24]. Figure 5.9 shows good results for the input conductance at the probe aperture, but a little discrepancy is observed for the results of the input susceptance at the probe aperture. Since the imaginary component of the probe input admittance is strongly dependent on the field distributions at the aperture, the discrepancy of this component may indicate the imperfection of our probe aperture. This is probably caused by a slight curving nature of the flange and four non-smooth filled holes around the aperture which are used to connect the adjustable shorter to the flange while calibrating.

Figures 5.10 to 5.12 show the real and imaginary components of the experimental input admittances of the waveguide probe when the probe is placed against various material layers such as an acrylic layer of 0.06 inch, a plexiglass layer of 0.06 inch and a teflon layer of 0.51625 inch, respectively. As before, these figures show both the experimental data and the smoothed curves of the data. It was found that the contact between the material layer and the waveguide probe is very important. In our configuration the material layer to be measured is backed by free space, an unintentional air gap may exist if the material layer is not tightly attached to the probe aperture. This

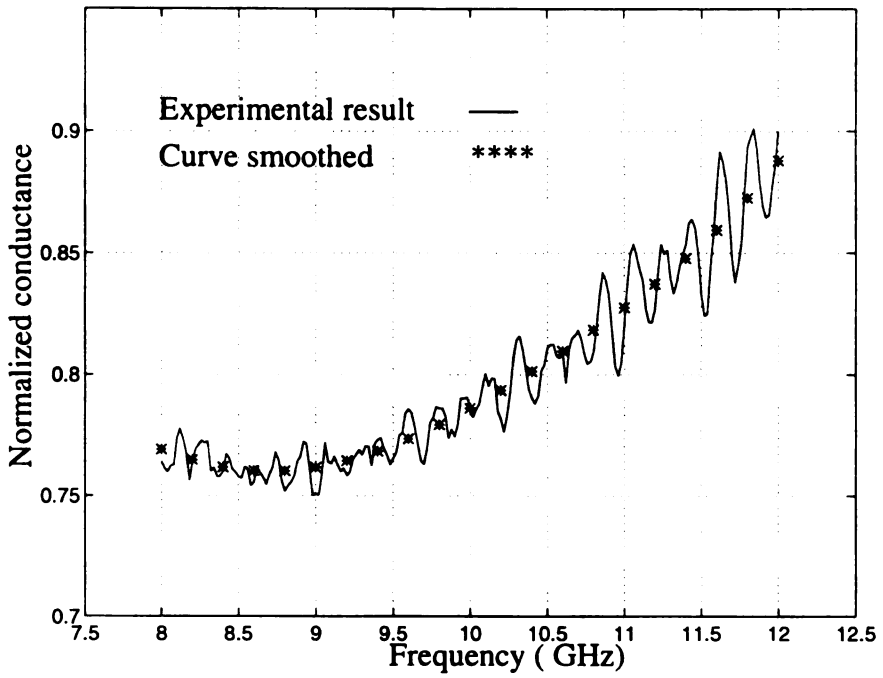

(a)

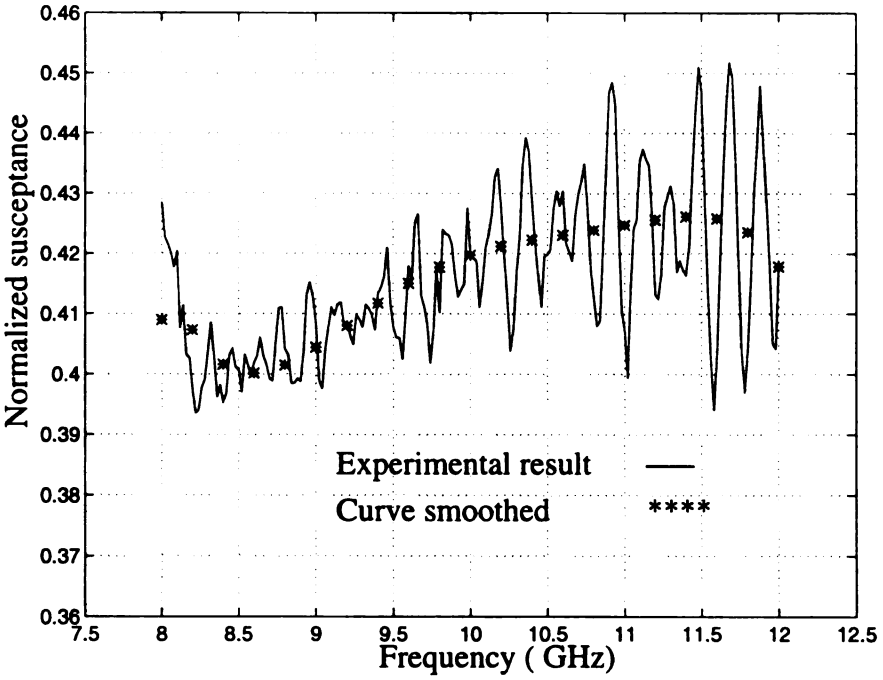

(b)

Figure 5.8 Experimental input conductances and susceptances of a waveguide probe ($a = 0.4$ *in*, $b = 0.9$ *in*) as functions of frequency when the probe is open to free space.

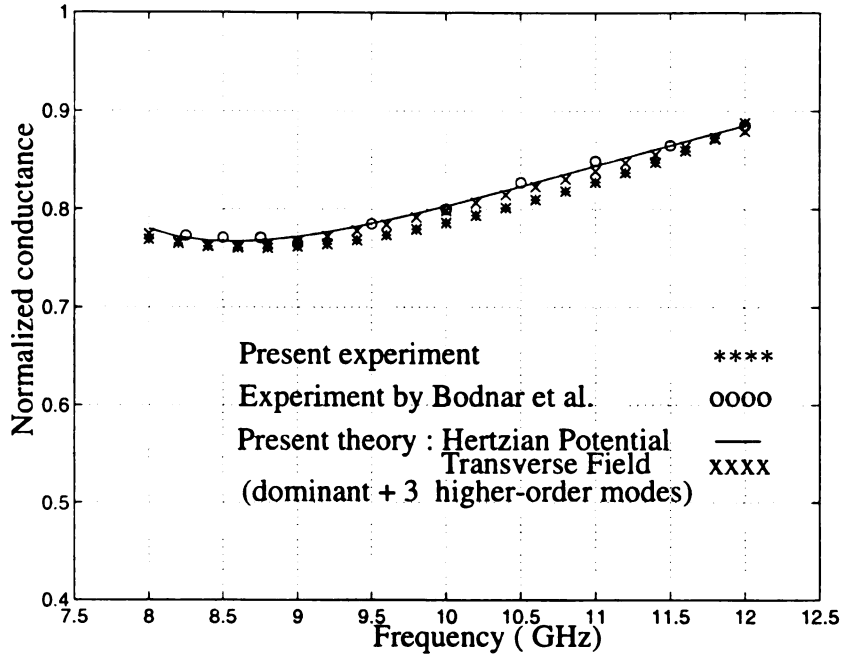

(a)

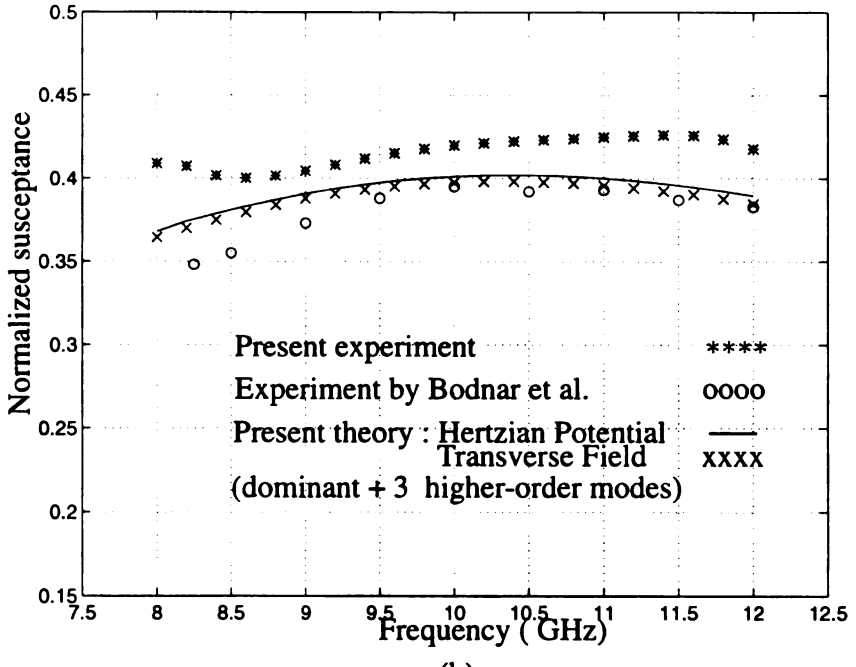

(b)

Figure 5.9 Comparison of input conductances and susceptances of a waveguide probe (a = 0.4 *in*, b = 0.9 *in*) as functions of frequency when the probe is open to free space with the existing experimental results of Bodnar et al.[24].

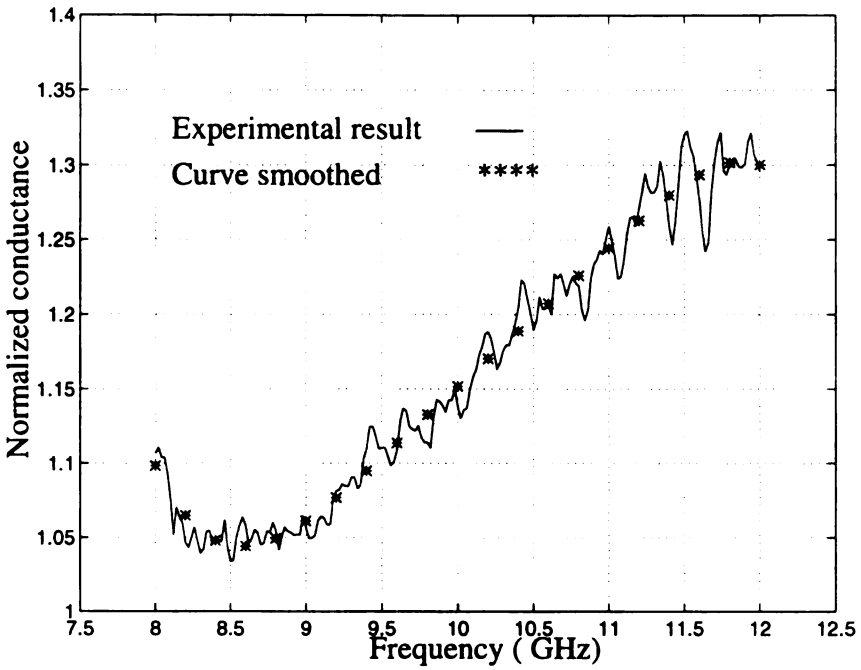

(a)

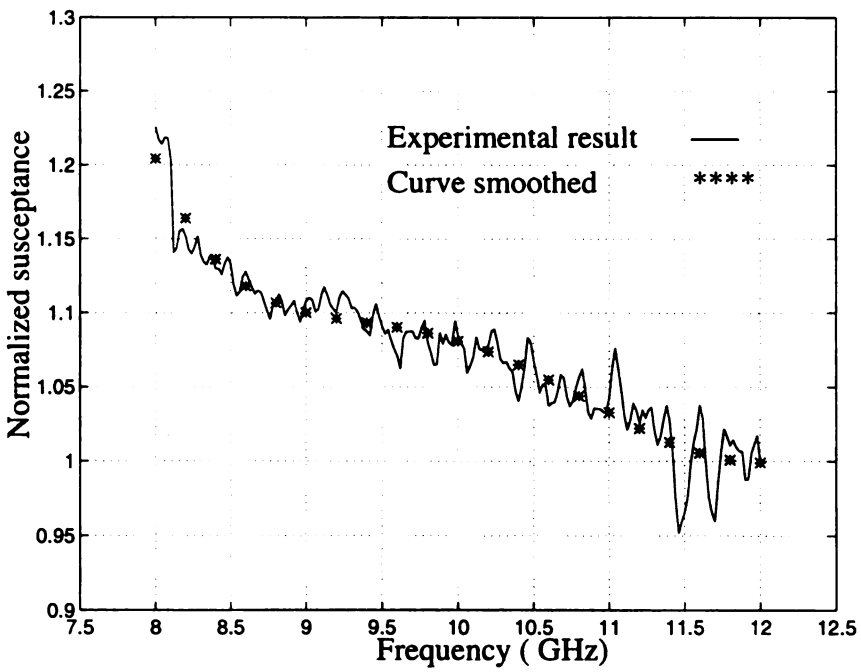

(b)

Figure 5.10 Experimental input conductances and susceptances of a waveguide probe ($a = 0.4$ *in*, $b = 0.9$ *in*) as functions of frequency when the probe is placed against a material layer (acrylic) with a thickness of 0.06 *inch*.

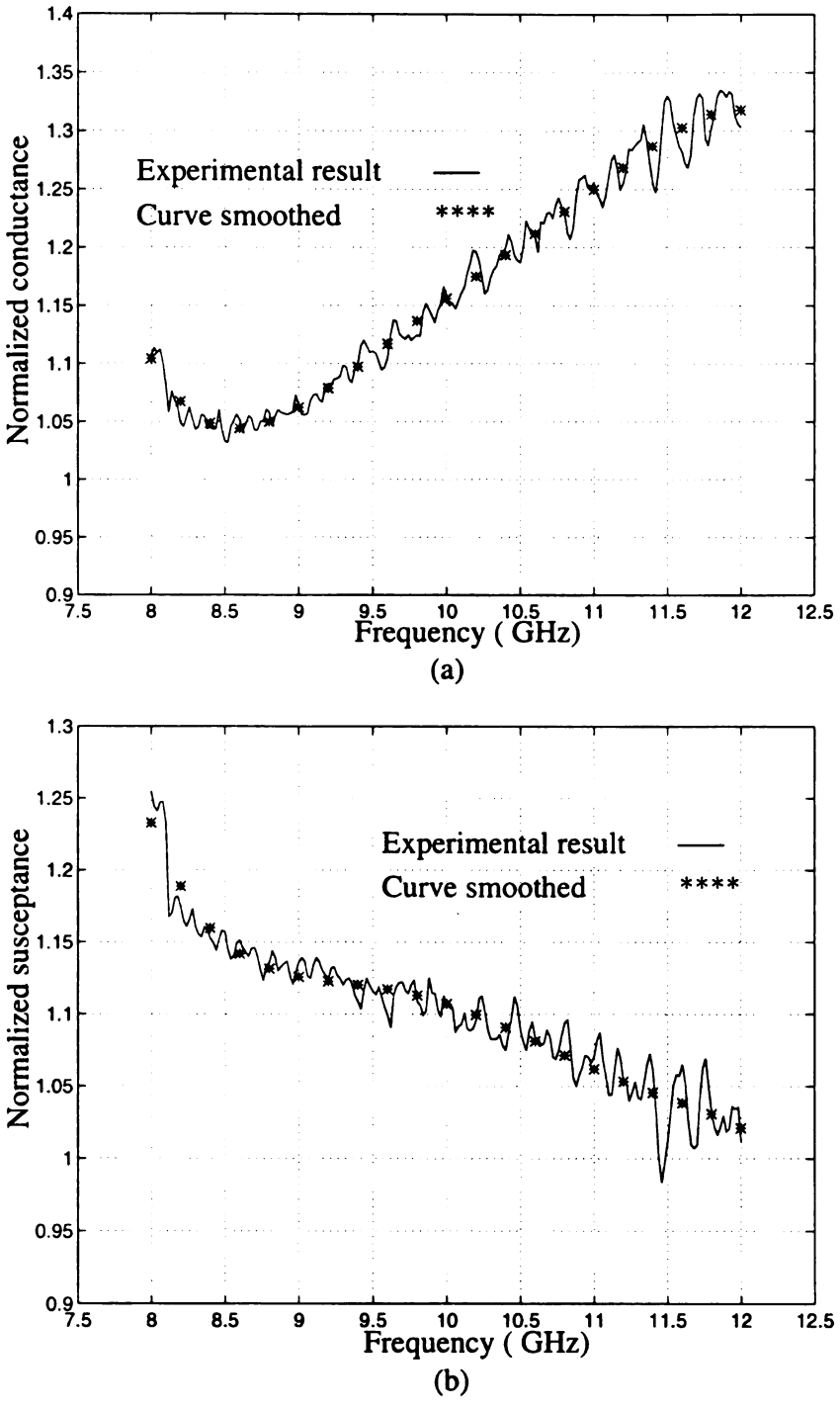

Figure 5.11 Experimental input conductances and susceptances of a waveguide probe ($a = 0.4$ *in*, $b = 0.9$ *in*) as functions of frequency when the probe is placed against a material layer (plexiglass) with a thickness of 0.06 *inch*.

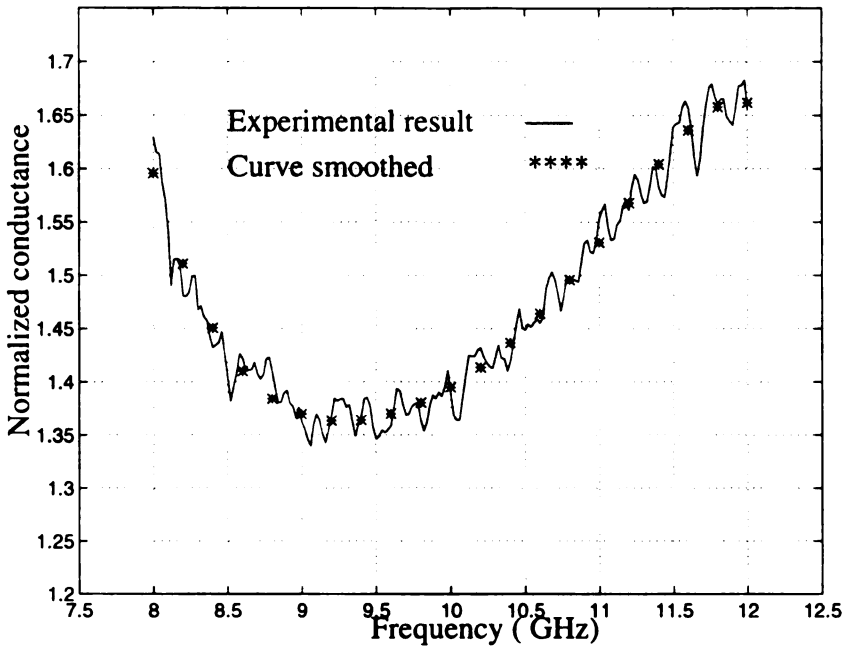

Figure 5.12 Experimental input conductances and susceptances of a waveguide probe ($a = 0.4$ *in*, $b = 0.9$ *in*) as functions of frequency when the probe is placed against a material layer (teflon) with a thickness of 0.51625 *inch*.

may cause considerable inaccuracy in the measurement as well as the inverse results on the EM parameters of the materials.

Figure 5.13 shows the real and imaginary components of the experimental input admittances of the waveguide probe when it is placed against two layers of liquid material, distilled water, with thickness's of 0.2344 inch and 0.3125 inch. These two sets of measurements will be both used later to inversely determine the complex permittivity of the distilled water via an inverse technique. The purpose is to verify the precision of the reading of the thickness for a liquid material layer which is difficult to determine accurately in a tank.

Figure 5.14 shows the real and imaginary components of the experimental input admittances of the waveguide probe when the probe is placed against a layer of liquid material, acetone, with a thickness of 0.345 inch. The figures show both the experimental data and the smoothed curves of the data.

Figure 5.15 shows the real and imaginary components of the experimental input admittances of a waveguide probe when the probe is placed against a layer of anisotropic material, epoxy/glass-fiber, with a thickness of 0.1105 inch. These figures show the measured results at four different orientations of the waveguide aperture with respect to a reference axis of the material layer. As defined in section 5.2., the measurements at 0, 30, 45 and 90 degrees mean that the experiments are conducted when glass fibers in the first ply of the material layer are making an angle of 0, 30, 45 and 90 degrees, respectively, with the direction of the electric field of the dominant mode at the probe aperture.

The smoothed curves of the above experimental results are shown in Fig. 5.18. These curves represent the real and imaginary components of the smoothed waveguide input admittances when the probe is placed against the epoxy/glass-fiber layer. These data will

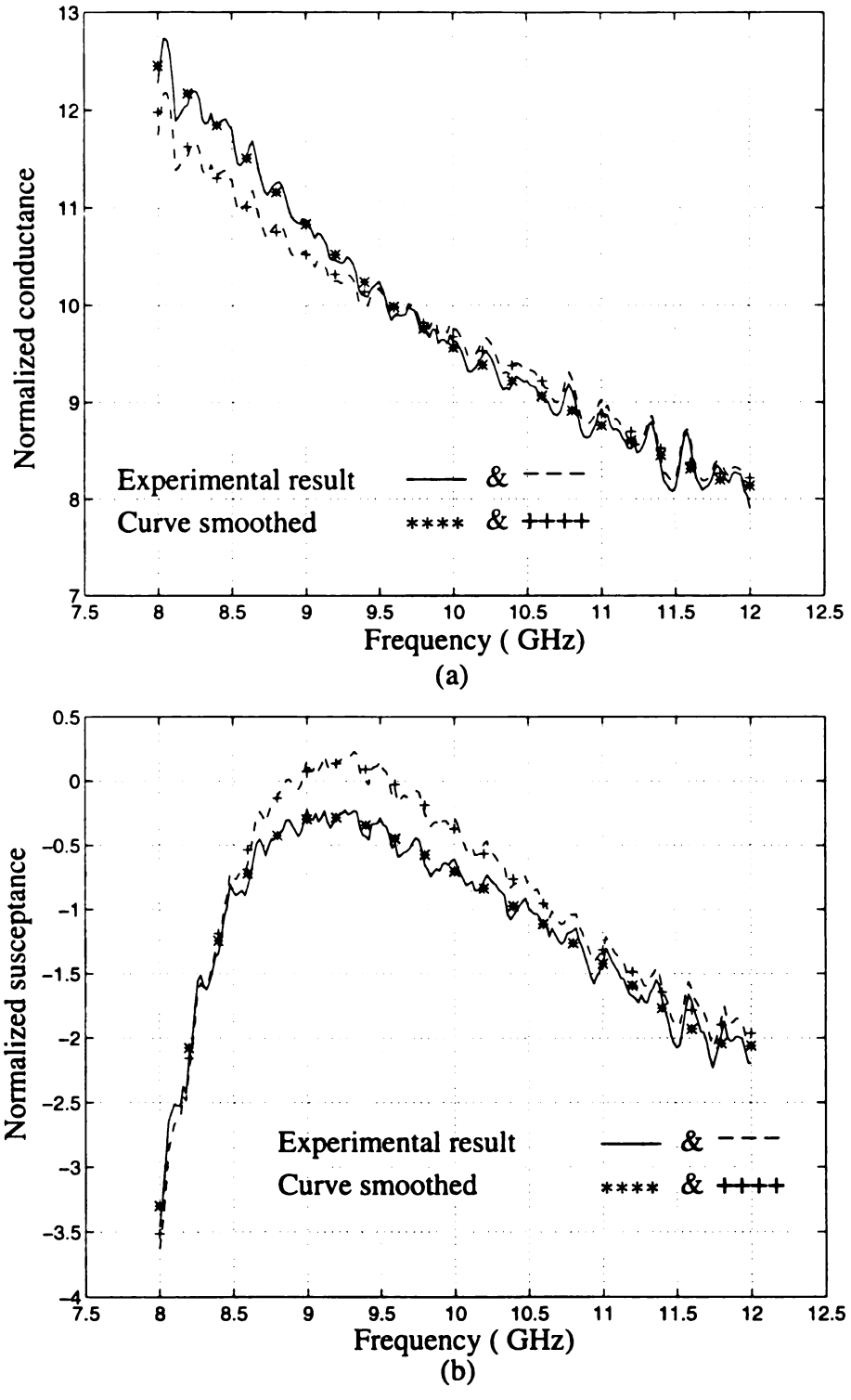

Figure 5.13 Experimental input conductances and susceptances of a waveguide probe (a = 0.4 *in*, b = 0.9 *in*) as functions of frequency when the probe is placed against two liquid material layers (distilled water) with thickness's of 0.2344 *inch* (dash line) and 0.3125 *inch* (solid line).

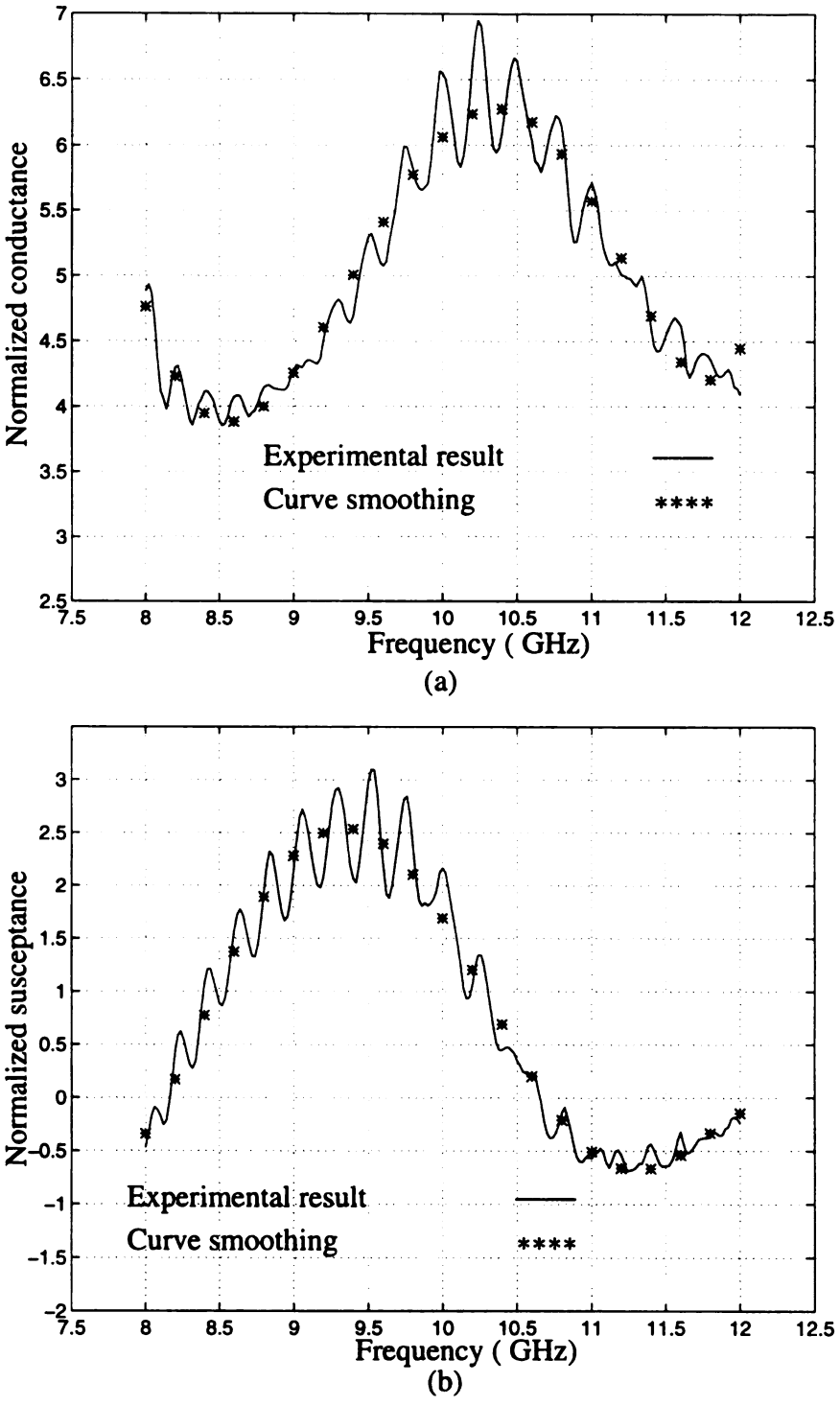

Figure 5.14 Experimental input conductances and susceptances of a waveguide probe ($a = 0.4$ *in*, $b = 0.9$ *in*) as functions of frequency when the probe is placed against a liquid material layer (acetone) with a thickness of 0.345 *inch*.

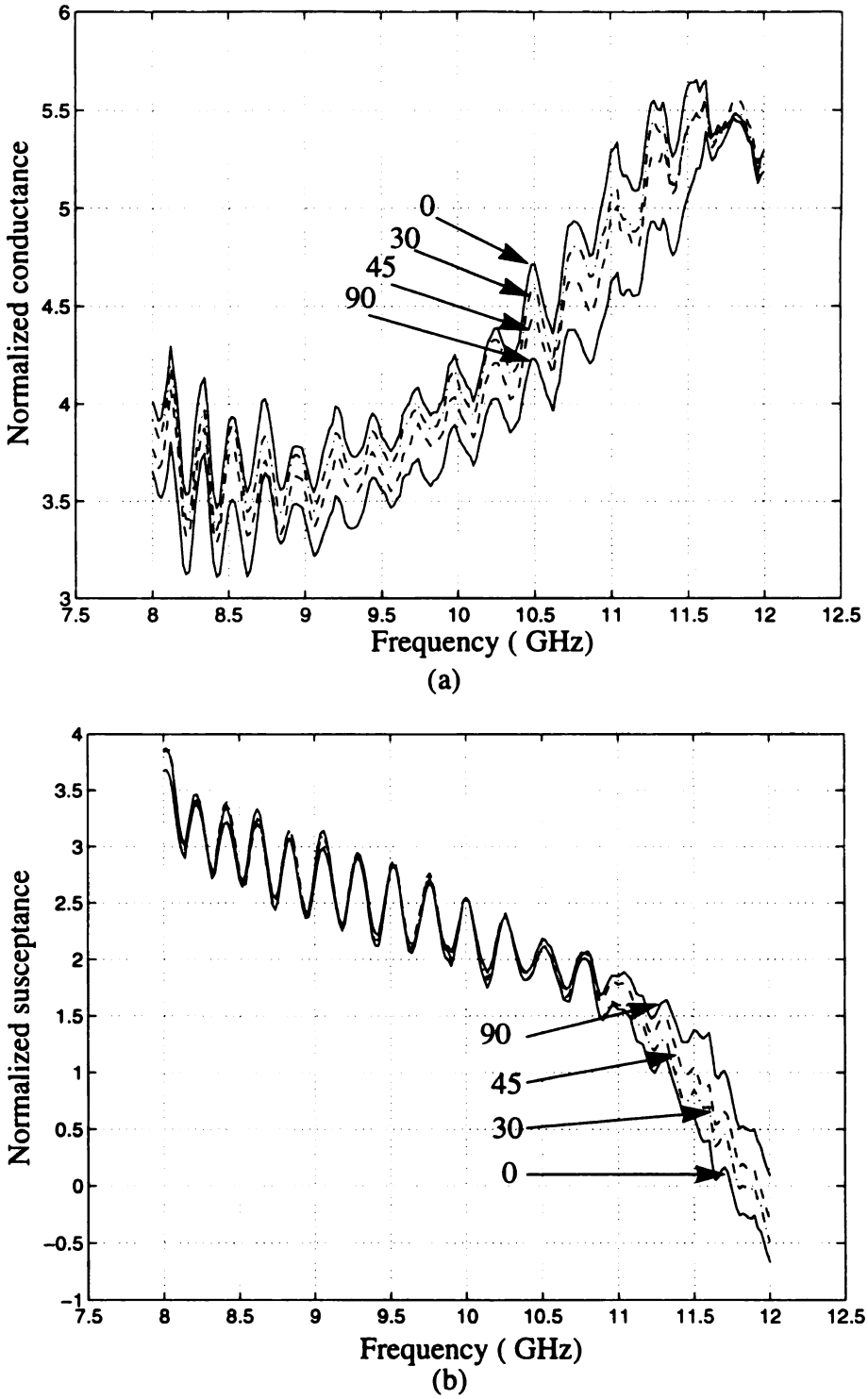

Figure 5.15 Experimental input conductances and susceptances of a waveguide probe ($a = 0.4$ *in*, $b = 0.9$ *in*) when the probe is placed against a layer of anisotropic material (Epoxy/Glass-Fiber) with a thickness of 0.1105 *inch* measured at four different orientations with respect to a reference axis of the material layer.

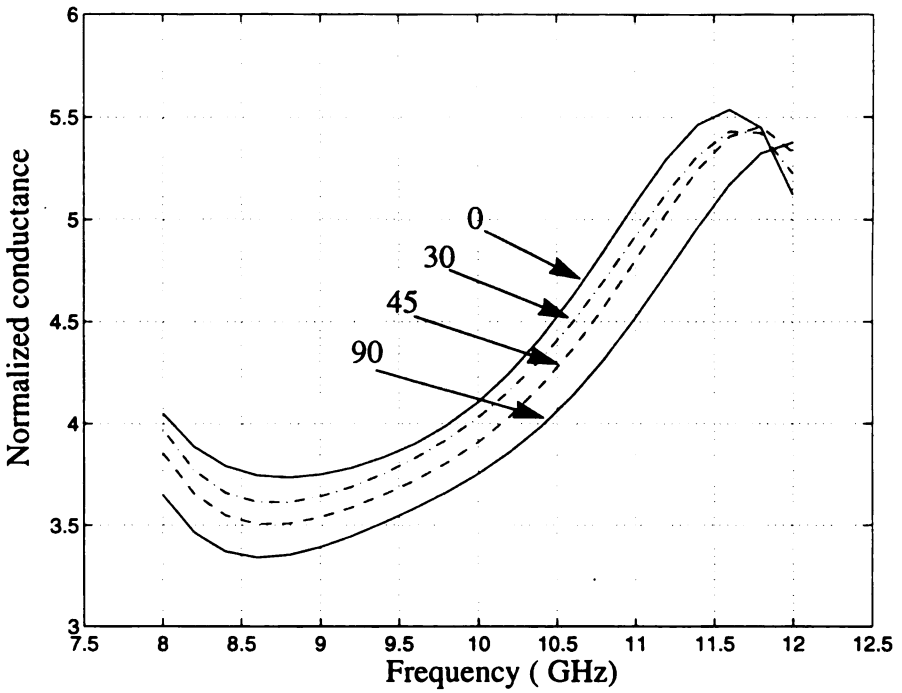

(a)

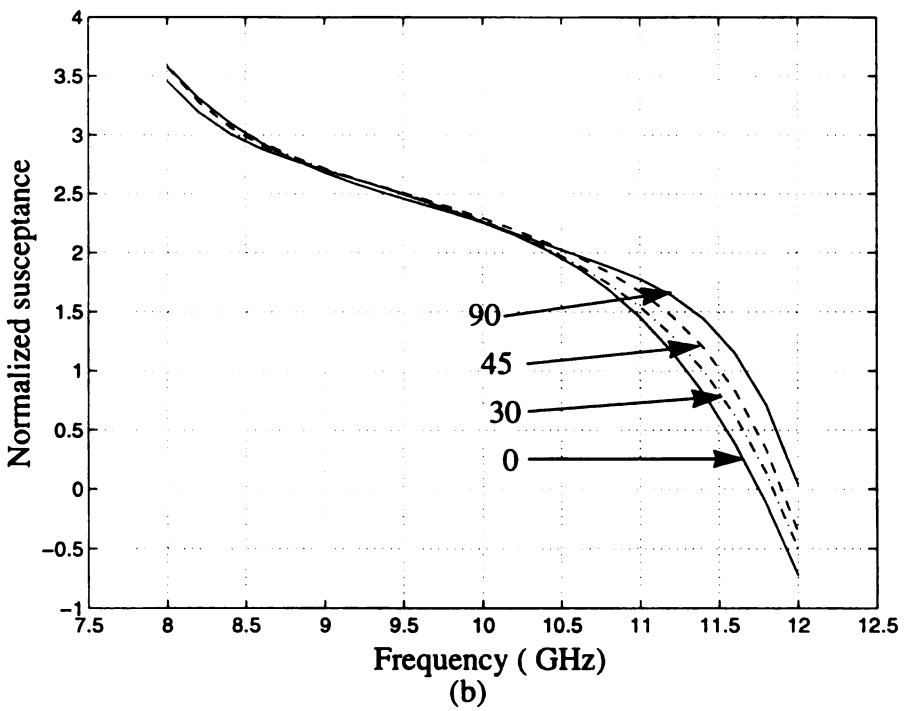

(b)

Figure 5.16 Smoothed curves of the experimental input admittances of a waveguide probe ($a = 0.4$ *in*, $b = 0.9$ *in*) when the probe is placed against an anisotropic material layer (Epoxy/Glass-Fiber) with a thickness of 0.1105 *inch* measured at four different orientations with respect to a reference axis of the material layer.

be used in the next section to inversely determine the complex permittivities of the anisotropic material layer.

Figure 5.15 shows the real and imaginary components of the experimental input admittances of a waveguide probe when the probe is placed against a layer of anisotropic material, dielectric-fiber, with a thickness of 0.053 inch. These figures show the measured results at four different orientations of the waveguide aperture with respect to a reference axis of the material layer.

Figure 5.18 shows the smoothed curves of the experimental results of Fig. 5.15. These curves represent the real and imaginary components of the smoothed waveguide input admittances when the probe is placed against the dielectric-fiber layer. These data will be used in the next section to inversely determine the complex permittivities of the anisotropic material layer.

5.4.Inverse Technique and Results

Theoretical development up to this point has been to express the effect of material parameters on the reflection coefficient or the input admittance of a waveguide probe. In this section, the material parameters as functions of the reflection coefficient or the input admittance of a waveguide probe are determined numerically by using an inversion technique based on the Newton's iterative method [45].

The newton's method, an extension of the Newton-Raphson method, is well known to have a key relationship of

$$x_{k+1} = x_k - \left(f_k'\right)^{-1} \cdot f_k \tag{5.4.1}$$

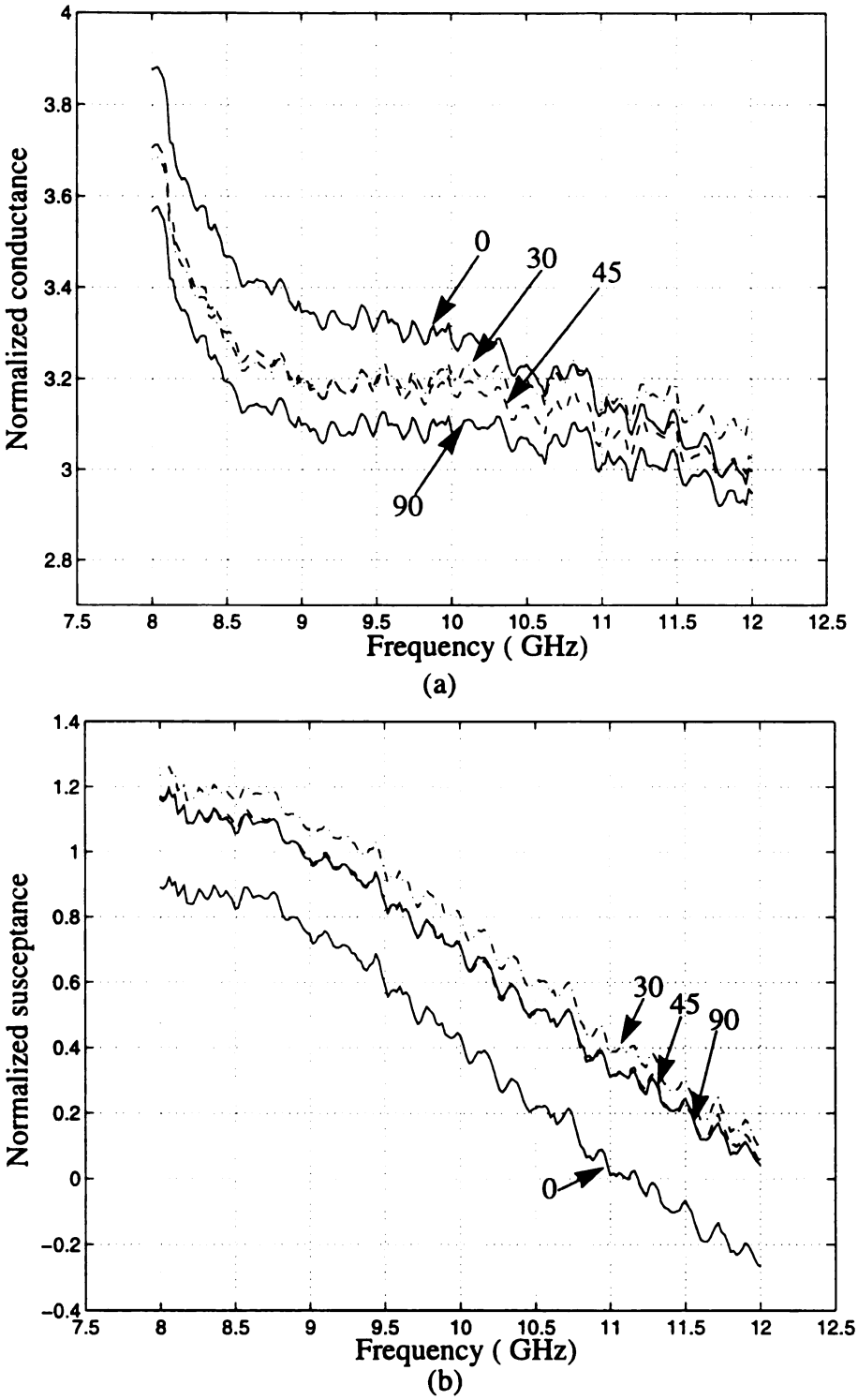

Figure 5.17 Experimental input conductances and susceptances of a waveguide probe ($a = 0.4$ *in*, $b = 0.9$ *in*) when the probe is placed against a layer of anisotropic material (dielectric-fiber from Boeing) with a thickness of 0.053 *inch* measured at four different orientations with respect to a reference axis of the material layer.

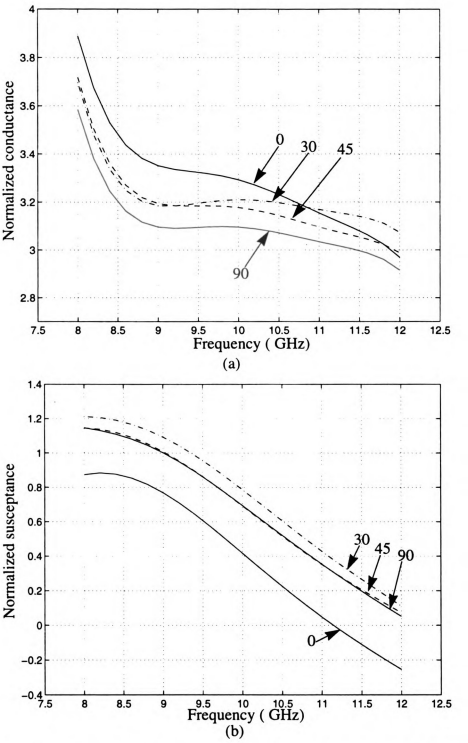

Figure 5.18 Smoothed curves of the experimental input admittances of a waveguide probe ($a = 0.4$ *in*, $b = 0.9$ *in*) when the probe is placed against an anisotropic material layer (dielectric-fiber from Boeing) with a thickness of 0.053 *inch* measured at four different orientations with respect to a reference axis of the material layer.

It also follows that, in order to extend the method to higher dimensions, an analogue of the derivative $f'(x)$ is developed to be an $n \times n$ matrix J_k which can be determined by evaluating the Jacobian matrix $J(\vec{x})$ whose entries are the partial derivatives

$$(J)_{i,j} = \frac{\partial f_i(\vec{x})}{\partial x_j} \qquad ,1 \le i,j \le n \tag{5.4.2}$$

As an example, suppose that we are using the Newton's method to solve three equations for three unknowns simultaneously, say,

$$F(\vec{x}) = \begin{bmatrix} f_1(x_1, x_2, x_3) \\ f_2(x_1, x_2, x_3) \\ f_3(x_1, x_2, x_3) \end{bmatrix} \tag{5.4.3}$$

and

$$\vec{x} = \begin{bmatrix} x_1 \\ x_2 \\ x_3 \end{bmatrix}. \tag{5.4.4}$$

Then the Jacobian matrix can be evaluated as

$$J(\vec{x}) = \begin{bmatrix} \dfrac{\partial f_1}{\partial x_1} & \dfrac{\partial f_1}{\partial x_2} & \dfrac{\partial f_1}{\partial x_3} \\ \dfrac{\partial f_2}{\partial x_1} & \dfrac{\partial f_2}{\partial x_2} & \dfrac{\partial f_2}{\partial x_3} \\ \dfrac{\partial f_3}{\partial x_1} & \dfrac{\partial f_3}{\partial x_2} & \dfrac{\partial f_3}{\partial x_3} \end{bmatrix}. \tag{5.4.5}$$

With this definition, we have, as the analogue of eq. (5.4.1),

$$\vec{x}_{k+1} = \vec{x}_k - (J_k)^{-1} F_k \tag{5.4.6}$$

where $F_k = F(\vec{x}_k)$, $J_k = J(\vec{x}_k)$ and $\vec{x}_k$ denotes the k^{th} iterative values of $\vec{x}$.

In the programming implementation, the Jacobian matrix is carried out by using a finite difference approximation for each component of J_k. That is,

$$(J_k)_{i,j} = \frac{f_i(\vec{x}_k) - f_i(\vec{x}_{k'})}{(\vec{x}_k)_j - (\vec{x}_{k'})_j} \approx \left(\frac{\partial f_i(\vec{x})}{\partial x_j} \right)_{x = x_k} \tag{5.4.7}$$

where $(x_k - x_{k'}) = \delta$ denotes a preset difference.

To solve n equations for n unknowns, this Newton's iterative method can be regarded as an n-dimensional analogue of the secant method. Substituting eq. (5.4.7) in eq. (5.4.6), the $(k+1)^{th}$ iterative value of $\vec{x}$ is calculated. If $F(\vec{x}_{k+1}) \approx 0$ is satisfied at some preset accuracy then the problem is solved with $\vec{x}_{k+1}$ to be the roots of equation $F(\vec{x}) = 0$ and the iterative process is terminated. Otherwise, a new approximation will be generated to continue the iterative procedure defined by the recursion formula (5.4.6).

As developed earlier, since the reflection coefficient or the input admittance of the waveguide probe is an implicit function of the material parameters such as permittivity ε, permeability μ and the thickness of the material layer, etc., the inversion of material parameters can be achieved by the Newton's iterative method. Let $\vec{R}_m$ be a vector representing the n different measured reflection coefficients or the input admittance of the waveguide probe with the unknown material layer, and $\vec{R}_{th}$ be the corresponding vector for the n theoretical reflection coefficients or the input admittances at the probe aperture. The nonlinear equation, $F(\vec{x}) = 0$, with n unknowns is constructed as

$$F(\vec{x}) = \vec{R}_{th}(\vec{x}) - \vec{R}_m = 0 \tag{5.4.8}$$

With an appropriate set of guess values $\vec{x}_0$ and the use of the recursion formula given in eq. (5.4.6), the correct material parameters, $\vec{x}$, can be determined inversely that lead to the n measured reflection coefficients or the input admittances.

With the assumption of free-space permeability ($\mu = \mu_0$) for all measured materials discussed in the preceding sections, the complex permittivities of these materials are inversely determined from the measured waveguide input admittances. For an isotropic material layer, one measurement of the waveguide input admittance is needed to inversely determine the complex permittivity of the material layer via the inverse technique, while, for an anisotropic material layer, three measurements of the waveguide input admittance will be required to inversely determine three complex permittivities with respect to the three principal axes of the material layer.

In Fig. 5.19, we show the permittivities of the open space inversely determined from the measured input admittances of the waveguide probe as shown in Fig. 5.8. Two sets of results obtained by the inverse technique based on two different methods, the Hertzian potential method and the transverse field method, which have been addressed in Chapter 3 and 4, are shown in this figure. The marks with '*' represent the results which are inversely determined from technique based on Hertzian potentials, and the marks with 'o' represent that from the technique based on the transverse field method. Both methods give good and consistent results for the complex permittivities of free space.

Since the computation time of the inverse procedure based on the transverse field method is longer than that based on the Hertzian potential method, the inverse results of the measured complex permittivities of the following isotropic materials were determined by employing the technique based on Hertzian potentials only. On the other hand, the measured permittivities of the anisotropic materials were determined by using the technique based on the transverse field method.

Figure 5.20 shows the measured complex permittivity of an acrylic layer with a thickness of 0.06 *inch*. The results indicate $\varepsilon_r \approx 2.5 \sim 2.7$ and $\varepsilon_i \approx -0.1 \sim 0$ for the most part of frequency range. These results are quite consistent with that obtained by Li [46].

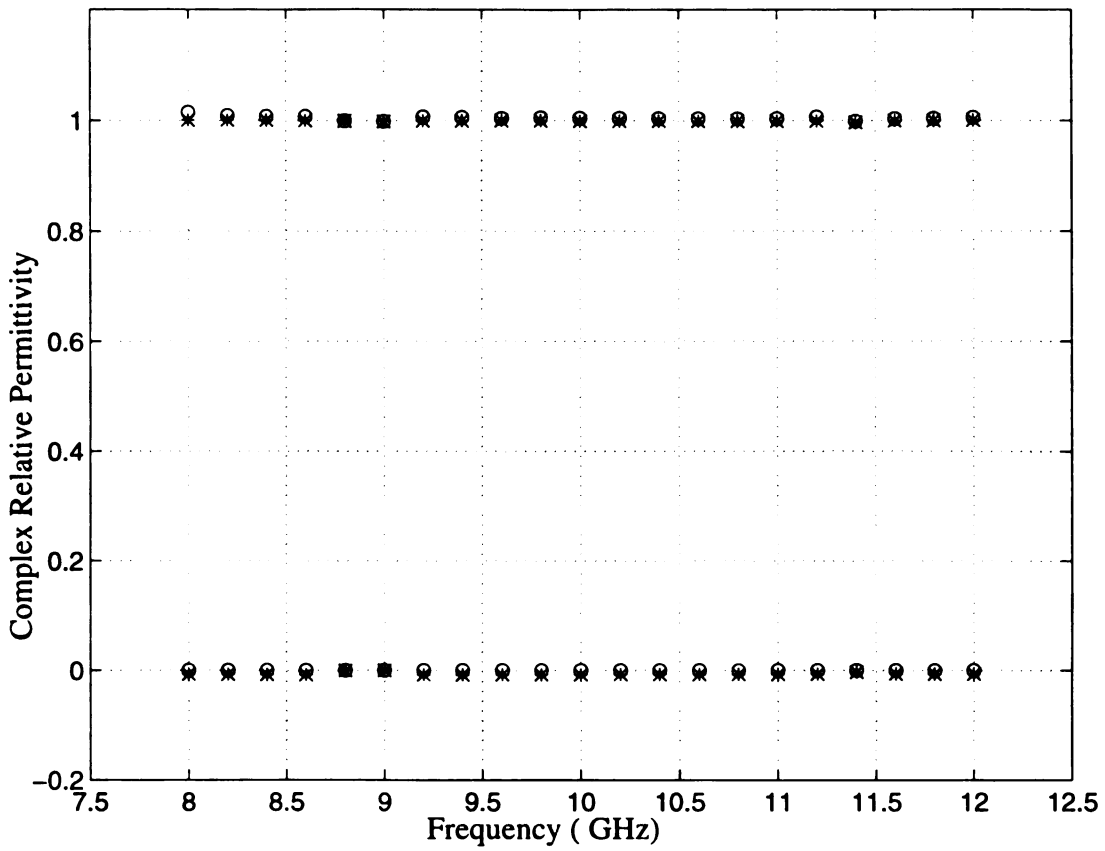

Figure 5.19 The inverse results of the complex relative permittivities of free space determined by employing two different methods. The '*' marks represent the results based on the Hertzian potential method, while the 'o'marks represent that based on transverse field method. The upper curves show the real part of the complex relative permittivities, while the lower curves show the imaginary part.

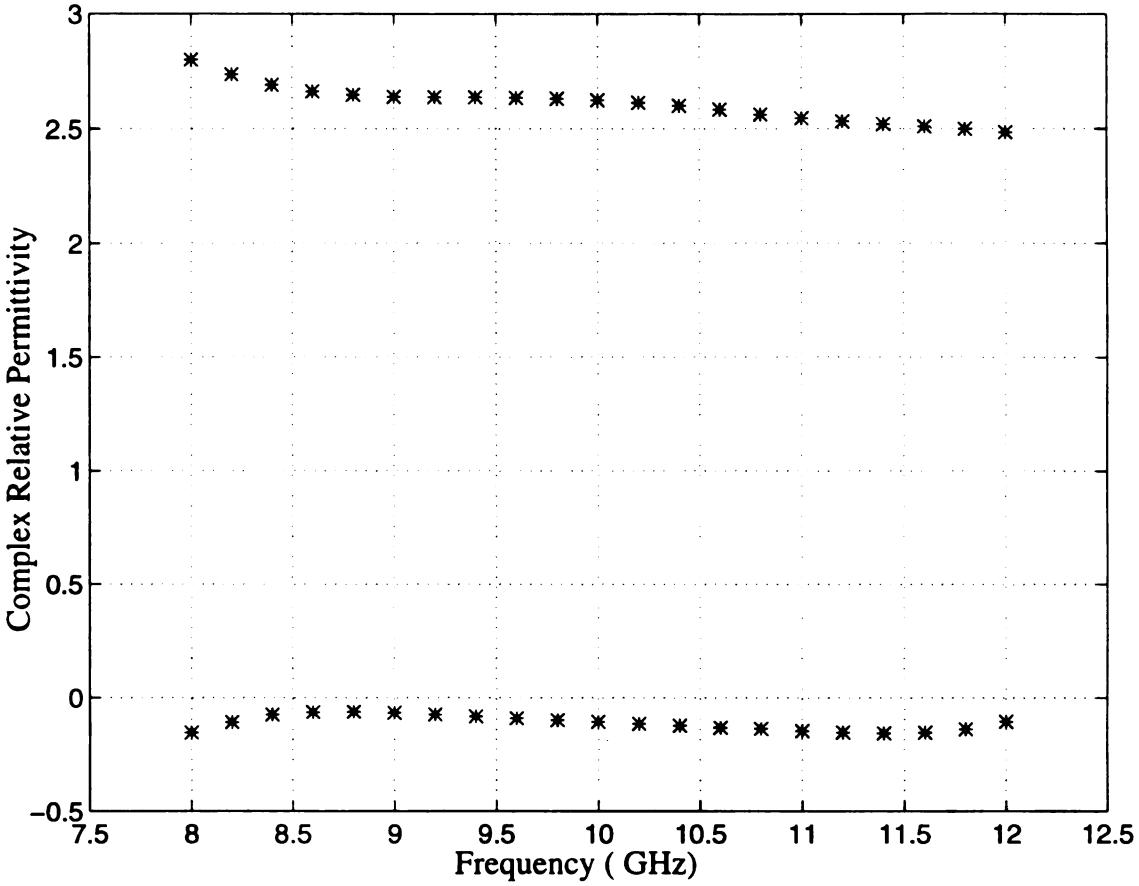

Figure 5.20 The inverse results of complex relative permittivity of a material layer (acrylic) which has a dielectric constant of ε_r = 2.5~2.7 and a thickness of 0.06 *inch*. The upper curve shows the real part of complex relative permittivity, while the lower curve shows the imaginary part.

Figure 5.21 shows the measured complex permittivity of a plexiglass layer with a thickness of 0.06 *inch*. The results indicate $\varepsilon_r \approx 2.5 \sim 2.7$ and $\varepsilon_i \approx -0.1 \sim 0$ which are close to the published results.

Figure 5.22 shows the measured complex permittivity of an teflon layer with a thickness of 0.51625 *inch*. The results indicate $\varepsilon_r \approx 2.05$ and $\varepsilon_i \approx 0$ for the most part of the frequency range. These results are considered to be quite accurate.

Figure 5.23 shows the complex permittivity of a layer of distilled water inversely determined from the measured input admittances of the waveguide probe as shown in Fig. 5.13. Two set of results are obtained from two measurements of distilled water with two different thicknesses of 0.2344 *inch* and 0.3125 *inch*. Both cases give very consistent results on the real and imaginary components of the permittivities. At 10 GHz, the measured results indicate $\varepsilon_r \approx 59$ and $\varepsilon_i \approx -17$ which agree very well with the published results of Metaxas and Meredith et al. [47] who gave $\varepsilon_r \approx 59$ and $\varepsilon_i \approx -20 \sim -30$. While there is a good agreement between the real components of the permittivity, the discrepancy of the imaginary components of the permittivity is probably due to different degrees of pureness of distilled water used in the experiments.

Figure 5.24 shows the measured complex permittivity of a layer of acetone with a thickness of 0.345 *inch*. The results indicate $\varepsilon_r \approx 6 \sim 8$ and $\varepsilon_i \approx 0$ for the most part of the frequency range. These results are considered to be reasonable.

The measured complex tensor permittivities of a layer of anisotropic material, an epoxy/glass-fiber supplied by Composite Material Laboratory of Michigan State University, with a thickness of 0.1105 *inch*, are shown in Fig. 5.25. In the figure, the real components of three complex relative permittivities in the three principal directions are shown in the upper graph (a), while the imaginary components of the corresponding permittivities are in the lower graph (b). Both graphs contain two sets of results; the solid

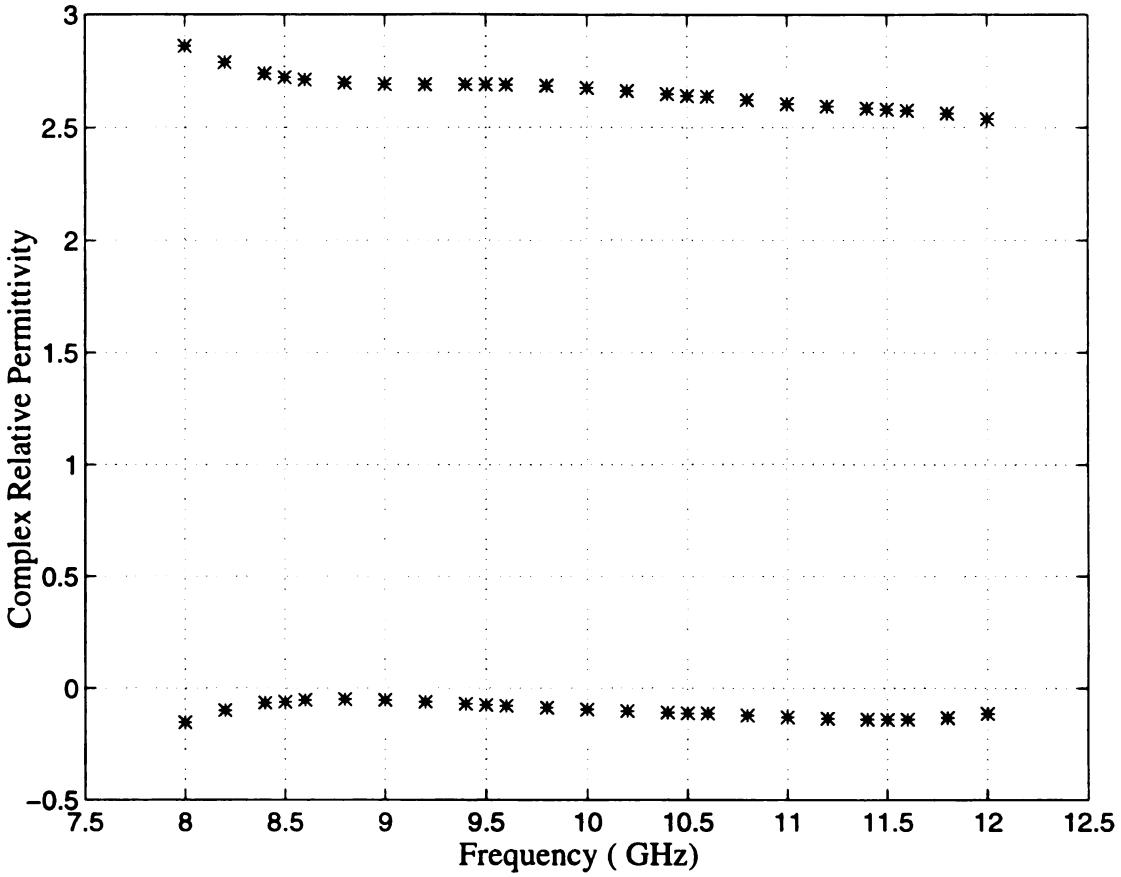

Figure 5.21 The inverse results of complex relative permittivity of a material layer (plexiglass) which has a dielectric constant of $\varepsilon_r = 2.59$ and a thickness of 0.06 *inch*. The upper curve shows the real part of complex relative permittivity, while the lower curve shows the imaginary part.

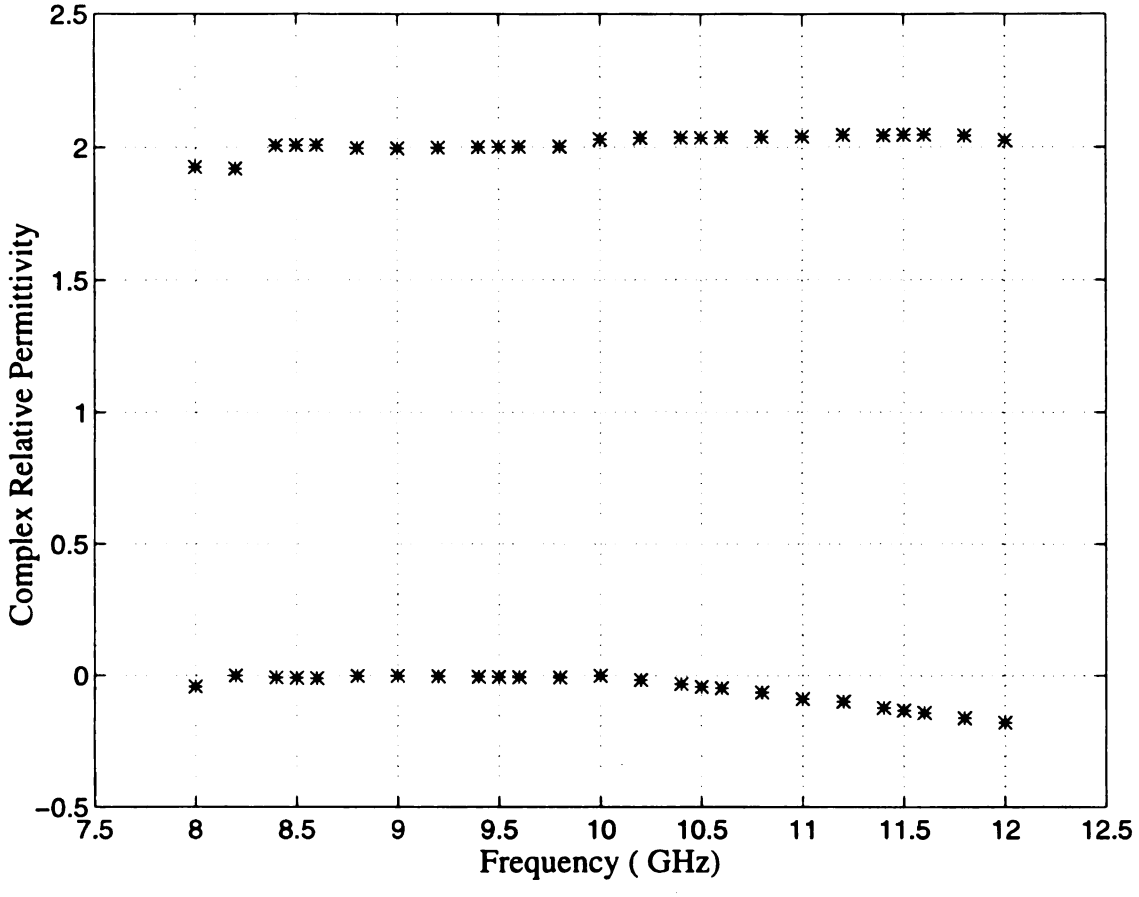

Figure 5.22 The inverse results of complex relative permittivity of a material layer (teflon) which has a dielectric constant of $\varepsilon_r = 2.046$ and a thickness of 0.51625 *inch*. The upper curve shows the real part of complex relative permittivity, while the lower curve shows the imaginary part.

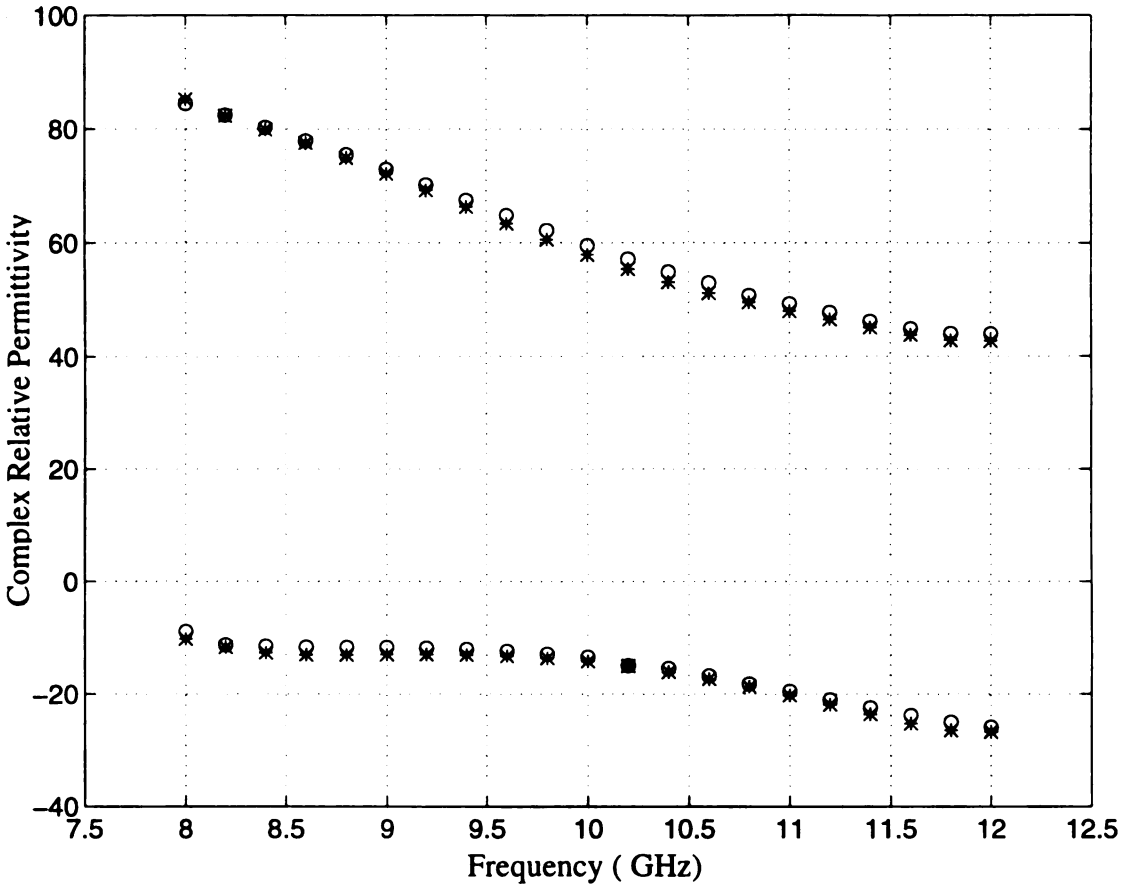

Figure 5.23 The inverse results of complex relative permittivities of two material layers (distilled water) with two different thickness's of 0.2344 *inch* and 0.3125 *inch*. The upper curves of the graph show the real part of complex relative permittivity, while the lower curves show the imaginary part.

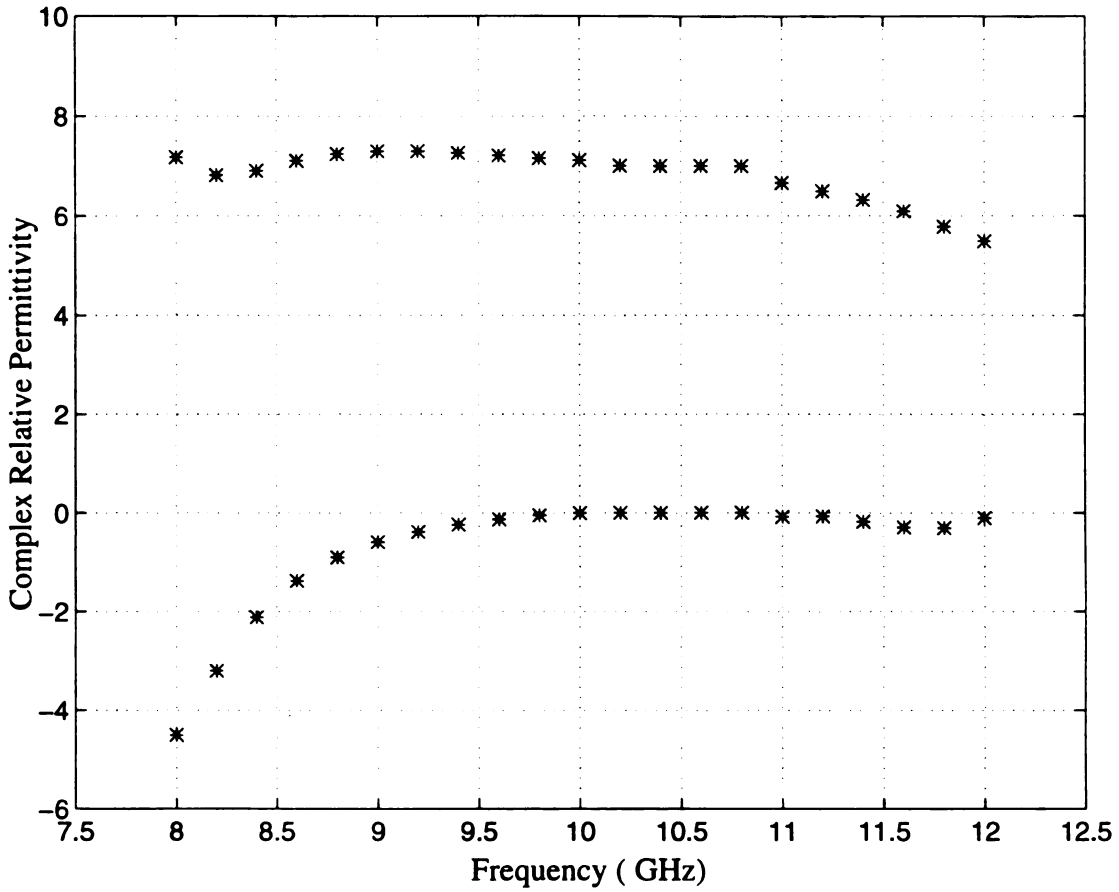

Figure 5.24 The inverse results of complex relative permittivity of a material layer (acetone) which has a thickness of 0.345 *inch*. The upper curve shows the real part of complex relative permittivity, while the lower curve shows the imaginary part.

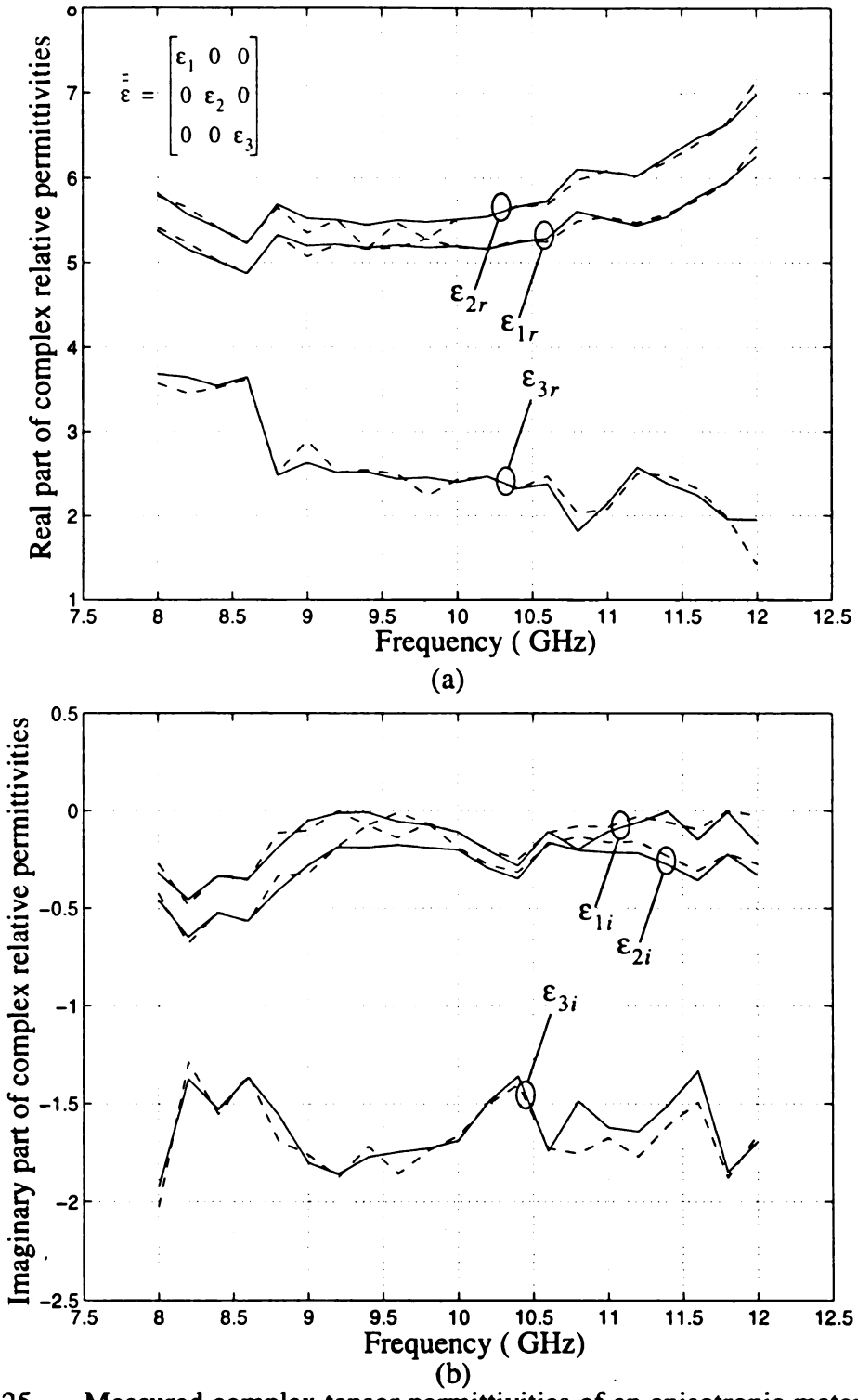

Figure 5.25 Measured complex tensor permittivities of an anisotropic material layer (epoxy/glass-fiber) with a thickness of 0.1105 *inch*. The solid lines represent the measured results inversely determined by employing three measurements of the probe input admittances with the probe orientations of 0, 45 and 90 degrees with respect to a principal axis of the material, while the dash lines represent the corresponding results with the probe orientation of 0, 30 and 90 degrees.

lines represent the measured permittivities obtained by employing three different measurements of the probe input admittances with the probe orientations of 0, 45 and 90 degrees with respect to a principal axis of the material, and the dash lines represent those with the probe orientations of 0, 30 and 90 degrees. As shown in the figure, both cases give quite consistent results on the real and imaginary components of the permittivities. It is also important to note that these measured permittivities are inversely determined by assuming a dominant TE_{10} mode only for the aperture electric field in the solution of the matrix equation. As discussed in Chapter 4, since the effect of the higher order modes in the aperture electric field is insignificant when the waveguide probe is attached to an anisotropic material layer, the inverse results with only a dominant mode consideration should be sufficiently accurate.

Figure 5.26 shows the measured complex tensor permittivities of a layer of anisotropic material, a dielectric-fiber manufactured by Boeing Airplane Company, with a thickness of 0.053 $inch$. The results are determined inversely by employing three measurements of the probe input admittances with the probe orientations of 0, 30 and 90 degrees with respect to a principal axis of the material. In the figure, we only show the real and imaginary components of the principal permittivities in the transverse directions, while the permittivity in the perpendicular direction is omitted because it is found to be of highly unstable giving a value between 10 to 10000 for both real and imaginary components. The difficulty encountered in this case will be discussed in the next section.

5.5.Analysis on the Effects of Material Parameters

The reflection coefficient or the input admittance of a waveguide probe placed against a layer of material has been shown in the preceding chapters to be a function of the EM parameters of the material, such as permittivity, permeability, conductivity and sample thickness. In our measurements, with the assumption of having free-space permeability

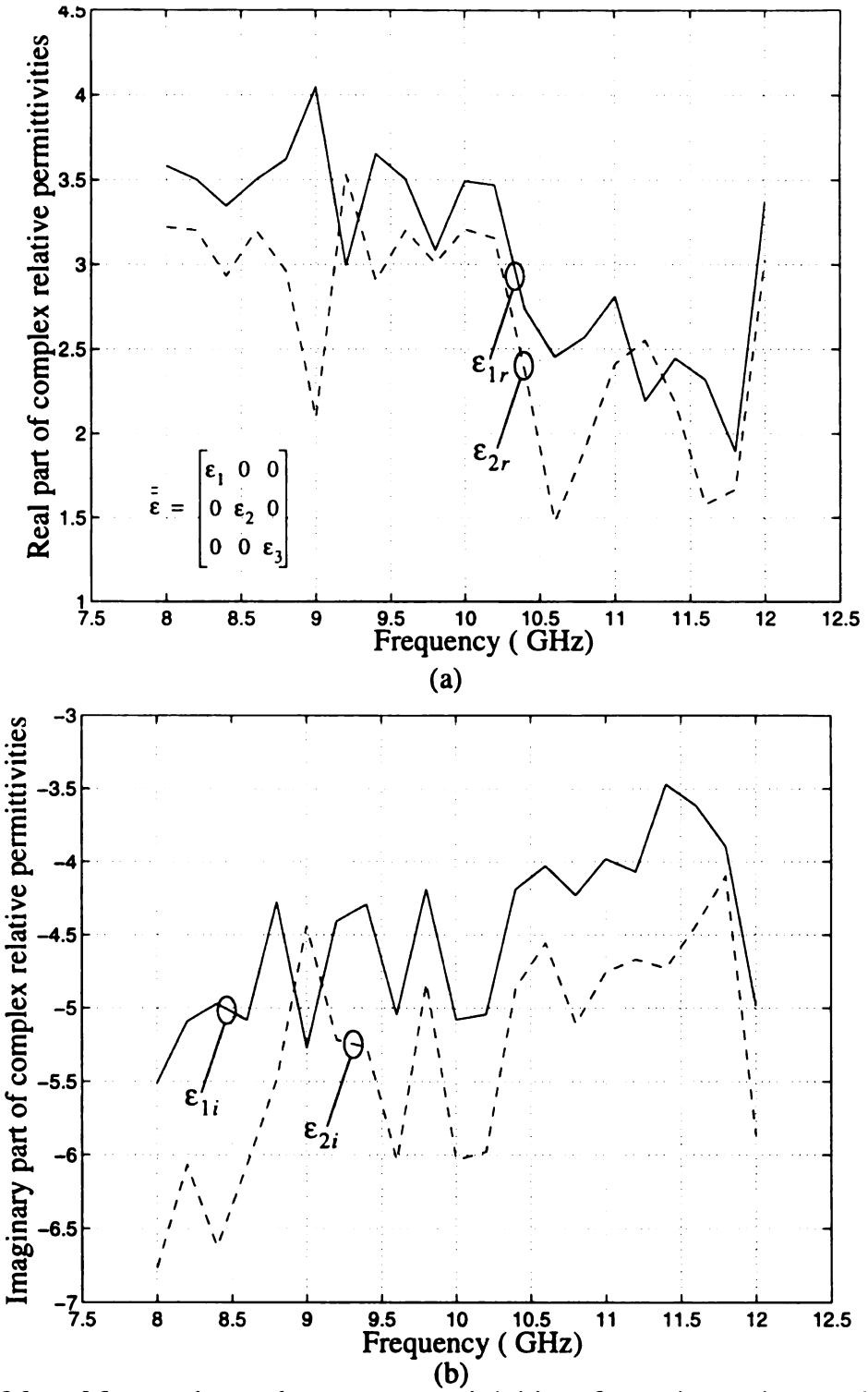

Figure 5.26 Measured complex tensor permittivities of an anisotropic material layer (dielectric-fiber) with a thickness of 0.053 *inch*. The results are determined inversely by employing three measurements of the probe input admittances with the probe orientations of 0, 30 and 90 degrees with respect to a principal axis of the material. The complex permittivity in the direction perpendicular to the waveguide aperture is determined to be unstable and is omitted.

and fixed known thickness for the material layer, there is no difficulty in determining the permittivity and conductivity of isotropic materials inversely; however, for anisotropic materials, there exist some constraints. In this section we will discuss the effects of the material parameters on the input admittance of the probe and the constraints one needs to consider in the measurements of anisotropic materials.

As discussed in the preceding section, we have difficulty in the inverse determination of the EM parameters of a layer of anisotropic dielectric-fiber manufactured by Boeing Airplane Company. In that measurement, the conductivity in the direction perpendicular to the waveguide aperture was found to be highly unstable. To find out the reason for causing this problem, we develop the following scheme.

Let's assume that a waveguide probe is placed against an anisotropic material layer with three principal complex permittivities of $\varepsilon_1 = 5.4 - j5.3$, $\varepsilon_2 = 5.8 - j6.4$ and $\varepsilon_3 = 3.8 - j5.7$. For this kind of materials, we can first plot the input admittance of the waveguide probe as a function of the material thickness. If we further change one of the imaginary components of three principal complex permittivities in the theoretical calculation, the effects of the specific conductivity associated with the thickness on the probe input admittance can be sought.

Figure 5.27 shows the real and imaginary components of the input admittance of a waveguide probe as functions of the material thickness when the probe is placed against a layer of anisotropic material at an operating frequency of 10 GHz. In the figure, the anisotropic material is assumed to have three principal complex permittivities of $\varepsilon_1 = 5.4 - jx$, $\varepsilon_2 = 5.8 - j6.4$ and $\varepsilon_3 = 3.8 - j5.7$, where x takes the values of 0.3, 10.3 and 1000.3 in three different cases. Since the aperture electric field is dominated by the dominant TE_{10} mode which has an electric field in the y-direction only, changing the material conductivity in the x direction does not change the induced current in the material layer, leading to an insignificant change in the probe input admittance. This phenomenon

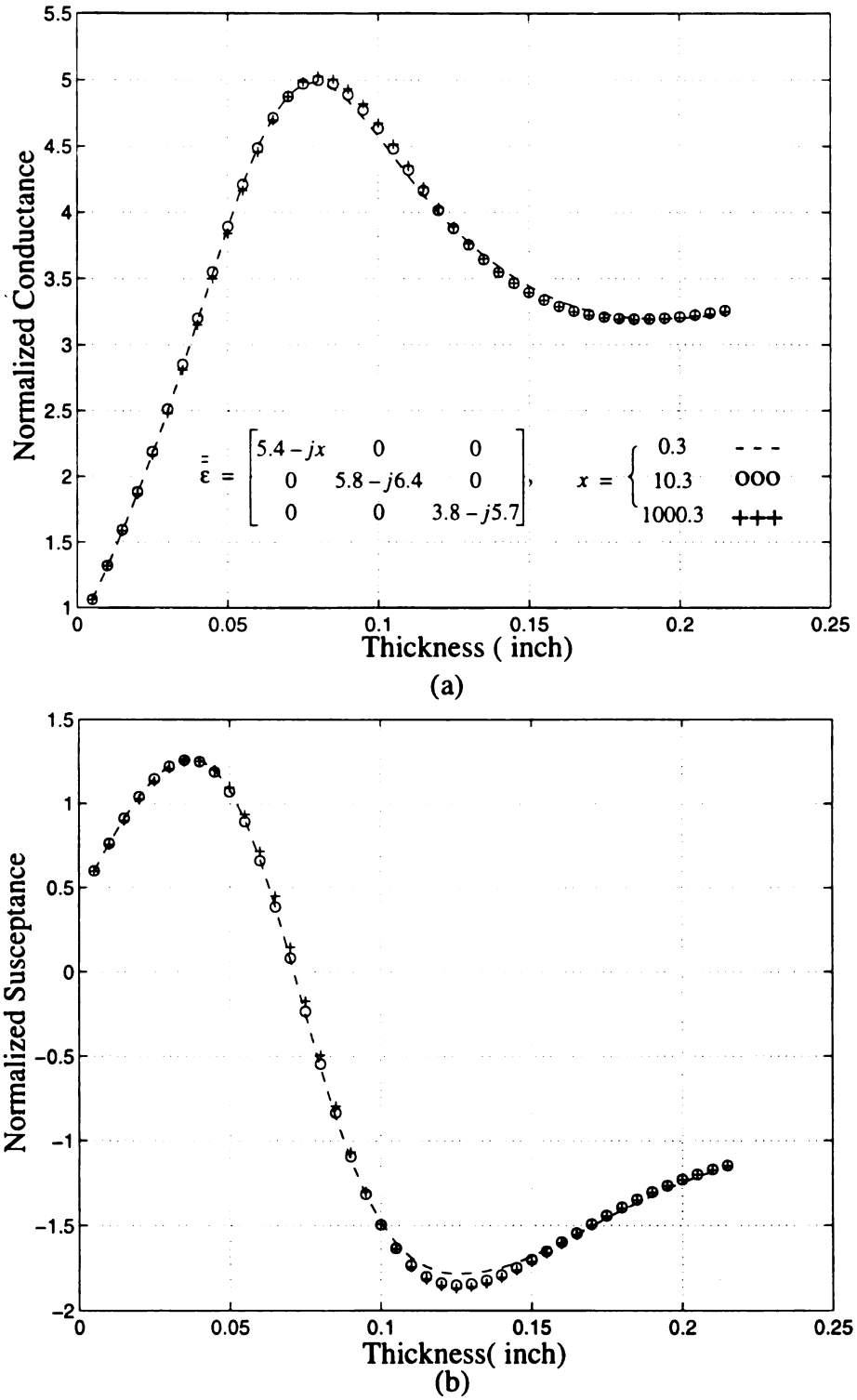

Figure 5.27 Input admittance of a waveguide probe as a function of the material thickness at 10 GHz when the probe is placed against an anisotropic material layer supplied by Boeing Airplane Company with various conductivities in the x direction.

can be verified from the figure that shows almost identical curves for the three different cases of x.

At the same operating frequency of 10 GHz, Fig. 5.28 shows the real and imaginary components of the input admittance of a waveguide probe as functions of the material thickness when the probe is placed against a layer of anisotropic material with three principal complex permittivities of $\varepsilon_1 = 5.4 - j5.3$, $\varepsilon_2 = 5.8 - jx$ and $\varepsilon_3 = 3.8 - j5.7$, where x is assumed to have values of 0.4, 10.4 and 1000.4 in three different cases. Since the electric field of the dominant TE_{10} mode is in the y-direction, the change in the material conductivity in the y direction should cause a great change in the probe input admittance. We can observe in this figure that the probe input admittances for three different cases are highly distinguishable over a range of material thickness. It is also noted that when the measured anisotropic material is highly conductive in the y-direction, the probe input admittance becomes independent of the material thickness because the material layer essentially becomes a short circuit.

Similarly, Fig. 5.29 shows the real and imaginary components of the input admittance of a waveguide probe as functions of the material thickness when the probe is placed against a layer of anisotropic material with three principal complex permittivities of $\varepsilon_1 = 5.4 - j5.3$, $\varepsilon_2 = 5.8 - j6.4$ and $\varepsilon_3 = 3.8 - jx$, where x assumes the values of 0.7, 10.7 and 1000.7 in three different cases. In the figure, we found that when the anisotropic material is highly conductive (such as x=10.7 and 1000.7) in the direction perpendicular to the waveguide aperture, the probe input admittance remains nearly constant for the material thickness smaller than 0.07 inch. This phenomenon is maybe due to the fact that the induced current in the perpendicular direction of a thin conducting layer is quite small and is independent of the conductivity in the perpendicular direction.

From Fig. 5.26, we found that three principal permittivities of the dielectric-fiber from Boeing Airplane Company are approximately of $\varepsilon_1 = 3.5 - j5$, $\varepsilon_2 = 3.2 - j6$ and ε_3

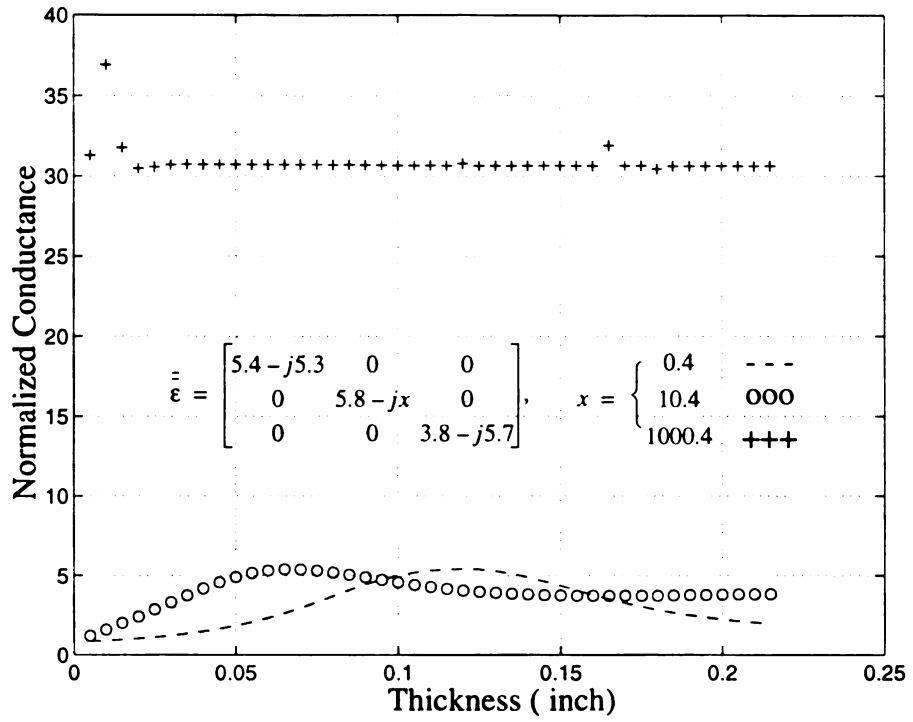

(a)

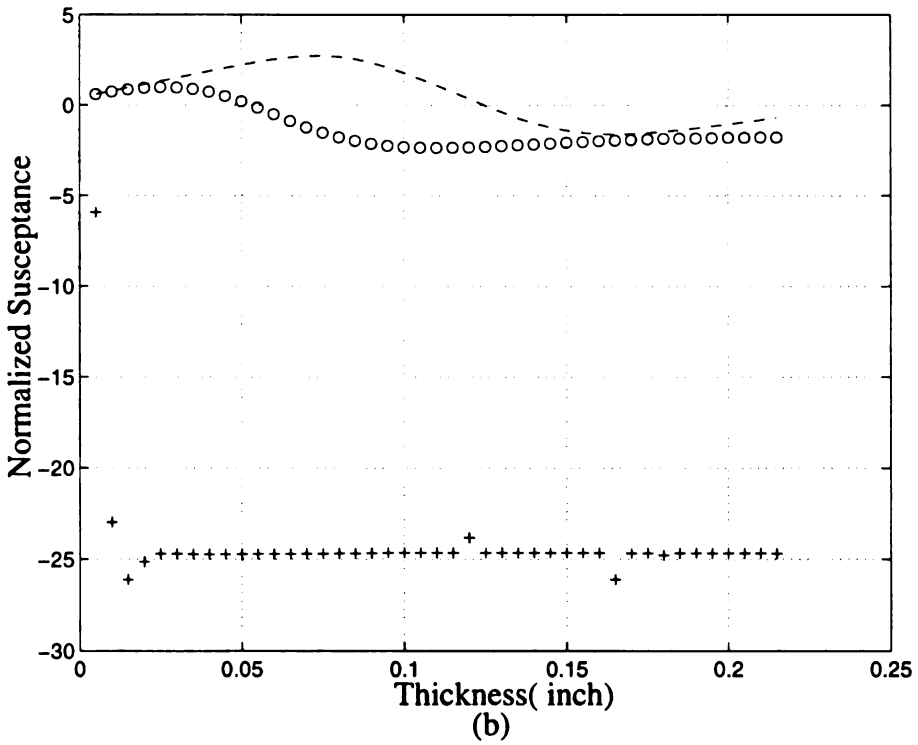

(b)

Figure 5.28 Input admittance of a waveguide probe as a function of the material thickness at 10 GHz when the probe is placed against an anisotropic material layer supplied by Boeing Airplane Company with various conductivities in the y direction.

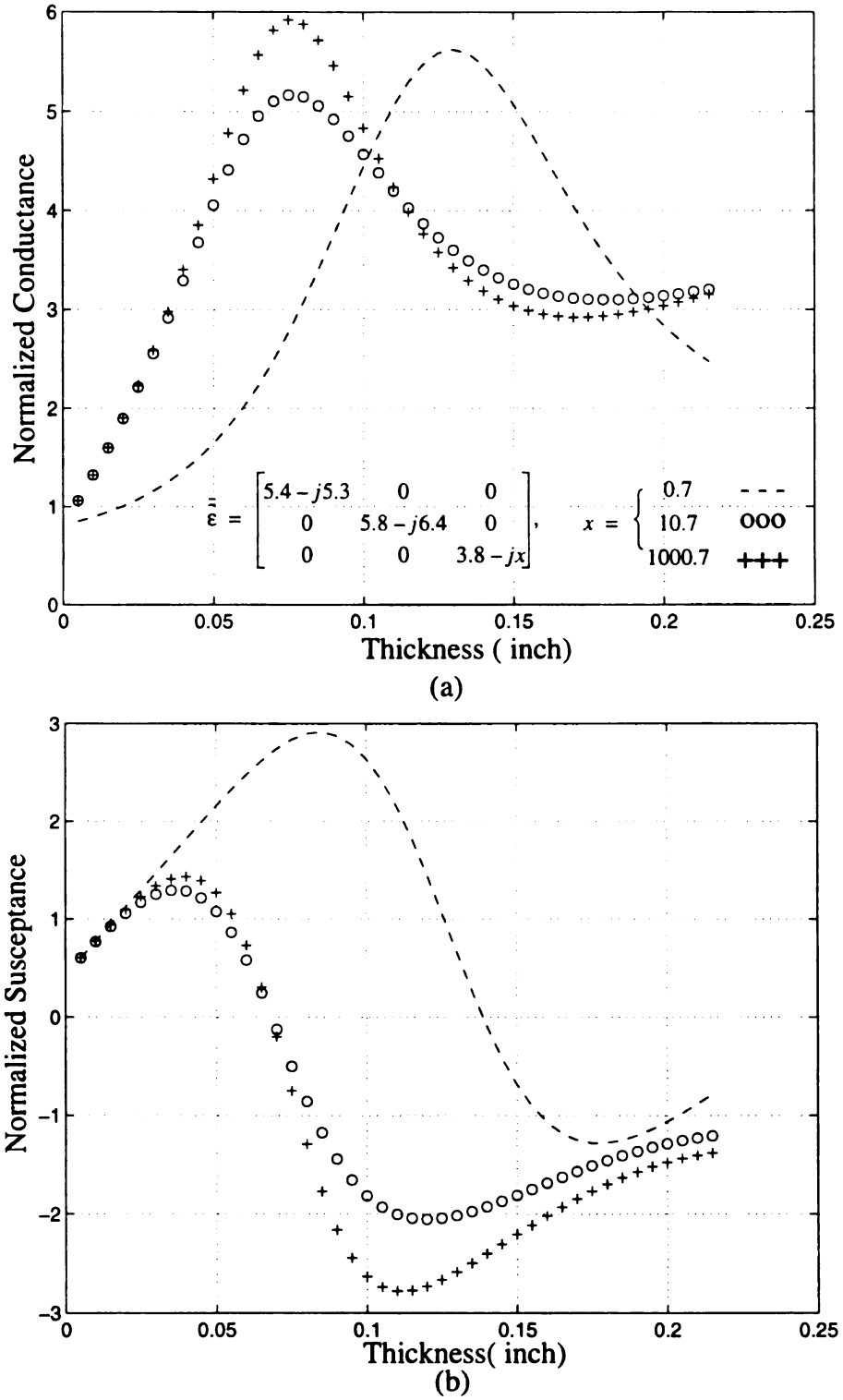

Figure 5.29 Input admittance of a waveguide probe as a function of the material thickness at 10 GHz when the probe is placed against an anisotropic material layer supplied by Boeing Airplane Company with various conductivities in the z direction.

with an unstable value of between 10 to 10000, which is just the same order of quantities used in the calculation of the results shown in Figs. 5.27-5.29. The thickness of this dielectric-fiber is 0.053 inch and at this thickness the conductivity in the z direction causes very small change in the probe input admittance. Therefore, it is very difficult to inversely determine the ε_3 (in the z-direction) from the measured probe input admittance.

Employing the similar scheme, the measurement using a waveguide probe placed against a layer of epoxy/glass-fiber supplied by MSU Composite Material Laboratory can also be analyzed. From Fig. 5.25, we found that three principal permittivities of the epoxy/glass-fiber at 10 GHz are approximate of $\varepsilon_1 = 5.1 - j0.2$, $\varepsilon_2 = 5.3 - j0.3$ and $\varepsilon_3 = 2.5 - j1.7$. From a plot of the probe input admittance as a function of the material thickness, if we further change one of the imaginary components of three principal complex permittivities in the theoretical calculation, the effect of the specific conductivity associated with the thickness on the probe input admittance can be determined.

Figure 5.30 shows the real and imaginary components of the input admittance of a waveguide probe as functions of the material thickness when the probe is placed against a layer of anisotropic material at an operating frequency of 10 GHz. The anisotropic material is assumed to have three principal complex permittivities of $\varepsilon_1 = 5.4 - jx$, $\varepsilon_2 = 5.8 - j0.4$ and $\varepsilon_3 = 3.8 - j1.7$, where x takes the values of 0.3, 10.3 and 1000.3 in three different cases. As mentioned earlier, since the aperture electric field is dominated by the dominant TE_{10} mode which has no electric field in the x direction, the change in the material conductivity in the x direction has insignificant effect on the probe input admittance, as shown in the figure.

Figure 5.31 shows the real and imaginary components of the input admittance of a waveguide probe as functions of the material thickness at 10 GHz when the probe is placed against a layer of anisotropic material with three principal complex permittivities of $\varepsilon_1 = 5.4 - j0.3$, $\varepsilon_2 = 5.8 - jx$ and $\varepsilon_3 = 3.8 - j1.7$, where x assumes the values of

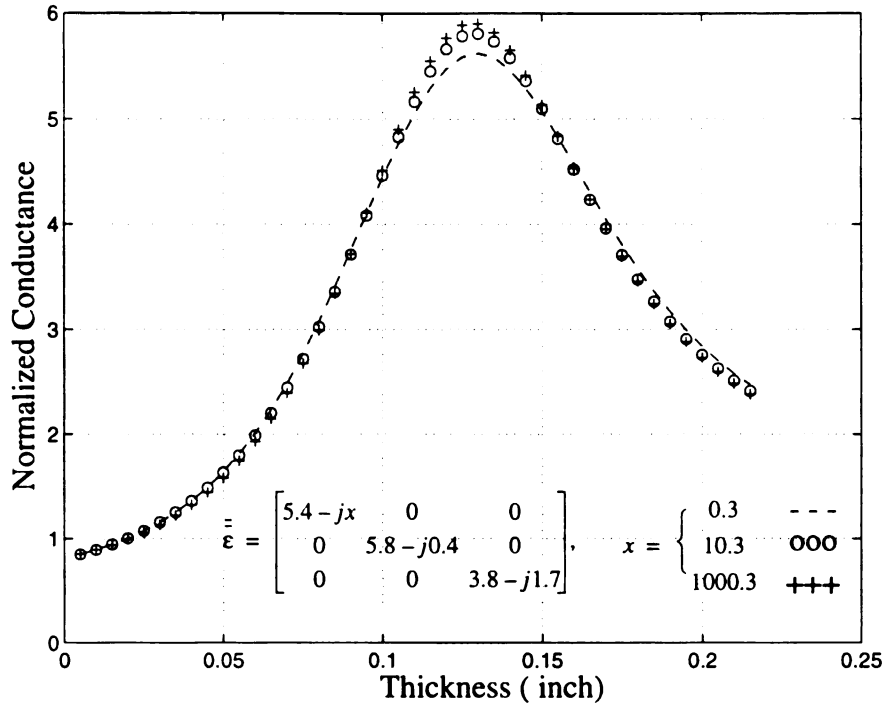

(a)

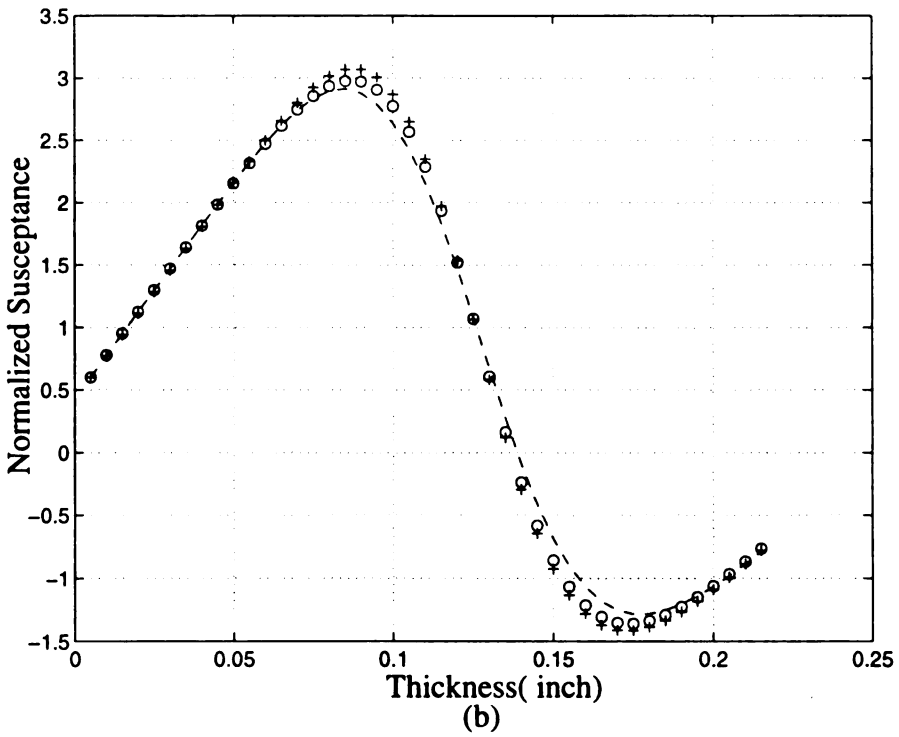

(b)

Figure 5.30 Input admittance of a waveguide probe as a function of the material thickness at 10 GHz when the probe is placed against an anisotropic material layer supplied by MSU Composite Material Laboratory with various conductivities in the x direction.

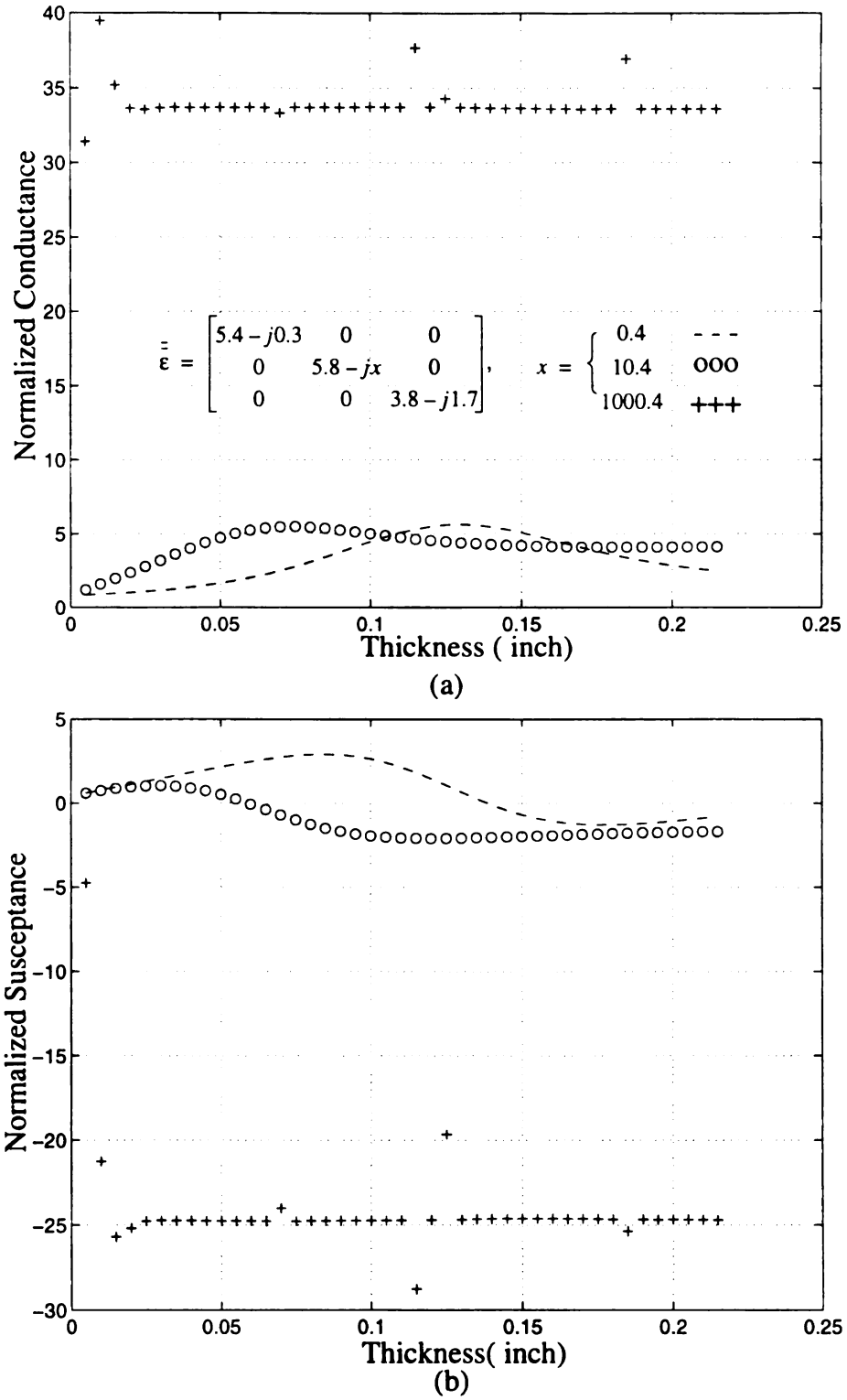

Figure 5.31 Input admittance of a waveguide probe as a function of the material thickness at 10 GHz when the probe is placed against an anisotropic material layer supplied by MSU Composite Material Laboratory with various conductivities in the y direction.

0.4, 10.4 and 1000.4 in three different cases. As shown in the figure, the probe input admittances for three different cases are very different over a range of material thickness because the change in the conductivity in the y-direction will cause significant change in the induced current in the material layer.

Figure 5.32 shows the real and imaginary components of the input admittance of a waveguide probe as functions of the material thickness at 10 GHz when the probe is placed against a layer of anisotropic material with three principal complex permittivities of $\varepsilon_1 = 5.4 - j0.3$, $\varepsilon_2 = 5.8 - j0.4$ and $\varepsilon_3 = 3.8 - jx$, where x has the values of 1.7, 10.7 and 1000.7 in three different cases. In the figure, we found that when the anisotropic material becomes highly conductive in the direction perpendicular to the waveguide aperture, the effect of the conductance on the probe input admittance become significant if the material layer is thicker than about 0.07 inch. Since the thickness of the epoxy/glass-fiber is 0.1103 inch which is thicker than 0.07 inch, we can then inversely determine three principal complex permittivities of the epoxy/glass-fiber without any difficulty.

We also analyzed the measurement using a waveguide probe placed against a layer of isotropic material with a complex permittivity of $\varepsilon = 2.046 - j0.1$. In Fig. 5.33, we show the real and imaginary components of the probe input admittance as functions of the material thickness at 10 GHz when the probe is placed against a layer of isotropic material with a complex permittivity of $\varepsilon = 2.046 - jx$, where x has the values of 0.1, 0.2 and 0.5 in three different cases. We found that those probe input admittances of three cases are clearly distinguishable. It is also noted that when the material is highly conductive, the probe input admittance becomes independent of the material thickness, which is the same phenomenon as in the anisotropic materials and is not shown in this figure.

Figure 5.34 shows the real and imaginary components of the probe input admittance as functions of the material thickness at 10 GHz when the probe is placed against a layer of isotropic material with a complex permittivity of $\varepsilon = x - j0.1$, where x assumes the

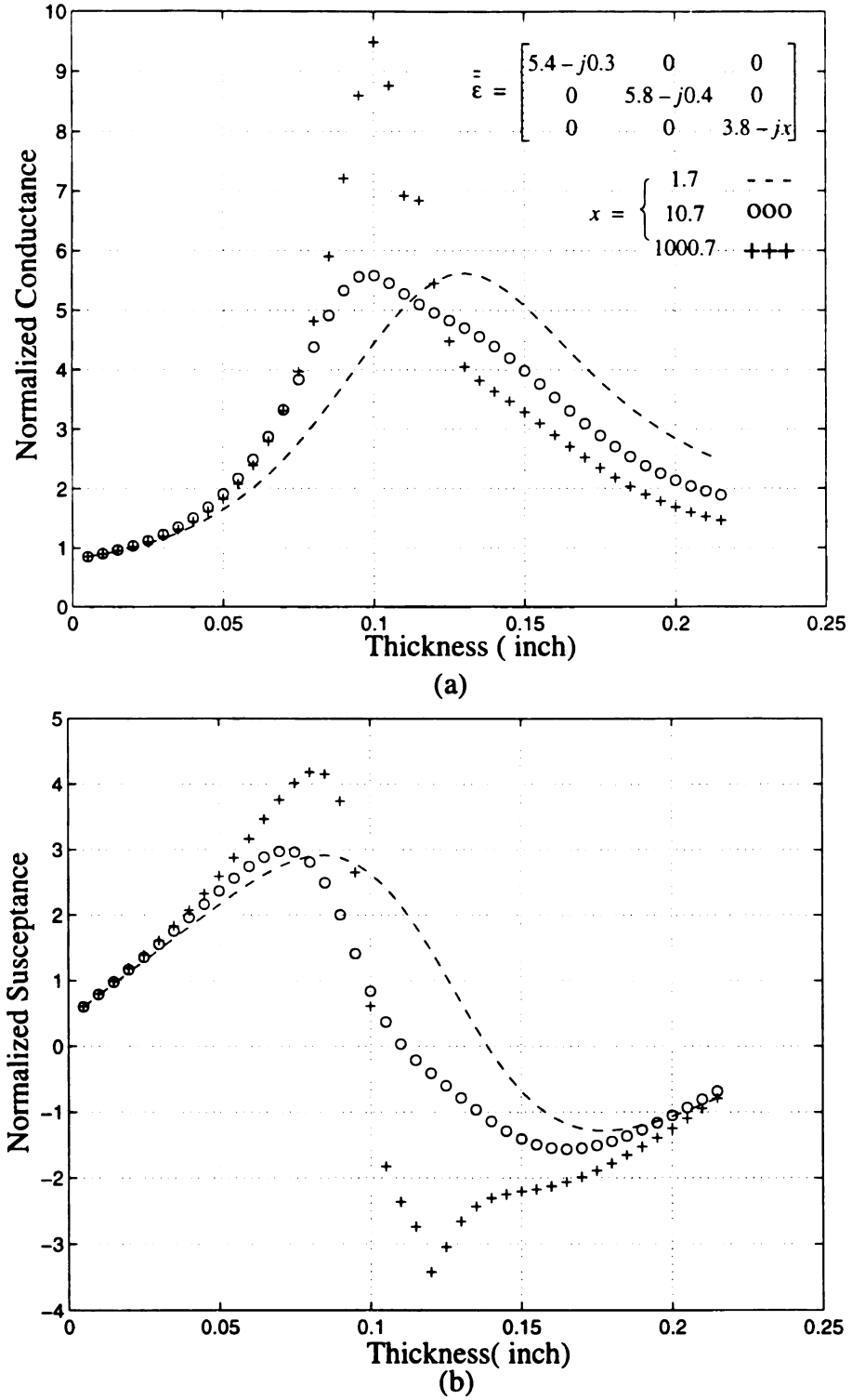

Figure 5.32 Input admittance of a waveguide probe as a function of the material thickness at 10 GHz when the probe is placed against an anisotropic material layer supplied by MSU Composite Material Laboratory with various conductivities in the z direction.

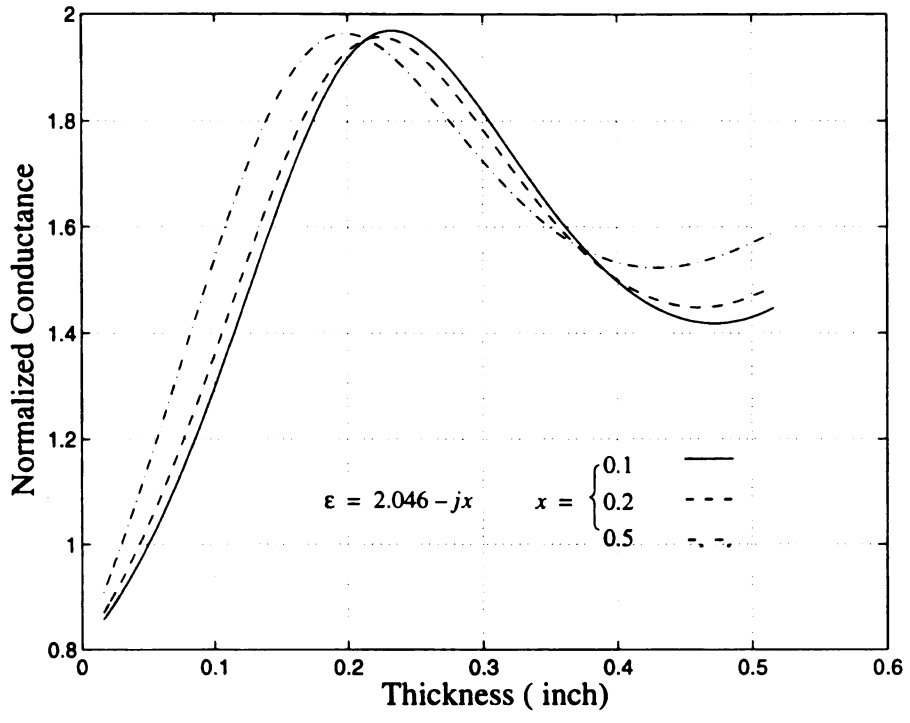

Figure 5.33 Input admittance of a waveguide probe as a function of the material thickness at 10 GHz when the probe is placed against an isotropic material layer with various conductivities.

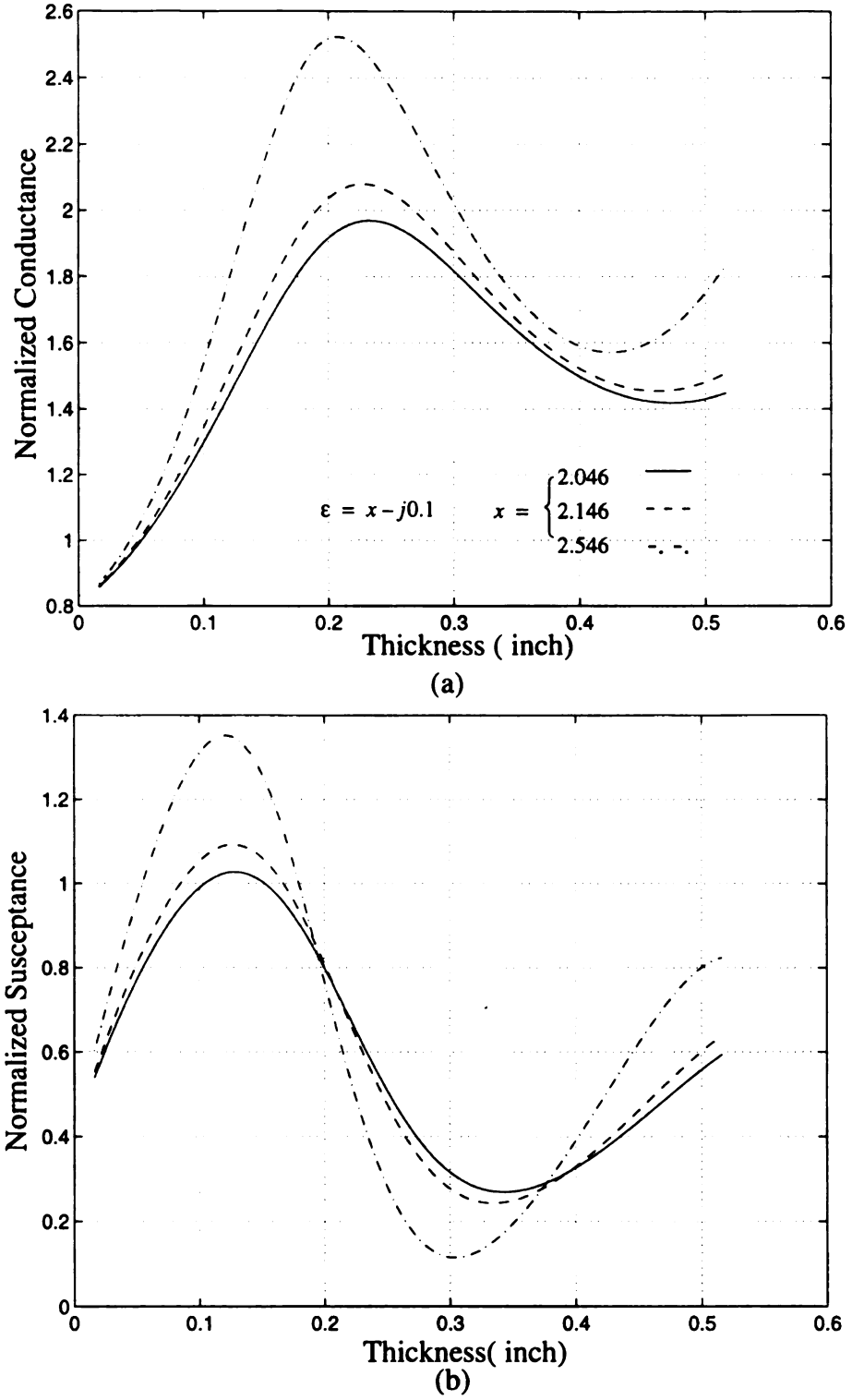

Figure 5.34 Input admittance of a waveguide probe as a function of the material thickness at 10 GHz when the probe is placed against an isotropic material layer with various permittivities.

values of 2.046, 2.146 and 2.546 in three different cases. In this figure, the probe input admittances clearly show distinguishable differences between three different cases, even when the change in the permittivity is of small quantity.

To summarize this analysis, we found that for the measurement of the EM properties of isotropic materials the thickness of the material is not important factor; while for anisotropic material, the material layer needs to be thicker than some value if accurate results on the EM parameters are sought.

CHAPTER 6

CONCLUSIONS

The purpose of this research was to determine the EM properties of materials nondestructively using a waveguide probe system over the X-band of 8 to 12 GHz. In this chapter, we review the techniques we have developed as well as the limitations for the use of this waveguide probe system. Finally, suggestions for future studies are addressed.

There are two major contributions from this research: two proposed theoretical techniques for the measurement of the EM properties of isotropic and anisotropic materials using a waveguide probe system, and the development of the experimental procedure for this system to achieve the nondestructive measurement of materials.

To measure the EM properties of a layer of material, a nondestructive measurement can be achieved by placing a waveguide probe system, which consists of an open-ended rectangular waveguide terminated on a flange and a network analyzer, against the material layer.

In Chapters 3 and 4, we have conducted theoretical and numerical analyses of the waveguide probe system attached to a layer of assumed known material. In these analyses, the reflection coefficient and other relevant quantities such as the input

admittance and the EM fields of the probe aperture were formulated as functions of the assumed EM parameters of the material layer.

The theoretical analyses of the system were based on two coupled integral equations developed for the aperture electric field by matching the tangential EM fields across the probe aperture. The method of moments was applied to solve these electric field integral equations numerically. After the Galerkin's method was used to convert these EFIE's into a matrix equation, the unknown aperture electric field can be determined numerically. Then, the reflection coefficient or the input admittance of the probe aperture can be calculated.

The technique presented in Chapter 3 employed the EM fields expressed in terms of Hertzian potentials to construct two EFIE's for the electric field at the waveguide aperture. Since the EM fields expressed in terms of Hertzian potentials are only suitable in an isotropic medium, this technique was then limited to the measurement of the EM parameters of isotropic materials. The numerical results on the input admittances of the waveguide probe obtained with this method were compared with the existing results published by other workers and they showed a good agreement between them. It was also found that a good convergence in the numerical calculation can be achieved when only the first four waveguide modes (TE_{10}, TE_{30}, TE_{12} and TM_{12}) were used.

The technique presented in Chapter 4 used the EM fields determined by the transverse field method to construct two EFIE's for the aperture electric field. Since the transverse field method can deal with a general case of the EM fields inside an anisotropic medium and a degenerate case of the EM fields inside an isotropic medium, this technique is suitable for the measurement of the EM parameters of both isotropic and anisotropic materials. The numerical examples illustrated in Chapter 3 for isotropic materials were also recalculated by the transverse field method and compared with the existing results. The results showed that our numerical results using four modes for both techniques agreed

well to each other, as well as to other published results. We also conducted the theoretical calculation of the input admittance of the waveguide probe placed against a layer of assumed known anisotropic material. The numerical results indicated that the aperture electric field is dominated by the dominant TE_{10} mode when the waveguide probe is attached to an anisotropic material layer, while using a dominant TE_{10} mode plus one higher order mode TE_{20} in the numerical calculation, we can obtain a good convergence on the probe input admittance.

Chapter 5 described the experiments and the inverse procedure for the nondestructive measurement of EM properties of materials. A series of experiments were conducted to measure the input admittances of the waveguide probe system attached to various materials, which included solid and liquid materials, as well as isotropic and anisotropic materials over the frequency range of 8 to 12 GHz. Two calibration procedures for the waveguide probe system were developed and discussed in detail. In the calibration procedure, we found that an oscillation of less than 5% amplitude along the measured data occurred probably due to the inaccuracy in the hardware and software of the calibration method. Therefore, a better calibration technique is needed for improving the accuracy of the measurement. It was suggested that a better method may be to use the HP waveguide calibration kits with an HP network analyzer to calibrate the waveguide probe system.

An inverse procedure to determine the EM parameters of the measured materials from the measured input admittances of the waveguide probe was described in Chapter 5. The measured probe input admittances were used to determine the conductivity and permittivity of the measured materials inversely by this numerical inverse procedure. The inverse results showed that the inverse procedure based on the Newton's iterative method provided a stable and efficient method to evaluate the EM properties of isotropic materials; while for anisotropic materials, the measured EM parameters are sensitive to the guess values given in the computer program. This was due to the increasing

complexity in the inverse procedure for determining three unknown complex permittivities of the anisotropic material simultaneously. The analysis of this difficulty was also presented detailedly in Chapter 5.

As mentioned in section 5.3., since we assume that the material layer to be measured is backed by free space in our configuration, an unintentional air gap may occur if the material layer was too thin or too light to secure a tight contact with the aperture. This may cause considerable inaccuracy because the EM fields excited inside the material layer were found to localize around the probe aperture. Therefore, the extension of the analysis of the waveguide probe system with a stratified material layer is suggested to further improve the accuracy of the measurement.

Finally, the forward procedures presented in Chapters 3 and 4 showed that the reflection coefficient and the input admittance at the probe aperture can be expressed as functions of the assumed EM properties such as the conductivity, permittivity, permeability and thickness of the material layer. Thus, it is possible to determine these quantities of interest simultaneously. However, it may require a faster computer to solve more quantities simultaneously.

APPENDIX

APPENDIX A

2-D FOURIER TRANSFORM OF SINUSOIDAL FUNCTIONS OVER WAVEGUIDE APERTURE

In this appendix the two-dimensional Fourier transforms of the sinusoidal functions are derived analytically. The simplified expressions of the notations are used to facilitate the implementation of a computer program. The shorthand notations of the transforms given in Chapter 4 are first rewritten in eqs. (A.1) to (A.4). They are based on the mode indices of the basis and testing functions represented as $[p, q]$ and $[l, r]$, respectively. On the other hand, to use these notations in Chapter 3, the mode indices are replaced by $[(2p-1), (2q-2)]$ and $[(2l-1), (2r-2)]$, respectively, for the basis and testing functions.

$$\iint t_y^e \equiv \int_0^b \int_0^a t_\alpha^y(x, y)\, e^{jk_x x} e^{jk_y y}\, dx dy$$

$$= \left(\int_0^a \sin\left[\frac{l\pi x}{a}\right] [\cos(k_x x) + j\sin(k_x x)]\, dx \right) \times$$

$$\left(\int_0^b \cos\left[\frac{r\pi y}{b}\right] [\cos(k_y y) + j\sin(k_y y)]\, dy \right)$$

$$\equiv [s_{11}(k_x) + s_{12}(k_x)]\, [s_{13}(k_y) + s_{14}(k_y)] \qquad \text{(A.1)}$$

$$\iint e_y^e \equiv \int_0^b \int_0^a e_\beta^y (x', y')\, e^{-jk_x x'} e^{-jk_y y'} dx' dy'$$

$$= \left(\int_0^a \sin\left[\frac{p\pi x'}{a}\right] [\cos(k_x x') - j\sin(k_x x')]\, dx' \right) \times$$

$$\left(\int_0^b \cos\left[\frac{q\pi y'}{b}\right] [\cos(k_y y') - j\sin(k_y y')]\, dy' \right)$$

$$\equiv [s_{21}(k_x) + s_{22}(k_x)]\, [s_{23}(k_y) + s_{24}(k_y)] \tag{A.2}$$

$$\iint t_x^e \equiv \int_0^b \int_0^a t_\alpha^x (x, y)\, e^{jk_x x} e^{jk_y y} dx dy$$

$$= \left(\int_0^a \cos\left[\frac{l\pi x}{a}\right] [\cos(k_x x) + j\sin(k_x x)]\, dx \right) \times$$

$$\left(\int_0^b \sin\left[\frac{r\pi y}{b}\right] [\cos(k_y y) + j\sin(k_y y)]\, dy \right)$$

$$\equiv [s_{31}(k_x) + s_{32}(k_x)]\, [s_{33}(k_y) + s_{34}(k_y)] \tag{A.3}$$

$$\iint e_x^e \equiv \int_0^b \int_0^a e_\beta^x (x', y')\, e^{-jk_x x'} e^{-jk_y y'} dx' dy'$$

$$= \left(\int_0^a \cos\left[\frac{p\pi x'}{a}\right] [\cos(k_x x') - j\sin(k_x x')]\, dx' \right) \times$$

$$\left(\int_0^b \sin\left[\frac{q\pi y'}{b}\right] [\cos(k_y y') - j\sin(k_y y')]\, dy' \right)$$

$$\equiv [s_{41}(k_x) + s_{42}(k_x)]\, [s_{43}(k_y) + s_{44}(k_y)] \tag{A.4}$$

The following derivations list the analytical results of the single finite integrals which represent sub-items of each inversion. Each result divides into two conditions as shown in the following.

$$s_{11}(k_x) \equiv \int_0^a \sin\left[\frac{l\pi x}{a}\right] \cos(k_x x)\, dx$$

$$= \begin{cases} \dfrac{a\pi l\,(1+\cos ak_x)}{l^2\pi^2 - a^2 k_x^{\,2}} & for \quad k_x \neq \dfrac{l\pi}{a} \\ 0 & for \quad k_x = \dfrac{l\pi}{a} \end{cases} \tag{A.5}$$

$$s_{12}(k_x) \equiv j\int_0^a \sin\left[\frac{l\pi x}{a}\right] \sin(k_x x)\, dx$$

$$= j\begin{cases} \dfrac{a\pi l \sin ak_x}{l^2\pi^2 - a^2 k_x^{\,2}} & for \quad k_x \neq \dfrac{l\pi}{a} \\ \dfrac{a}{2}\left[1-\delta(k_x)\right] & for \quad k_x = \dfrac{l\pi}{a} \end{cases} \tag{A.6}$$

$$s_{13}(k_y) \equiv \int_0^b \cos\left[\frac{r\pi y}{b}\right] \cos(k_y y)\, dy$$

$$= \begin{cases} \dfrac{-b^2 k_y \sin bk_y}{r^2\pi^2 - b^2 k_y^{\,2}} & for \quad k_y \neq \dfrac{r\pi}{b} \\ \dfrac{b}{2}\varepsilon_{k_y} & for \quad k_y = \dfrac{r\pi}{b} \end{cases} \tag{A.7}$$

$$s_{14}(k_y)' \equiv j\int_0^b \cos\left[\frac{r\pi y}{b}\right] \sin(k_y y)\, dy$$

$$= j\begin{cases} \dfrac{-b^2 k_y\,(1-\cos bk_y)}{r^2\pi^2 - b^2 k_y^{\,2}} & for \quad k_y \neq \dfrac{r\pi}{b} \\ 0 & for \quad k_y = \dfrac{r\pi}{b} \end{cases} \tag{A.8}$$

$$s_{21}(k_x) \equiv \int_0^a \sin\left[\frac{p\pi x'}{a}\right] \cos(k_x x')\, dx'$$

$$= \begin{cases} \dfrac{a\pi p\,(1+\cos ak_x)}{p^2\pi^2 - a^2 k_x^{\,2}} & for \quad k_x \neq \dfrac{p\pi}{a} \\ 0 & for \quad k_x = \dfrac{p\pi}{a} \end{cases} \tag{A.9}$$

$$s_{22}(k_x) \equiv -j\int_0^a \sin\left[\frac{p\pi x'}{a}\right] \sin(k_x x')\, dx'$$

$$= -j\begin{cases} \dfrac{a\pi p \sin ak_x}{p^2\pi^2 - a^2 k_x^{\,2}} & for \quad k_x \neq \dfrac{p\pi}{a} \\ \dfrac{a}{2}\left[1-\delta(k_x)\right] & for \quad k_x = \dfrac{p\pi}{a} \end{cases} \tag{A.10}$$

$$s_{23}(k_y) \equiv \int_0^b \cos\left[\frac{q\pi y'}{b}\right] \cos(k_y y')\, dy'$$

$$= \begin{cases} \dfrac{-b^2 k_y \sin bk_y}{q^2\pi^2 - b^2 k_y^{\,2}} & for \quad k_y \neq \dfrac{q\pi}{b} \\ \dfrac{b}{2}\varepsilon_{k_y} & for \quad k_y = \dfrac{q\pi}{b} \end{cases} \tag{A.11}$$

$$s_{24}(k_y) \equiv -j\int_0^b \cos\left[\frac{q\pi y'}{b}\right] \sin(k_y y')\, dy'$$

$$= -j\begin{cases} \dfrac{-b^2 k_y\,(1-\cos bk_y)}{q^2\pi^2 - b^2 k_y^{\,2}} & for \quad k_y \neq \dfrac{q\pi}{b} \\ 0 & for \quad k_y = \dfrac{q\pi}{b} \end{cases} \tag{A.12}$$

$$s_{31}(k_x) \equiv \int_0^a \cos\left[\frac{l\pi x}{a}\right] \cos(k_x x)\, dx$$

$$= \begin{cases} \dfrac{a^2 k_x \sin a k_x}{l^2\pi^2 - a^2 k_x^2} & \text{for} \quad k_x \neq \dfrac{l\pi}{a} \\ \dfrac{a}{2}\varepsilon_{k_x} & \text{for} \quad k_x = \dfrac{l\pi}{a} \end{cases} \tag{A.13}$$

$$s_{32}(k_x) \equiv j\int_0^a \cos\left[\frac{l\pi x}{a}\right] \sin(k_x x)\, dx$$

$$= j\begin{cases} \dfrac{-a^2 k_x (1 + \cos a k_x)}{l^2\pi^2 - a^2 k_x^2} & \text{for} \quad k_x \neq \dfrac{l\pi}{a} \\ 0 & \text{for} \quad k_x = \dfrac{l\pi}{a} \end{cases} \tag{A.14}$$

$$s_{33}(k_y) \equiv \int_0^b \sin\left[\frac{r\pi y}{b}\right] \cos(k_y y)\, dy$$

$$= \begin{cases} \dfrac{b\pi r (1 - \cos b k_y)}{r^2\pi^2 - b^2 k_y^2} & \text{for} \quad k_y \neq \dfrac{r\pi}{b} \\ 0 & \text{for} \quad k_y = \dfrac{r\pi}{b} \end{cases} \tag{A.15}$$

$$s_{34}(k_y) \equiv j\int_0^b \sin\left[\frac{r\pi y}{b}\right] \sin(k_y y)\, dy$$

$$= j\begin{cases} \dfrac{-b\pi r \sin b k_y}{r^2\pi^2 - b^2 k_y^2} & \text{for} \quad k_y \neq \dfrac{r\pi}{b} \\ \dfrac{b}{2}[1 - \delta(k_y)] & \text{for} \quad k_y = \dfrac{r\pi}{b} \end{cases} \tag{A.16}$$

$$s_{41}(k_x) \equiv \int_0^a \cos\left[\frac{p\pi x'}{a}\right] \cos(k_x x')\, dx'$$

$$= \begin{cases} \dfrac{a^2 k_x \sin a k_x}{p^2\pi^2 - a^2 k_x^2} & \text{for} \quad k_x \neq \dfrac{p\pi}{a} \\ \dfrac{a}{2}\varepsilon_{k_x} & \text{for} \quad k_x = \dfrac{p\pi}{a} \end{cases} \tag{A.17}$$

$$s_{42}(k_x) \equiv -j\int_0^a \cos\left[\frac{p\pi x'}{a}\right] \sin(k_x x')\, dx'$$

$$= -j\begin{cases} \dfrac{-a^2 k_x (1 + \cos a k_x)}{p^2\pi^2 - a^2 k_x^2} & \text{for} \quad k_x \neq \dfrac{p\pi}{a} \\ 0 & \text{for} \quad k_x = \dfrac{p\pi}{a} \end{cases} \tag{A.18}$$

$$s_{43}(k_y) \equiv \int_0^b \sin\left[\frac{q\pi y'}{b}\right] \cos(k_y y')\, dy'$$

$$= \begin{cases} \dfrac{b\pi q (1 - \cos b k_y)}{q^2\pi^2 - b^2 k_y^2} & \text{for} \quad k_y \neq \dfrac{q\pi}{b} \\ 0 & \text{for} \quad k_y = \dfrac{q\pi}{b} \end{cases} \tag{A.19}$$

$$s_{44}(k_y) \equiv -j\int_0^b \sin\left[\frac{q\pi y'}{b}\right] \sin(k_y y')\, dy'$$

$$= -j\begin{cases} \dfrac{-b\pi q \sin b k_y}{q^2\pi^2 - b^2 k_y^2} & \text{for} \quad k_y \neq \dfrac{q\pi}{b} \\ \dfrac{b}{2}[1 - \delta(k_y)] & \text{for} \quad k_y = \dfrac{q\pi}{b} \end{cases} \tag{A.20}$$

As given in Chapters 3 and 4, these inversion functions are used to define the following notations such as

$$\phi_{12u}(k_x) \equiv [s_{11}(k_x) + s_{12}(k_x)]\,[s_{21}(k_x) + s_{22}(k_x)] \tag{A.21}$$

$$\phi_{12v}(k_y) \equiv [s_{13}(k_y) + s_{14}(k_y)]\,[s_{23}(k_y) + s_{24}(k_y)] \tag{A.22}$$

to be used in $D_{\alpha\beta}^{yy}$, and

$$\phi_{34u}(k_x) \equiv [s_{31}(k_x) + s_{32}(k_x)]\,[s_{41}(k_x) + s_{42}(k_x)] \tag{A.23}$$

$$\phi_{34v}(k_y) \equiv [s_{33}(k_y) + s_{34}(k_y)]\,[s_{43}(k_y) + s_{44}(k_y)] \tag{A.24}$$

in $D_{\alpha\beta}^{xx}$, and

$$\phi_{32u}(k_x) \equiv [s_{31}(k_x) + s_{32}(k_x)]\,[s_{21}(k_x) + s_{22}(k_x)] \tag{A.25}$$

$$\phi_{32v}(k_y) \equiv [s_{33}(k_y) + s_{34}(k_y)]\,[s_{23}(k_y) + s_{24}(k_y)] \tag{A.26}$$

in $D_{\alpha\beta}^{xy}$, and

$$\phi_{14u}(k_x) \equiv [s_{11}(k_x) + s_{12}(k_x)]\,[s_{41}(k_x) + s_{42}(k_x)] \tag{A.27}$$

$$\phi_{14v}(k_y) \equiv [s_{13}(k_y) + s_{14}(k_y)]\,[s_{43}(k_y) + s_{44}(k_y)] \tag{A.28}$$

in $D_{\alpha\beta}^{yx}$.

If we further denote S_{xy}^{a} as the finite integral result for the multiplication of two sinusoidal functions with different arguments and S_{xy}^{b} as the result with the same argument, where xy is the index of the above sub-inversion functions, then eqs. (A.21) to (A.28) can be tabulated in Table A.1 to be used in Chapter 4 and Table A.2 in Chapter 3 if the symmetric

Table A.1 Summary for simplified expressions of notations used in Chapter 4.

Function / Condition	$D^{yy}_{\alpha\beta}$	$D^{yx}_{\alpha\beta}$	$D^{xy}_{\alpha\beta}$	$D^{xx}_{\alpha\beta}$
	$\phi_{12u}(k_x)$	$\phi_{14u}(k_x)$	$\phi_{32u}(k_x)$	$\phi_{34u}(k_x)$
$k_x \neq \frac{l\pi}{a} \wedge k_x \neq \frac{p\pi}{a}$	$\left(S^a_{11}+S^a_{12}\right)\times\left(S^a_{21}+S^a_{22}\right)$	$\left(S^a_{11}+S^a_{12}\right)\times\left(S^a_{41}+S^a_{42}\right)$	$\left(S^a_{31}+S^a_{32}\right)\times\left(S^a_{21}+S^a_{22}\right)$	$\left(S^a_{31}+S^a_{32}\right)\times\left(S^a_{41}+S^a_{42}\right)$
$k_x \neq \frac{l\pi}{a} \wedge k_x = \frac{p\pi}{a}$	$\left(S^a_{11}+S^a_{12}\right)S^b_{22}$	$\left(S^a_{11}+S^a_{12}\right)S^b_{41}$	$\left(S^a_{31}+S^a_{32}\right)S^b_{22}$	$\left(S^a_{31}+S^a_{32}\right)S^b_{41}$
$k_x = \frac{l\pi}{a} \wedge k_x \neq \frac{p\pi}{a}$	$S^b_{12}\left(S^a_{21}+S^a_{22}\right)$	$S^b_{12}\left(S^a_{41}+S^a_{42}\right)$	$S^b_{31}\left(S^a_{21}+S^a_{22}\right)$	$S^b_{31}\left(S^a_{41}+S^a_{42}\right)$
$k_x = \frac{l\pi}{a} \wedge k_x = \frac{p\pi}{a}$	$S^b_{12}S^b_{22}$	$S^b_{12}S^b_{41}$	$S^b_{31}S^b_{22}$	$S^b_{31}S^b_{41}$
Function / Condition	$D^{yy}_{\alpha\beta}$	$D^{yx}_{\alpha\beta}$	$D^{xy}_{\alpha\beta}$	$D^{xx}_{\alpha\beta}$
	$\phi_{12v}(k_y)$	$\phi_{14v}(k_y)$	$\phi_{32v}(k_y)$	$\phi_{34v}(k_y)$
$k_y \neq \frac{r\pi}{a} \wedge k_y \neq \frac{q\pi}{a}$	$\left(S^a_{13}+S^a_{14}\right)\times\left(S^a_{23}+S^a_{24}\right)$	$\left(S^a_{13}+S^a_{14}\right)\times\left(S^a_{43}+S^a_{44}\right)$	$\left(S^a_{33}+S^a_{34}\right)\times\left(S^a_{23}+S^a_{24}\right)$	$\left(S^a_{33}+S^a_{34}\right)\times\left(S^a_{43}+S^a_{44}\right)$
$k_y \neq \frac{r\pi}{a} \wedge k_y = \frac{q\pi}{a}$	$\left(S^a_{13}+S^a_{14}\right)S^b_{23}$	$\left(S^a_{13}+S^a_{14}\right)S^b_{44}$	$\left(S^a_{33}+S^a_{34}\right)S^b_{23}$	$\left(S^a_{33}+S^a_{34}\right)S^b_{44}$
$k_y = \frac{r\pi}{a} \wedge k_y \neq \frac{q\pi}{a}$	$S^b_{13}\left(S^a_{23}+S^a_{24}\right)$	$S^b_{13}\left(S^a_{43}+S^a_{44}\right)$	$S^b_{34}\left(S^a_{23}+S^a_{24}\right)$	$S^b_{34}\left(S^a_{43}+S^a_{44}\right)$
$k_y = \frac{r\pi}{a} \wedge k_y = \frac{q\pi}{a}$	$S^b_{13}S^b_{23}$	$S^b_{13}S^b_{44}$	$S^b_{34}S^b_{23}$	$S^b_{34}S^b_{44}$

Table A.2 Summary for simplified expressions of notations used in Chapter 3.

Function / Condition	$D^{yy}_{\alpha\beta}$	$D^{yx}_{\alpha\beta}$	$D^{xy}_{\alpha\beta}$	$D^{xx}_{\alpha\beta}$
	$\phi^{e}_{12u}(k_x)$	$\phi^{o}_{14u}(k_x)$	$\phi^{o}_{32u}(k_x)$	$\phi^{e}_{34u}(k_x)$
$k_x \neq \frac{l\pi}{a} \wedge k_x \neq \frac{p\pi}{a}$	$S^a_{11}S^a_{21} + S^a_{12}S^a_{22}$	$S^a_{11}S^a_{42} + S^a_{12}S^a_{41}$	$S^a_{31}S^a_{22} + S^a_{32}S^a_{21}$	$S^a_{31}S^a_{41} + S^a_{32}S^a_{42}$
$k_x \neq \frac{l\pi}{a} \wedge k_x = \frac{p\pi}{a}$	$S^a_{11}S^b_{22}$	$S^a_{12}S^b_{41}$	$S^a_{32}S^b_{22}$	$S^a_{31}S^b_{41}$
$k_x = \frac{l\pi}{a} \wedge k_x \neq \frac{p\pi}{a}$	$S^b_{12}S^a_{21}$	$S^b_{12}S^a_{42}$	$S^b_{31}S^a_{22}$	$S^b_{31}S^a_{41}$
$k_x = \frac{l\pi}{a} \wedge k_x = \frac{p\pi}{a}$	$S^b_{12}S^b_{22}$	0	0	$S^b_{31}S^b_{41}$
Function / Condition	$D^{yy}_{\alpha\beta}$	$D^{yx}_{\alpha\beta}$	$D^{xy}_{\alpha\beta}$	$D^{xx}_{\alpha\beta}$
	$\phi^{e}_{12v}(k_y)$	$\phi^{o}_{14v}(k_y)$	$\phi^{o}_{32v}(k_y)$	$\phi^{e}_{34v}(k_y)$
$k_y \neq \frac{r\pi}{a} \wedge k_y \neq \frac{q\pi}{a}$	$S^a_{13}S^a_{23} + S^a_{14}S^a_{24}$	$S^a_{13}S^a_{44} + S^a_{14}S^a_{43}$	$S^a_{33}S^a_{24} + S^a_{34}S^a_{23}$	$S^a_{33}S^a_{43} + S^a_{34}S^a_{44}$
$k_y \neq \frac{r\pi}{a} \wedge k_y = \frac{q\pi}{a}$	$S^a_{13}S^b_{23}$	$S^a_{14}S^b_{44}$	$S^a_{34}S^b_{23}$	$S^a_{33}S^b_{44}$
$k_y = \frac{r\pi}{a} \wedge k_y \neq \frac{q\pi}{a}$	$S^b_{13}S^a_{23}$	$S^b_{13}S^a_{44}$	$S^b_{34}S^a_{24}$	$S^b_{34}S^a_{43}$
$k_y = \frac{r\pi}{a} \wedge k_y = \frac{q\pi}{a}$	$S^b_{13}S^b_{23}$	0	0	$S^b_{34}S^b_{44}$

Note that in this table *l*, *p*, *r* and *q* represent *(2l-1)*, *(2p-1)*, *(2r-2)* and *(2q-2)*, respectively.

properties of these notations are considered. Note that in Table A.2 the mode indices need to be replaced by $[(2p-1), (2q-2)]$ and $[(2l-1), (2r-2)]$ instead of $[p, q]$ and $[l, r]$.

BIBLIOGRAPHY

BIBLIOGRAPHY

[1] E. Tanabe and W. T. Joines, "A nondestructive method for measuring the complex permittivity of dielectric materials at microwave frequencies using an open transmission line resonator," *IEEE Trans. Instrum. Meas.*, vol. IM-25, pp. 222-226, Sept. 1976.

[2] J. R. Mosig et al., "Reflection of an open-ended coaxial line and application to non-destructive measurement of material," *IEEE Trans. Instrum. Meas.*, vol. IM-30, pp. 46-51, (Jan.) 1981.

[3] M. A. Stuchly and S. S. Stuchly, "Coaxial line reflection method for measuring dielectric properties of biological substances at radio and microwave frequencies - a review," *IEEE Trans. Instrum. Meas.*, vol. IM-29, pp. 176-183, (Sept.) 1980.

[4] G. B. Gajda and S. S. Stuchly, "Numerical analysis of open-ended coaxial lines," *IEEE Trans. Microwave Theory and Techniques*, vol. MTT-31, pp. 380-384, May 1983.

[5] S. Fan, K. Staebell, and D. Misra, "Static analysis of an open-ended coaxial line terminated by layered media," *IEEE Trans. Instrum. Meas.*, vol. IM-39, pp. 425-437, Apr. 1990.

[6] S. Fan and D. Misra, "A study on the metal-flanged open-ended coaxial line terminating in a conductor-backed dielectric layer," 1990 IEEE Instrumentation and Measurement Technology Conference Record, pp. 43-46.

[7] D. K. Misra et al., "Noninvasive electrical characterization of materials at microwave frequencies using an open-ended coaxial line: Test of an improved calibration technique," *IEEE Trans. Microwave Theory and Techniques*, vol. MTT-38, pp. 8-14, Jan. 1990.

[8] Belhadj-Tahar, N. E., and A. Fourrier-Lamer, and H. de Chanterac., "Broad-band simultaneous measurement of complex permittivity and permeability using a coaxial discontinuity," *IEEE Trans. Microwave Theory and Techniques*, vol. MTT-38, pp. 1-7, Jan. 1990.

[9] H. Zheng and C. E. Smith, "Permittivity measurements using a short open-ended coaxial line proe," *IEEE Trans. Microwave and Guided Wave Lett.*, vol. 1, no. 11, Nov. 1991.

[10] L. L. Li, N. H. Ismail, L. S. Taylor and C. C. Davis, "Flanged coaxial microwave probes for measuring thin moisture layers," *IEEE Trans. Biomedical Eng.*, vol. 39, pp. 49-57, Jan. 1992.

[11] B. Chevalier, M. Chatard-Moulin, J. P. Astier and P. Y. Guillon, "High-temperature complex permittivity measurements of composite materials using an open-ended waveguide," *J. Electromagn. Waves Applic.*, vol. 6, no. 9, pp. 1259-1275, 1992.

[12] C. L. Lee, "Measurement of electromagnetic properties of material via coaxial probe systems," Ph.D. Dissertation, Dept. Elec. Eng., Michigan State Univ., East Lansing, Michigan, 1993.

[13] W. Barry, "A broad-band, automated, stripline technique for the simultaneous measurement of complex permittivity and permeability," *IEEE Trans. Microwave Theory and Techniques*, vol. MTT-34, pp. 80-84, Jan. 1986.

[14] R. M. Pannell and B. W. Jervis, "Two simple methods for the measurement of dielectric permittivity of low-loss microstrip substates," *IEEE Trans. Microwave Theory and Techniques*, vol. MTT-29, no. 4, pp. 383-386, Apr. 1981.

[15] B. Terselius and B. Ranby, "Cavity perturbation measurements of the dielectric properties of vnlcanizing rubber and polyethylene compounds," *J. Microwave Power*, vol. 13, pp. 327-335, Jan. 1978.

[16] A. Parkash, J. K. Vaid, and A. Mansingh, "Measurement of dielectric parameters at microwave frequencies by cavity perturbation technique," *IEEE Trans. Microwave Theory and Techniques*, vol. MTT-27, pp. 791-795, Jan. 1979.

[17] C. B. Rosenberg, N. A. Hermiz, and R. J. Cook, "Cavity resonator measurements of the complex permittivity of low-loss liquids," *Proc. IEE*, pt. H, vol. 129, pp. 71-76, 1982.

[18] W. B. Wier, "Automatic measurement of complex dielectric constant and permeability at microwave frequencies," *Proc. IEEE*, vol. 62, no. 1, pp. 33-36, Jan., 1982.

[19] M. C. Decreton and F. E. Gardiol, "Simple nondestructive method for the measurement of complex permittivity," *IEEE Trans. Instrum. Meas.*, vol. IM-23, pp. 434-438, Dec. 1974.

[20] M. C. Decreton and M. S. Ramachandraiah, "Nondestructive measurement of complex permittivity for dielectric slabs," *IEEE Trans. Microwave Theory and Techniques*, vol. MTT-23, pp. 1077-1080, Dec. 1975.

[21] J. Galejs, "Admittance of a waveguide radiating into stratified plasma," *IEEE Trans. Antennas and Propagation.*, vol. AP-13, pp. 64-70, Jan. 1965.

[22] W. F. Croswell, R. C. Rudduck, and D. M. Hatcher, "The admittance of a rectangular waveguide radiating into a dielectric slab," *IEEE Trans. Antennas and Propagation*, vol. AP-15, pp. 627-633, Sept.1967.

[23] C. P. Wu, "Integral equation solutions for the radiation from a waveguide through a dielectric slab," *IEEE Trans. Antennas and Propagation*, vol. AP-17, pp. 733-739, Nov. 1969.

[24] D. G. Bodnar and D. T. Paris, "New variational principle in electromagnetics," *IEEE Trans. Antennas and Propagation.*, vol. AP-18, pp. 216-223, March 1970.

[25] A. R. Jamieson and T. E. Rozzi, "Rigorous analysis of cross polarization in flange-mounted rectangular waveguide radiators," *Electronics Letters*, vol. 13, pp. 742-744, Nov. 24, 1977.

[26] R. H. MacPhie and A. I. Zaghloul, "Radiation from a rectangular waveguide with infinite flange - exact solution by the correlation matrix method," *IEEE Trans. Antennas and Propagation*, vol. AP-28, pp. 497-503, July 1980.

[27] J. L. Tsalamengas and N. K. Uzunoglu, "Radiation from a dipole in the proximity of a general anisotropic grounded layer," *IEEE Trans. Antennas and Propagation*, vol. AP-*33*, pp. 165-172, 1985.

[28] V. Teodoridis, T. Sphicopoulos, and F. E. Gardiol, "The reflection from an open-ended rectangular waveguide terminated by a layered dielectric medium," *IEEE Trans. Microwave Theory and Techniques*, vol. MTT-33, pp. 359-366, May 1985.

[29] M. A. Morgan, D. L. Fisher, and E. A. Milne, "Electromagnetic scattering by stratified inhomogeneous anisotropic media," *IEEE Trans. Antennas and Propagation*, vol. AP-*35*, pp. 191-197, Feb. 1986.

[30] H. Baudrand, J.-W. Tao, and J. Atechian, "Study of radiating properties of open-ended rectangular waveguides," *IEEE Trans. Antennas and Propagation*, vol. AP-*36*, pp. 1071-1077, Aug. 1988.

[31] J. L. Tsalamengas and N. K. Uzunoglu, "Radiation properties of a flanged parallel-plate waveguide loaded with an $\mathfrak{E}-\mu$ general anisotropic slab," *IEEE Trans. Antennas and Propagation*, vol. AP-*38*, pp. 369-379, March 1990.

[32] R. D. Graglia and P. L. E. Uslenghi, "Electromagnetic scattering from anisotropic materials, Part I: General theory," *IEEE Trans. Antennas and Propagation*, vol. AP-*32*, pp. 867-869, Aug. 1993.

[33] J. A. Stratton, *Electromagnetic Theory,* McGram-Hill, New York, 1941, pp. 392-395.

[34] C. A. Balanis, *Advanced Engineering Electromagnetics,* Wiley, New York, 1989, Chap. 6.

[35] J. Galejs, *Antennas in Inhomogeneous Media,* Oxford, Pergamon, 1969, pp. 39-44, 105-109.

[36] T. M. Roberts, "Explicit eigenmodes for anisotropic media," *IEEE Trans. Magnetics*, vol. 26, pp.3064-3071, 1990.

[37] T. M. Roberts, H. A. Sabbagh, and L. D. Sabbagh, "Electromagnetic interactions with an anisotropic slab," *IEEE Trans. Magnetics*, vol. 24, pp. 3193-3200, Nov. 1988.

[38] T. M. Roberts, H. A. Sabbagh, and L. D. Sabbagh, "Electromagnetic scattering for a class of anisotropic layered media," *J. Math. Phys.*, vol. 29, pp. 2675-2681, Dec. 1991.

[39] R. E. Collin, *Field Theory of Guided Waves,* 2nd ed., IEEE Press, New York, 1991, Chap. 5, 11.

[40] A. Sommerfeld, *Partial Differential Equations in Physics,* Academic Press, New York, 1965.

[41] J. Song, "Scattering of arbitrarily-polarized EM waves by a discontinuity in a grounded dielectric sheet and propagation of EM pulses excited by an electric dipole in conducting media," Ph.D. Dissertation, Dept. Elec. Eng., Michigan State Univ., East Lansing, Michigan, 1993.

[42] W. C. Chew, *Waves and Fields in Inhomogeneous Media*, Van Nostrand Reinhold Company, New York, 1990.

[43] E. F. da Silva and M. K. McPhun, "Calibration techniques for one port measurement," *Microwave J.*, pp. 97-100, June 1978.

[44] L. N. Ridenour, *Technique of Microwave Measurements,* McGram-Hill, New York, 1947, pp. 473-496.

[45] R. L. Johnston, *Numerical Methods - A Software Approach,* Wiley, New York, 1982, Chap. 4.

[46] C. L. Li and K. M. Chen, "Determination of electromagnetic properties of materials using flanged open-ended coaxial probe -- full-wave analysis," *IEEE Trans. Microwave Theory and Techniques*, vol. MTT-44, pp. 19-27, Feb. 1995.

[47] A. C. Metaxas and R. J. Meredith, *Industrial Microwave Heating,* Peregrinus, London, 1983, pp. 58-60.